



Simon Oberhollenzer, BSc

Numerical studies on slope stability analysis

MASTERARBEIT

zur Erlangung des akademischen Grades

Diplom-Ingenieur

Masterstudium Bauingenieurwissenschaften – Geotechnik und Wasserbau

eingereicht an der

Technischen Universität Graz

Betreuer

Ass.Prof. Dipl.-Ing. Dr.techn., Franz Tschuchnigg

Institut für Bodenmechanik und Grundbau

Eidesstattliche Erklärung

Ich erkläre an Eides statt, dass ich die vorliegende Arbeit selbstständig verfasst, andere als die angegebenen Quellen/Hilfsmittel nicht benutzt, und die den benutzten Quellen wörtlich und inhaltlich entnommenen Stellen als solche kenntlich gemacht habe.

Graz, am

.....

(Unterschrift)

Statutory declaration

I declare that I have authored this thesis independently, that I have not used other than the declared sources / resources, and that I have explicitly marked all material which has been quoted either literally or by content from the used sources.

Graz,

.....

(signature)

Acknowledgement

It is a great pleasure to acknowledge my deepest thanks and gratitude to Ass.Prof. Dipl.-Ing. Dr.techn. Franz Tschuchnigg, for suggesting the topic of this thesis as well as his guidance, patience, motivation and enthusiasm throughout this process.

I also want to thank my friends and colleagues for their encouragement and for making the years of study a pleasure. A special note of thanks to Laurin *Rattino* Hauser and Alex *Barbarossa* Putzer for their friendship and support.

Finally I would like to express my gratitude to my parents *Hånsi* and *Guzza* as well as my girlfriend *Lünski* for supporting me where- and whenever possible. Without their help I would not have been able to complete my studies.

Kurzfassung

Die Grenz-Gleichgewichtsverfahren nach Bishop (1955) oder Morgenstern & Price (1965) finden in der Geotechnik eine breite Verwendung zur Bestimmung des Sicherheitsfaktors (FoS). Unterschiedliche Annahmen zur Form des Versagens, sowie der Kräfte zwischen den Lamellen verhindern eine einheitliche Definition des Sicherheitsfaktors. Diese Annahmen sind bei *displacement based finite element analyses* oder *finite element limit analyses* hingegen nicht notwendig. Aufgrund der Tatsache, dass der letztere Berechnungstyp auf eine assoziierte Fließregel beschränkt ist, empfahl Davis (1968) die Verwendung von reduzierten Festigkeitsparametern, um ein nicht-assoziertes Verhalten zu simulieren (Davis A). Die Anwendung dieser an bewährten Böschungen sowie an Beispielen von Griffiths und Lane (1999) führen, im Vergleich zu den *strength reduction finite element analyses* (SRFEA), zu sehr konservativen Ergebnissen. Modifizierte Vorgehensweisen der ursprünglichen Idee (Davis B, Davis C) resultieren nach wie vor in einem konservativen Sicherheitsfaktor, zeigen jedoch eine bessere Übereinstimmung mit der SRFEA. Weitere Parameterstudien haben verifiziert, dass ein Anstieg im Reibungswinkel ϕ' , Kohäsion c' und Maß an nicht-Assoziativität λ zu größeren Differenzen zwischen Davis A und SRFEA führen. Für Davis B und Davis C wirken sich Kohäsion c' und Reibungswinkel ϕ' gering auf die Differenzen aus.

Standardmäßig wird bei einer *strength reduction finite element analysis* die Poisson's Zahl ν konstant gehalten, während Reibungswinkel ϕ' und Kohäsion c' reduziert werden. Basierend auf dem Mohr-Coulomb Fehlerkriterium kann die $\phi - \nu$ Ungleichheit $\sin\phi' \geq 1 - 2\nu$ abgeleitet werden. Für hohe Sicherheitsfaktoren wird die Bedingung verletzt. Numerische Untersuchungen haben ergeben, dass die $\phi - \nu$ Ungleichheit keinen Einfluss auf den Sicherheitsfaktor nimmt, jedoch mit höherer Poisson Zahl ν die Anzahl an *failure points* sinkt.

In den meisten Fällen ist die Spannungssituation *in situ* unbekannt. Daher ist die Auswirkung des ursprünglichen Spannungsniveaus auf den Sicherheitsfaktor von großem Interesse. Eine weitere Studie zeigt, dass die ursprüngliche Spannungsverteilung keinen Einfluss auf den FoS nimmt. Unabhängig vom Ausgangspunkt des Spannungspfades wird dieser immer am selben Mohr-Coulomb-Fehlerkriterium versagen.

Abstract

Limit equilibrium methods by Bishop (1955) or Morgenstern & Price (1965) are commonly used in practical geotechnical engineering to determine the factor of safety (FoS). Varying assumptions about the shape of failure mechanisms as well as interslice forces make an unique definition of the safety factor next to impossible. On the other hand, *displacement based finite element analyses* and *finite element limit analyses* don't need those assumptions to perform. Due to the fact that the latter one is limited to associated plasticity, Davis (1968) suggested the use of reduced strength parameters in order to generate a non-associated behaviour (Davis A). Applying this approach on reinforced slopes and on examples taken from Griffiths and Lane (1999) lead to very conservative results compared to *strength reduction finite element analyses* (SRFEA) with non-associated plasticity. Modified versions of the original approach (Davis B, Davis C) still result in a conservative factor of safety but achieve a far better agreement with the SRFEA. Further parameter studies have verified that an increase in friction angle ϕ' , cohesion c' and degree of non-associativity λ lead to larger differences between Davis A and SRFEA. For Davis B and Davis C, these differences are weakly affected by cohesion c' and friction angle ϕ' .

It is common practice that in a *strength reduction finite element analysis* the Poisson's ratio ν is kept constant while friction angle ϕ' and cohesion c' get reduced. Deriving from the Mohr-Coulomb failure criterion, the relation $\sin\phi' \geq 1 - 2\nu$, known as the $\phi - \nu$ inequality obviously gets violated for high safety factors. Numerical analyses proved that the $\phi - \nu$ inequality does not affect the factor of safety. It should be noted that with increasing Poisson's ratio the number of *failure points* decreases.

In most cases the stress situation *in situ* is unknown. Therefore, the influence of the initial stress state on the factor of safety is of interest. A further study established shows that the initial stress level has no impact on the FoS. For any point situated along the failure mechanism, the origin of its stress path is of no importance. Failure will always occur along the same Mohr-Coulomb criterion.

Table of contents

1	Introduction	1
2	Analytical method of defining a FoS	3
2.1	Definition of limit equilibrium.....	3
2.2	Limit equilibrium analysis	4
2.2.1	Ordinary method	4
2.2.2	Bishop's simplified method.....	5
2.2.3	Janbu's simplified method	6
2.2.4	Morgenstern & Price method.....	6
2.2.5	Spencer's method	7
3	Numerical methods of defining a FoS.....	9
3.1	Strength reduction finite element analysis (SRFEA)	9
3.1.1	Introduction to displacement based finite element analysis	9
3.1.2	Flow rule	11
3.1.3	SRFEA in Plaxis 2D	11
3.1.4	Difficulties by calculating with a non-associated flow rule	12
3.2	Finite element limit analysis (FELA)	14
3.2.1	Introduction to limit analysis	14
3.2.2	Introduction to finite element limit analysis	16
3.2.3	Strength reduction according to Sloan (2013)	21
3.2.4	Safety analysis of Optum G2.....	23
3.3	Davis approach	24
3.3.1	Necessity of the Davis approach in finite element limit analysis	24
3.3.2	Equality of stress and velocity characteristics.....	24
3.3.3	Modifications of the original Davis approach	26
4	Davis in combination with structural elements	28
4.1	Reinforced embankment	28
4.1.1	General information.....	28
4.1.2	Factor of safety according to SRFEA and LEA.....	31

4.1.3	Factor of safety according to Davis A and Davis B	36
4.1.4	Mesh study.....	38
4.2	Upstream slope	41
4.2.1	General information.....	41
4.2.2	Safety analysis of case 1	44
4.2.3	Safety analyses of case 2	46
5	Slope stability analyses based on six paper examples	50
5.1	Introduction	50
5.2	Example 1	51
5.2.1	General information and paper results	51
5.2.2	Slope stability analysis on example 1	51
5.3	Example 2	54
5.3.1	General information and paper results	54
5.3.2	Slope stability analysis on example 2	54
5.4	Example 3	57
5.4.1	General information and paper results	57
5.4.2	Slope stability analysis on example 3	58
5.5	Example 4	62
5.5.1	General information and paper results	62
5.5.2	Slope stability analysis on example 4	62
5.6	Example 5	65
5.6.1	General information and paper results	65
5.6.2	Slope stability analysis on example 5	65
5.7	Example 6	70
5.7.1	General information and paper results	70
5.7.2	Slope stability analysis on example 6	71
5.8	Comparison of Davis A, Davis B and Davis C	75
5.8.1	General information.....	75
5.8.2	Study 1: Variation of φ' and λ	75

5.8.3	Study 2: Variation of c' and λ for $\varphi' = 30^\circ$	76
5.8.4	Comparison of the results	77
6	$\varphi - v$ inequality.....	83
6.1	Derivation of the $\varphi - v$ inequality	83
6.2	Scheme of analysis	84
6.3	Analysis	84
6.3.1	General information.....	84
6.3.2	Comparison of the results	86
7	Influence of the initial stress condition on the FoS.....	91
7.1	$\varphi - v$ inequality with K_0 procedure	91
7.2	Influence of K_0 on the FoS.....	96
8	Conclusion	100
9	Literatur.....	102
10	Appendix	105
10.1	Safety analysis of Optum G2.....	105
10.1.1	FELA (Optum G2)	105
10.1.2	SRFEA (Optum G2)	106
10.2	Reinforced embankment	107
10.2.1	Influence of construction steps on the FoS.....	107
10.2.2	Safety analyses on modified cross section 1 and cross section2.....	108
10.2.3	Cross section 2: Influence of strength parameters φ' and c' on FoS.....	109
10.2.4	Influence of extensional stiffness and tensile strength N_p on FoS.....	109
10.2.5	Mesh study: Safety values for SRFEA and FELA	110
10.3	Upstream slope.....	113
10.3.1	Input parameters for modelling soil nails and Maccaferri grid	113
10.3.2	Excavation steps for SRFEA	114
10.3.3	Additional studies on the upstream slope	115
10.4	Slope stability analyses based on six paper examples	120
10.4.1	Example 1	120

10.4.2	Example 2	121
10.4.3	Example 3	123
10.4.4	Example 4	124
10.4.5	Example 5	125
10.4.6	Example 6	127
10.4.7	Comparison of Davis A, Davis B and Davis C	128
10.5	$\varphi - v$ inequality.....	132
10.6	Influence of the initial stress condition on the FoS.....	134

List of figures

Fig. 1	Definition of FoS in LEA (according to Abramson et al. 2002)	3
Fig. 2	Ordinary method (according to Aryal 2006)	4
Fig. 3	Bishop's simplified method (according to Aryal 2006).....	5
Fig. 4	Janbu's simplified method (according to Aryal 2006).....	6
Fig. 5	Morgenstern & Price method (according to Aryal 2006)	6
Fig. 6	Selected shapes of the interslice force function (according to Egger 2012)	7
Fig. 7	Spencer's method (according to Aryal 2006).....	7
Fig. 8	Comparison of associated and non-associated flow rule (according to Egger 2012).....	11
Fig. 9	Standard strength reduction (Plaxis 2D)	12
Fig. 10	User-defined strength reduction (Plaxis 2D)	12
Fig. 11	SRFEA according to different dilatancy angles ψ'	13
Fig. 12	Bifurcation of the failure mechanism for $\psi' = 0^\circ$: Step = 190 (a), step = 240 (b), step = 292 (c)	14
Fig. 13	Forces acting on soil body (according to Sloan 2013).....	16
Fig. 14	Lower-bound mesh (according to Sloan 2013).....	17
Fig. 15	Zero thickness elements (D_1 , D_2) (according to Sloan 2013).....	18
Fig. 16	Upper-bound elements (according to Sloan 2013).....	20
Fig. 17	Zero thickness elements for the upper-bound solution (according to Sloan 2013)	21
Fig. 18	Velocity boundary condition (according to Sloan 2013).....	21
Fig. 19	Strength reduction process in FELA (according to Sloan 2013)	22
Fig. 20	Element of interest (a), Mohr stress circle (b), Mohr strain circle (c) (according to Tschuchnigg 2015a)	25
Fig. 21	Comparison of stress and velocity characteristics (a), Davis approach (b) (according to Tschuchnigg 2015a).....	26
Fig. 22	Reinforced embankment: Soil composition (a), water table (b)	28
Fig. 23	Reinforced embankment: Comparison of cross section 1 and cross section 2	29
Fig. 24	Reinforced embankment: Loading conditions	30
Fig. 25	Reinforced embankment: Mesh refinement (step 1 - 5)	30
Fig. 26	Cross section 1: ϕ - c reduction	31
Fig. 27	Cross section 1 ($\psi' = 0^\circ$): Incremental shear strains	32
Fig. 28	Cross section 1 ($\psi' = \phi'$): Incremental shear strains.....	32
Fig. 29	Cross section 1: Failure mechanisms of LEA.....	33

Fig. 30	Cross section 2: φ - c reduction	34
Fig. 31	Cross section 2 ($\psi' = 0^\circ$): Incremental shear strains	34
Fig. 32	Cross section 2 ($\psi' = \varphi'$): Incremental shear strains	35
Fig. 33	Cross section 2: Failure mechanism according to LEA	35
Fig. 34	Modified cross section 1: (a) Soil composition, (b) water table	36
Fig. 35	Adaptive mesh refinement: Concentration at the toe for the lower bound .	37
Fig. 36	Cross section 2 according to FELA: (a) lower bound: adaptive mesh refinement; (b) upper bound: adaptive mesh refinement; (c) lower bound: failure mechanism; (d) upper bound: failure mechanism	37
Fig. 37	Mesh study: Comparison of SRFEA.....	39
Fig. 38	Mesh study: Comparison of SRFEA and FELA.....	40
Fig. 39	Upstream slope: (a) Soil layers, (b) inclined water table.....	41
Fig. 40	Upstream slope - case 1: Dimensions and structural elements	42
Fig. 41	Upstream slope - case 2: Dimensions and structural elements	43
Fig. 42	Upstream slope: Modelling of structural elements in Plaxis 2D (a) and Optum G2 (b)	44
Fig. 43	Upstream slope: Mesh refinement Plaxis 2D	44
Fig. 44	Case 1 - Comparison of the failure mechanisms: (a) total displacements for SRFEA with associated plasticity, (b) circular failure mechanism according to LEA, (c) total displacements for lower-bound FELA, (d) total displacements for upper-bound FELA	45
Fig. 45	Case 1 - Davis A: (a) adaptive mesh refinement of upper-bound FELA; (b) total displacements of upper-bound FELA; (c) total displacements of SRFEA	45
Fig. 46	Case 2 - Comparison of water pressure distributions: (a) Plaxis 2D with phreatic water table; (b) Optum G2 with steady state ground water flow; (c) Optum G2 with steady state ground water flow with modifications	47
Fig. 47	Original water table (black dashed line), lowered water table (red full line)	47
Fig. 48	Case 2 according to the original water table - total displacements: (a) SRFEA ($\psi' = \varphi'$), (b) FELA lower-bound, (c) FELA upper-bound	47
Fig. 49	Case 2 according to the lowered water table - total displacements: (a) SRFEA ($\psi' = \varphi'$), (b) FELA lower-bound, (c) FELA upper-bound	48
Fig. 50	Case 2 according to the original water table - total displacements: (a) SRFEA ($\psi' = 0^\circ$), (b) Davis B - FELA upper-bound mesh refinement, (c) Davis B - FELA upper-bound	48

Fig. 51	Case 2 according to the lowered water table - total displacements: (a) SRFEA ($\psi' = 0^\circ$), (b) Davis B - FELA upper-bound mesh refinement, (c) Davis B - FELA upper-bound	48
Fig. 52	Example 1: Geometry (according Griffiths & Lane 1999)	51
Fig. 53	Example 1: (a) coarse mesh (233 elements); (b) fine mesh (959 elements); (c) coarse mesh: total displacements after safety analysis; (d) fine mesh: total displacements after safety analysis	52
Fig. 54	Example 1: (a) FELA - lower-bound failure mechanism, (b) FELA - upper-bound failure mechanism.....	53
Fig. 55	Example 2: Geometry (according to Griffiths & Lane 1999)	54
Fig. 56	Example 2: Failure mechanisms of SRFEA ($\psi' = 0^\circ$, fine mesh, 15-noded elements) (a) and LEA (b).....	55
Fig. 57	Example 3: Geometry (according to Griffiths & Lane 1999)	57
Fig. 58	Example 3: Comparison of SRFEA and FELA results.....	59
Fig. 59	Example 3 with $c_{u2} / c_{u1} = 1$: (a) SRFEA - Plaxis 2D; (b) SRFEA - Optum G2; (c) FELA, lower bound - Optum G2.....	60
Fig. 60	Example 3 with $c_{u2} / c_{u1} = 0.6$: (a) SRFEA - Plaxis 2D; (b) SRFEA - Optum G2; (c) FELA, lower bound - Optum G2.....	60
Fig. 61	Example 3 with $c_{u2} / c_{u1} = 0.2$: (a) SRFEA - Optum G2; (b) FELA, lower bound - Optum G2.....	60
Fig. 62	Example 3 with $c_{u2}/c_{u1} = 0.4$: (a) Circular failure leads to a FoS = 1.28; (b) three line wedge leads to a FoS = 0.92.....	60
Fig. 63	Example 3: Comparison of FELA and LEA results.....	61
Fig. 64	Example 4: Geometry (according to Griffiths & Lane 1999)	62
Fig. 65	Example 4 with $c_{u2} / c_{u1} = 2$: (a) SRFEA - Plaxis 2D; (b) SRFEA - Optum G2; (c) FELA, upper bound - Optum G2	63
Fig. 66	Example 4 with $c_{u2} / c_{u1} = 1.5$: (a) SRFEA - Plaxis 2D; (b) SRFEA - Optum G2; (c) FELA, upper bound - Optum G2	63
Fig. 67	Example 4 with $c_{u2} / c_{u1} = 0.75$: (a) SRFEA - Optum G2; (b) FELA, upper bound - Optum G2.....	63
Fig. 68	Example 4: Comparison of FELA, SRFEA and LEA results	64
Fig. 69	Example 5: Geometry (according to Griffiths & Lane 1999)	65
Fig. 70	Example 5: Comparison of SRFEA ($\psi' = 0^\circ$, 6-noded elements).....	66
Fig. 71	Example 5: Comparison of SRFEA ($\psi' = \phi'$) results	67
Fig. 72	Example 5: Comparison of SRFEA ($\psi' = \phi'$), FELA and LEA results.....	67

Fig. 73	Example 5 - SRFEA, 6-noded: Comparison of Davis approaches and SRFEA ($\psi' = 0^\circ$)	69
Fig. 74	Example 5 - SRFEA, 15-noded: Comparison of Davis approaches and SRFEA ($\psi' = 0^\circ$).....	69
Fig. 75	Example 5 - FELA: Comparison of Davis approaches and SRFEA ($\psi' = 0^\circ$).....	70
Fig. 76	Example 6: Geometry (according to Griffiths & Lane 1999)	70
Fig. 77	Example 6 without free surface – failure mechanism: Comparison of SRFEA ($\psi' = \phi'$) with 15-noded elements (a), FELA (b) and LEA (c)	71
Fig. 78	Example 6 with free surface – failure mechanism: Comparison of SRFEA ($\psi' = \phi'$) with 15-noded elements (a), FELA (b) and LEA (c).....	73
Fig. 79	Example 6 with free surface – failure mechanism: Comparison of SRFEA ($\psi' = 0^\circ$) (a), FELA (b) and FELA with Davis B ($\psi' = 0^\circ$) parameters (c)	74
Fig. 80	Geometry of slope 1 (a) and slope 2 (b).....	75
Fig. 81	Range where modification of Davis C is required to ensure $\phi^* \geq \psi'$	77
Fig. 82	Study 1 - slope 1: Standard SRFEA, user-defined SRFEA, Davis A, Davis B and Davis C results for different λ and ϕ'	79
Fig. 83	Study 1 - slope 1: Differences between Davis A and standard SRFEA, Davis B and user-defined SRFEA and Davis C and standard SRFEA for different λ and ϕ'	80
Fig. 84	Study 2 - slope 1: Standard SRFEA, user-defined SRFEA, Davis A, Davis B and Davis C results for different λ and c'	81
Fig. 85	Study 2 - slope 1: Differences between Davis A and standard SRFEA, Davis B and user-defined SRFEA and Davis C and standard SRFEA for different λ and c'	82
Fig. 86	$\phi - v$ inequality: Geometry of the slope.....	85
Fig. 87	$\phi - v$ inequality - failure points: Comparison of gravity loading and the following nil-step ($\phi'_1 = 37^\circ$, $v_1 = 0.2$, $c' = 2 \text{ kN/m}^2$, $E' = 10^4 \text{ kN/m}^2$, $\gamma_{\text{unsat}} = 16 \text{ kN/m}^3$).....	85
Fig. 88	$\phi - v$ inequality: Comparison of SRFEA, Davis A and Davis B for different v ($\gamma_{\text{unsat}} = 16 \text{ kN/m}^3$, $E' = 10^4 \text{ kN/m}^2$, $\phi'_1 = 37^\circ$, $\psi' = 0^\circ$).....	89
Fig. 89	$\phi - v$ inequality: SRFEA ($\psi' = 0^\circ$) according to $v = 0.146$	90
Fig. 90	$\phi - v$ inequality : SRFEA ($\psi' = 0^\circ$) according to v_{mod}	90
Fig. 91	Geometry of slope 1 (a) and slope 2 (b).....	91
Fig. 92	Location of point A and point B	98

Fig. 93	Stress paths of point A.....	98
Fig. 94	Stress paths of point B.....	99
Fig. 95	FELA - Optum G2: <i>Strength Reduction</i> (in <i>Solids</i>) with (a) <i>Lower</i> and (b) <i>Upper</i> element type	105
Fig. 96	FELA - Optum G2: <i>Limit Analysis</i> (Multiplier: <i>Load</i>) with (a) <i>Lower</i> and (b) <i>Upper</i> element type	105
Fig. 97	FELA - Optum G2: <i>Limit Analysis</i> (Multiplier: <i>Gravity</i>) with (a) <i>Lower</i> and (b) <i>Upper</i> element type	105
Fig. 98	SRFEA - Optum G2: (a): Strength reduction in the soil (<i>Solids</i>), (b) strength reduction in the structural elements (<i>Struts</i>).....	106
Fig. 99	Construction in one step.....	107
Fig. 100	Construction in three steps	107
Fig. 101	Construction in five steps.....	107
Fig. 102	Study 1 – slope 2: Standard SRFEA, user-defined SRFEA, Davis A, Davis B as well as Davis C results for different λ and φ'	130
Fig. 103	Study 1 – slope 2: Differences between Davis A and standard SRFEA, Davis B and user-defined SRFEA as well as Davis C and standard SRFEA for different λ and φ'	131

List of tables

Tab. 1	Comparison of the equilibrium, normal force and tangential force conditions (according to Egger 2012).....	8
Tab. 2	Comparison of resulting interslice force inclination, λ and $f(x)$ conditions (according to Egger 2012).....	8
Tab. 3	Comparison of Davis A, B and C (according to Tschuchnigg 2015a).....	27
Tab. 4	Reinforced embankment: Material parameters.....	29
Tab. 5	Influence of mesh density on the factor of safety.....	30
Tab. 6	Cross section 1: Overview of safety factors according to SRFEA.....	32
Tab. 7	Cross section 1: Overview of safety factors according to LEA.....	33
Tab. 8	Cross section 1: Comparison of SRFEA and LEA.....	33
Tab. 9	Cross section 1: Differences between SRFEA and LEA.....	34
Tab. 10	Cross section 2: Comparison of SRFEA and LEA.....	35
Tab. 11	Cross section 2: Differences between SRFEA and LEA.....	35
Tab. 12	Cross section 2 (LC1): Comparison of SRFEA.....	38
Tab. 13	Cross section 2 (LC1): Comparison of FELA.....	38
Tab. 14	Cross section 2 (LC1): Comparison of Davis A and Davis B with SRFEA ($\psi' = 0^\circ$).....	38
Tab. 15	Upstream slope: Material parameters.....	43
Tab. 16	Case 1: Comparison of LEA and SRFEA.....	46
Tab. 17	Case 1: Comparison of FELA.....	46
Tab. 18	Case 1: Comparison of Davis A and Davis B with SRFEA ($\psi' = 0^\circ$).....	46
Tab. 19	Case 2: Comparison of SRFEA.....	49
Tab. 20	Case 2: Comparison of FELA.....	49
Tab. 21	Case 2: Comparison of Davis A and Davis B with SRFEA ($\psi' = 0^\circ$).....	49
Tab. 22	Example 1: Set 1 - 4.....	51
Tab. 23	Example 1: SRFEA ($\psi' = 0^\circ$) and LEA results for $E' = 10^4 \text{ kN/m}^2$ and $\nu = 0.25$	52
Tab. 24	Example 1: SRFEA ($\psi' = \varphi'$) and FELA results for $E' = 10^4 \text{ kN/m}^2$ and $\nu = 0.25$	53
Tab. 25	Example 1: Davis A and Davis B results for $E' = 10^4 \text{ kN/m}^2$ and $\nu = 0.25$	53
Tab. 26	Example 1: Comparison of Davis A and Davis B with the SRFEA ($\psi' = 0^\circ$) for $E' = 10^4 \text{ kN/m}^2$ and $\nu = 0.25$	54
Tab. 27	Example 2: SRFEA ($\psi' = 0^\circ$) and LEA results for $E' = 10^4 \text{ kN/m}^2$ and $\nu = 0.25$	55

Tab. 28	Example 2: SRFEA ($\psi' = \varphi'$) and FELA results for $E' = 10^4$ kN/m ² and $\nu = 0.25$	56
Tab. 29	Example 2: Davis A and Davis B results for $E' = 10^4$ kN/m ² and $\nu = 0.25$...	56
Tab. 30	Example 2: Comparison of Davis A and Davis B with the SRFEA ($\psi' = 0^\circ$) for $E' = 10^4$ kN/m ² and $\nu = 0.25$	56
Tab. 31	Example 3: Set 1 - 4	58
Tab. 32	Example 3: SRFEA and FELA results for set 1 and $E_u = 5000$ kN/m ²	59
Tab. 33	Example 4: SRFEA and FELA results for set 1 and $E_u = 5000$ kN/m ²	63
Tab. 34	Example 5: Set 1 - 6	66
Tab. 35	Example 5: Comparison of Davis A and Davis B results with SRFEA ($\psi' = 0^\circ$).....	68
Tab. 36	Example 6 without free surface: Comparison of SRFEA ($\psi' = \varphi'$) and FELA	72
Tab. 37	Example 6 without free surface: Comparison of Davis A and Davis B.....	72
Tab. 38	Example 6 without free surface: Comparison of Davis A and Davis B with SRFEA ($\psi' = 0^\circ$).....	72
Tab. 39	Example 6 with free surface: Comparison of SRFEA ($\psi' = \varphi'$) and FELA..	73
Tab. 40	Example 6 with free surface: Comparison of Davis A and Davis B.....	74
Tab. 41	Example 6 with free surface: Comparison of Davis A and Davis B with SRFEA ($\psi' = 0^\circ$)	74
Tab. 42	Study 1: Soil properties.....	76
Tab. 43	Study 2 - soil properties	76
Tab. 44	Study 1 - slope 1 ($c' = 2$ kPa): Comparison of SRFEA ($\psi' = 0^\circ$), Davis A and Davis B	78
Tab. 45	Study 1 - slope 1 ($c' = 2$ kPa): Comparison of Davis A and Davis B with SRFEA ($\psi' = 0^\circ$).....	78
Tab. 46	$\varphi - \nu$ inequality: Variation of the strength and stiffness parameters	85
Tab. 47	$\varphi - \nu$ inequality: Soil parameters used for the evaluation	86
Tab. 48	Failure points: SRFEA ($\psi' = \varphi'$), Plaxis 2D	87
Tab. 49	Yield function: SRFEA ($\psi' = \varphi'$), Optum G2.....	87
Tab. 50	Yield function: FELA, upper-bound ($\psi' = \varphi'$), Optum G2.....	88
Tab. 51	$\varphi - \nu$ inequality: SRFEA results according to non-associated plasticity (Plaxis 2D).....	88
Tab. 52	Soil parameters used for analyses	92
Tab. 53	Variation 1 - 4: Calculation phases (Plaxis 2D)	92
Tab. 54	K_0 values for the several Poisson's ratios	93

Tab. 55	Slope 1 - SRFEA ($\psi' = \varphi'$): Failure points and safety factors for several ν ..94
Tab. 56	Slope 2 - SRFEA ($\psi' = \varphi'$): Failure points and safety factors for the several ν95
Tab. 57	SRFEA results (FoS) according to associated and non-associated plasticity.....96
Tab. 58	Slope 1 - SRFEA ($\psi' = \varphi'$): σ'_3 / σ'_197
Tab. 59	Strength reduction in the soil (according to Krabbenhøft et al. 2016)106
Tab. 60	Strength reduction in structural elements (according to Krabbenhøft et al. 2016)106
Tab. 61	Influence of construction steps on the factor of safety: Overview of the safety factors.....108
Tab. 62	Modified cross section 1: Comparison of SRFEA and LEA108
Tab. 63	Modified cross section 1: Differences between SRFEA and LEA108
Tab. 64	Modified cross section 2: Comparison of SRFEA and LEA108
Tab. 65	Modified cross section 1: Differences between SRFEA and LEA.....109
Tab. 66	Cross section 1: Influence of strength parameters φ' and c' on FoS109
Tab. 67	EA = 750 kN/m ² : Variation of tensile strength109
Tab. 68	EA = 500 kN/m ² : Variation of tensile strength110
Tab. 69	SRFEA ($\psi' = \varphi'$): Plaxis 2D - no adaptive mesh refinement110
Tab. 70	SRFEA ($\psi' = \varphi'$): Optum G2 - no adaptive mesh refinement111
Tab. 71	SRFEA ($\psi' = \varphi'$): Optum G2 - adaptive mesh refinement.....111
Tab. 72	FELA: Optum G2 - no adaptive mesh refinement112
Tab. 73	FELA: Optum G2 - adaptive mesh refinement112
Tab. 74	Input parameters for the Maccaferri grid113
Tab. 75	Input parameters for the soil nails113
Tab. 76	Single phases for SRFEA performed in Plaxis 2D114
Tab. 77	Original water table (no modifications in Optum G2): Comparison of total displacements and mesh refinements.....115
Tab. 78	Original water table (no modifications in Optum G2): Comparison of SRFEA results.....116
Tab. 79	Original water table (no modifications in Optum G2): Comparison of FELA results.....116
Tab. 80	Horizontal water table (no modifications in Optum G2): Comparison of total displacements and mesh refinements.....116
Tab. 81	Horizontal water table (no modifications in Optum G2): Comparison of SRFEA results117

Tab. 82	Horizontal water table: Safety factors according to FELA.....	117
Tab. 83	Horizontal water table (no modifications in Optum G2): Comparison of Davis A and Davis B with SRFEA ($\psi' = 0^\circ$).....	117
Tab. 84	No water table: Comparison of total displacements and mesh refinements.....	118
Tab. 85	No water table: Comparison of SRFEA results	118
Tab. 86	No water table: Comparison of FELA results	119
Tab. 87	No water table: Comparison of Davis A and Davis B with SRFEA ($\psi' = 0^\circ$).....	119
Tab. 88	Example 1: Check calculations	120
Tab. 89	Example 1: Further calculations for set 1 - part 1	120
Tab. 90	Example 1: Further calculations for set 1 - part 2.....	121
Tab. 91	Example 2: Check calculations	121
Tab. 92	Example 2: Further calculations for set 1 - part 1	122
Tab. 93	Example 2: Further calculations for set 1 - part 2.....	122
Tab. 94	Example 3: Overview of the calculations.....	123
Tab. 95	Example 4: Overview of the calculations.....	124
Tab. 96	Example 5: Check calculations	125
Tab. 97	Example 5: Further calculations for set 2	126
Tab. 98	Example 6: Overview of the calculations - part 1.....	127
Tab. 99	Example 6: Overview of the calculations - part 2.....	127
Tab. 100	Study 1 - slope 1: Overview of the calculations.....	128
Tab. 101	Study 1 - slope 2: Overview of the calculations.....	128
Tab. 102	Study 2 - slope 1: Overview of the calculations.....	129
Tab. 103	Case 1: Overview of the calculations	132
Tab. 104	Case 2: Overview of the calculations	133
Tab. 105	$\varphi - v$ inequality with K_0 procedure: Overview of the calculations.....	134
Tab. 106	Influence of K_0 on FoS: Overview of the calculations with $K_0 = 0.25$	134
Tab. 107	Influence of K_0 on FoS: Overview of the calculations with $K_0 = 0.4$	134

List of symbols and abbreviations

Capital letters

A^e	area of element
A_q	boundary area of soil mass subjected to unknown surface tractions
A_t	boundary area of soil mass subjected to fixed surface tractions
A_w	boundary area of soil mass subjected to fixed velocities
B	strain–displacement matrix
$\bar{\mathbf{B}}$	global strain–displacement matrix for mesh multiplied by the element areas
\mathbf{B}^e	strain–displacement matrix for element e
$\bar{\mathbf{B}}^e$	strain–displacement matrix for element e multiplied by its area
\mathbf{B}_j	strain–displacement matrix for node j of an element
$\bar{\mathbf{B}}_j$	strain–displacement matrix for node j of an element multiplied by the element area
D	material stiffness matrix
\mathbf{D}^e	elastic material stiffness matrix
D	diameter
E	interslice normal force
E'	Young's modulus of the soil
E_u	undrained soil stiffness
E_{50}^{ref}	reference secant modulus from triaxial test
E_{oed}^{ref}	reference tangential modulus from oedometer test
E_{ur}^{ref}	reference unloading / reloading modulus
G	self-weight of the slice; self-weight of the failure body
H	slope height
K	stiffness matrix
\mathbf{K}^i	stiffness matrix according to step i
K_0	earth pressure coefficient at rest
L	length of discontinuity; length of element edge
$L_{spacing}$	spacing
N	shape function matrix
N'	effective base normal force acting on shear surface
N_j	linear shape function for node j
N_P	tensile strength
\mathbf{P}_{ext}^i	vector of external force according to step i

\mathbf{P}_{int}^i	vector of internal force according to step i
P_P	pole point for planes
Q	collapse load
Q_n, Q_s	normal and tangential (shear) loads per unit thickness acting on element edge of length L
R	radius of circular failure surface about origin O
S	shear force acting at the base of a slice
T	interslice shear force
$T_{skin,axial}$	axial skin resistance (soil - structural element interaction)
$T_{skin,lateral}$	lateral skin resistance (soil - structural element interaction)
V	volume of soil mass
\dot{W}	rate of internal energy dissipation less rate of work done by external loads
\dot{W}_{ext}, P_{ext}	rate of work expended by external forces
\dot{W}_{int}, P_{int}	rate of internal energy dissipation

Small letters

\mathbf{c}	vector of constants
c^*	reduced cohesion according to Davis (1968)
c'	effective cohesion
c'_a	effective cohesion divided by factor of safety
$c'_{mob.}$	mobilized effective cohesion during SRFEA
c_u	undrained shear strength
$c_{u,mob.}$	mobilized undrained shear strength during SRFEA
$f(x)$	interslice force function
\mathbf{g}	vector of fixed body forces at a point
\mathbf{g}^e	vector of fixed body forces for element e
g_x, g_y	fixed body forces in x- and y-directions
g_x^e, g_y^e	fixed body forces in x- and y-directions for element e
\mathbf{h}	global vector of unknown body forces; vector of unknown body forces at a point
\mathbf{h}^e	vector of unknown body forces for element e
h_x, h_y	unknown body forces in x- and y-directions
h_x^e, h_y^e	unknown body forces in x- and y-directions for element e
l	slice base length
m	power for stress dependency of stiffness

m^*	gravity multiplier for slope equal to $\bar{\gamma}/\gamma$
n, s	local Cartesian coordinates in normal and tangential directions
p'	mean of effective stress
p_g	permanent load
p_q	live load
\mathbf{q}	vector of unknown tractions acting on area A_q
q	deviatoric stress
q_n, q_s	unknown normal and tangential (shear) stresses acting on element edge
q_n^j, q_s^j	unknown normal and tangential (shear) stresses acting on element edge at node j
\mathbf{t}	vector of fixed surface tractions acting on area A_t
t_n^j, t_s^j	fixed surface tractions in normal and tangential (shear) directions at node j
\mathbf{u}	vector of displacement field (chapter 3.1.1); global vector of unknown nodal velocities (chapter 3.2.2)
\mathbf{u}^e	vector of unknown nodal velocities for element e
\mathbf{u}^j	vector of unknown velocities at node j
$\Delta\mathbf{u}$	vector of incremental displacements
u	pore water pressure
u_n, u_s	unknown velocities in normal and tangential (shear) directions
u_x, u_y	unknown velocities in x- and y-directions
u_n^j, u_s^j	unknown velocities in normal and tangential (shear) directions for node j
u_x^j, u_y^j	unknown velocities in x- and y-directions for node j
$\Delta u_n, \Delta u_s$	velocity jumps across discontinuity in normal and tangential directions
\mathbf{v}	vector of nodal displacements
$\delta\mathbf{v}$	vector of sub-incremental nodal displacements according to step i
$\Delta\mathbf{v}^i$	vector of incremental nodal displacements according to step i
\mathbf{w}	fixed velocities on surface A_w
w_n, w_s	fixed velocities in normal and tangential (shear) directions
w_n^j, w_s^j	fixed velocities in normal and tangential (shear) directions for node j
x, y	Cartesian coordinates

Greek letters

α	slope angle
α_{slice}	inclination in the middle of the slice
$\dot{\alpha}$	plastic multiplier rate multiplied by element area

A	amount of non-associativity ($\varphi' - \psi'$)
β	strength factor according to Davis (1968)
β_0	strength factor according to Davis (1968) at initial conditions
$\beta_{failure}$	strength factor according to Davis (1968) at failure
γ	unit weight
$\bar{\gamma}$	mean of upper and lower bounds on maximum unit weight for slope
γ_{LB}, γ_{UB}	lower and upper bounds on unit weight
γ_{unsat}	unsaturated unit weight
γ_{sat}	saturated unit weight
δ	width of velocity discontinuity
$\delta\gamma$	engineering shear strain increment
$\delta\gamma_{max}$	maximum engineering shear strain increment
$\delta\varepsilon_1$	major principle strain increment
$\delta\varepsilon_3$	minor principle strain increment
$\delta\varepsilon_n$	zero direct strain increment
$\delta\varepsilon_{vol}$	volumetric strain increment
$\Delta\varepsilon$	vector of incremental strains
$\Delta\varepsilon^P$	vector of incremental plastic strains
ε	vector of strains
$\dot{\varepsilon}^P$	vector of plastic strain rates
η	inclination to vertical direction
θ	modification factor to determine $\nu_{mod.}$
κ	inclination to horizontal direction
λ	scale factor of the assumed function $f(x)$
$\dot{\lambda}$	plastic multiplier rate
ν	Poisson's ratio
ν_{choice}	chosen Poisson's ratio to fulfil clearly $\varphi - \nu$ inequality
$\nu_{mod.}$	modified Poisson's ratio to fulfil $\varphi - \nu$ inequality
σ	vector of stress field (chapter 3.1.1); global vector of unknown nodal stresses (chapter 3.2.2)
σ^e	vector of unknown stresses for element e
σ^i	vector of the actual stress state i
σ^{i-1}	vector of the previous stress state $i - 1$
σ^j	vector of unknown stresses at node j
$\Delta\sigma$	vector of the stress increment

$\sigma_{xx}, \sigma_{yy}, \tau_{xy}$	Cartesian stresses
σ_n	normal stress
σ'_1	major effective principal stress
σ'_3	minor effective principal stress
σ'_k	effective normal stress based on velocity characteristics
σ'_s	effective normal stress which defines failure criterion according to Coulomb
σ^j_{nn}	normal stress at node j
$\sigma^j_{xx}, \sigma^j_{yy}, \tau^j_{xy}$	Cartesian stresses at node j
τ	shear stress
τ_f	shear strength
τ_k	shear stress based on velocity characteristics
$\tau_{mob.}$	mobilized shear stress
τ^j_{ns}	shear stress at node j
τ_s	shear stress which defines failure criterion according to Coulomb
φ'	effective friction angle
φ^*	reduced effective friction angle according to Davis (1968)
φ_u	undrained friction angle (=0°)
φ'_a	effective friction angle divided by factor of safety
$\varphi'_{failure}$	effective friction angle at failure
$\varphi'_{mob.}$	mobilized effective friction angle during SRFEA
$\varphi'_{red.}$	reduced effective friction angle during SRFEA
ψ'	dilatancy angle
$\psi'_{failure}$	dilatancy angle at failure
$\psi'_{mob.}$	mobilized dilatancy angle during SRFEA

Abbreviations

CS	cross section
EA	extensional stiffness
FEA	finite element analysis
FELA	finite element limit analysis
FoS	factor of safety
FoS _F	factor of safety according to force equilibrium
FoS _{Gravity}	factor of safety based on gravity
FoS _{Load}	factor of safety based on a load

FoS _{LB}	factor of safety obtained with lower bound analysis
FoS _M	factor of safety according to moment equilibrium
FoS _{Mean}	averaged factor of safety obtained with upper and lower bound analyses
FoS _{UB}	factor of safety obtained with upper bound analysis
HMC	Hardening Mohr-Coulomb (model)
HS	Hardening Soil (model)
LC	loading condition
LEA	limit equilibrium analysis
LEM	limit equilibrium method
MC	Mohr-Coulomb
M&P	Morgenstern & Price method
SRFEA	strength reduction finite element analysis
w. t.	water table

1 Introduction

In this thesis, several different numerical studies based on *strength reduction finite element analyses* and *finite element limit analyses* have been conducted in order to prove modifications of the Davis approach as well as the effects of the $\varphi - v$ inequality and the initial stress condition on the factor of safety regarding slope stability analyses.

In geotechnical engineering no uniform definition of the factor of safety (FoS) exists. For many bearing capacity problems the FoS is usually defined as the load capacity. However, for slope stability analyses it is more common that the strength parameters are used to define the safety factor (Tschuchnigg et al. 2015b).

The limit equilibrium methods by Janbu (1954), Bishop (1955) and Morgenstern & Price (1965) are based on the method of slices and have a wide tradition in slope stability analysis (Tschuchnigg et al. 2015). Despite the long-lasting experience with *limit equilibrium analysis* (LEA), all methods do show several disadvantages. Assumptions regarding the shape of the failure mechanism and the forces acting between the slices lead to no unique definition of the factor of safety. Furthermore, it cannot be guaranteed that the failure mechanism is kinematically admissible.

Therefore, *displacement based finite element analyses* became increasingly popular over the last decades. The FoS is no longer defined as the ratio of driving and resisting forces and moments along a failure surface. Instead, friction angle φ' and cohesion c' are simultaneously reduced until no equilibrium can be satisfied. Consequently, the ratio of initial strength parameters to mobilized strength parameters is the most widespread definition of the safety factor in *strength reduction finite element analyses* (SRFEA). It has been previously shown that LEA and SRFEA according to associated plasticity yield to similar results when employing a Mohr-Coulomb failure criterion. As mentioned by Tschuchnigg (2015b), large differences between friction angle φ' and dilatancy angle ψ' may lead to numerical problems without any clear definition of the factor of safety.

Alternatively, rigorous upper and lower bounds on the factor of safety are determined in *finite element limit analyses* (FELA). As FELA is restricted to associated plasticity, Davis (1968) proposed reduced strength parameters to simulate a non-associated behaviour. This approach causes good agreements if the FoS is expressed by maximising loads for a given strength (Tschuchnigg et al. 2015b). In the event that the definition of safety is based on the strength parameters, the mentioned approach leads to very conservative results. Therefore, two modifications (Davis B and Davis C) were developed by

Tschuchnigg (2015b). Both correlate better with the non-associated SRFEA. The first two chapters are meant to give the reader some essential background knowledge which helps the understanding of LEA, SRFEA, FELA and the basic concept by Davis.

Numerical studies according to associated and non-associated plasticity are performed on two reinforced slopes and on examples taken from Griffiths and Lane (1999). The calculations aim to clarify how well the original Davis and the modified procedures correlate with non-associated SRFEA. In addition, it should be determined how the strength parameters friction angle φ' , dilatancy angle ψ' and cohesion c' affect the differences between Davis procedures and SRFEA. For comparison, the numerical analyses are supplemented by limit equilibrium analyses after Morgenstern & Price. Summing up, the aim of this section lies in a better understanding of the efficiency of the Davis approach modifications as well as in highlighting the boundaries of the LEA.

The *strength reduction finite element analysis* will be run by several programs with a constant Poisson's ratio ν . At the same time, the friction angle φ' and cohesion c' are reduced. Based on the Mohr-Coulomb failure criterion the relation $\sin\varphi' \geq 1 - 2\nu$ is formed. This equation is known as the $\varphi - \nu$ inequality. In combination with a high safety factor, the relation might be violated. The main goal of this section is to clarify through numerical analyses to what extent the $\varphi - \nu$ inequality influences the factor of safety.

In geotechnical engineering the stress conditions *in situ* are in most cases unknown. Finite element programs like Plaxis 2D provide several tools to generate the initial stress level with respect to different boundary conditions. Here, a further study aims at investigating whether the initial stress condition influences the safety factor.

2 Analytical method of defining a FoS

2.1 Definition of limit equilibrium

„At the moment of failure, the shear strength is fully mobilized along the failure surface when the critical state conditions are reached“ (Nash 1987)

This quote states that a limit equilibrium is defined as the ratio of shear strength to the factor of safety whereby the shear strength is generally related to the Mohr-Coulomb failure criterion (Aryal 2006). The relation is expressed in accordance to Eq. (1). In it, the soil strength τ_f is expressed in terms of the cohesion and friction angle of the soil material and the shear stress $\tau_{mob.}$ is affected by external forces acting on the domain.

$$\tau_{mob.} = \frac{\tau_f}{FoS} \quad (1)$$

$$\tau_f = c' + \tan \varphi'$$

The factor of safety offers three definitions pursuant to Abramson (2002). Eq. (1) mentions the first option that is expressed by means of shear strength and mobilized shear stress. In a second option, the FoS can be related to the equilibrium of driving and resisting forces (Eq. (2)). The acting moments are covered by a third one (Eq. (3)) (Abramson et al. 2002).

$$FoS_F = \frac{\text{Sum of resisting forces}}{\text{Sum of driving forces}} = \frac{S}{G \sin \alpha} \quad (2)$$

$$FoS_M = \frac{\text{Sum of resisting moments}}{\text{Sum of driving moments}} = \frac{R \int_0^L S dl}{Gx} \quad (3)$$

It might not always be clear if forces or moments should be counted to either the resisting side or the driving one. If one imagines the self-weight at the toe of a slope, the moment might act in another direction than the rest of the self-weight (Fig. 1). The moments of the toe can either be subtracted from the driving side or added to the resistant side.

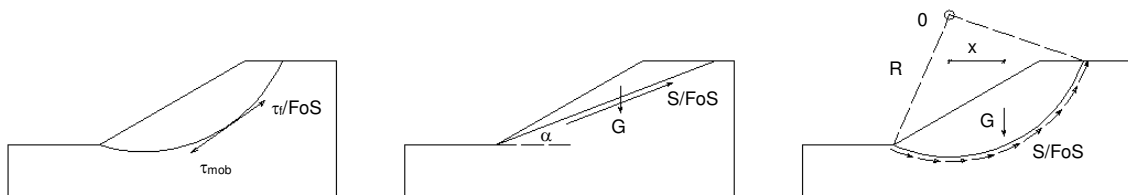


Fig. 1 Definition of FoS in LEA (according to Abramson et al. 2002)

2.2 Limit equilibrium analysis

In practical engineering, slope stability analyses are mostly performed by using limit equilibrium analyses. Over the years, different methods were developed, using various assumptions. In this section, the most common methods including their respective characteristics will be discussed. All of the limit equilibrium methods have some disadvantages in common. First, the failure mechanism has to be defined *a priori* in the form of a circular or three-line wedge. Furthermore, the kinematic admissibility is not ensured. Eventually, all programs used to perform LEA need to conduct a global search in order to determine the failure mechanism with the lowest factor of safety (Schweiger 2016).

Limit equilibrium analyses were developed over the past century. Based on the *Ordinary Method of Slices* from Fellenius (1936), *Bishop's simplified method* (1955) went a step further and took normal forces between the slices into account while neglecting shear forces and neither satisfying all the equilibrium conditions. During the sixties, several methods taking into account normal and shear forces acting between the slices were developed. Not all of them fulfilled both equilibrium of moments and forces. Spencer's as well as Morgenstern & Price's method do satisfy the two equations, each with a different assumption about the interslice forces (Egger 2012). The following chapters will describe the different methods briefly.

2.2.1 Ordinary method

The ordinary method of Fellenius defines a failure surface with a circular shape and a satisfied moment equilibrium. Normal and tangential interslice forces are not taken into account and force equilibrium is not given either (Fig. 2). No iterative process is necessary to solve the equation needed for a definition of the FoS. As a result, the factor of safety is easy to calculate through the moments equilibrium (see Eq. (4)). It should be noted that the ordinary method provides most of the time the lowest safety values compared to the following methods (Aryal 2006).

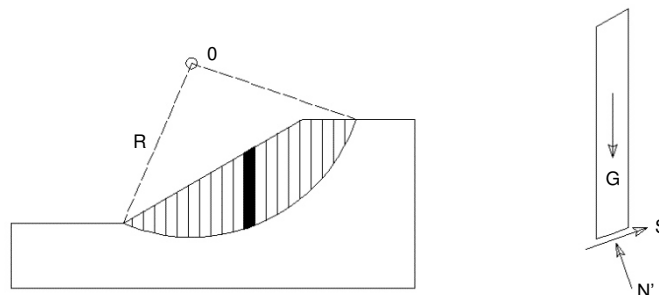


Fig. 2 Ordinary method (according to Aryal 2006)

$$FoS_m = \frac{\sum(c'l + N' \tan \varphi')}{\sum G \sin \alpha} \quad (4)$$

$$N' = (G \cos \alpha - ul) \quad (5)$$

c'	cohesion acting along the slice base length
l	slice base length
N'	effective base normal force acting on shear surface
G	self-weight of the slice
u	pore water pressure
α_{slice}	inclination in the middle of the slice

2.2.2 Bishop's simplified method

One of the most common limit equilibrium methods in practical engineering is the Bishop's method (1955). It assumes a circular failure surface and satisfies vertical force equilibrium in order to determine N' (Eq. (6)), in contrast to the *Swedish method*. At the same time, it also satisfies the moment equilibrium to determine the factor of safety. The normal interslice forces E_1 and E_2 get concerned, unlike the shear stresses, as Fig. 3 illustrates.

$$N' = \frac{1}{m_\alpha} \sum \left(G - \frac{c'l \sin \alpha}{FoS} - ul \cos \alpha \right) \quad (6)$$

$$m_\alpha = \cos \alpha \left(1 + \tan \alpha \frac{\tan \varphi'}{FoS} \right) \quad (7)$$

Eq. (4) can be used due to the circular failure mechanism as well as the fulfilled moment equilibrium. It is apparent that both Eq. (4) and Eq. (6) include the factor of safety and need to be solved iteratively until FoS is equal to FoS_M (Abramson et al. 2002).

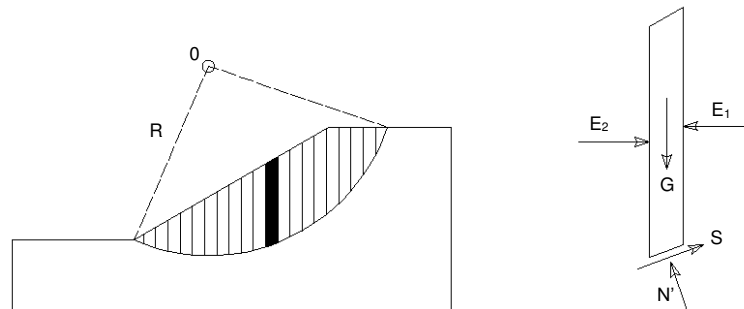


Fig. 3 Bishop's simplified method (according to Aryal 2006)

2.2.3 Janbu's simplified method

The simplified method by Janbu (1954) got developed for a non-circular failure mechanism where both horizontal and vertical force equilibrium are used to determine the factor of safety. In contrast, the ordinary as well as the simplified Bishop method use moment equilibrium to determine the FoS. As shown below, shear forces acting in between the slices are neglected, but the normal forces are taken into account. The normal force N' is determined in accordance to Eq. (6). By using Eq. (8), the factor of safety FoS_F is determined iteratively until FoS (Eq. (6)) is equal to FoS_F (Aryal 2006).

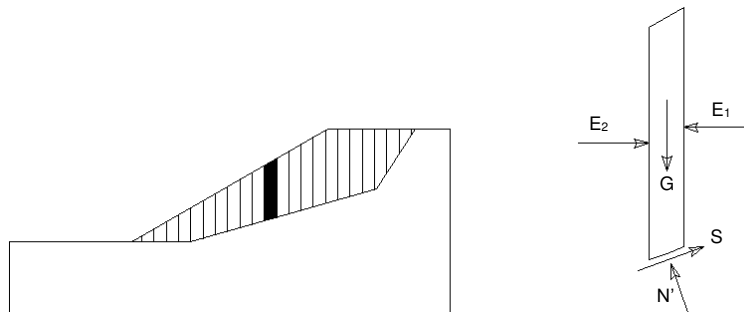


Fig. 4 Janbu's simplified method (according to Aryal 2006)

$$FoS_F = \frac{\sum (c'l + (N - ul) \tan \varphi') \sec \alpha}{\sum W \tan \alpha + \sum \Delta E} \quad (8)$$

$$\sum \Delta E = E_2 - E_1$$

2.2.4 Morgenstern & Price method

The three described methods satisfied either the moment equilibrium or the force equilibrium. Morgenstern & Price (1965) define the factor of safety by fulfilling both moment and force equilibrium. In addition to normal interslice forces, shear forces are concerned, as shown in Fig. 5.

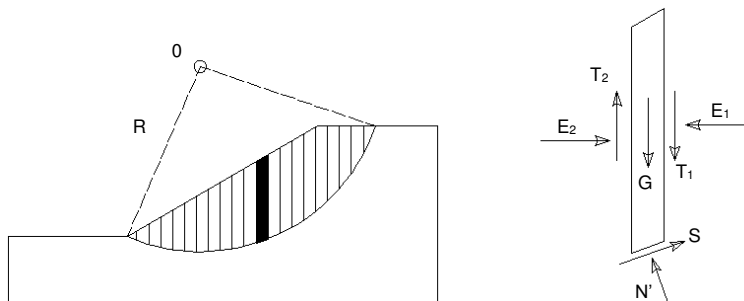


Fig. 5 Morgenstern & Price method (according to Aryal 2006)

The inclination of the resulting interslice force can vary along the slip surface, according to Eq. (9). The interslice force functions $f(x)$ might show either constant, half-sine, trapezoidal or user-defined shapes (Fig. 6). Lambda is thereby a scaling factor of $f(x)$.

$$T = E \cdot \lambda \cdot f(x) \tag{9}$$

$f(x)$ interslice force function along the slipping plane
 λ scale factor of the assumed function $f(x)$

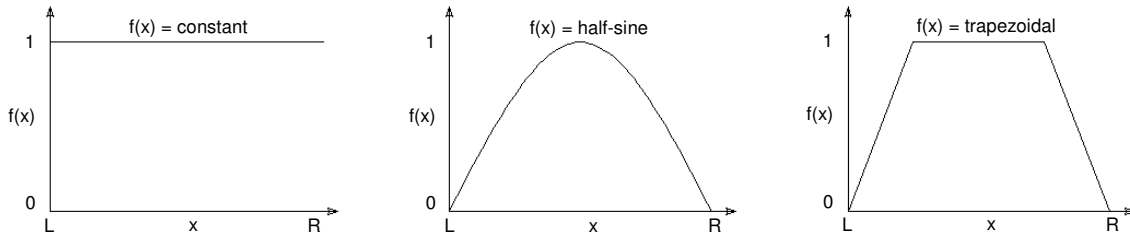


Fig. 6 Selected shapes of the interslice force function (according to Egger 2012)

An iterative procedure is necessary to guarantee the equality of both factors of safety, according to force and moment equilibrium. To comply with this condition, it must be confirmed that Eq. (10) and Eq. (11) are the same (Egger 2012).

$$FoS_F = \frac{\sum\{[c'l + (N - ul) \tan \varphi'] \sec \alpha\}}{\sum[G - (T_2 - T_1)] \tan \alpha + \sum(E_2 - E_1)} \tag{10}$$

$$FoS_M = \frac{\sum[c'l + (N - ul) \tan \varphi']}{\sum G \sin \alpha} \tag{11}$$

2.2.5 Spencer's method

Spencer's approach (1967) is similar to the procedure proposed by Morgenstern & Price, with one big difference. The inclination of the interslice forces is constant along the slipping surface. As a consequence, the interslice force function $f(x)$ is equal to unity (Tab. 2) and the scale factor $\lambda = \tan^{-1} (T / E)$. The factor of safety is determined the same way as in 2.2.4 (Aryal 2006).

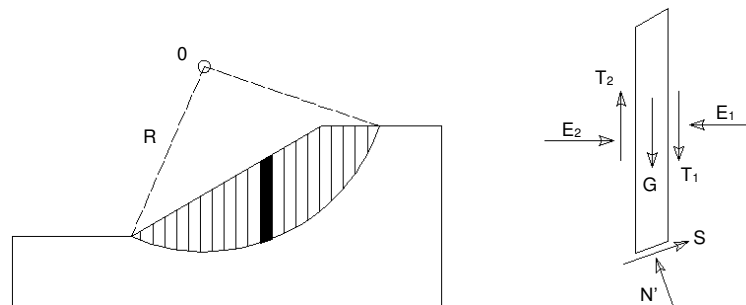


Fig. 7 Spencer's method (according to Aryal 2006)

Finally, Tab. 1 and Tab. 2 compare the discussed limit equilibrium methods and show the satisfied requirements in the respective method.

Tab. 1 Comparison of the equilibrium, normal force and tangential force conditions (according to Egger 2012)

<i>Limit equilibrium method</i>	<i>Moment equilibrium</i>	<i>Force equilibrium</i>	<i>Normal-force E</i>	<i>Tangential force T</i>
Ordinary	Yes	No	No	No
Simplified Bishop	Yes	No	Yes	No
Simplified Janbu	No	Yes	Yes	No
Morgenstern-Price	Yes	Yes	Yes	Yes
Spencer	Yes	Yes	Yes	Yes

Tab. 2 Comparison of resulting interslice force inclination, λ and $f(x)$ conditions (according to Egger 2012)

<i>Limit equilibrium method</i>	<i>Inclination of resulting interslice force</i>	λ	$f(x)$
Ordinary	No	No need	No need
Simplified Bishop	Horizontal	No need	No need
Simplified Janbu	Horizontal	No need	No need
Morgenstern-Price	Variable	Variable	Variable
Spencer	Constant inclination	Constant	1.0

3 Numerical methods of defining a FoS

This section tries to convey a basic understanding of both the *displacement based finite element analysis* as well as the *finite element limit analysis*. Furthermore, a particular note is made of the strength reduction techniques that define the factor of safety.

3.1 Strength reduction finite element analysis (SRFEA)

3.1.1 Introduction to displacement based finite element analysis

The introduction derives from the scientific manual of Plaxis 2D (2016), because *strength reduction finite element analyses* were performed using this software. The basic characteristics of the *displacement based finite element analysis* are described in this chapter. First of all, it is assumed that all deformations are very small and the original geometry can be used for the formulation. This domain can get discretized by either 6-noded or 15-noded elements, as defined by the user. Each node is characterized by a number of degrees of freedom which correspond to the unknown displacement components. The distribution of the displacements \mathbf{u} within elements depends on the shape function \mathbf{N} and the nodal values of displacements \mathbf{v} (Eq. (12)). The number of nodes decides how the displacements vary within the element and determine the polynomial form of the distribution (Brinkgreve et al. 2016).

$$\mathbf{u} = \mathbf{N} \mathbf{v} \quad (12)$$

A strain interpolation matrix \mathbf{B} , containing derivatives of the shape function, is introduced in order to extrapolate the strains from the nodal displacements (Eq. (13)).

$$\boldsymbol{\varepsilon} = \mathbf{B} \mathbf{v} \quad (13)$$

The equilibrium equation is satisfied according to Eq. (14). The formulation allows the introduction of boundary tractions \mathbf{t} and body forces \mathbf{h} . Since the actual stress state $\boldsymbol{\sigma}^i$ is unknown, an incremental process is introduced according to Eq. (15), where $\boldsymbol{\sigma}^{i-1}$ is the known stress state of the previous step and $\Delta\boldsymbol{\sigma}$ is the applied stress increment. The differences between external and internal forces get balanced due to the stress increment (Brinkgreve et al. 2016).

$$\int \mathbf{B}^T \Delta\boldsymbol{\sigma} dV = \int \mathbf{N}^T \mathbf{h}^i dV + \int \mathbf{N}^T \mathbf{t}^i dS - \int \mathbf{B}^T \boldsymbol{\sigma}^{i-1} dV \quad (14)$$

$$\boldsymbol{\sigma}^i = \boldsymbol{\sigma}^{i-1} + \Delta\boldsymbol{\sigma} \quad (15)$$

Except for a linear elastic material behaviour, no linear correlation between strains and stresses is given. Therefore, iterative procedures are introduced to satisfy equilibrium everywhere in the domain. The elasto-plastic material behaviour includes a non-linear material stiffness matrix \mathbf{D} (Eq. (16)) (Brinkgreve et al. 2016).

$$\boldsymbol{\sigma} = \mathbf{D}\boldsymbol{\varepsilon} \quad (16)$$

The standard procedure of a *displacement based finite element analysis* starts by applying a displacement increment $\Delta\mathbf{u}$, while using the strain interpolation matrix \mathbf{B} to determine the strain increment $\Delta\boldsymbol{\varepsilon}$. Eq. (17) is used to evaluate the stress increment whereas \mathbf{D}^e represents the elastic material stiffness. Depending on the material behaviour, the vector of incremental plastic strains $\Delta\boldsymbol{\varepsilon}^p$ is equal to zero for a linear material behaviour. Otherwise, it can be determined according to Vermeer (Brinkgreve et al. 2016).

$$\Delta\boldsymbol{\sigma} = \mathbf{D}^e(\Delta\boldsymbol{\varepsilon} - \Delta\boldsymbol{\varepsilon}^p) \quad (17)$$

Substituting the incremental stress strain connection into the equilibrium Eq. (14), the resulting correlation can be written as follows:

$$\mathbf{K}^i \Delta\mathbf{v}^i = \mathbf{P}_{ext}^i - \mathbf{P}_{int}^{i-1} \quad (18)$$

\mathbf{K}^i	stiffness matrix according to step i
$\Delta\mathbf{v}^i$	incremental displacement vector according to step i
\mathbf{P}_{ext}^i	external force vector according to step i
\mathbf{P}_{int}^{i-1}	internal force vector according to step $i - 1$

Due to the non-linear connection of stress and strain increments, the stiffness matrix is determined in an iterative procedure that satisfies both equilibrium and compatibility. The incremental displacement vector $\Delta\mathbf{v}^i$ is defined as the sum of sub-incremental displacement vectors $\delta\mathbf{v}$, applied to the domain. The global stiffness matrix \mathbf{K} approximately defines the material behaviour and can be written according to Eq. (19). The more exact the stiffness matrix is determined, the less iteration steps are required to fulfil an equilibrium (Brinkgreve et al. 2016).

$$\mathbf{K} = \int \mathbf{B}^T \mathbf{D} \mathbf{B} \, dV \quad (19)$$

3.1.2 Flow rule

The flow rule is a key factor in finite element analyses, whereby a choice between associated and non-associated plasticity needs to be taken. To illustrate the explanation, an elastic perfectly plastic material is assumed. As long as the stress increment is located in the elastic area, the corresponding strain increment can be calculated by Hooke's law. When reaching the failure limit, no further stress increments can be carried by the material and as a result, plastic strains occur. Eventually, the flow rule decides how the plastic strains will develop at failure (Nordal 2014).

Considering an associated flow rule, the plastic strains act perpendicularly to the yield function. Assuming Coulomb's failure criterion, the dilatancy angle ψ' is equal to the friction angle φ' of the soil. Consequently, the plastic volumetric strains get overestimated. Assuming a non-associated flow rule, plastic strains act perpendicularly to the plastic potential only, but not to the yield function anymore. The dilatancy angle ψ' is smaller compared to the friction angle φ' and the plastic volumetric strains get reduced with a decreasing ψ' , as shown in Fig. 8. The non-associated flow rule is representing the soil behaviour in a more realistic way and is therefore more appropriate for modelling (Nordal 2014).

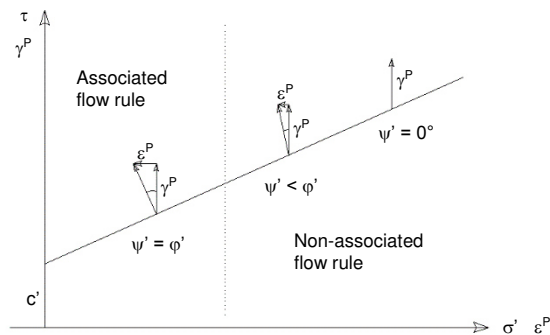


Fig. 8 Comparison of associated and non-associated flow rule (according to Egger 2012)

3.1.3 SRFEA in Plaxis 2D

Plaxis 2D enables the user to run a safety analysis where simultaneously the strength parameters $\tan\varphi'$ and c' are reduced until the point where no equilibrium can be achieved anymore. During undrained conditions, the undrained shear strength c_u needs to be reduced. The factor of safety is defined in Eq. (20).

$$FoS = \frac{\tan \varphi'}{\tan \varphi'_{mob.}} = \frac{c'}{c'_{mob.}} = \frac{c_u}{c_{u,mob.}} \quad (20)$$

For associated plasticity, both friction angle φ' and dilatancy angle ψ' get reduced at the same time. While highlighting the non-associated flow rule, it should be noted that as long as the reduced friction angle φ' is greater compared to the dilatancy angle ψ' , the latter one is kept constant (Fig. 9a). At the point where $\varphi' = \psi'$, both get simultaneously reduced, as shown in Fig. 9b (Brinkgreve et al. 2016).

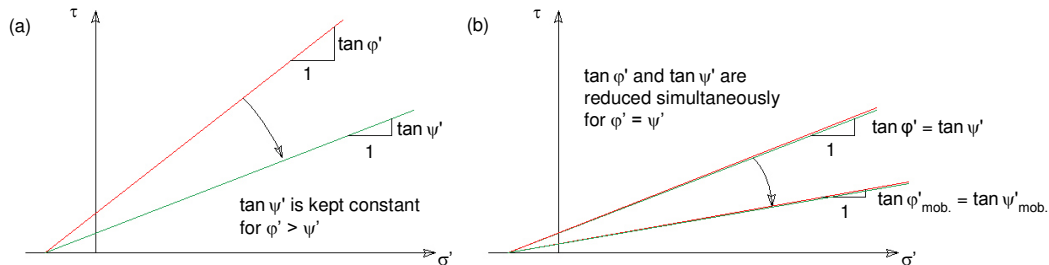
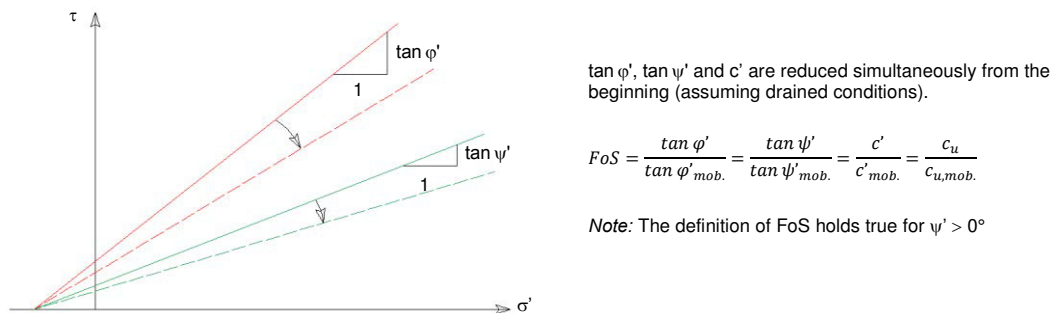


Fig. 9 Standard strength reduction (Plaxis 2D)

Additional calculations are performed with a user-defined Mohr-Coulomb model where all $\tan \varphi'$, $\tan \psi'$ and c' get concurrently reduced throughout the entire reduction (also for $\varphi' > \psi'$). The user-defined strength reduction for a non-associated flow rule is illustrated in Fig. 10. It is of importance that for an associated flow rule and a dilatancy angle ψ' equal to zero, the standard strength reduction and the user-defined strength reduction result in the same factor of safety.



$$FoS = \frac{\tan \varphi'}{\tan \varphi'_{mob.}} = \frac{\tan \psi'}{\tan \psi'_{mob.}} = \frac{c'}{c'_{mob.}} = \frac{c_u}{c_{u,mob.}}$$

Note: The definition of FoS holds true for $\psi' > 0^\circ$

Fig. 10 User-defined strength reduction (Plaxis 2D)

3.1.4 Difficulties by calculating with a non-associated flow rule

A SRFEA performed with non-associated materials may lead to numerical instabilities without any clear defined failure mechanism. This is due to the fact that the solution of the governing equations is not unique and the failure mechanism changes with reduced strength parameters. The bifurcation and kinematics of the failure mechanism lead to a reduction in the factor of safety, compared to the associated plasticity (Tschuchnigg et al. 2015a).

The following *strength reduction finite element analysis* is inspired by Tschuchnigg (2015a) and should demonstrate the influence of the dilatancy angle on slope stability analyses. A 10 m high slope disposed to the horizontal at an angle of about 45° is discretised by 1060 15-noded elements. A Mohr-Coulomb material model is implemented with a friction angle $\varphi' = 45^\circ$ and a cohesion $c' = 6 \text{ kN/m}^2$. To estimate the importance of the flow rule, calculations with dilatancy angles $\psi' = 0^\circ, 5^\circ, 10^\circ$ and 45° are performed. After a gravity loading is applied, the SRFEA is performed. The importance of the flow rule can be identified on Fig. 11. The factor of safety amounts to 1.53 by assuming associated plasticity. On the other hand, no clear value can be defined for a high degree of non-associativity ($\psi' = 0^\circ$). The safety factors vary between 1.28 and 1.36, depending on the number of steps taken (Fig. 11). As a consequence, the determination of one value for the factor of safety is not possible! An approach could be made by either choosing the lowest value 1.28 in order to be at the safe side (step 240) or by rather overestimating the safety and choosing 1.35 (step 292). The most realistic and therefore favoured approach is an averaged value approximately equal to 1.30 (step 190).

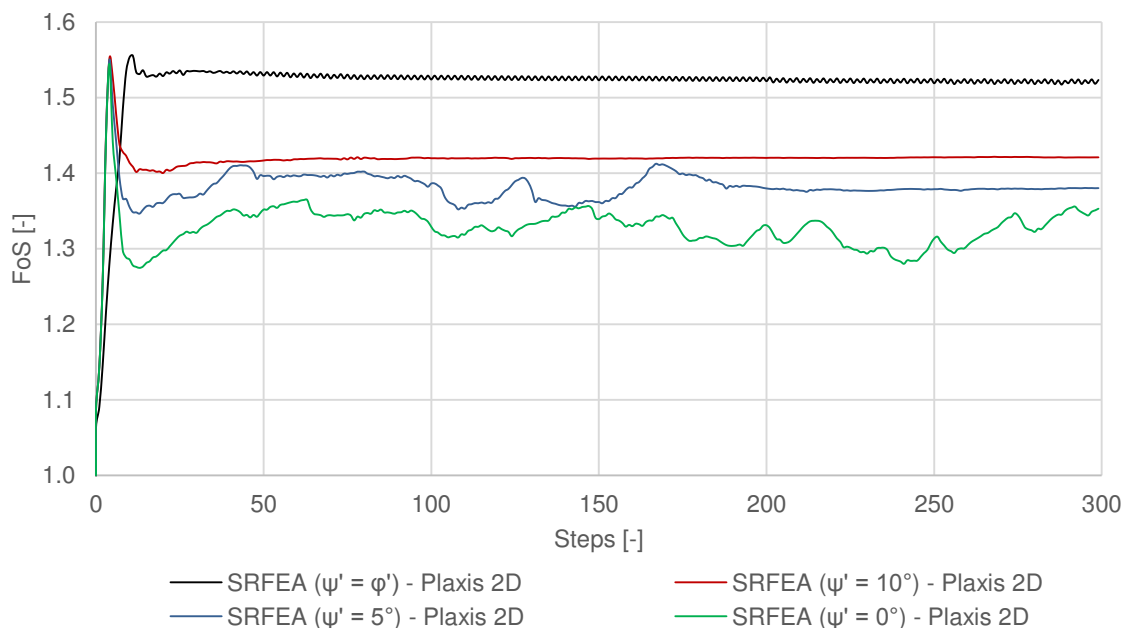


Fig. 11 SRFEA according to different dilatancy angles ψ'

Fig. 12 demonstrates the change of the failure mechanism depending on the number of steps taken for the case $\psi' = 0^\circ$. The shape of the incremental shear strains vary widely in all three cases. To summarize, the oscillation of the factor of safety is the consequence of the bifurcation of the failure mechanism (Tschuchnigg et al. 2015a).

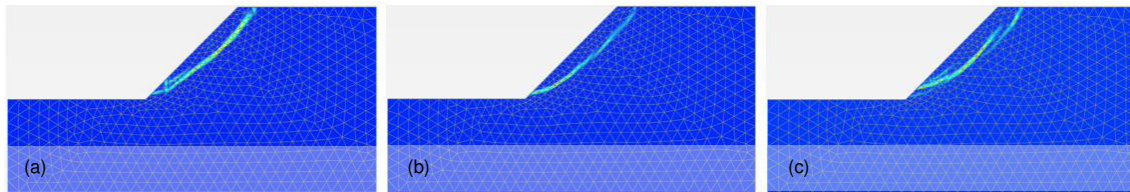


Fig. 12 Bifurcation of the failure mechanism for $\psi' = 0^\circ$: Step = 190 (a), step = 240 (b), step = 292 (c)

3.2 Finite element limit analysis (FELA)

3.2.1 Introduction to limit analysis

Limit analysis was developed in different fields during the 90s, ranging from metal deformation processing to the design of reinforced concrete structures. In recent years, the limit analysis was furthermore applied to soil mechanics (Chen 2007). The power lies in the constricting of the true collapse load from below as well as from above, by definition of lower and upper bounds. The difference between those two bounds represents the error margin of the solution (Tschuchnigg et al. 2015b).

The original procedure of defining the factor of safety is performed by an increase of applied load until failure is reached. A limit analysis enables the definition of a collapse load without performing an elasto-plastic analysis. Some well-defined assumptions are necessary to perform a FELA. First, it should be noted that strain softening is being ignored and elastic-perfectly plastic stress strain correlation is used. The Mohr-Coulomb failure criterion is the assumed condition where plastic flow occurs and nothing can be said about the total plastic strains because of unlimited plastic flow. The changes in geometry at the time of failure are small and as a consequence, for equilibrium equations, the original geometry is used. Due to the lack of changes in the geometry, the virtual work equation can be applied (Chen 2007).

The theorems of the limit analysis can be transferred to any solid body if the material shows perfect plasticity and no hardening or softening is at risk. Furthermore, the yield surface is assumed to be convex and in consequence, the strain rates are derivable from the flow rule ($\psi' = \varphi'$). As a third criterion, changes of geometry at limit load are neglected. If the failure load is reached, all stresses remain constant and only plastic strain increments occur. The elastic strain increments are assumed to be small and set to zero because they are not influencing the collapse at the limit load. Moreover, the initial stresses and deformations do not affect the plastic limit (failure load). The following two paragraphs are going to impart knowledge for both lower- and upper-bound theorems (Chen 2007).

The lower-bound theorem is representing a stress state where equilibrium equations, the stress boundary conditions and yield criterion are satisfied (statically admissible stress field). In respect to a lower-bound solution, the load would be smaller compared to the actual collapse quantity and could be applied to the elastic perfectly plastic material without reaching failure. This chapter is considered to be appropriate to address the topic of discontinuities in the stresses. They cause the division of the material into several stress zones. The mentioned zones are satisfying the equilibrium and do not violate the yield condition. Furthermore, the stress fields are continuous in each zone, but there might be a different one in two neighbouring zones. The tangential component of stress along the two zones may be different, but all the normal directed components, on the other hand, continue across boundaries. The equilibrium and yield criteria are satisfied in the lower-bound theorem, but the soil kinematics are not concerned (Chen 2007).

By applying the upper-bound theorem, the loads exceed the collapse quantity and cannot be carried by the soil body because the work done by the external forces is exceeding the internal dissipation. The theorem sets the external work equal to the internal rate. This happens under the terms that the assumed failure mechanism satisfies the mechanical boundary conditions. Moreover, the worst case upper-bound solution must be determined using the work equation. The mechanism has to fulfil the condition that changes in displacements within the soil body are kinematically admissible. No gaps and overlaps should occur. The upper-bound satisfies the velocity boundary conditions as well as the strain and velocity compatibility condition. It is of uppermost importance that the distribution of stresses does not have to satisfy an equilibrium (Chen 2007).

3.2.2 Introduction to finite element limit analysis

For comprehensibility reasons, the chapter is split into two parts. The first one discusses the finite element lower-bound formulation while the latter one deals with the formulation of the finite element upper-bound.

Finite-element lower-bound formulation

This section is set up according to the formulation of Lyamin & Sloan (2002a). For a better understanding, Fig. 13 represents a soil body with a volume V , loaded by several different forces. Along boundary A , forces \mathbf{q} , \mathbf{t} and \mathbf{w} might act. Additionally, the two body forces \mathbf{g} and \mathbf{h} are acting over the volume and might represent the unit weight as well as an unknown body force (Sloan 2013).

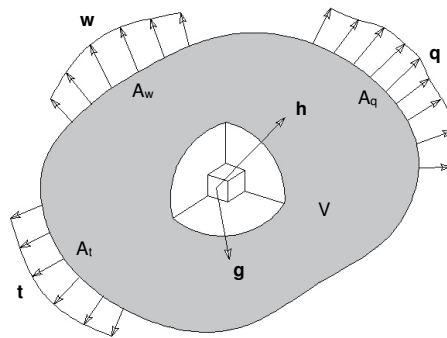


Fig. 13 Forces acting on soil body (according to Sloan 2013)

The lower bound calculation defines a statically feasible stress field with a satisfying equilibrium in the whole system that must find a balance with the acting forces at the boundaries, stick the yield criterion anywhere in the system and define the maximum possible load (collapse load) too. Referring the collapse load to Eq. (21), in terms of a slope stability analysis $Q_1 = 0$ and $\mathbf{h} = \gamma$, the variable has to be optimized.

$$Q = \int_{A_q} Q_1(\mathbf{q})dA + \int_V Q_2(\mathbf{h})dV \quad (21)$$

The soil body gets discretised by using 3-noded elements. The nodes of the linear elements consist of a vector of three unknown stresses and a vector of two unknown body forces which might be equal to zero if any of the two body forces are acting (Fig. 14). The nodal stresses and element body forces are the primary unknowns in the non-linear equation system. Equilibrium equality constraints have to be ensured for each element, for each discontinuity and for each stress boundary condition. The normal and

shear stresses (n,s) acting along stress discontinuities are continuous. Furthermore, the yield function $f(\sigma^i)$ has to be equal or smaller than zero at all nodes (Sloan 2013).

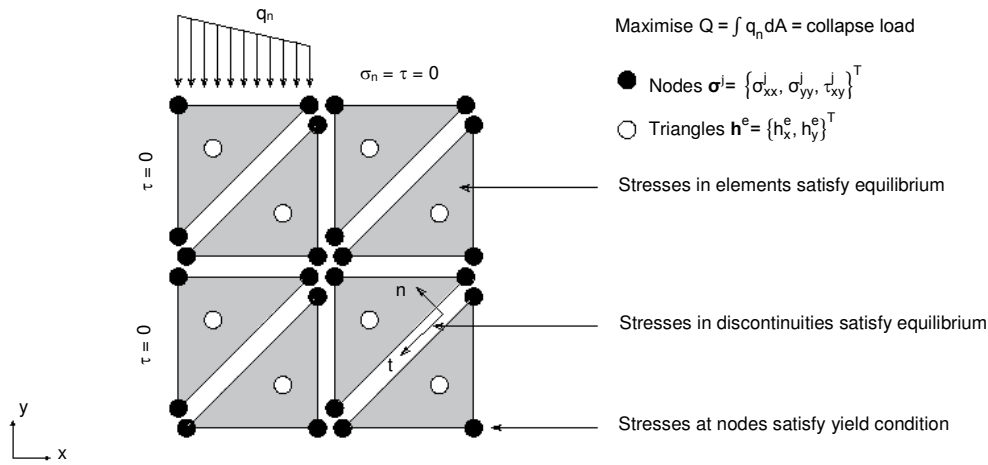


Fig. 14 Lower-bound mesh (according to Sloan 2013)

For a bearing capacity problem, the external traction q gets expanded until collapse occurs (Fig. 14). Based on the fact that the stresses vary linearly over the edge, the resulting forces acting in a normal and tangential way are defined according to Eq. (22). The stresses q^1 and q^2 are acting at the nodes and can be connected linearly because 3-noded elements with edge length L are used (Sloan 2013).

$$\begin{Bmatrix} Q_n \\ Q_s \end{Bmatrix} = \frac{L}{2} \left(\begin{Bmatrix} q_n^1 \\ q_s^1 \end{Bmatrix} + \begin{Bmatrix} q_n^2 \\ q_s^2 \end{Bmatrix} \right) \quad (22)$$

With the use of a Cartesian coordinate system and by summing up all the loaded edges, the collapse load can be defined as $c_1^T \sigma$, where c_1 is representing a vector of constants and σ the global vector of unknown nodal stresses. If body loads are acting instead of external forces, $c_2^T h$ is defining the critical condition. It should be noted that c_2 is the area on which the global vector of body loads h is acting on. As mentioned before, the continuum equilibrium has to be fulfilled for each element. By substituting Eq. (24) to Eq. (23), the condition to satisfy (Eq. (25)) is met (Sloan 2013).

$$\begin{aligned} \frac{\partial \sigma_{xx}}{\partial x} + \frac{\partial \tau_{xy}}{\partial y} + h_x + g_x &= 0 \\ \frac{\partial \sigma_{yy}}{\partial y} + \frac{\partial \tau_{xy}}{\partial x} + h_y + g_y &= 0 \end{aligned} \quad (23)$$

$$\boldsymbol{\sigma} = \sum_{i=1}^3 N_j \boldsymbol{\sigma}^j \quad (24)$$

$$[\mathbf{B}_1^T \mathbf{B}_2^T \mathbf{B}_3^T] \boldsymbol{\sigma}^e = -(\mathbf{h}^e + \mathbf{g}^e) \quad (25)$$

The \mathbf{B} -matrices are covering the compatibility and contain the area of the element A^e and constants which depend on the coordinates. When multiplying Eq. (25) on both sides with A^e , an implementation of stress discontinuities is possible. If Eq. (26) is satisfied, equilibrium at any point in the domain is given.

$$[\bar{\mathbf{B}}_1^T \bar{\mathbf{B}}_2^T \bar{\mathbf{B}}_3^T] \boldsymbol{\sigma}^e = -(\mathbf{h}^e + \mathbf{g}^e) A^e \quad (26)$$

$$\text{where } \bar{\mathbf{B}}_j^T = A^e \mathbf{B}_1^T = \begin{bmatrix} b_j & 0 & c_j \\ 0 & c_j & b_j \end{bmatrix} \quad (27)$$

To model areas of discontinuity, zero thickness elements are used because their utilization is increasing the accuracy of the collapse load.

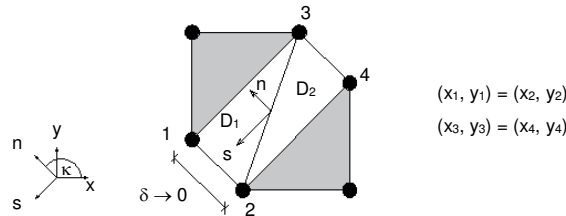


Fig. 15 Zero thickness elements (D_1, D_2) (according to Sloan 2013)

The shear and the normal stress have to be the same on both sides of the discontinuity. To comply Eq. (26), δ is set to zero. It can be seen, that $(x_1, y_1) = (x_2, y_2)$ and $(x_3, y_3) = (x_4, y_4)$ (Fig. 15). Therefore, the Eq. (28) changes and provides the evidence that $\bar{\mathbf{B}}_1^T \boldsymbol{\sigma}^1 = \bar{\mathbf{B}}_1^T \boldsymbol{\sigma}^2$ (Sloan 2013).

$$[\bar{\mathbf{B}}_1^T \bar{\mathbf{B}}_1^T 0] \boldsymbol{\sigma}^e = 0 \quad (28)$$

As a consequence, normal and shear stresses are continuous along the discontinuity, while the tangential normal stress may differ at the same nodes (Eq. (29)).

$$\begin{Bmatrix} \sigma_{nn}^1 \\ \tau_{ns}^1 \end{Bmatrix} = \begin{Bmatrix} \sigma_{nn}^2 \\ \tau_{ns}^2 \end{Bmatrix}, \begin{Bmatrix} \sigma_{nn}^3 \\ \tau_{ns}^3 \end{Bmatrix} = \begin{Bmatrix} \sigma_{nn}^4 \\ \tau_{ns}^4 \end{Bmatrix} \quad (29)$$

To fulfil the stress boundary condition, the boundary nodes have to match the tractions \mathbf{t} which is acting on the surface. This condition can be written as follows.

$$\begin{Bmatrix} \sigma_{nn}^1 \\ \tau_{ns}^1 \end{Bmatrix} = \begin{Bmatrix} t_n^1 \\ t_s^1 \end{Bmatrix}, \begin{Bmatrix} \sigma_{nn}^2 \\ \tau_{ns}^2 \end{Bmatrix} = \begin{Bmatrix} t_n^2 \\ t_s^2 \end{Bmatrix} \quad (30)$$

The yield condition is the last one to be satisfied in the finite-element lower-bound. It is fulfilled when $f(\boldsymbol{\sigma}^i) \leq 0$ holds true at any node in the domain (Sloan 2013).

Finite-element upper-bound formulation

The formulation of the upper-bound described in this chapter refers to Lyamin & Sloan (2002b), with some modifications related to discontinuities by Krabbenhøft et al. (2005).

A finite element upper-bound formulation searches for a velocity distribution \mathbf{u} that satisfies compatibility, the flow rule as well as the velocity boundary conditions \mathbf{w} along A_w (Fig. 13). It attempts thereby to minimize the internal power dissipation minus the work done by external forces, according to Eq. (31) (Sloan 2013).

$$\dot{W} = P_{int} - \int_{A_t} \mathbf{t}^T \mathbf{u} dA - \int_V \mathbf{g}^T \mathbf{u} dV \quad (31)$$

$$P_{int} = \int_V \boldsymbol{\sigma}^T \dot{\boldsymbol{\epsilon}}^p dV \quad (32)$$

The enhanced value for \dot{W} to the rate of work expended by external forces P_{ext} (Eq. 33)) defines the upper bound of the *finite element limit analysis* (Sloan 2013).

$$P_{ext} = \int_{A_q} \mathbf{q}^T \mathbf{u} dA - \int_V \mathbf{h}^T \mathbf{u} dV \quad (33)$$

In a similar way, if compared to the lower-bound, the 3-noded elements are characterized by a linear distribution of the velocities \mathbf{u} and a constant stress field $\boldsymbol{\sigma}$. By using this kind of 3-noded elements, rigorous upper bounds can be set. The primary unknowns are nodal velocities, element stresses and plastic multipliers. They get determined by minimizing the internal power dissipation less the external work done by external forces. As evident in Fig. 16, each nodal vector is composed of two velocities. Three unknown stress components and one unknown plastic multiplier rate $\dot{\lambda}$ get assigned to each element. In the next step, the plastic strains get calculated while considering an

associated flow rule and satisfying the consistency requirement $\dot{\lambda} f(\boldsymbol{\sigma}^e) = 0$. Two multipliers get introduced to model velocity discontinuities in order to fulfil the associated flow rule. The velocity boundary conditions is ensured on the corresponding nodal boundaries. The stresses in all elements create the yield condition $f(\boldsymbol{\sigma}^e) \leq 0$ (Sloan 2013).

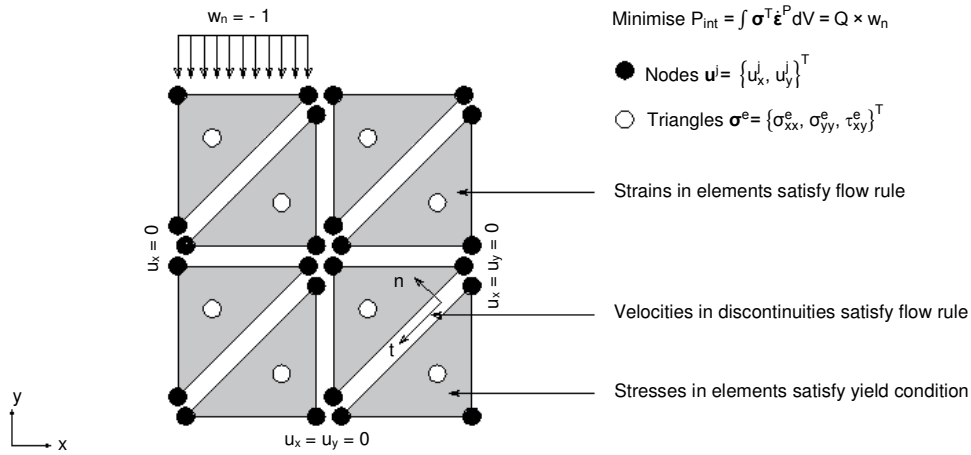


Fig. 16 Upper-bound elements (according to Sloan 2013)

The stress distribution over each element is constant, therefore the internal power dissipation P_{int} can be written as shown in Eq. (34). Within the element the plastic strains $\dot{\epsilon}^p$ are constant and can be defined as $\mathbf{B}^e \mathbf{u}^e$. The variables $\boldsymbol{\sigma}$ and \mathbf{u} are representing the global vector of element stresses and of nodal velocities.

$$P_{int} = \int_V \boldsymbol{\sigma}^T \dot{\epsilon}^p dV = \sum_e (\boldsymbol{\sigma}^T \dot{\epsilon}^p V)^e = \sum_e \boldsymbol{\sigma}^T \mathbf{B}^e \mathbf{u}^e = \boldsymbol{\sigma}^T \bar{\mathbf{B}} \mathbf{u} \quad (34)$$

The second part of Eq. (31) containing the tractions \mathbf{t} and body forces \mathbf{h} can be combined to $\mathbf{c}^T \mathbf{u}$. The final correlation is written as follows (Sloan 2013).

$$\dot{W} = \boldsymbol{\sigma}^T \bar{\mathbf{B}} \mathbf{u} - \mathbf{c}^T \mathbf{u} \quad (35)$$

In addition to Eq. (35), a continuum flow rule has to be confirmed, according to Eq. (36) where $\dot{\lambda}$ is the plastic multiplier. To ensure that plastic strains $\dot{\epsilon}^p$ occur only at the yield surface, $\dot{\lambda} f(\boldsymbol{\sigma}^e) = 0$ (Sloan 2013).

$$\dot{\epsilon}^p = \dot{\lambda} \nabla f(\boldsymbol{\sigma}^e), \quad \dot{\lambda} \geq 0 \quad (36)$$

In summary, any 3-noded element has to fulfil the flow rule constraints, as shown in Eq. (37) where $\dot{\alpha} = \mathbf{A}^e \dot{\lambda}$ (Sloan 2013).

$$\bar{\mathbf{B}}^e \mathbf{u}^e = \dot{\alpha} \nabla f(\boldsymbol{\sigma}^e), \quad \dot{\alpha} \geq 0, \quad \dot{\alpha} f(\boldsymbol{\sigma}^e) = 0 \quad (37)$$

The discontinuity flow rule is satisfied in a similar way as for the lower-bound. Two 3-noded elements with zero thickness (Fig. 17) model discontinuities. Additionally, two plastic multipliers are applied to simulate the normal and tangential jumps Δu_n and Δu_s along the discontinuity (Sloan 2013). The velocity components in discontinuities satisfy the associated flow rule and are defined according to Eq. (38).

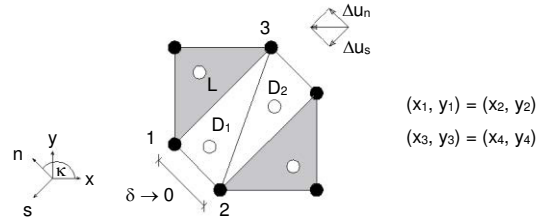


Fig. 17 Zero thickness elements for the upper-bound solution (according to Sloan 2013)

$$\Delta u_n = \frac{\dot{\alpha} \partial f}{\partial \sigma_n}$$

$$\Delta u_s = \frac{\dot{\alpha} \partial f}{\partial \tau} \quad (38)$$

$$\dot{\alpha} \geq 0, \quad \dot{\alpha} f(\sigma_n, \tau) = 0$$

In addition to the discontinuity flow rule, the velocity boundary conditions have to be fulfilled, according to Eq. (39), at any nodes that are charged by velocities (Fig. 18) (Sloan 2013).

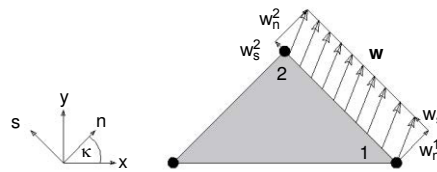


Fig. 18 Velocity boundary condition (according to Sloan 2013)

$$\begin{Bmatrix} u_n^1 \\ u_s^1 \end{Bmatrix} = \begin{Bmatrix} w_n^1 \\ w_s^1 \end{Bmatrix}, \quad \begin{Bmatrix} u_n^2 \\ u_s^2 \end{Bmatrix} = \begin{Bmatrix} w_n^2 \\ w_s^2 \end{Bmatrix} \quad (39)$$

3.2.3 Strength reduction according to Sloan (2013)

The FELA factor of safety as mentioned above gets commonly expressed in terms of loads. In slope stability analyses, however, the factor of safety is effectively defined according to the strength parameters of the soil. Sloan (2013) developed the following method which is implemented into Optum G2, the software used to perform FELA. As a

first step, a factor of safety equal to unity is assumed ($F_0 = 1$). Subsequently, the available strength gets computed according to Eq. (40) and Eq. (41).

$$c'_a = c'/F_0 \quad (40)$$

$$\varphi'_a = \tan^{-1}(\tan \varphi'/F_0) \quad (41)$$

According to c'_a and φ'_a , the upper and the lower bounds of the unit weight (γ_{LB} , γ_{UB}) are computed which can be ensured by the slope. Using both bounds of the unit weight, the m_o^* value can be derived from Eq. (42) (Sloan 2013).

$$m^* = (\gamma_{LB} + \gamma_{UB})/2\gamma \quad (42)$$

If the m^* value is greater than 1, the previous factor of safety increases by 0.1, otherwise it decreases by 0.1. In one specific kind of iterative process, c'_a and φ'_a form according to an updated FoS. Subsequently, m_1 is calculated according to Eq. (42) again. If $(m_1^* - 1)(m_o^* - 1) > 0$, m_o^* is equal to m_1^* and F_o equal to F_1 . As long as m^* is not equal to unity, the factor of safety gets modified as mentioned above. The iterative procedure of strength reduction in *finite element limit analyses* is shown in Fig. 19. The values are taken from Sloan (2013).

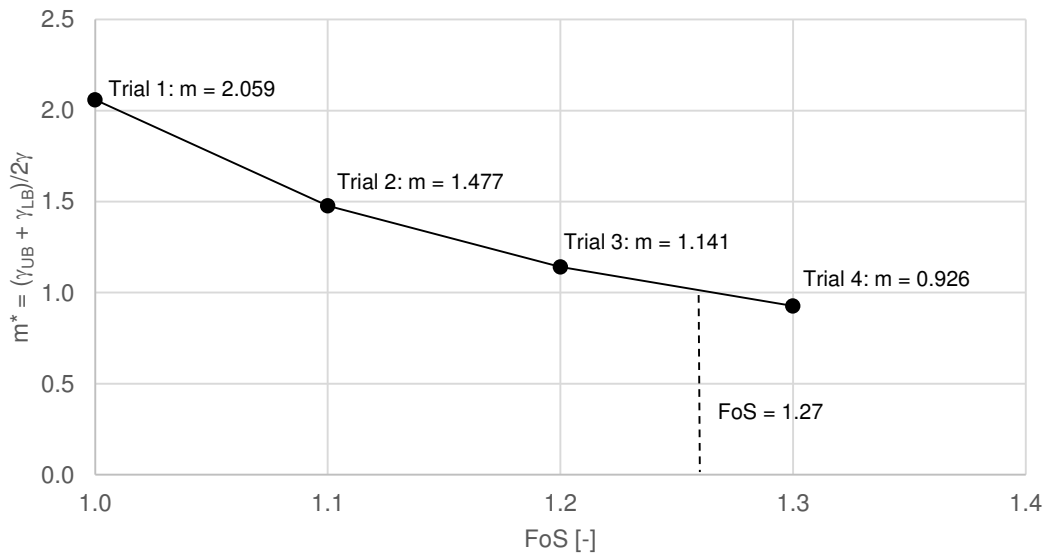


Fig. 19 Strength reduction process in FELA (according to Sloan 2013)

3.2.4 Safety analysis of Optum G2

The iterative strength reduction process described in 3.2.3 is automatically performed in Optum G2. This can be achieved by combining the program-internal analysis type options *Strength Reduction* with *Upper* and *Lower* elements. Since the mentioned analysis type is limited to approximately 1000 elements, alternatives are needed for a finer discretisation. The type *Limit Analysis* with *Upper* and *Lower* elements provide the use of more elements but misses a definition of the FoS according to the strength parameters. As shown in Eq. (43) and Eq. (44), the safety factors are based on optimizing loads and gravity for a given strength. The latter option is more appropriate in connection with slope stability (Krabbenhøft et al. 2016).

$$FoS_{Load} = \frac{Load_{Failure}}{Load} \quad (43)$$

$$FoS_{Gravity} = \frac{Gravity_{Failure}}{Gravity} \quad (44)$$

When choosing the second option, there is, however, a possibility to define the FoS with respect to the strength parameters manually. The strength parameters φ' and c' get reduced to a $FoS_{Gravity} = 1$. In succession, the ratio of the initial strength parameters to the ones at failure defines the safety (Krabbenhøft et al. 2016). Appendix 10.1.1 gives an overview of the several options that Optum G2 offers.

Although the analysis type *Strength Reduction* is limited to approximately 1000 elements, an adaptive mesh refinement can lead to more precise results. Thereby, it should be noted that refinements according to plastic shear (*Shear Dissipation*) or plastic total strains (*Total Dissipation*) are commonly used. Apart from this choice, the refinement is still automatically executed by Optum G2 (Krabbenhøft et al. 2016).

Moreover, it shall be mentioned at this place that *Strength Reduction* analyses can also be performed with 6-noded and 15-noded elements, assuming associated plasticity. Therefore, the strength parameters define the FoS, according to Eq. (20). Furthermore, Optum G2 enables the user to reduce the strength of structural elements by keeping the soil properties constant (appendix 10.1.2).

3.3 Davis approach

3.3.1 Necessity of the Davis approach in finite element limit analysis

As mentioned in the previous chapter, the limit analysis is always dealing with an associated flow rule. Due to the fact that in a plastic field, stress and velocity characteristics are equal only for the associated flow rule ($\varphi' = \psi'$), some modifications of the strength parameters c' and φ' are necessary to guarantee the equality of the characteristics and to generate a kind of non-associated behaviour. Therefore, the modified parameters c^* and φ^* are used with an associated flow rule as input parameters (Eq. (45) and Eq. (46)) (Tschuchnigg 2015a).

$$\begin{aligned} c^* &= \beta c' \\ \tan \varphi^* &= \beta \tan \varphi' \end{aligned} \quad (45)$$

$$\beta_{failure} = \beta = \frac{\cos \psi' \cos \varphi'}{1 - \sin \psi' \sin \varphi'} \quad (46)$$

3.3.2 Equality of stress and velocity characteristics

To demonstrate the correlation between the stress and velocity characteristics, an element ABCD is imagined. The principal stresses σ'_1 and σ'_3 as well as the principal strains $\delta\varepsilon_1$ and $\delta\varepsilon_3$ are acting on the element ABCD inclined to the vertical axis at an angle of η (Fig. 20a). The failure criterion is defined by Coulomb, according to the normal stress σ'_s and shear stress τ_s , as it can be seen in Fig. 20b. The pole point P_P is defined as the point of intersection where the Mohr circle meets extensions of lines acting parallel to major and minor principle stress directions. Davis introduced the term stress characteristics, visualized as the red lines, connecting P_P with (I) and (II). The stress characteristics are disposed about $45^\circ - \varphi' / 2$ to the major principal stress direction (Tschuchnigg 2015a).

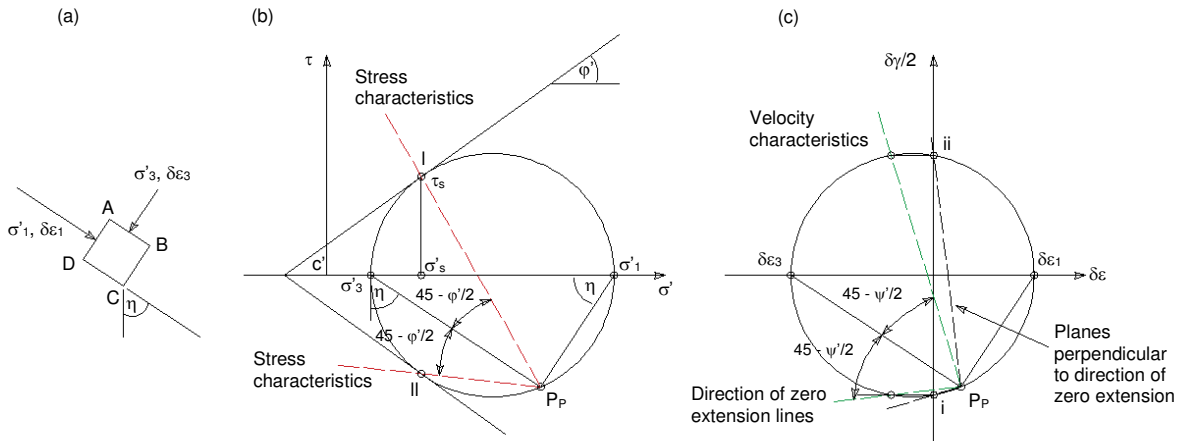


Fig. 20 Element of interest (a), Mohr stress circle (b), Mohr strain circle (c) (according to Tschuchnigg 2015a)

Fig. 20c represents the corresponding Mohr strain circle with the major and minor strain increments $\delta\varepsilon_1$ and $\delta\varepsilon_3$ acting along the abscissa. The shear strain increments $\delta\gamma/2$ are applied to the ordinate axis.

The ratio of volumetric strain increment $\delta\varepsilon_{vol}$ to the related maximal shear strain increment $\delta\gamma_{max}$ defines the dilatancy. The approach by Davis deals with plane strain conditions with a dilatancy angle according to Eq. (47).

$$\sin \psi' = \frac{\delta\varepsilon_{vol}}{\delta\gamma_{max}} = \frac{\delta\varepsilon_n}{\delta\gamma_{max}} = \frac{\delta\varepsilon_1 + \delta\varepsilon_2}{\delta\gamma_{max}} \quad (47)$$

As shown in Fig. 20c, the black dashed lines connecting P_P with (i) or (ii) are representing planes perpendicular to the direction of zero extension. It should be noticed that (i) and (ii) represent points of zero extension ($\delta\varepsilon_n = 0$). The direction of zero extension is determined by drawing horizontal lines from (i) and (ii) and connecting the intersection point of the Mohr strain circle with the pole point P_P . The lines representing the direction of zero extension are marked in green (Fig. 20c) and are named velocity characteristics, because according to Davis they are equal to the slip lines. The velocity characteristics are disposed about $45^\circ - \varphi' / 2$ to the principal stress direction. Consequently, the stress and velocity characteristics are equal for an associated flow rule ($\varphi' = \psi'$). Assuming a non-associated flow rule, the stress characteristics are not equal to the slip lines (Tschuchnigg 2015a). This relation is shown in Fig. 21a.

Concerning a non-associated flow rule, the stress ratio according to the zero extension lines rather than the stresses related to the stress characteristics has to be applied. In succession, the shear and normal stresses τ_k and σ'_k are not cutting the Mohr-Coulomb failure criterion (Fig. 21b). According to Davis, the modified strength parameters φ^* and

c^* should be used in combination with an associated flow rule. The combination of σ'_k and τ_k matches remarkably well with the modified strength parameters (Tschuchnigg 2015a).

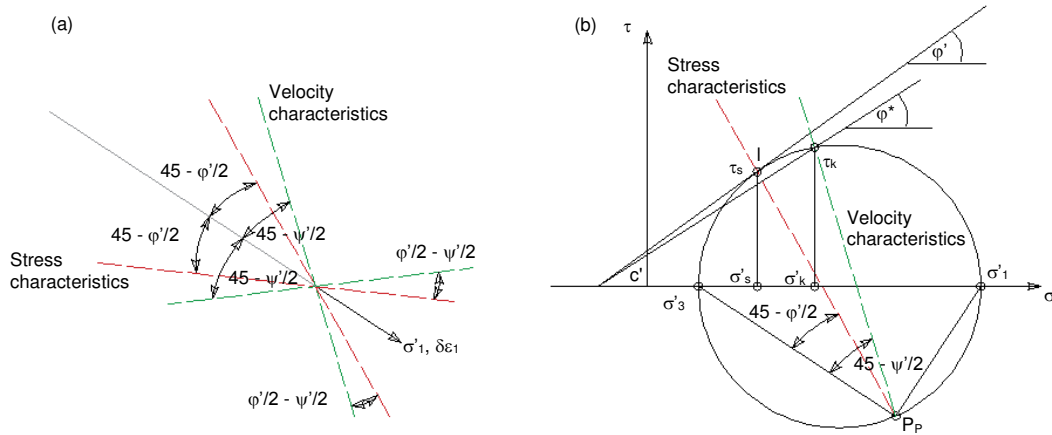


Fig. 21 Comparison of stress and velocity characteristics (a), Davis approach (b) (according to Tschuchnigg 2015a)

The strength parameters φ^* and c^* are dependent on the factor β (Eq. (46)). The amount of β is diminishing with a decreasing dilatancy angle and an increasing degree of non-associativity (Tschuchnigg 2015a).

The original approach by Davis is called Davis A, because Tschuchnigg developed two modifications which are subject of discussion in the following chapter.

3.3.3 Modifications of the original Davis approach

Based on the fact that the original approach by Davis leads to very conservative results if the factor of safety gets expressed by the strength parameters of the soil, Tschuchnigg (2015a) developed two procedures which are still conservative compared to the non-associated FoS, but less than Davis A.

Davis B

In Davis B, the β value is determined iteratively because of a change in the degree of non-associativity λ ($\varphi' - \psi'$). The factor of safety of the previous iteration step modifies the dilatancy angle ψ' as well as the friction angle φ' , according to Eq. (48).

$$\beta_{failure} = \frac{\cos\left(\tan^{-1}\left(\frac{\tan\varphi'}{FoS}\right)\right)\cos\left(\tan^{-1}\left(\frac{\tan\psi'}{FoS}\right)\right)}{1 - \sin\cos\left(\tan^{-1}\left(\frac{\tan\varphi'}{FoS}\right)\right)\sin\left(\tan^{-1}\left(\frac{\tan\psi'}{FoS}\right)\right)} \quad (48)$$

For the sake of completeness, a factor of safety equal to unity is assumed for the first step. Consequently, Eq. (48) becomes equal to Eq. (46). The value $\beta_{failure}$ gets calculated until no change in factor of safety occurs anymore.

Davis C

Davis C is similar to procedure B, with the difference of an unmodified dilatancy angle ψ' due to the iterations, as shown in Eq. (49) (Tschuchnigg 2015a).

$$\beta_{failure} = \frac{\cos\left(\tan^{-1}\left(\frac{\tan\varphi'}{FoS}\right)\right)\cos\psi'}{1 - \sin\cos\left(\tan^{-1}\left(\frac{\tan\varphi'}{FoS}\right)\right)\sin\psi'} \quad (49)$$

In the same way as for Davis B, β_0 gets calculated with a factor of safety equal to unity. As long as the dilatancy angle ψ' is zero, procedures B and C remain the same. To perform Davis B and Davis C, either in Plaxis 2D or Optum G2, the input parameters get calculated manually and each iteration step is a separate calculation.

Tab. 3 Comparison of Davis A, B and C (according to Tschuchnigg 2015a)

	Davis A	Davis B	Davis C
β	Constant	Varies	Varies
ψ'	$\beta_{failure} = f(\varphi', \psi')$	$\beta_{failure} = f(\varphi'_{failure}, \psi'_{failure})$	$\beta_{failure} = f(\varphi'_{failure}, \psi')$
Note:	φ^* could theoretically become smaller than ψ'	φ^* cannot be smaller than ψ'	φ^* could theoretically become smaller than ψ'

4 Davis in combination with structural elements

The following chapters show calculations performed on a reinforced embankment as well as on an upstream slope. The two examples are not linked together and can therefore be discussed separately. They, however, are connected due to the simple fact that both are reinforced by structural elements. In addition to LEA, SRFEA and FELA, further calculations based on Davis A and Davis B are performed with FELA. The approach results are compared with the non-associated SRFEA performed in Plaxis 2D in order to clarify how well both match.

4.1 Reinforced embankment

4.1.1 General information

The covered embankment gets reinforced by horizontal geotextile layers at the toe of the embankment. The four soil layers, namely *backfill material*, *sandy top layer*, *gravel layer* and *clay layer* define the soil composition (Fig. 22a). A horizontal water table is defined on top of the *sandy top layer*. Assuming drained conditions, the three underlying layers are fully saturated.

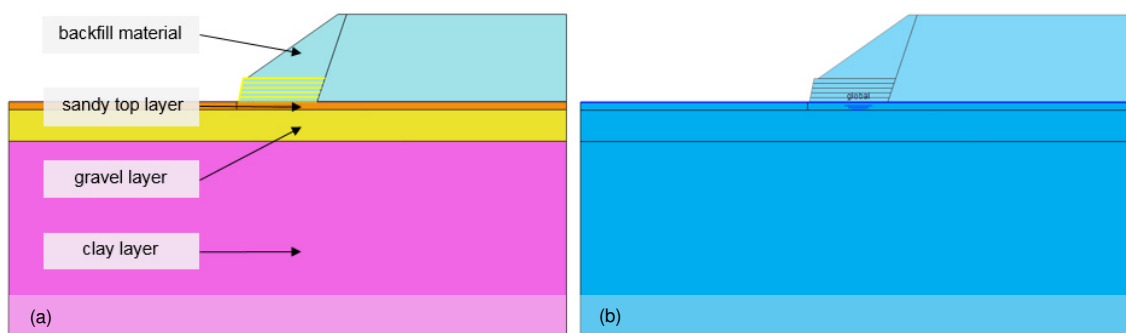


Fig. 22 Reinforced embankment: Soil composition (a), water table (b)

This study deals with two different cross sections of the reinforced embankment. Both are similar in many aspects. For the sake of completeness, the differences of cross section 1 (CS1) and cross section 2 (CS2) are described in the following. Both models are 35.5 m long, 20.6 m high and show an embankment height equal to 5.6 m. The cross section 1 is characterized by an embankment inclination of about $\alpha_1 = 36^\circ$, while cross section 2 is slightly flatter ($\alpha_2 = 35^\circ$). Additionally, the amount of horizontal geogrid layers is different. Fig. 23 shows that 5 horizontal geogrid layers are installed in CS1, while 6 layers are present in CS2. The geogrids are 5 m long for both cross sections and show a vertical distance of about 0.3 m. In consequence, the height of the geogrids package for CS1 is 1.2 m and for CS2 1.5 m.

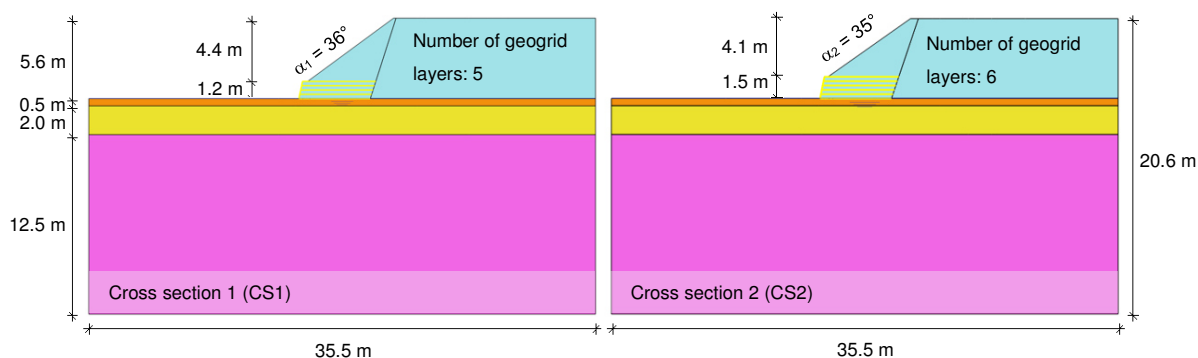


Fig. 23 Reinforced embankment: Comparison of cross section 1 and cross section 2

The Hardening Soil (HS) model and the Hardening Mohr-Coulomb (HMC) model, both assuming a Mohr-Coulomb failure criterion, are used for finite element analyses in Plaxis 2D (Schanz 1998) and Optum G2 (Doherty & Muir Wood 2013). Additionally, *limit equilibrium analyses*, assuming a Mohr-Coulomb failure criterion, are performed. The material parameters, listed in Tab. 4, are used as an input. The reinforcements get modelled by 5 m long geogrids with elastic properties and an extensional stiffness $EA = 10000 \text{ kN/m}^2$.

Tab. 4 Reinforced embankment: Material parameters

	Unit	Backfill material	Sandy top layer	Gravel layer	Clay layer
$\gamma_{unsat}, \gamma_{sat}$	(kN/m ³)	21; 21.5	21; 21.5	21; 21.5	20; 20.5
E_{50}^{ref}	(kN/m ²)	$40 \cdot 10^3$	$40 \cdot 10^3$	$25 \cdot 10^3$	$30 \cdot 10^3$
E_{oed}^{ref}	(kN/m ²)	$40 \cdot 10^3$	$40 \cdot 10^3$	$25 \cdot 10^3$	$30 \cdot 10^3$
E_{ur}^{ref}	(kN/m ²)	$120 \cdot 10^3$	$120 \cdot 10^3$	$75 \cdot 10^3$	$90 \cdot 10^3$
m	(-)	0.5	0.5	0.5	0.8
c'	(kN/m ²)	5	0	0	30
φ'	(°)	37	35	35	20
ψ'	(°)	0; φ'	0; φ'	0; φ'	0; φ'

This study includes three loading conditions. Loading condition 1 excludes any external load, only its self-weight is acting. The permanent load $p_g = 19 \text{ kN/m}^2$, acting along the whole crest, is taken into account in loading condition 2. In addition to p_g , the live load $p_q = 63 \text{ kN/m}^2$, is part of loading condition 3 (Fig. 24).

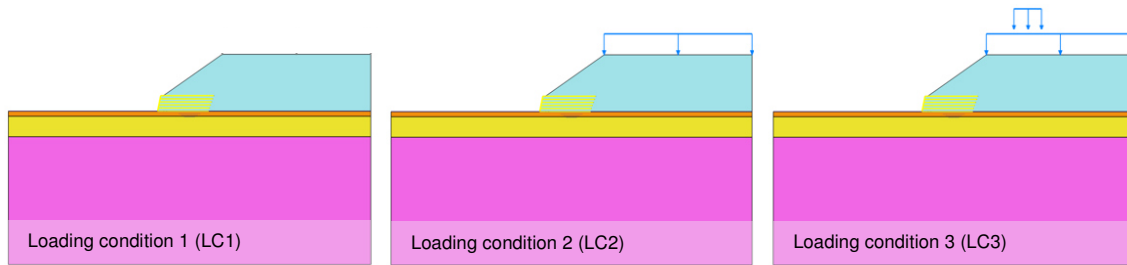


Fig. 24 Reinforced embankment: Loading conditions

Due to the similarity of both cross sections, the mesh refinement is only shown for CS2. In Plaxis 2D, the discretization of the domain is carried out using 15-noded elements. As Fig. 25 shows, the mesh gets refined until the safety factor remains almost constant. Due to the fact that the failure mechanism develops behind the reinforcements, this area shall be the subject of refinements. In order to secure no change in factor of safety for any loading condition, 10913 elements are used. It should be noticed that the higher the number of elements, the smaller the change in the factor of safety gets. This correlation becomes clear in Tab. 5. In order to decrease the FoS from 1.70 to 1.69, 700 additional elements are needed. To decrease the factor of safety from 1.67 to 1.66, about 5900 elements are needed. This behaviour gets elaborated with more details in chapter 4.1.4.

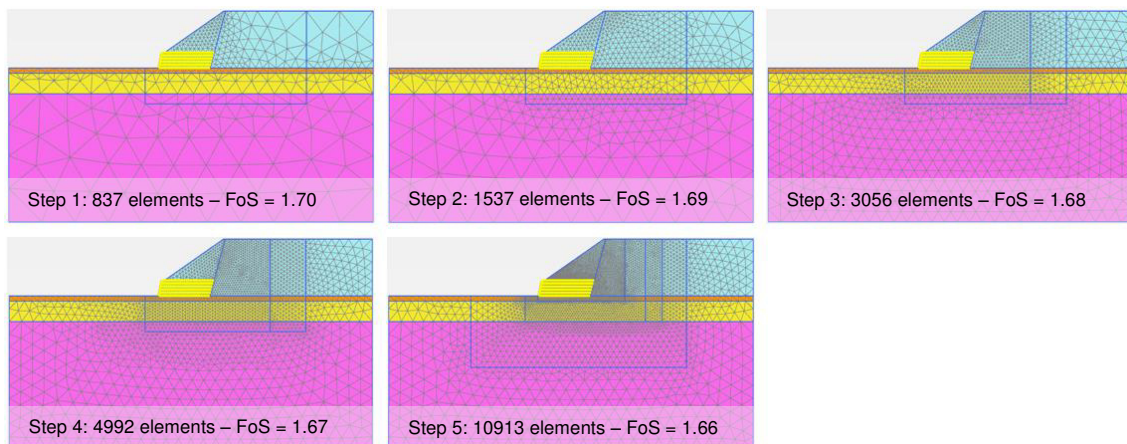


Fig. 25 Reinforced embankment: Mesh refinement (step 1 - 5)

Tab. 5 Influence of mesh density on the factor of safety

Unit	837 elements	1537 elements	3056 elements	4992 elements	10913 elements	
SRFEA ($\psi' = \varphi'$)	(-)	1.70	1.69	1.68	1.67	1.66

It should be noted that for all SRFEA carried out in Plaxis 2D, the initial stresses are calculated according to the K_0 procedure where no embankment is present. In addition, the construction of the embankment gets modelled in one step, followed by either the safety analysis on its own or a loading phase with an additional safety analysis (LC2 and

LC3). Subdividing the process of construction into more phases has no influence on the factor of safety (appendix 10.2.1).

4.1.2 Factor of safety according to SRFEA and LEA

It was mentioned earlier that the flow rule might have a strong influence on the factor of safety in strength reduction analyses. Fig. 26 illustrates the safety factors over reduction steps for cross section 1. The dashed lines, representing the non-associated calculations ($\psi' = 0^\circ$), differ strongly from the full lines ($\psi' = \phi'$). Logically, loading condition 1 with associated plasticity shows the highest FoS, equal to 1.66. In comparison, the non-associated calculation results in a safety factor equal to 1.52 which corresponds to a difference of about 9.2 %. The factors of safety for loading conditions 2 and 3 are listed in Tab. 6. It can be seen that the differences in the factor of safety rise from 9.2 % to 11.7 %. Furthermore, Fig. 26 shows a slightly erratic result for non-associated plasticity due to the so-called bifurcation of failure mechanism, as mentioned in section 3.1.4.

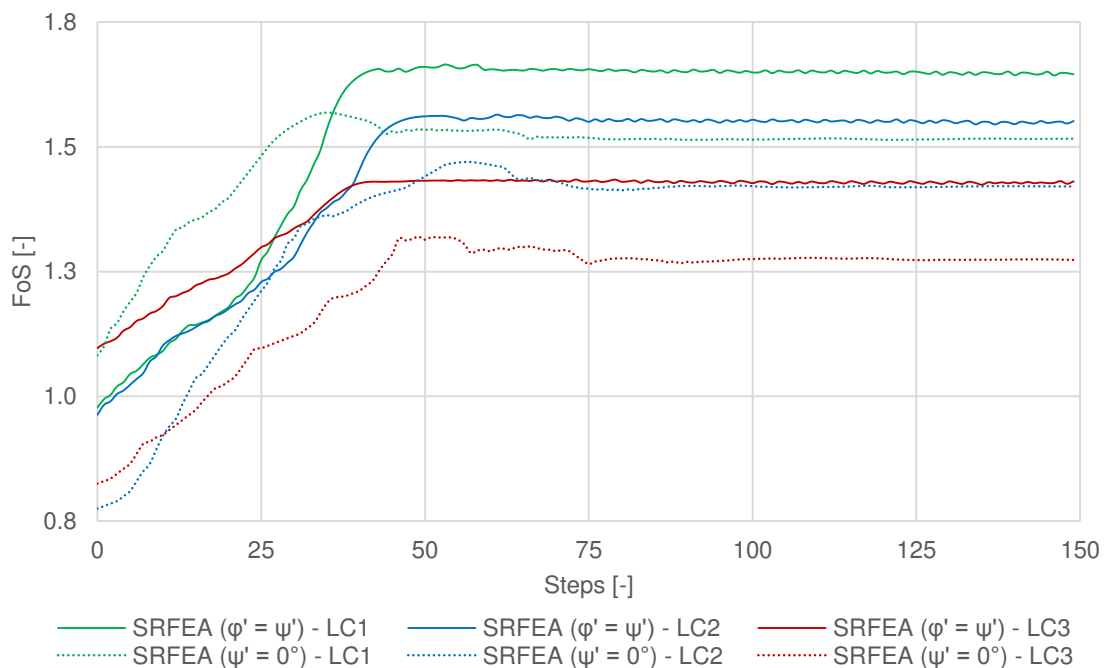


Fig. 26 Cross section 1: ϕ - c reduction

Tab. 6 Cross section 1: Overview of safety factors according to SRFEA

SRFEA			
	<i>Loading condition 1</i>	<i>Loading condition 2</i>	<i>Loading condition 3</i>
<i>SRFEA ($\psi' = \varphi'$)</i>	1.66	1.56	1.43
<i>SRFEA ($\psi' = 0^\circ$)</i>	1.52	1.42	1.28
<i>% Difference</i>	9.2	9.9	11.7

The incremental shear strains for the non-associated calculations ($\psi' = 0^\circ$) show a similar failure mechanism for all three loading conditions (Fig. 27).

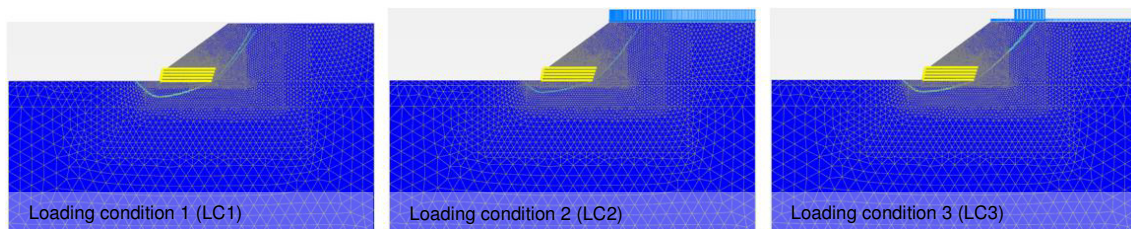


Fig. 27 Cross section 1 ($\psi' = 0^\circ$): Incremental shear strains

It can be established that by comparing the shape of incremental shear strains for both associated and non-associated plasticity, all six failure mechanisms show good agreement (Fig. 27 and Fig. 28). Due to the additional dynamic load, the failure mechanism in loading condition 3 is slightly flatter in the upper part. Again, both associated and non-associated calculations show the same failure mechanism. Because of numerical problems at the toe of the embankment, a concentration of incremental shear strains gets developed below the lowest layer of geogrids for all associated calculations (Fig. 28). As a consequence, the failure mechanism is not as clear defined as for the non-associated calculations.

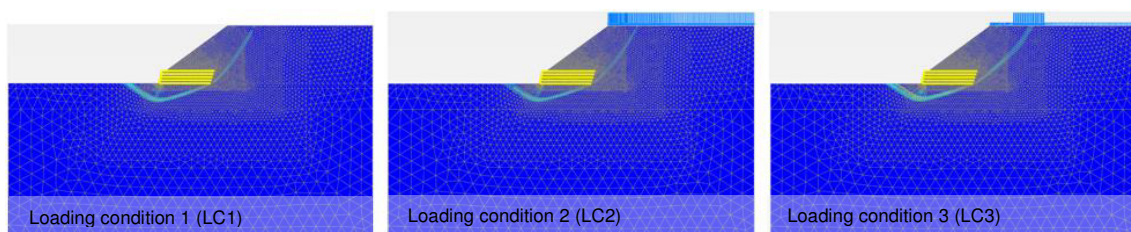


Fig. 28 Cross section 1 ($\psi' = \varphi'$): Incremental shear strains

In addition, limit equilibrium analyses, using the Morgenstern & Price method, are performed for cross section 1. A square area, with a side length of 10 m and 200 intervals in the x and the y direction, is used to search for the circular failure mechanism with the lowest factor of safety. The safety factors of LC1, LC2 and LC3 are listed in Tab. 7.

Tab. 7 Cross section 1: Overview of safety factors according to LEA

LEA (Morgenstern & Price)			
	<i>Loading condition 1</i>	<i>Loading condition 2</i>	<i>Loading condition 3</i>
<i>LEA</i>	1.72	1.62	1.50

Fig. 29 highlights the critical failure mechanisms for the different loading conditions. They are in good agreement with the course of incremental shear strains obtained from SRFEA.

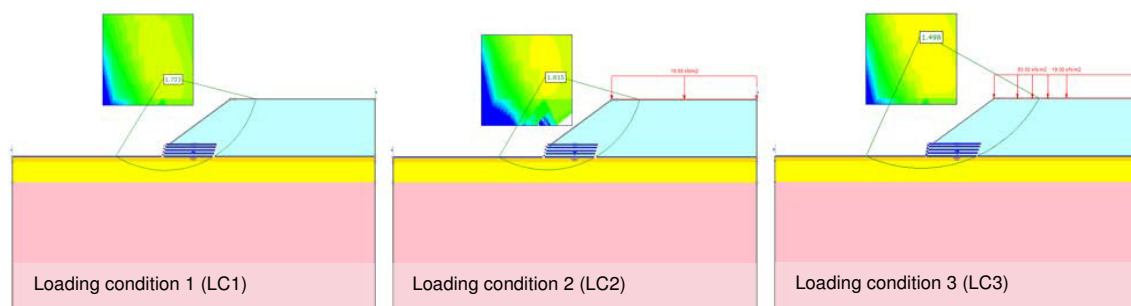


Fig. 29 Cross section 1: Failure mechanisms of LEA

Now, comparing the SRFEA and the LEA, it is remarkable that the safety factors obtained from the LEA are in better agreement with the associated calculations of Plaxis 2D and give a slightly higher FoS than the SRFEA. A complete comparison is listed below. The differences between the LEA and the associated SRFEA vary between 3.5 % and 4.7 %. In contrast, compared to the LEA, the non-associated safety factors are between 11.6 % and 14.7 % lower.

Tab. 8 Cross section 1: Comparison of SRFEA and LEA

LEA, SRFEA			
	<i>Loading condition 1</i>	<i>Loading condition 2</i>	<i>Loading condition 3</i>
<i>LEA (M&P)</i>	1.72	1.62	1.50
<i>SRFEA ($\psi' = \phi'$)</i>	1.66	1.56	1.43
<i>SRFEA ($\psi' = 0^\circ$)</i>	1.52	1.42	1.28

Tab. 9 Cross section 1: Differences between SRFEA and LEA

% Differences			
	Loading condition 1	Loading condition 2	Loading condition 3
<i>LEA (M-P) - SRFEA ($\psi' = \varphi'$)</i>			
$= 100 (\text{LEA (M-P) - SRFEA } (\psi' = \varphi')) / \text{LEA (M-P)}$	3.5	3.7	4.7
<i>LEA (M-P) - SRFEA ($\psi' = 0^\circ$)</i>			
$= 100 (\text{LEA (M-P) - SRFEA } (\psi' = 0^\circ)) / \text{LEA (M-P)}$	11.6	12.3	14.7

The same safety analyses are performed for cross section 2. For the sake of completeness, the results are presented in Fig. 30, Fig. 31, Fig. 32 and Fig. 33 as well as in Tab. 10 and Tab. 11. It should be noted that all statements made for cross section 1 hold true for cross section 2 as well.

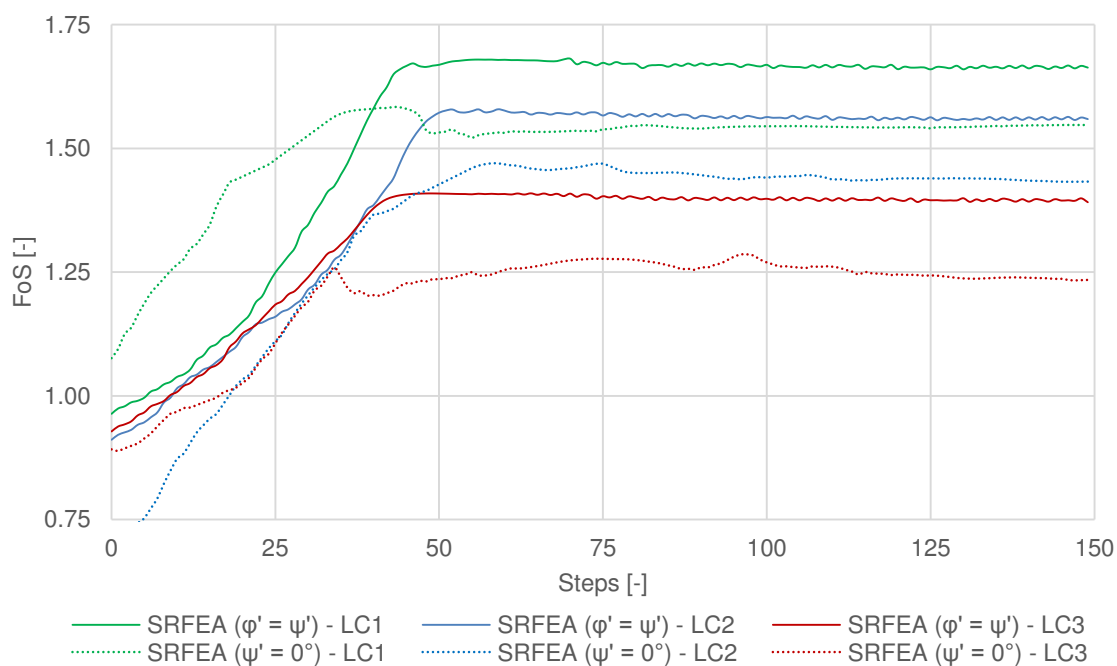


Fig. 30 Cross section 2: $\varphi - c$ reduction

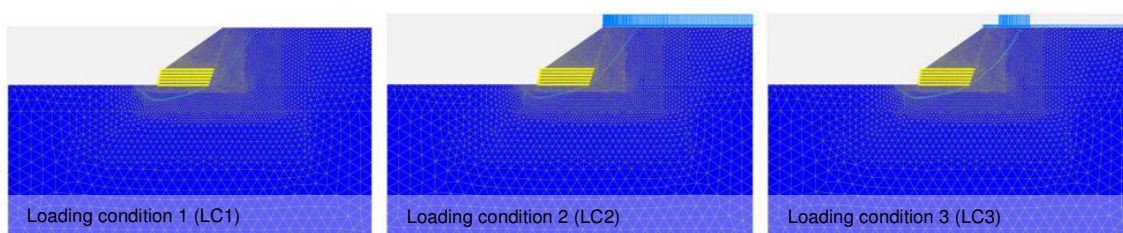


Fig. 31 Cross section 2 ($\psi' = 0^\circ$): Incremental shear strains

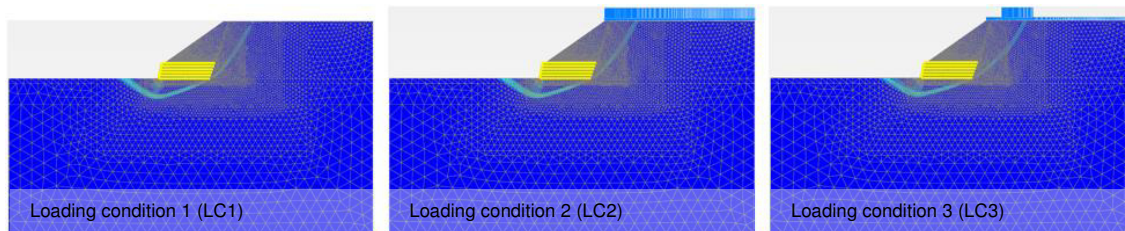


Fig. 32 Cross section 2 ($\psi' = \varphi'$): Incremental shear strains

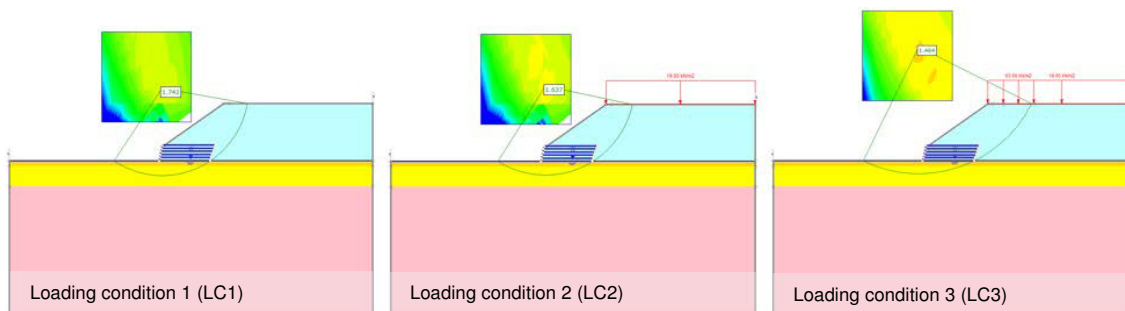


Fig. 33 Cross section 2: Failure mechanism according to LEA

Tab. 10 Cross section 2: Comparison of SRFEA and LEA

LEA, SRFEA			
	Loading condition 1	Loading condition 2	Loading condition 3
LEA (M-P)	1.74	1.64	1.46
SRFEA ($\psi' = \varphi'$)	1.66	1.56	1.40
SRFEA ($\psi' = 0^\circ$)	1.55	1.43	1.22

Tab. 11 Cross section 2: Differences between SRFEA and LEA

% Differences			
	Loading condition 1	Loading condition 2	Loading condition 3
LEA (M-P) - SRFEA ($\psi' = \varphi'$)			
= 100 (LEA (M-P) - SRFEA ($\psi' = \varphi'$)) / LEA (M-P)	4.6	4.9	4.1
LEA (M-P) - SRFEA ($\psi' = 0^\circ$)			
= 100 (LEA (M-P) - SRFEA ($\psi' = 0^\circ$)) / LEA (M-P)	10.9	12.8	16.4

Due to the uncertainty of the soil parameters and geometry, additional calculations are performed for cross section 1 and cross section 2. Appendix 10.2.2 includes the SRFEA and the LEA on two modified cross sections where both embankments are disposed about 37° . The modified cross sections 1 and 2 still include 5 or rather 6 horizontal

geogrid layers (see chapter 4.1.1). As shown in Fig. 34, the cohesionless *sandy top layer* gets used for backfilling. To avoid near-surface failure mechanisms, a *modified backfill material* with $c' = 100$ kPa is used. This is done because the slope inclination is larger than the friction angle of the backfill material. The results underline the expectation that the factor of safety based on the limit equilibrium technique is in better agreement with analyses according to associated plasticity.

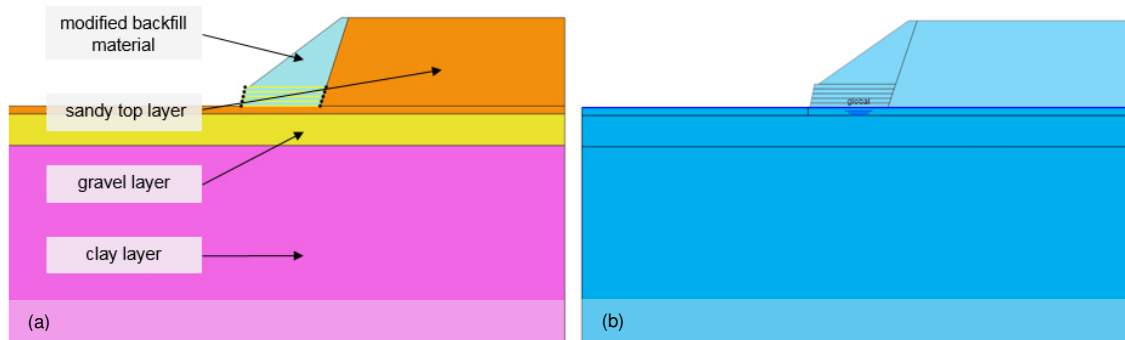


Fig. 34 Modified cross section 1: (a) Soil composition, (b) water table

A further study, attached to appendix 10.2.3, shows that the cohesion has a larger impact on the factor of safety than the friction angle. The influence of extensional stiffness EA and tensile strength N_p is discussed in appendix 10.2.4.

4.1.3 Factor of safety according to Davis A and Davis B

This chapter deals with *finite element limit analyses* performed on cross section 2 (CS2) while considering loading condition 1 (LC1). In addition to the standard upper and lower bound calculation with associated plasticity, Davis A and Davis B are calculated as well. It should be noted that for this example the latter one is equal to Davis C, because all soil layers show a dilatancy angle ψ' equal to zero. FELA are performed with adaptive mesh refinement. As mentioned in chapter 4.1.2, a concentration of incremental shear strains occurs for SRFEA with associated flow rule below the geogrid layers. The same problem arises in Optum G2 for the lower bound analyses. Fig. 35 shows that the mesh gets refined automatically at the toe of the embankment.

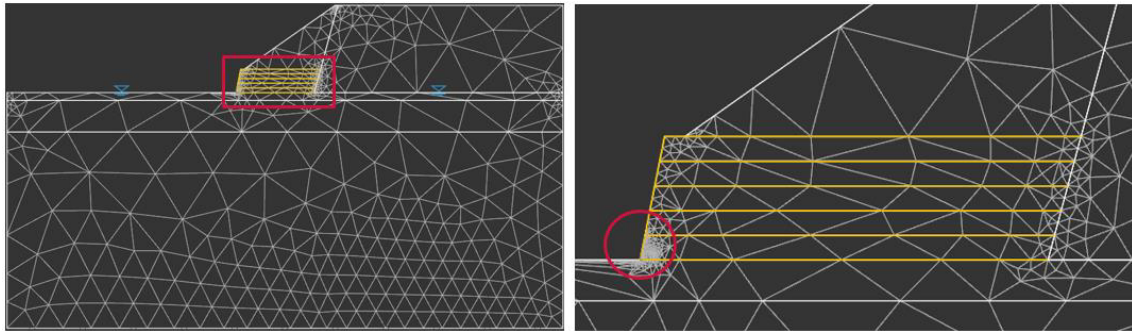


Fig. 35 Adaptive mesh refinement: Concentration at the toe for the lower bound

To overcome this numerical problem, tension gets allowed between the geotextile layers (*tension cut-off*: No). This assumption is acceptable due to the fact that the geotextiles get bend up at the edges. Taking these modifications into account, the meshes for lower and upper bounds get refined according to Fig. 36a and Fig. 36b. The area around the reinforcements gets refined according to the shear dissipations. A $FoS_{LB} = 1.91$ and a $FoS_{UB} = 1.95$ are yielded by the FELA. The deformed meshes of Fig. 36c and Fig. 36d represent the failure mechanisms for the lower and upper bound calculations. It should be noted that the distribution of incremental shear strains is equal to those based on the SRFEA.

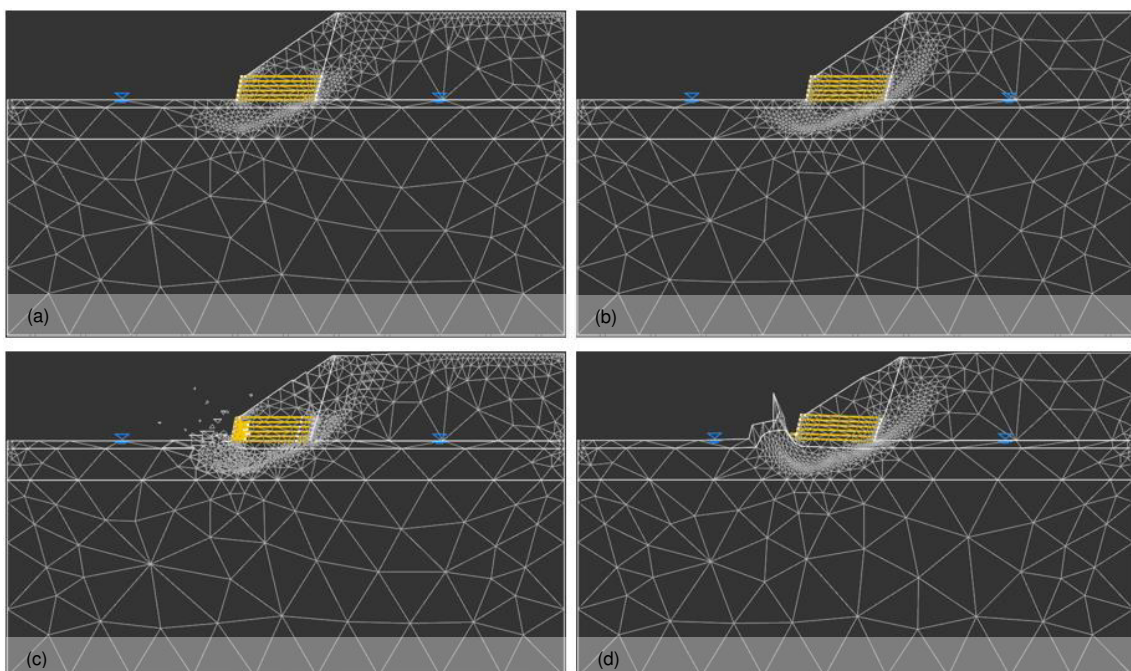


Fig. 36 Cross section 2 according to FELA: (a) lower bound: adaptive mesh refinement; (b) upper bound: adaptive mesh refinement; (c) lower bound: failure mechanism; (d) upper bound: failure mechanism

Moreover, the SRFEA and the FELA are performed with modified strength parameters c^* and φ^* , according to Eq. (46). Tab. 12 and Tab. 13 highlight that SRFEA and FELA are in good agreement. It is apparent that Davis A is about 14 % conservative compared

to a SRFEA with non-associated plasticity (Tab. 14). The FoS_{Mean} based on Davis B is still conservative at only about 3.1 %. By using Eq. (48), three iterative modifications of the strength parameters are necessary to guarantee no change in the safety factor.

Tab. 12 Cross section 2 (LC1): Comparison of SRFEA

SRFEA			
	$\psi' = \varphi'$ Plaxis 2D	$\psi' = 0^\circ$ Plaxis 2D	Davis A ($\psi' = 0^\circ$) Plaxis 2D
FoS	1.66	1.55	1.35

Tab. 13 Cross section 2 (LC1): Comparison of FELA

FELA			
	$\psi' = \varphi'$ Optum G2	Davis A ($\psi' = 0^\circ$) Optum G2	Davis B ($\psi' = 0^\circ$) Optum G2
FoS_{Mean}	1.66	1.35	1.49

Tab. 14 Cross section 2 (LC1): Comparison of Davis A and Davis B with SRFEA ($\psi' = 0^\circ$)

% Difference	
Davis A	Davis B
$= 100 (FELA (Davis A) - SRFEA (\psi' = 0^\circ)) / FELA (Davis A)$	$= 100 (FELA (Davis B) - SRFEA (\psi' = 0^\circ)) / FELA (Davis B)$
- 14.0	- 3.1

4.1.4 Mesh study

The aim of the following studies is to find out if safety analyses can be performed with less elements when having implemented an adaptive mesh refinement. As mentioned earlier, Optum G2 can run SRFEA and FELA with and without adaptive mesh refinement. Keep in mind that by choosing a *Strength Reduction* analysis with *Lower* and *Upper* element types, a FELA is performed. If more than 1000 elements are needed, a FELA can also be carried out manually by reducing the strength parameters cohesion and friction angle until the gravity multiplier ($FoS_{Gravity}$) is equal to unity (Krabbenhøft et al. 2016).

Cross section 2 with associated plasticity and no external loads (LC1) is subject of several SRFEA and FELA according to different numbers and types of elements. In the first part of the study, both SRFEA are performed in Plaxis 2D and Optum G2 with 6-noded and 15-noded elements. As shown in Fig. 37, about 10500 elements are needed

to reach a safety factor equal to 1.66, by performing a SRFEA with 15-noded elements in Plaxis 2D. As mentioned above, the number of elements while using analysis type *Strength Reduction* is limited to approximately 1000 elements. This number refers to the input value. The adaptive mesh refinement may increase or decrease the number of elements. By turning on the adaptive mesh refinement and using 15-noded elements, about 1300 elements are necessary to reach a FoS = 1.66. Concurrently, if no adaptive mesh refinement is concerned, the evolution of safety factors is similar to the performance obtained in Plaxis 2D.

As presented in Fig. 37, all analyses performed with 6-noded elements result in higher safety factors compared to the ones that are based on 15-noded elements. However, the statements for 15-noded elements are valid for 6-noded elements too. The determined safety values are listed in appendix 10.2.5.

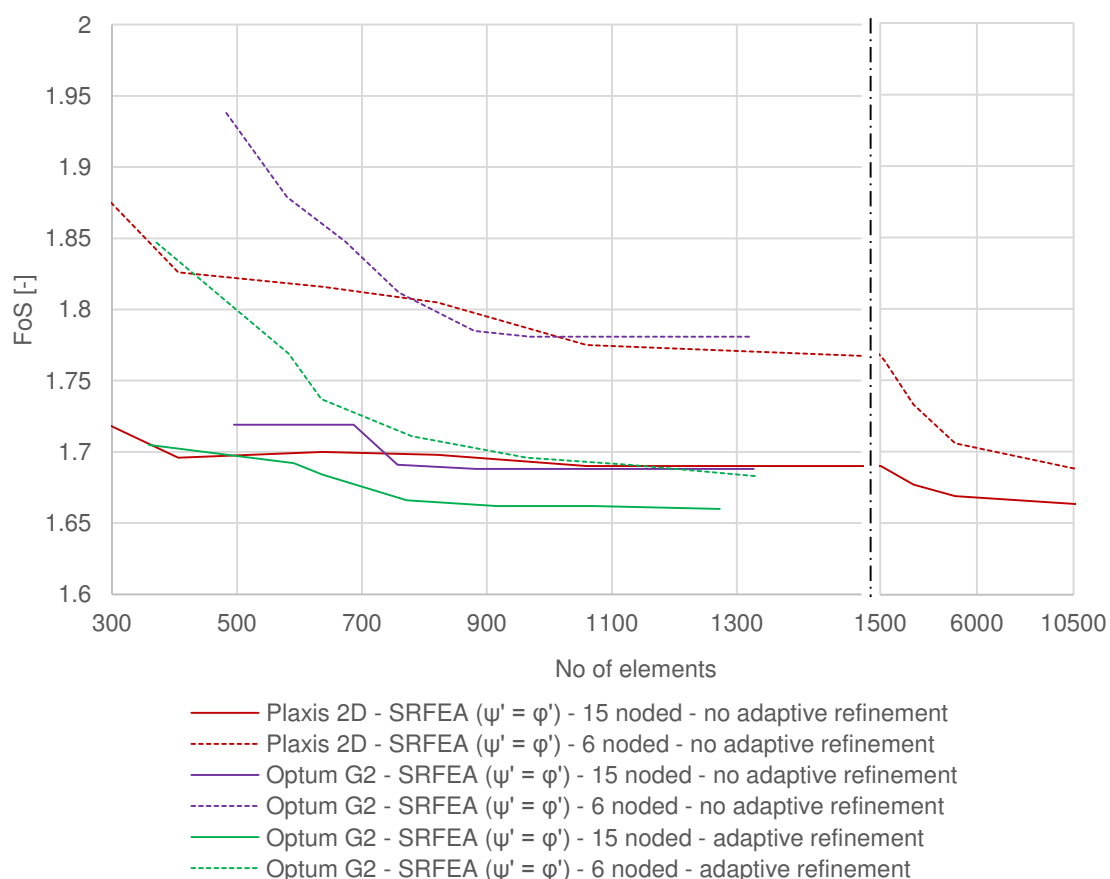


Fig. 37 Mesh study: Comparison of SRFEA

The question arises, how well the adaptive mesh refinement works for a FELA. As Fig. 38 shows, the difference of upper and lower bound reduces significantly once the adaptive mesh refinement is turned on. From this follows that the error of the result with adaptive mesh refinement is significantly smaller. Furthermore, it becomes clear that the

upper bound is close to the results obtained with the SRFEA. The safety values of all FELA are listed in appendix 10.2.5.

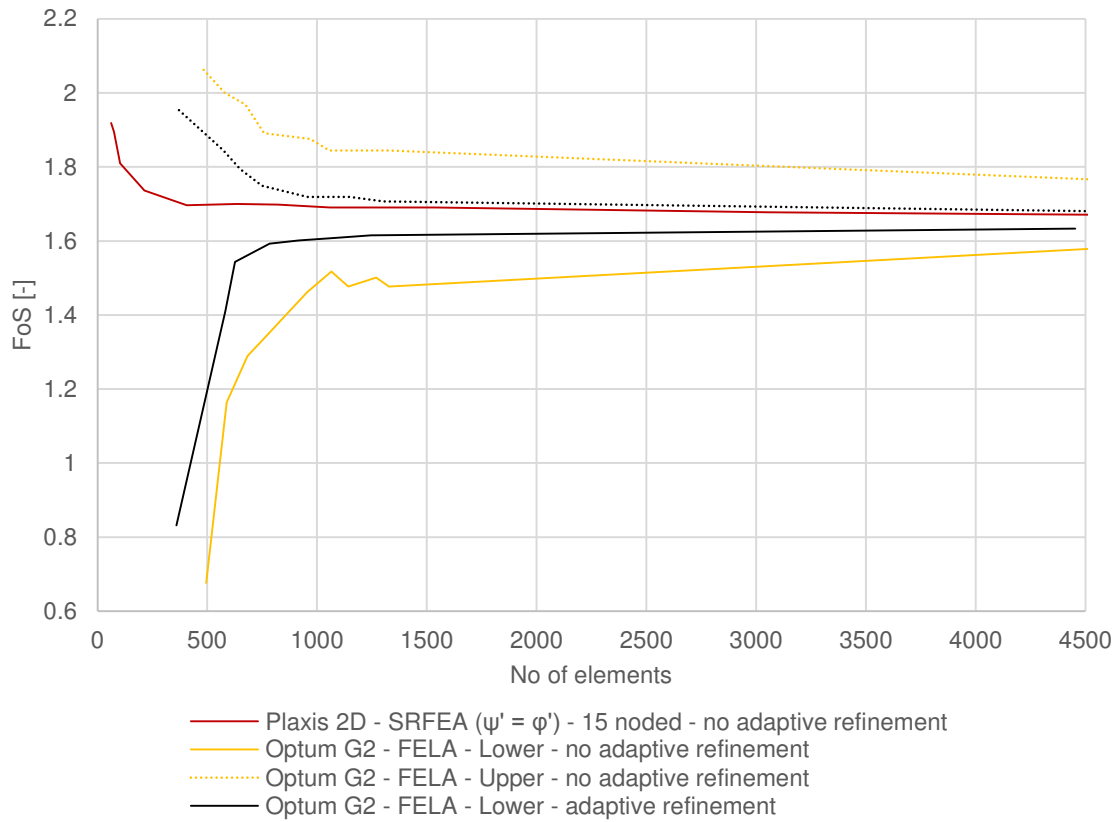


Fig. 38 Mesh study: Comparison of SRFEA and FELA

4.2 Upstream slope

4.2.1 General information

This example deals with a reinforced upstream slope next to a reservoir. Here again, we distinguish between two cases. Case 1 represents the current status with a low safety factor, while case 2 considers several modifications in order to reach a higher safety value. The soil layering is characterized by three soil layers, as seen in Fig. 39a. The top layer marked in light blue represents *moraine material*. Underneath, marked in light green and brown, *fractured* as well as *intact rock layers* are situated. The water level can be found primarily in the fractured rock layer. A conservative approach is made by defining an inclined water table, as shown in Fig. 39b. As will be discussed later, stability analyses are performed on a modified water table too.

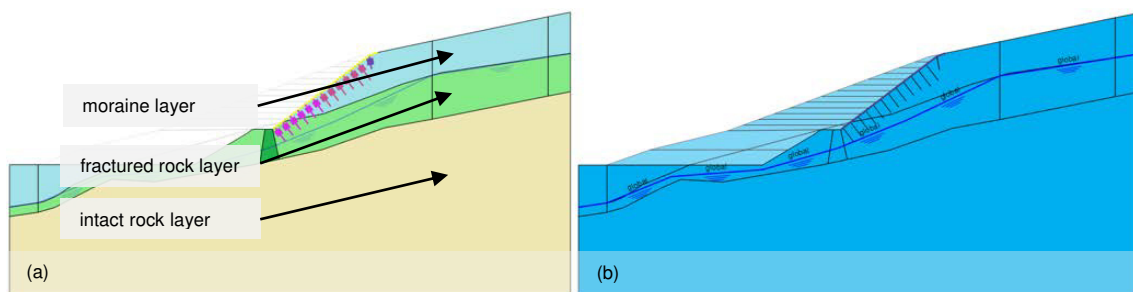


Fig. 39 Upstream slope: (a) Soil layers, (b) inclined water table

According to Fig. 40, the cross section of case 1 can be divided into an area below the berm, disposed about 30° towards the horizontal, and an area above the berm that is inclined by 37° towards the horizontal and is supported by several structural elements. To avoid shallow slides, a Maccaferri grid is installed. In addition, soil nails with spacings varying between 2 m to 3 m are present. The vertical nail on top of the slope is 4 m long and is characterized by a spacing equal to 2 m. The following 6 soil nails, the top two being 6 m, the bottom 4 being 5 m long, show a spacing of about 2.5 m. Referring to Fig. 40, the last six soil nails are 5 m long with a spacing equal to 3 m. At the berm, a pile trestle consisting of two GEWI piles which are connected with a ridgepole on top is installed. Below the berm, no further structures are present.

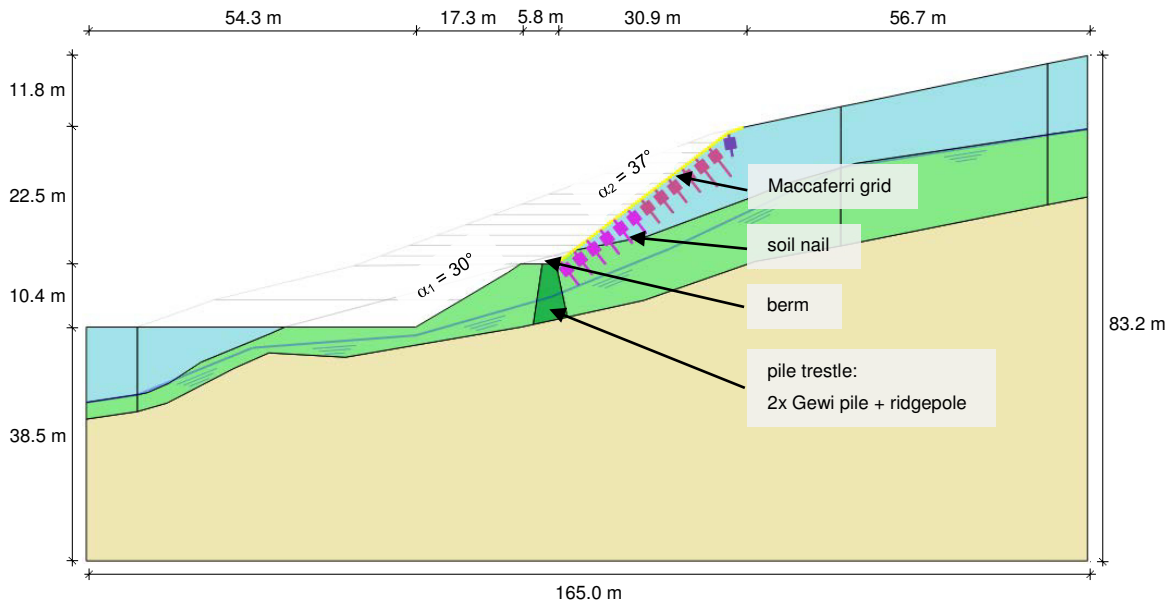


Fig. 40 Upstream slope - case 1: Dimensions and structural elements

Due to the unsafe conditions of case 1, the area below and above the berm gets flatted, according to Fig. 41. The slope above the berm is disposed about 30° to the horizontal and is divided by an additional intermediate berm. Furthermore, the Maccaferri grid and all soil nails get removed from the specified field. The pile trestle remains unchanged and the area below gets flatted to 26.7° . Case 2 will be calculated for the water table, as shown in Fig. 39b, as well as a lowered water level. Drainage rips disposed about 10° to the horizontal guarantee a long term reduction of the water table.

The Hardening Soil and Mohr-Coulomb models are used to model the soil layers in an appropriate way. The *moraine layer* and *fractured rock layer* are designed according to the HS model. Additionally, limit equilibrium analyses, assuming a Mohr-Coulomb failure criterion, are performed to work out if the safety factors are in good agreement with the associated results again. The input parameters for the SRFEA, the FELA and the LEA are listed in Tab. 15. It should be noted that SRFEA are performed in Plaxis 2D according to the standard procedure of $\varphi - c$ reduction by assuming a dilatancy angle $\psi'_1 = 0^\circ$ and $\psi'_2 = \varphi'$. All following calculations assume drained conditions and ignore external loads. Furthermore, the reservoir is assumed to be empty for both cases in order to generate the worst-case scenario.

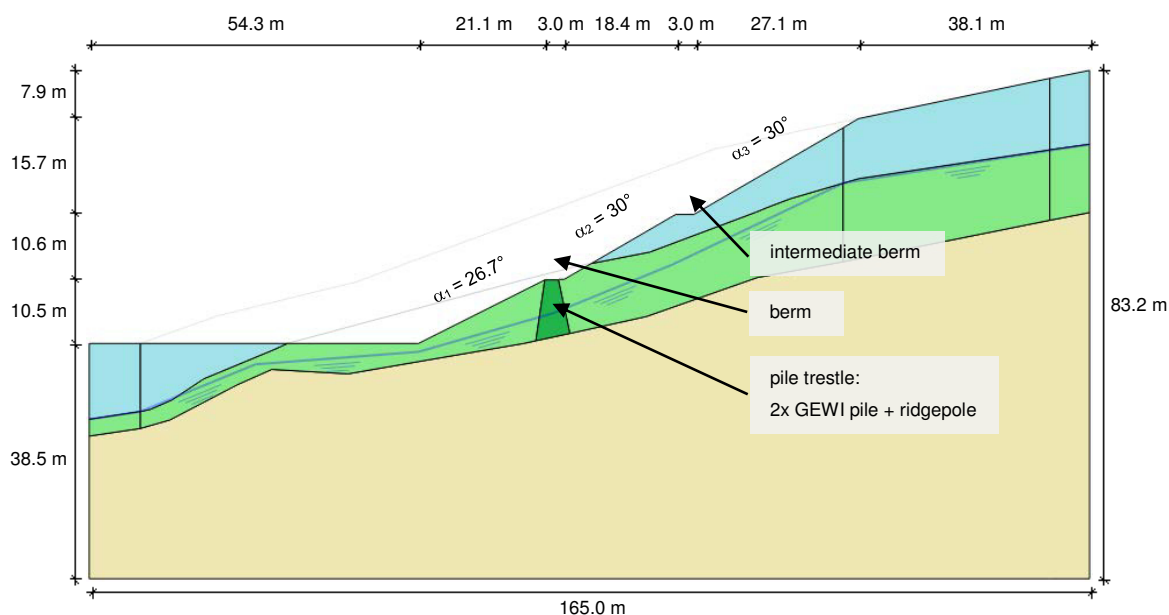


Fig. 41 Upstream slope - case 2: Dimensions and structural elements

Tab. 15 Upstream slope: Material parameters

	Unit	moraine layer	fractured rock layer	intact rock layer
<i>Model</i>	(-)	Hardening Soil	Hardening Soil	Mohr-Coulomb
$\gamma_{unsat}, \gamma_{sat}$	(kN/m ³)	22.0; 23.0	22.5; 23.0	22.5; 23.0
$E_{50}^{ref}, *E'$	(kN/m ²)	40·10 ³	50·10 ³	*5·10 ⁶
E_{50}^{oed}	(kN/m ²)	40·10 ³	50·10 ³	-
E_{ur}^{ref}	(kN/m ²)	120·10 ³	150·10 ³	-
m	(-)	0.5	0.5	-
c'	(kN/m ²)	10.0	15.0	25.0
φ'	(°)	31.0	31.0	35.0
ψ'	(°)	0.0; φ'	0.0; φ'	0.0; φ'

Instead of modelling the two GEWI piles with structural elements, the area of the pile trestle was defined with an increased cohesion of $c' = 18.5 \text{ kN/m}^2$. All the other soil properties correspond to the *fractured rock layer*. In Plaxis 2D, geogrids and embedded beam rows are used to model the Maccaferri grid and the soil nails. Optum G2 uses the equivalent option to the latter as a nail row (Krabbenhøft et al. 2016). Both structural elements show an elasto-plastic material behaviour. An overview of all input parameters is listed in appendix 10.3.1.

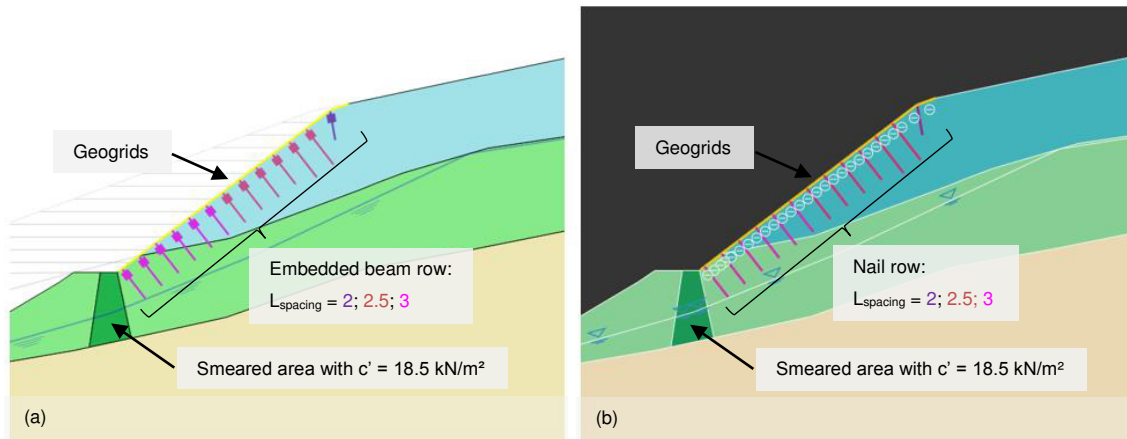


Fig. 42 Upstream slope: Modelling of structural elements in Plaxis 2D (a) and Optum G2 (b) SRFEA using 15-noded elements are carried out in Plaxis 2D. Referring to Fig. 43, the *moraine layer* and *fractured rock layer* are object of refinements. In particular, the domain behind and in between the nails as well as the direct environment of the pile trestle are object of refinements. 8932 elements are used for the discretisation. In a FELA, the mesh refinement is performed adaptively with 1000 starting elements.

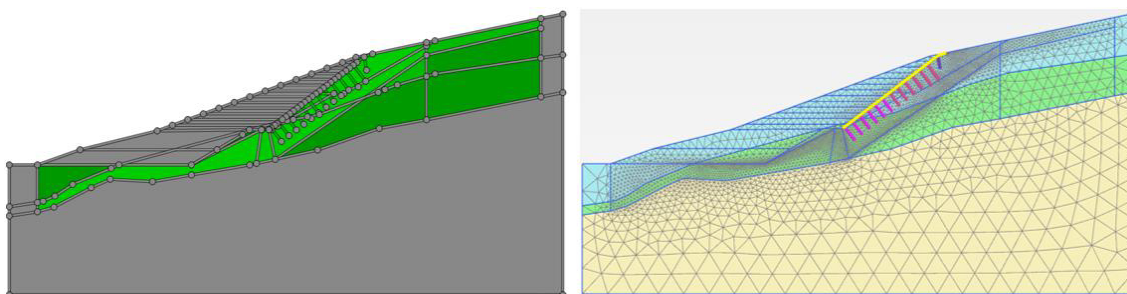


Fig. 43 Upstream slope: Mesh refinement Plaxis 2D

In Plaxis 2D, the initial stresses get determined by a K_0 procedure with an additional nil-step. Subsequently, the soil gets removed in 16 steps, followed by the SRFEA of case 1. Five more phases are considered adequate to flatten the slope and remove the structural elements before the strength reduction of case 2 is carried out. The individual excavation phases are shown in appendix 10.3.2.

4.2.2 Safety analysis of case 1

Again, it can be established that the FELA and SRFEA with associated plasticity are in good agreement with the LEA performed in Slide. In order to find the lowest FoS, the same square shape grid as discussed in section 4.1.2 is used. All three analyses show almost the same failure mechanism trough the toe of the reinforced part of the slope (Fig. 44). Referring to Tab. 16 and Tab. 17, the $FoS_{Mean} = 1.25$ according to the FELA is in good agreement with the SRFEA and the LEA. The strength reduction with non-

associated plasticity leads to a FoS = 1.12. Again, the analytical calculation is in better agreement with calculations based on associated plasticity.

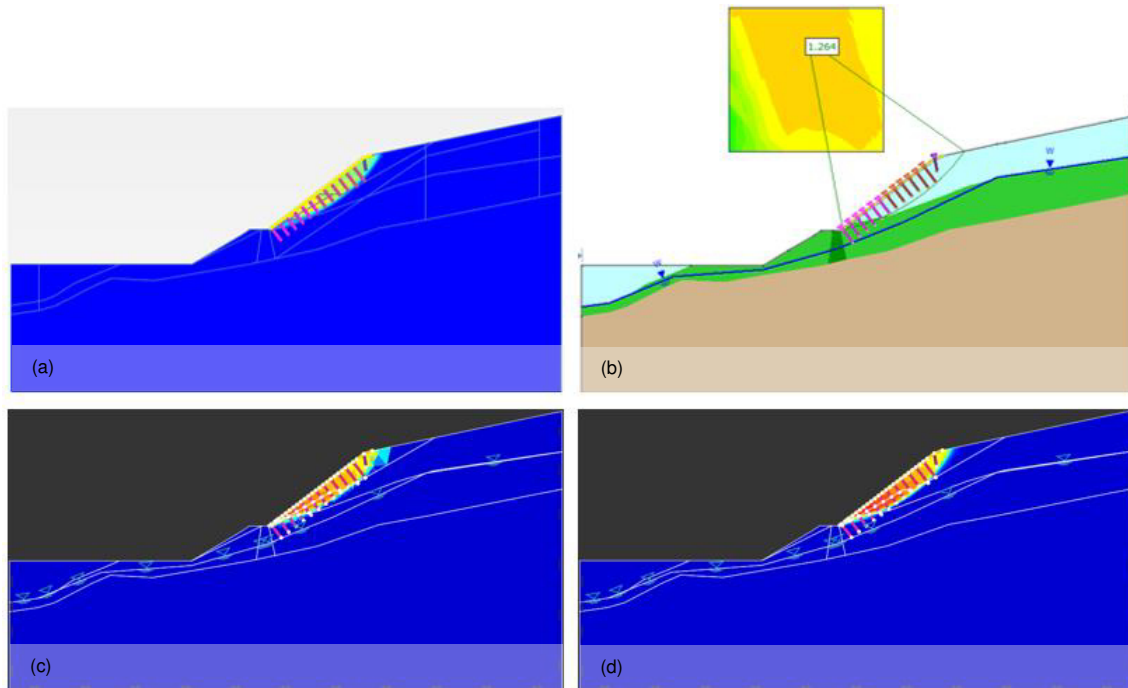


Fig. 44 Case 1 - Comparison of the failure mechanisms: (a) total displacements for SRFEA with associated plasticity, (b) circular failure mechanism according to LEA, (c) total displacements for lower-bound FELA, (d) total displacements for upper-bound FELA

In addition, it is of interest to determine how well Davis A and B correspond with the non-associated SRFEA ($\psi' = 0^\circ$). SRFEA and FELA based on the original approach (Davis A) only vary at about 0.9 %. The adaptively refined mesh for the upper-bound FELA is shown in Fig. 45a. Even if the safety factors based on the SRFEA and the FELA are in good agreement, it should be noted that a second deep-seated failure mechanism is weakly developed in Plaxis 2D (Fig. 45c). Furthermore, Davis B gets determined due to three iterations. All the proved failure mechanisms are very similar and do not interact with the defined water table.

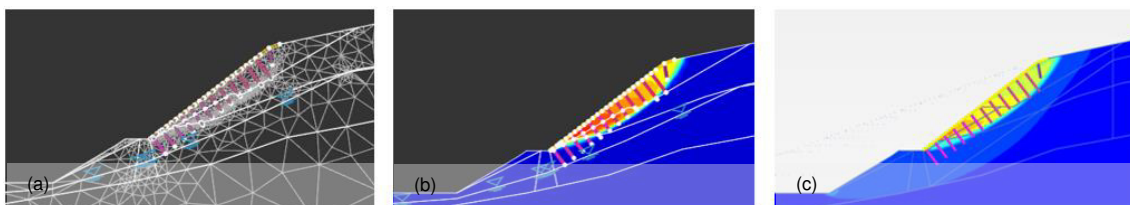


Fig. 45 Case 1 - Davis A: (a) adaptive mesh refinement of upper-bound FELA; (b) total displacements of upper-bound FELA; (c) total displacements of SRFEA

Tab. 18 compares the factors of safety based on Davis A and Davis B with the non-associated SRFEA. Both approaches are conservative in contrast to the SRFEA assuming a dilatancy angle $\psi' = 0^\circ$. The differences in the safety factor between

approach A and B are not as large as in the previous example. This is due to the fact that the failure mechanism is greatly dependent on the properties of structural elements.

Tab. 16 Case 1: Comparison of LEA and SRFEA

LEA, SRFEA

	<i>Morgenstern & Price Slide</i>	$\psi' = \varphi'$ <i>Plaxis 2D</i>	$\psi' = 0^\circ$ <i>Plaxis 2D</i>	<i>Davis A ($\psi' = 0^\circ$)</i> <i>Plaxis 2D</i>
<i>FoS</i>	*1.26	1.26	1.12	1.08

Tab. 17 Case 1: Comparison of FELA

FELA

	$\psi' = \varphi'$ <i>Optum G2</i>	<i>Davis A ($\psi' = 0^\circ$)</i> <i>Optum G2</i>	<i>Davis B ($\psi' = 0^\circ$)</i> <i>Optum G2</i>
<i>FoS_{Mean}</i>	1.25	1.07	1.09

Tab. 18 Case 1: Comparison of Davis A and Davis B with SRFEA ($\psi' = 0^\circ$)

% Difference

<i>Davis A</i>	<i>Davis B</i>
$= 100 (\text{FELA (Davis A)} - \text{SRFEA } (\psi' = 0^\circ)) / \text{FELA (Davis A)}$	$= 100 (\text{FELA (Davis B)} - \text{SRFEA } (\psi' = 0^\circ)) / \text{FELA (Davis B)}$
- 4.7	- 2.8

4.2.3 Safety analyses of case 2

Safety analyses in case 2 are performed according to the original as well as to a lowered water table. A phreatic water table is used for the SRFEA performed in Plaxis 2D. As a consequence, no flow is considered. Optum G2 does not allow the user to choose phreatic conditions and always determines a steady state groundwater flow. As long as the water table is not inclined, the phreatic and steady state calculations show the same results because no gradient is present (Krabbenhøft et al. 2016).

In order to compare the analysis based on an inclined phreatic water level with steady state groundwater flow conditions, some modifications in Optum G2 are needed. At each kink of the water table a hydrostatic pore water distribution along vertical lines is prescribed. As shown in Fig. 46c, the resulting pore water distribution is in very good agreement with the phreatic distribution of Plaxis 2D (Fig. 46a). The pore pressure distribution along the vertical lines does not show the appropriate scaling in Fig. 46c. Not

modifying the water pressure distribution would result in large FoS differences between the SRFEA and the FELA. Additional analyses attached to appendix 10.3.3 show results related to several water tables (without prescription of pore water pressures along lines).

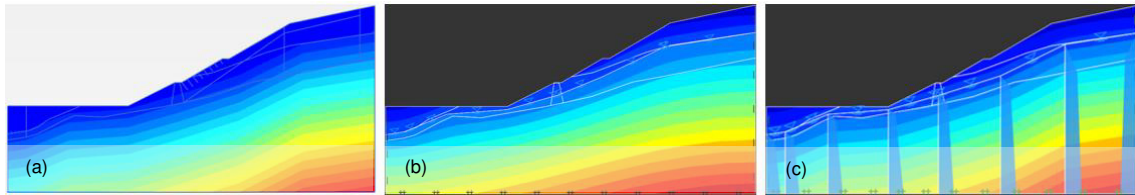


Fig. 46 Case 2 - Comparison of water pressure distributions: (a) Plaxis 2D with phreatic water table; (b) Optum G2 with steady state ground water flow; (c) Optum G2 with steady state ground water flow with modifications

The two discussed water tables are shown in Fig. 47. The black dashed line represents the original water table (used for case 1), whereas the red full line represents a long-term water lowering by horizontal drainage tubes installed above the berm.

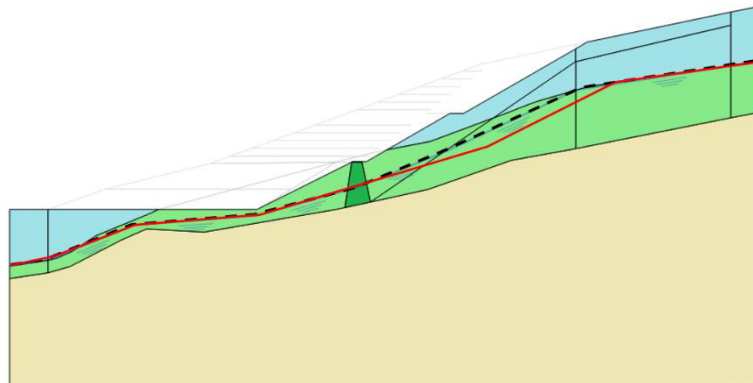


Fig. 47 Original water table (black dashed line), lowered water table (red full line)

Due to the changing conditions in the slope angle and removal of soil nails and geogrids, the failure mechanism changes. As shown in Fig. 48 and Fig. 49, the failure mechanism is shifted behind the pile trestle for both water tables. Moreover, one can see that the SRFEA and the FELA for both water tables fail in an analogous manner. The FELA and the SRFEA assuming associated plasticity present (as expected) a good agreement in the factor of safety (Tab. 19 and Tab. 20).

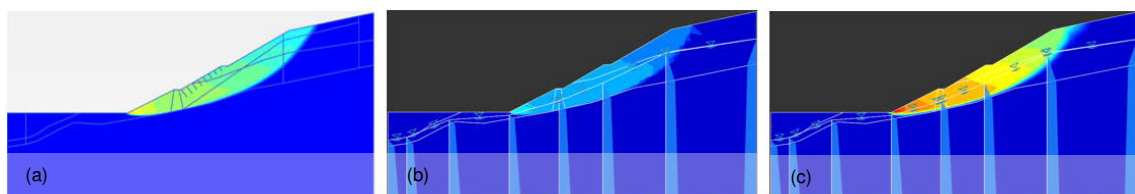


Fig. 48 Case 2 according to the original water table - total displacements: (a) SRFEA ($\psi' = \phi'$), (b) FELA lower-bound, (c) FELA upper-bound

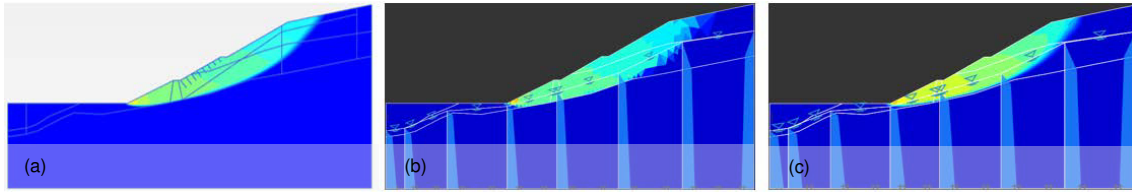


Fig. 49 Case 2 according to the lowered water table - total displacements: (a) SRFEA ($\psi' = \varphi'$), (b) FELA lower-bound, (c) FELA upper-bound

In addition, a non-associated SRFEA, Davis A and Davis B are applied to both the original and the lowered water table. For Davis B, the cohesion and friction angle are modified according to three iterative procedures. The results of adaptive mesh refinements in Optum G2 (Fig. 50b and Fig. 51b) present a higher mesh density along the slipping surface. Furthermore, the following two figures highlight that the failure mechanism of the SRFEA ($\psi' = 0^\circ$) is in good agreement with the failure mechanism of Davis B.

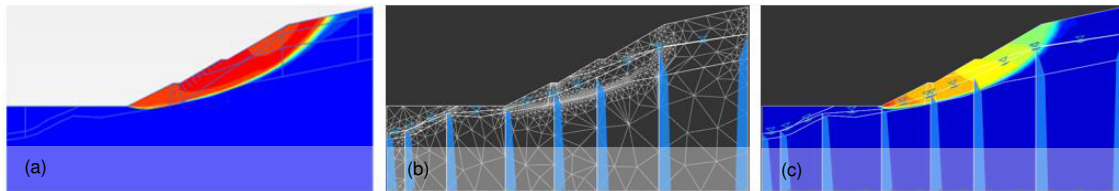


Fig. 50 Case 2 according to the original water table - total displacements: (a) SRFEA ($\psi' = 0^\circ$), (b) Davis B - FELA upper-bound mesh refinement, (c) Davis B - FELA upper-bound

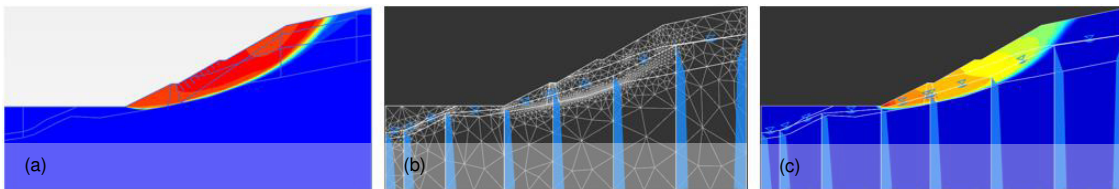


Fig. 51 Case 2 according to the lowered water table - total displacements: (a) SRFEA ($\psi' = 0^\circ$), (b) Davis B - FELA upper-bound mesh refinement, (c) Davis B - FELA upper-bound

By comparing the safety factors of Davis A and Davis B with a non-associated SRFEA, it becomes apparent that both are conservative, but the Davis B offers a better agreement with the calculation of Plaxis 2D (Tab. 21). Whereas procedure A deviates about 6.3 % to 7.6 % compared to the SRFEA, procedure B shows differences between 1.6 % and 1.7 %. It should be stressed that the lowering of the water table rises the FoS of the non-associated SRFEA at about 7.6 %.

Tab. 19 Case 2: Comparison of SRFEA

SRFEA			
	$\psi' = \varphi'$ Plaxis 2D	$\psi' = 0^\circ$ Plaxis 2D	Davis A ($\psi' = 0^\circ$) Plaxis 2D
FoS - original w. t.	1.29	1.19	1.10
FoS - lowered w. t.	1.38	1.28	1.16

Tab. 20 Case 2: Comparison of FELA

FELA			
	$\psi' = \varphi'$ Optum G2	Davis A ($\psi' = 0^\circ$) Optum G2	Davis B ($\psi' = 0^\circ$) Optum G2
FoS _{Mean} - original w. t.	1.31	1.12	1.17
FoS _{Mean} - lowered w. t.	1.39	1.19	1.26

Tab. 21 Case 2: Comparison of Davis A and Davis B with SRFEA ($\psi' = 0^\circ$)

% Difference		
	Davis A = 100 (FELA (Davis A) - SRFEA ($\psi' = 0^\circ$)) / FELA (Davis A)	Davis B = 100 (FELA (Davis B) - SRFEA ($\psi' = 0^\circ$)) / FELA (Davis B)
FoS - original w. t.	- 6.3	- 1.7
FoS - lowered w. t.	- 7.6	- 1.6

More safety analyses are performed on the upstream slope with modified water tables. Two studies including a horizontal water table and no water table are shown in appendix 10.3.3. Because no gradient arises in both cases, the SRFEA and the FELA are in good agreement without the need of prescribing the water pressure distribution along vertical lines.

5 Slope stability analyses based on six paper examples

5.1 Introduction

This chapter deals with six slope stability problems shown in *Slope stability analysis by finite elements* (Griffiths & Lane 1999). The paper's calculations are performed using 8-noded quadrilateral elements and a finite element program which is based on Program 6.2 (Smith & Griffith 1998). For all analyses, the authors assume plane strain conditions and neglect the formation of tension in the soil. A Mohr-Coulomb failure criterion is used for total and effective stress analyses whereby the latter assumes a dilatancy angle $\psi' = 0^\circ$. It should be noted that the initial stresses are calculated by gravity loading and, except for different water tables, no external forces are considered. Safety analyses are performed by reducing the strength parameters according to Eq. (20). If no global equilibrium and Mohr-Coulomb failure criterion are verified within a user-defined number of iteration steps, failure is assumed. Also, associated with this behaviour is a significant rise of nodal displacements (Griffiths & Lane 1999).

The six paper examples are subject of further analytical and numerical analyses. In addition to a SRFEA assuming a dilatancy angle $\psi' = 0^\circ$, *displacement-based finite element analyses* with associated plasticity are performed in Plaxis 2D and Optum G2. Again, it should be demonstrated that LEA are in good agreement with FELA and SRFEA, assuming associated plasticity. Moreover, the following calculations should prove that under certain conditions LEA end up with a different factor of safety. Again, Davis A and B are applied to all FELA. It is of main interest how well SRFEA assuming the modified strength parameters match with those calculations. Moreover, the paper examples shall continue to prove the better agreement of Davis B, compared to Davis A, with the non-associated calculations.

Given that all paper examples assume a dilatancy angle $\psi' = 0^\circ$, additional analyses are elaborated in section 5.8 with $\psi' \neq 0^\circ$ in order to prove the differences between Davis B and Davis C. Those results get compared with factors of safety that arise out of standard and user-defined SRFEA (see later).

5.2 Example 1

5.2.1 General information and paper results

The homogeneous slope is disposed 26.57° to the horizontal and has no foundation layer (Fig. 52). The soil body is characterized by a friction angle $\phi' = 20^\circ$, a dilatancy angle $\psi' = 0^\circ$ and the correlation $c' / \gamma H = 0.05$. Griffiths and Lane do not specify a Young's modulus E' and neither a Poisson's ratio ν and assert that elastic parameters do not have a big influence on the computed FoS. This statement will be discussed in detail later. The finite element analysis, using 200 quadrilateral elements leads to a safety factor equal to 1.40. A LEA, using Morgenstern & Price boundary conditions, shows a FoS = 1.38. (Griffiths & Lane 1999).

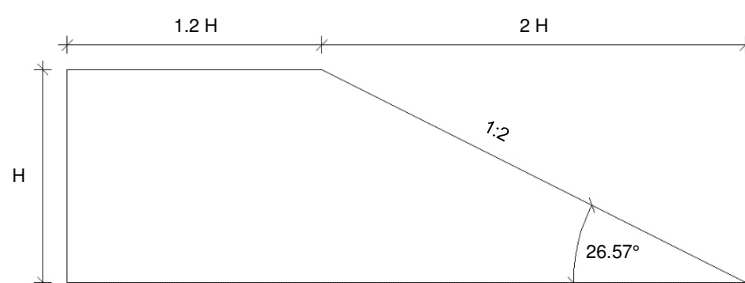


Fig. 52 Example 1: Geometry (according Griffiths & Lane 1999)

5.2.2 Slope stability analysis on example 1

Since the cohesion, unit-weight and height of the slope are not given precisely, four material sets are defined to prove the generalisation of the paper results, as long as the correlation $c' / \gamma H$ is equal to 0.05. The sets are listed in Tab. 22 and meet the mentioned correlation. In addition, it is of main interest how the factors of safety are affected by elastic parameters. Four different cases with varying standards are defined for each set. The Young's modulus E' differs between 10^4 and 10^6 kN/m², the Poisson's ratio ν between 0.25 and 0.35.

Tab. 22 Example 1: Set 1 - 4

Parameter	Unit	Set 1	Set 2	Set 3	Set 4
c'	(kN/m ²)	4	5	8	10
γ_{unsat}	(kN/m ³)	16	20	16	20
H	(m)	5	5	10	10

To evaluate the paper's result, both SRFEA with non-associated plasticity ($\psi' = 0^\circ$) and LEA in accordance to the Morgenstern & Price method are performed in Plaxis 2D and Slide. The numerical analyses are realized on a fine mesh and coarse mesh, both using 6-noded and 15-noded elements (Fig. 53). An overview of the calculations is listed in appendix 10.4.1. It is recognized that as long as the correlation $c' / \gamma H = 0.05$ is fulfilled, the FoS is not changing. The elastic parameters E' and ν do not affect the results for example 1. As shown in Fig. 53c and Fig. 53d, the failure mechanism is approximately the same for both meshes, while the shear band is defined more precise in the fine mesh.

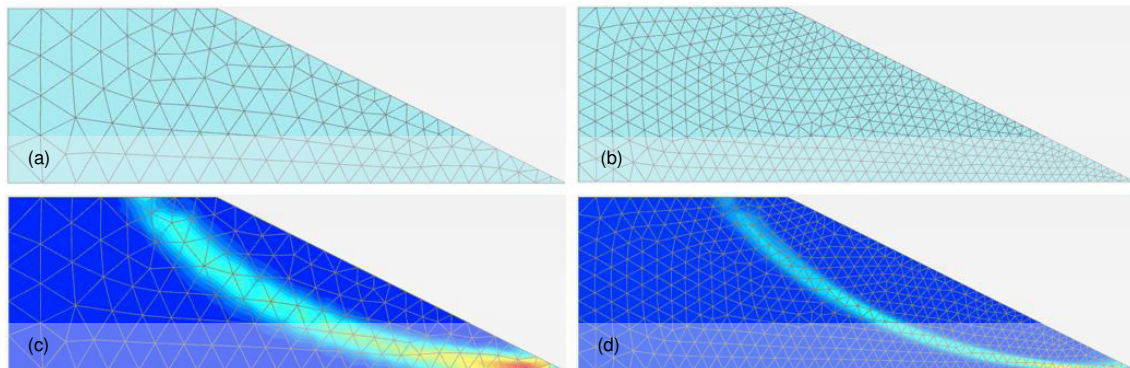


Fig. 53 Example 1: (a) coarse mesh (233 elements); (b) fine mesh (959 elements); (c) coarse mesh: total displacements after safety analysis; (d) fine mesh: total displacements after safety analysis

The FoS based on a LEA is in good agreement with the paper result, showing a difference of only 0.7 %. The SRFEA with the coarse mesh and 6-noded elements agrees the best with the papers calculations (Tab. 23).

Tab. 23 Example 1: SRFEA ($\psi' = 0^\circ$) and LEA results for $E' = 10^4$ kN/m² and $\nu = 0.25$

SRFEA ($\psi' = 0^\circ$)				LEA
Coarse mesh (233 elements)		Fine mesh (959 elements)		
15-noded	6-noded	15-noded	6-noded	Morgenstern & Price
1.35	1.39 (paper: 1.40)	1.35	1.36	1.37 (paper: 1.38)

Due to the fact that the safety factor is the same as long as the correlation $c' / \gamma H$ is equal to 0.05, further numerical studies using associated plasticity are performed for set 1 using a fine mesh with approximately 1000 elements. A look at the Tab. 24 shows that the SRFEA with 15-noded elements are in good agreement with the FELA, while the analyses using 6-noded elements show a slightly higher safety factor. The failure mechanism of the lower and upper bound FELA are presented in Fig. 54. It may be

mentioned that the distribution of incremental shear strains is in good agreement with the non-associated SRFEA.

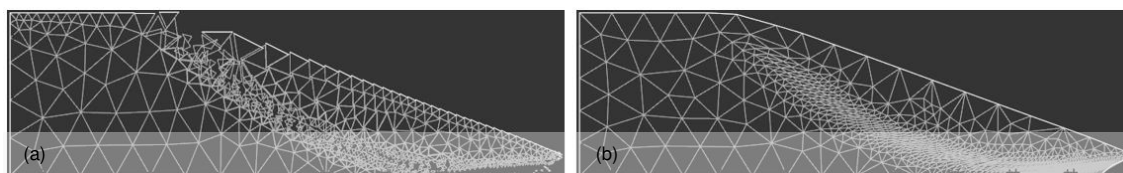


Fig. 54 Example 1: (a) FELA - lower-bound failure mechanism, (b) FELA - upper-bound failure mechanism

Tab. 24 Example 1: SRFEA ($\psi' = \phi'$) and FELA results for $E' = 10^4$ kN/m² and $\nu = 0.25$

Associated plasticity ($\psi' = \phi'$)			
	SRFEA Plaxis 2D	SRFEA Optum G2	FELA Optum G2
6-noded, *Lower	1.39	1.38	*1.36
15-noded, *Upper	1.38	1.37	*1.38
*Mean	-	-	*1.37

SRFEA and FELA with modified strength parameters, according to Davis A and Davis B, are in good agreement, as shown in Tab. 25. It should be pointed out that SRFEA with both 6-noded and 15-noded elements lead to approximately the same safety factor. When comparing those with SRFEA ($\psi' = 0^\circ$), it is obvious that both Davis approaches give lower safety factors with Davis B being less conservative. Davis A differs from the non-associated SRFEA about 3.9 % - 4.6 % while Davis B differs about 1.5 % - 2.3 %. To assist in understanding, the FoS_{Mean} (Davis A, Davis B), according to the FELA, gets compared with the 15-noded SRFEA ($\psi' = 0^\circ$) performed in Plaxis 2D (Tab. 26). All carried out calculations are listed in appendix 10.4.1.

Tab. 25 Example 1: Davis A and Davis B results for $E' = 10^4$ kN/m² and $\nu = 0.25$

Davis A ($\psi' = 0^\circ$), Davis B ($\psi' = 0^\circ$)					
	$\psi' = 0^\circ$ SRFEA Plaxis 2D	Davis A SRFEA Plaxis 2D	Davis B SRFEA Plaxis 2D	Davis A FELA Optum G2	Davis B FELA Optum G2
6-noded, *Lower	1.36	1.30	1.34	*1.28	*1.31
15-noded, *Upper	1.35	1.30	1.33	*1.30	*1.33
*Mean	-	-	-	*1.29	*1.32

Tab. 26 Example 1: Comparison of Davis A and Davis B with the SRFEA ($\psi' = 0^\circ$) for $E' = 10^4$ kN/m² and $\nu = 0.25$

% Difference		
	<i>Davis A</i>	<i>Davis B</i>
	= 100 (Davis A - SRFEA ($\psi' = 0^\circ$)) / Davis A	= 100 (Davis B - SRFEA ($\psi' = 0^\circ$)) / Davis B
<i>SRFEA_{6-noded}</i>		
Davis (SRFEA _{6-noded}) - SRFEA _{6-noded} ($\psi' = 0^\circ$)	- 4.6	- 1.5
<i>SRFEA_{15-noded}</i>		
Davis (SRFEA _{15-noded}) - SRFEA _{15-noded} ($\psi' = 0^\circ$)	- 3.9	- 1.5
<i>FELA</i>		
Davis (FELA _{Mean}) - SRFEA _{15-noded} ($\psi' = 0^\circ$)	- 4.7	- 2.3

5.3 Example 2

5.3.1 General information and paper results

For example 2, the slope of section 5.2 gets complemented by a foundation layer of thickness $H / 2$ ($D = 1.5$). The friction angle $\varphi' = 20^\circ$, the dilatancy angle $\psi' = 0^\circ$ and the correlation $c' / \gamma H = 0.05$ are given. Due to the foundation layer, the failure mechanisms of the *finite element* as well as the *limit equilibrium analysis* pass in both cases fractionally below the base of the slope. The safety factors remain unchanged (1.38 using the Morgenstern & Price method and 1.40 for the *finite element analysis*) (Griffiths & Lane 1999).

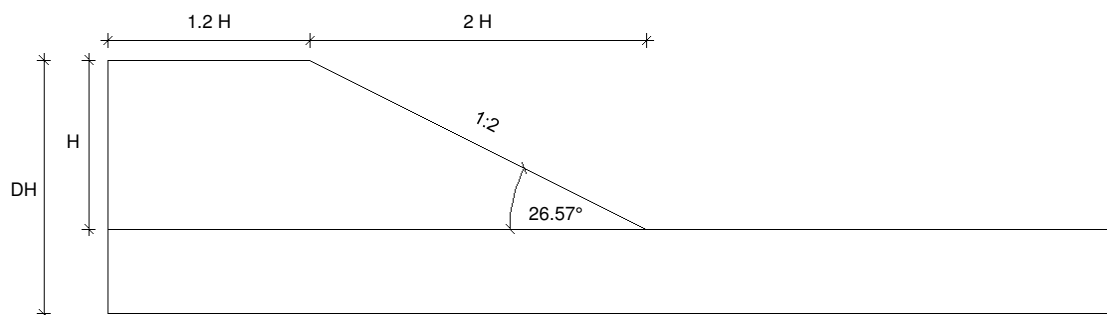


Fig. 55 Example 2: Geometry (according to Griffiths & Lane 1999)

5.3.2 Slope stability analysis on example 2

In a first step it was questioned if the 4 parameter sets, shown in Tab. 22, yield different safety factors. The reader is referred to appendix 10.4.2 for an overview of all performed analyses. It is recognized here too that as long as the correlation $c' / \gamma H = 0.05$ is fulfilled,

the FoS is not changing. Moreover, the Young’s modulus and Poisson’s ratio do not show any influence on the safety factor.

By looking at the following table, it becomes clear that the number of elements has an influence on the resulting safety factor. Simultaneously, the shape function is of decisive importance. The second column of Tab. 27 is in good agreement with the finite element paper result. The factor of safety stem from the LEA remains unchanged compared to example 1 and is equal to 1.37.

Tab. 27 Example 2: SRFEA ($\psi' = 0^\circ$) and LEA results for $E' = 10^4 \text{ kN/m}^2$ and $\nu = 0.25$

SRFEA ($\psi' = 0^\circ$)				LEA
Coarse mesh (254 elements)		Fine mesh (1004 elements)		
15-noded	6-noded	15-noded	6-noded	Morgenstern & Price
1.33	1.39 (paper: 1.40)	1.32	1.35	1.37 (paper: 1.38)

As Griffiths and Lane already demonstrated, the failure mechanism is changing slightly due to the additional foundation layer. One can observe at Fig. 56a that the distribution of incremental shear strains cuts the slope slightly below the base.

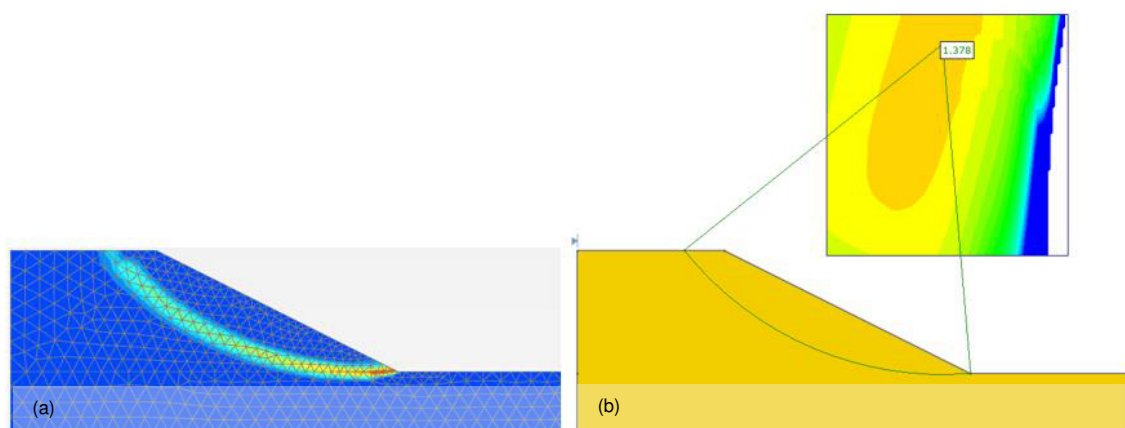


Fig. 56 Example 2: Failure mechanisms of SRFEA ($\psi' = 0^\circ$, fine mesh, 15-noded elements) (a) and LEA (b)

Comparing the averaged safety factor of FELA with SRFEA ($\psi' = 0^\circ$), it can be shown that analyses with 15-noded elements give exactly the same FoS. The calculations with 6-noded elements result in a slightly higher safety (Tab. 28).

Tab. 28 Example 2: SRFEA ($\psi' = \phi'$) and FELA results for $E' = 10^4 \text{ kN/m}^2$ and $\nu = 0.25$

Associated plasticity ($\psi' = \phi'$)			
	SRFEA Plaxis 2D	SRFEA Optum G2	FELA Optum G2
6-noded, *Lower	1.37	1.37	*1.35
15-noded, *Upper	1.36	1.36	*1.38
*Mean	-	-	*1.36

If we compare the non-associated SRFEA with Davis A and Davis B, it becomes clear that Davis B is less conservative compared to Davis A. Furthermore, Davis procedures in combination with SRFEA and 15-noded elements are in good agreement with FELA results (Tab. 29). It follows that the differences between Davis procedures and SRFEA with non-associated plasticity are the same (Tab. 30).

Tab. 29 Example 2: Davis A and Davis B results for $E' = 10^4 \text{ kN/m}^2$ and $\nu = 0.25$

Davis A ($\psi' = 0^\circ$), Davis B ($\psi' = 0^\circ$)					
	$\psi' = 0^\circ$ SRFEA Plaxis 2D	Davis A SRFEA Plaxis 2D	Davis B SRFEA Plaxis 2D	Davis A FELA Optum G2	Davis B FELA Optum G2
6-noded, *Lower	1.35	1.29	1.32	*1.27	*1.30
15-noded, *Upper	1.32	1.28	1.31	*1.29	*1.33
*Mean	-	-	-	*1.28	*1.31

Tab. 30 Example 2: Comparison of Davis A and Davis B with the SRFEA ($\psi' = 0^\circ$) for $E' = 10^4 \text{ kN/m}^2$ and $\nu = 0.25$

% Difference		
	Davis A = 100 (Davis A - SRFEA ($\psi' = 0^\circ$)) / Davis A	Davis B = 100 (Davis B - SRFEA ($\psi' = 0^\circ$)) / Davis B
SRFEA_{6-noded}		
Davis (SRFEA _{6-noded}) - SRFEA _{6-noded} ($\psi' = 0^\circ$)	- 4.7	- 2.3
SRFEA_{15-noded}		
Davis (SRFEA _{15-noded}) - SRFEA _{15-noded} ($\psi' = 0^\circ$)	- 3.1	- 0.8
FELA		
Davis (FELA _{Mean}) - SRFEA _{15-noded} ($\psi' = 0^\circ$)	- 3.1	- 0.8

5.4 Example 3

5.4.1 General information and paper results

Example 3 demonstrates slope stability analyses of an undrained clay with a thin weak layer. Instead of calculating with effective stresses, a total stress analysis using a Tresca failure criterion ($\phi_u = 0^\circ$) is presented. As shown in Fig. 57, the weak layer (c_{u2}) runs parallel to the slope (1:2) in the upper part, then it becomes horizontal in the foundation before it is redisposed at about 45° to the horizontal axis. The stability analysis is performed for several undrained shear strengths c_{u2} of the weak layer, while the strength of the surrounding material is kept constant and meets the correlation $c_{u1} / \gamma H = 0.25$ (Griffiths & Lane 1999).

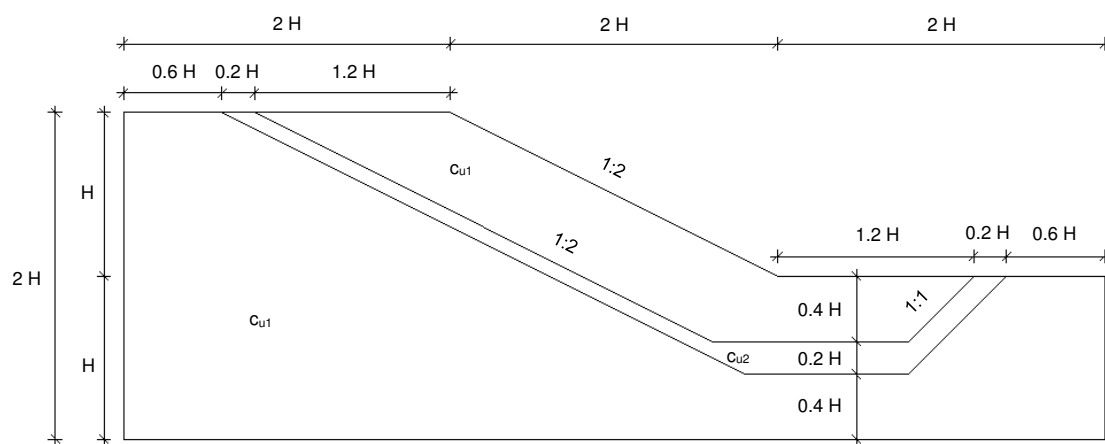


Fig. 57 Example 3: Geometry (according to Griffiths & Lane 1999)

A homogeneous slope ($c_{u1} = c_{u2}$) results in the expected circular failure mechanism. By gradually reducing the undrained shear strength c_{u2} in finite elements analysis, the failure mechanism changes and develops within the weak layer at a ratio of $c_{u2} / c_{u1} \approx 0.6$. In addition, LEA using Janbu's method are performed assuming both three-line wedge and circular failure mechanism. For $c_{u2} / c_{u1} > 0.6$, the behaviour is governed by the circular failure mechanism and is not significantly affected by the undrained shear strength of the thin layer. By dropping below the critical ratio, the linear failure mechanism along the thin layer takes over. The results illustrate the main disadvantage of LEA. If the failure mechanism is unknown *a priori*, the chosen shape might lead to an overestimation of safety (Griffiths & Lane 1999).

5.4.2 Slope stability analysis on example 3

The geometry of example 3 is subject for further analytical and numerical safety analyses. SRFEA using 6-noded as well as 15-noded elements are performed in both Plaxis 2D and Optum G2. The safety values get compared with FELA in a second step. In addition, LEA, based on Janbu (1954) and Morgenstern & Price (1965), are performed in Slide. For both methods, a circular and linear failure mechanism is investigated.

As shown in Tab. 31, four different parameter sets are considered to clarify if a variation of input parameters affects the resulting safety value. All four sets fulfil the correlation $c_{u1} / \gamma H = 0.25$. An undrained stiffness E_u equal to 5000 kN/m² as well as 7000 kN/m² is used for the calculations. As shown in appendix 10.4.3, the result is not affected by the variation of the input parameters as long as the correlation $c_{u1} / \gamma H = 0.25$ holds.

Tab. 31 Example 3: Set 1 - 4

Parameter	Unit	Set 1	Set 2	Set 3	Set 4
c_{u1}	(kN/m ²)	20	25	40	50
γ_{unsat}	(kN/m ³)	16	20	16	20
H	(m)	5	5	10	10

The parameter set 1 with an undrained stiffness $E_u = 5000$ kN/m² is used for further comparisons of SRFEA and FELA. It should be noted that the initial phase in Plaxis 2D, determined by gravity loading, does not satisfy the equilibrium for c_{u2} / c_{u1} ratios smaller than 0.5. Thereby an error message cancels the initial stress analysis because $M_{stage} = 1$ cannot be achieved and in consequence the $FoS < 1$. As can be seen in Tab. 32, there is a good agreement between 15-noded SRFEA and FELA. The safety analyses with 6-noded elements show a slightly higher safety factor. See Fig. 58 for a graphical representation of Tab. 32. It is obvious that the gradient of the curves is changing at a ratio of $c_{u2} / c_{u1} \approx 0.6$. For small differences between both undrained shear strengths, the failure mechanism remains circular (Fig. 59). By dropping below the critical ratio of $c_{u2} / c_{u1} \approx 0.6$, another failure mechanism along the thin layer forms and determines the safety factor.

Tab. 32 Example 3: SRFEA and FELA results for set 1 and $E_u = 5000 \text{ kN/m}^2$

Parameter	SRFEA Plaxis 2D		SRFEA Optum G2		FELA Optum G2		
	15-n	6-n	15-n	6-n	Lower	Upper	Mean
c_{u2} / c_{u1}							
1	1.46	1.47	1.45	1.46	1.44	1.46	1.45
0.9	1.44	1.45	1.43	1.44	1.42	1.45	1.44
0.8	1.42	1.44	1.41	1.42	1.40	1.43	1.42
0.7	1.39	1.41	1.39	1.40	1.37	1.41	1.39
0.6	1.36	1.38	1.36	1.37	1.34	1.38	1.36
0.5	1.17	1.24	1.17	1.20	1.15	1.20	1.17
0.4	-	1.01	0.95	0.97	0.93	0.98	0.95
0.3	-	-	0.72	0.75	0.71	0.75	0.73
0.2	-	-	0.50	0.51	0.49	0.52	0.50
0.1	-	-	0.27	0.28	0.26	0.28	0.27

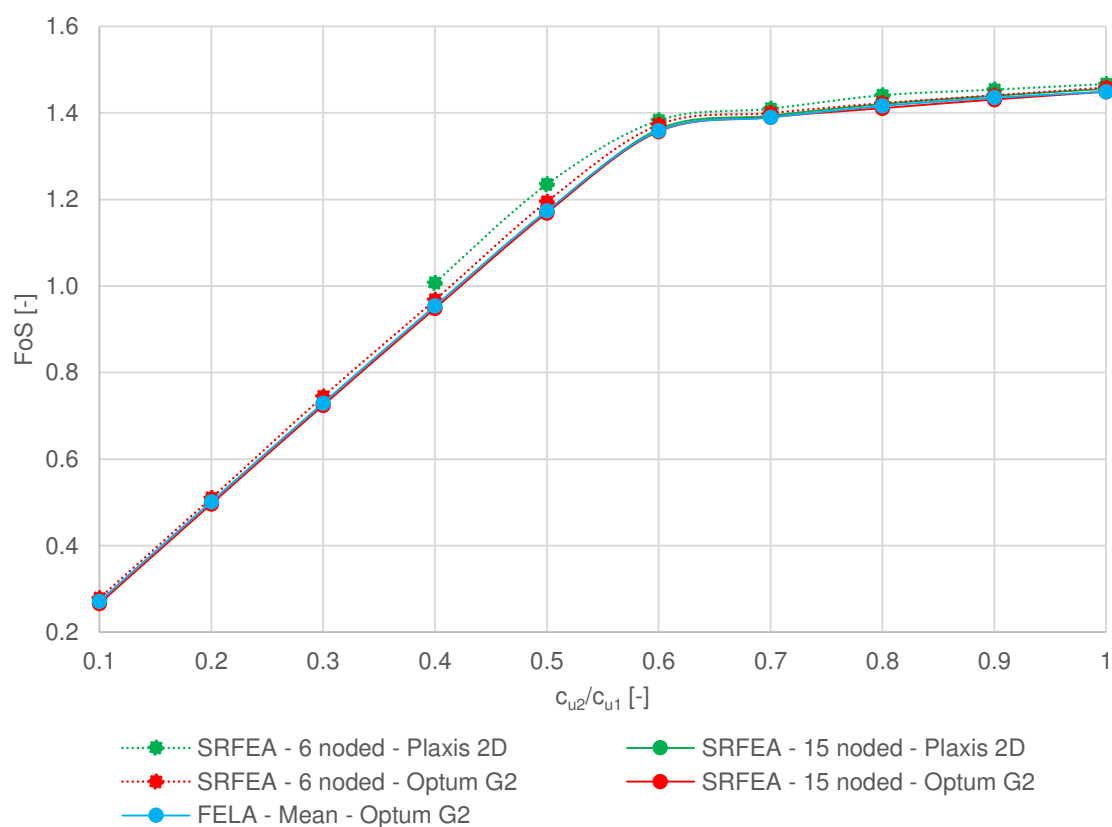


Fig. 58 Example 3: Comparison of SRFEA and FELA results

The change in failure mechanism is shown for three different ratios of undrained shear strength in Fig. 59, Fig. 60 and Fig. 61.

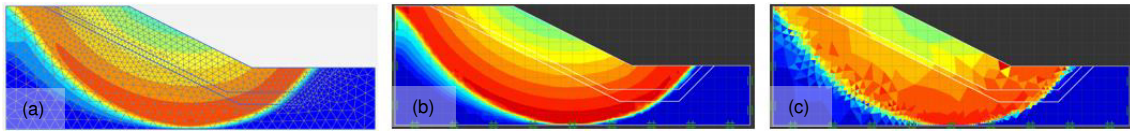


Fig. 59 Example 3 with $c_{u2} / c_{u1} = 1$: (a) SRFEA - Plaxis 2D; (b) SRFEA - Optum G2; (c) FELA, lower bound - Optum G2

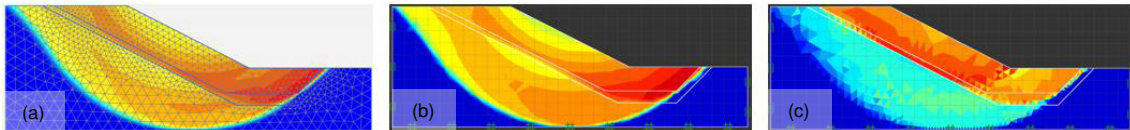


Fig. 60 Example 3 with $c_{u2} / c_{u1} = 0.6$: (a) SRFEA - Plaxis 2D; (b) SRFEA - Optum G2; (c) FELA, lower bound - Optum G2

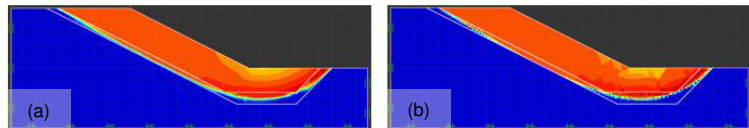


Fig. 61 Example 3 with $c_{u2} / c_{u1} = 0.2$: (a) SRFEA - Optum G2; (b) FELA, lower bound - Optum G2

Additionally, LEA are performed according to Morgenstern & Price and Janbu's simplified methods. Slide offers the possibility to define a circular as well as a three line wedge (linear) failure mechanism for both methods. Without any knowledge about the failure mechanisms, both options can lead to an overestimation of the safety (Fig. 62).

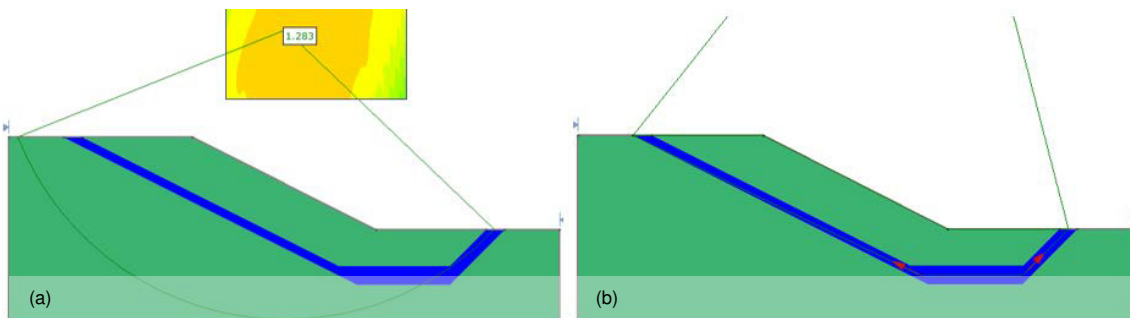


Fig. 62 Example 3 with $c_{u2} / c_{u1} = 0.4$: (a) Circular failure leads to a FoS = 1.28; (b) three line wedge leads to a FoS = 0.92

Above the critical ratio of $c_{u2} / c_{u1} \approx 0.6$, the failure mechanism is governed by a circular shape, while below it the three line wedge provides the appropriate mechanism. To conclude, the Morgenstern & Price method, compared to Janbu's method, leads to safety values which are in better agreement with FELA (Fig. 63).

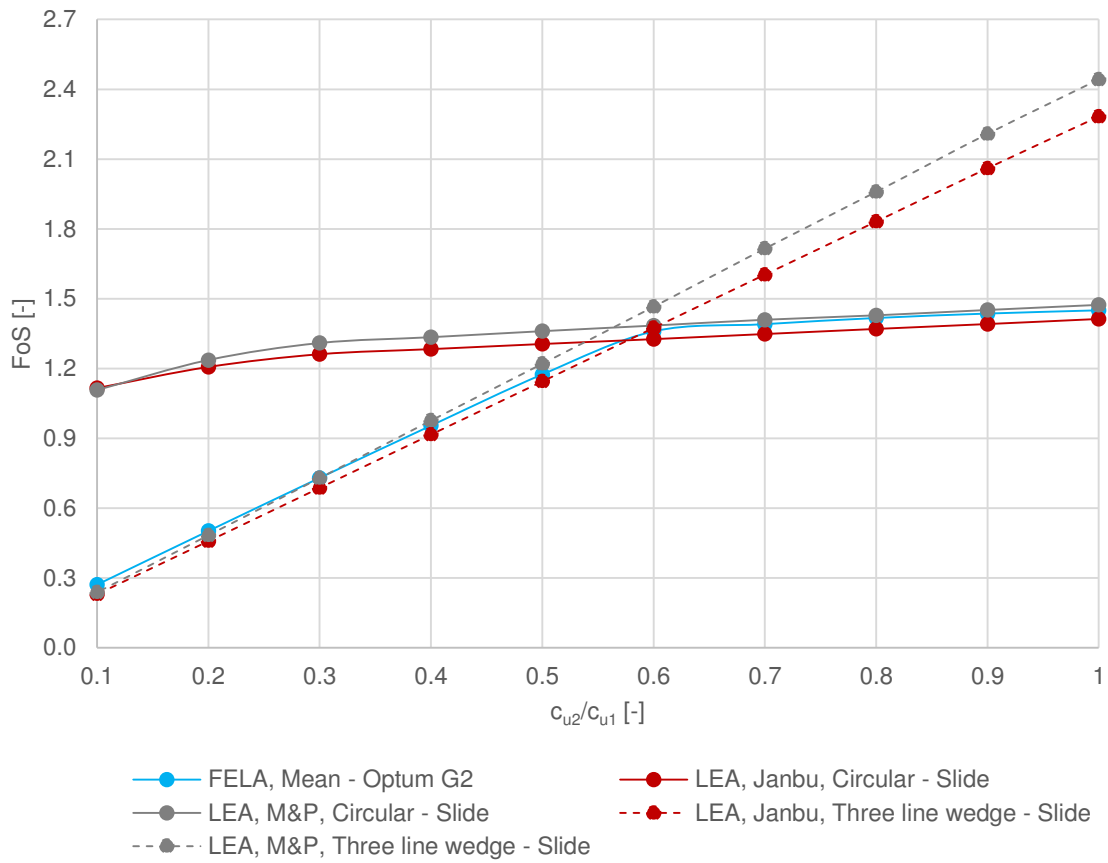


Fig. 63 Example 3: Comparison of FELA and LEA results

5.5 Example 4

5.5.1 General information and paper results

For example 4, the same geometry is used as in example 3, with the lack of the weak layer. However, a foundation layer with the undrained shear strength c_{u2} is taken into account (Fig. 64). For all analyses, $c_{u1} / \gamma H = 0.25$ holds true, while c_{u2} gets decreased stepwise. For $c_{u2} \gg c_{u1}$, a shallow failure mechanism cutting through the toe of the slope is observed, while for $c_{u2} \ll c_{u1}$, a deep-seated mechanism is developed. Griffiths and Lane come to the conclusion that the change in failure mechanism occurs approximately at a ratio of $c_{u2} / c_{u1} \approx 1.5$ for both FEA and LEA (Griffiths & Lane 1999).

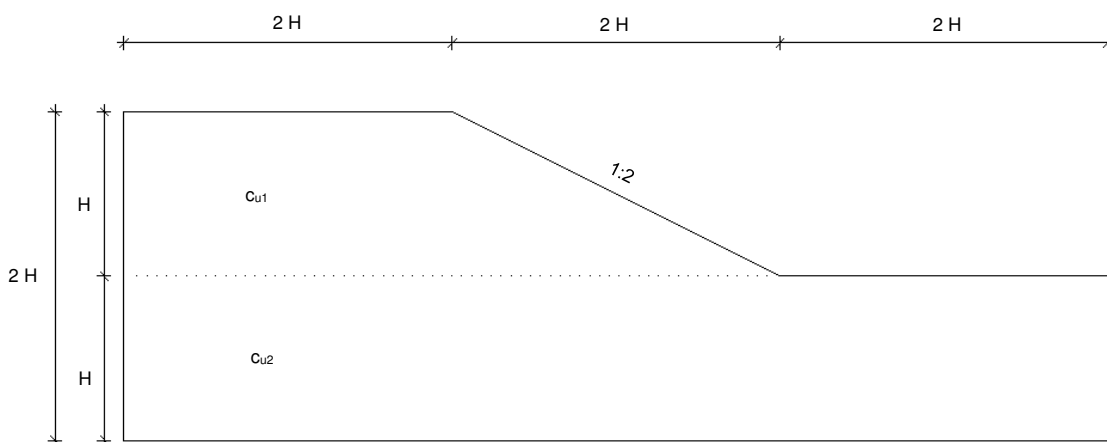


Fig. 64 Example 4: Geometry (according to Griffiths & Lane 1999)

5.5.2 Slope stability analysis on example 4

In this case, the calculations carried out in example 3 are performed, with the difference that the LEA is used with a circular failure mechanism and Morgenstern & Price method only. Appendix 10.4.4 proves that the variation of input parameters is not affecting the factor of safety as long as the correlation $c_{u1} / \gamma H = 0.25$ holds. Furthermore, the variation of undrained stiffness E_u does not affect the safety factors.

The parameter set 1 (Tab. 31) with an undrained stiffness of $E_u = 5000 \text{ kN/m}^2$ is used for further comparisons of SRFEA and FELA. Initial phases in Plaxis 2D, determined by gravity loading, do not satisfy an equilibrium for c_{u2} / c_{u1} ratios smaller than 0.75. As mentioned in the previous section, the FoS becomes smaller than 1 (for $c_{u2} / c_{u1} < 0.75$). The following table shows that the safety factors according to FELA and SRFEA are in good agreement. Again, the 6-noded strength reduction analyses result in slightly higher safety values. It's obvious, however, that the safety factors of all analyses fall faster when dropping below $c_{u2} / c_{u1} \approx 1.5$. For ratios larger than 1.5, the safety factor remains almost

constant, because the shallow failure mechanism does not interact with the foundation layer. This connection becomes clear by looking at Fig. 65, Fig. 66 and Fig. 67. By undercutting $c_{u2} / c_{u1} \approx 1.5$, another deep seated failure mechanism arises. With a further decrease of the undrained shear strength c_{u2} , the shallow failure mechanism disappears (Fig. 67).

Tab. 33 Example 4: SRFEA and FELA results for set 1 and $E_u = 5000 \text{ kN/m}^2$

Parameter	SRFEA Plaxis 2D		SRFEA Optum G2		FELA Optum G2		
	15-n	6-n	15-n	6-n	Lower	Upper	Mean
c_{u2} / c_{u1}							
4	2.04	2.07	2.02	2.05	1.99	2.05	2.02
3.5	2.04	2.07	2.02	2.04	1.99	2.05	2.02
3	2.04	2.07	2.02	2.04	1.99	2.05	2.02
2.5	2.04	2.07	2.02	2.04	1.99	2.05	2.02
2	2.04	2.07	2.02	2.04	1.99	2.05	2.02
1.5	2.02	2.04	2.02	2.04	1.99	2.05	2.02
1	1.46	1.47	1.45	1.46	1.44	1.46	1.45
0.75	1.15	1.17	1.15	1.16	1.14	1.16	1.15
0.5	-	-	0.85	0.86	0.84	0.86	0.85
0.25	-	-	0.54	0.55	0.53	0.55	0.54

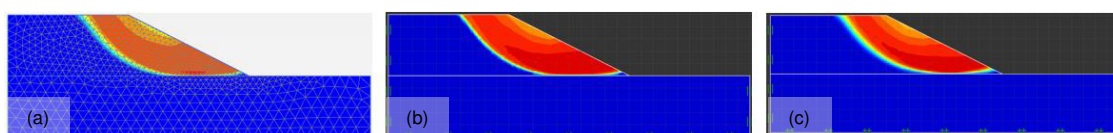


Fig. 65 Example 4 with $c_{u2} / c_{u1} = 2$: (a) SRFEA - Plaxis 2D; (b) SRFEA - Optum G2; (c) FELA, upper bound - Optum G2

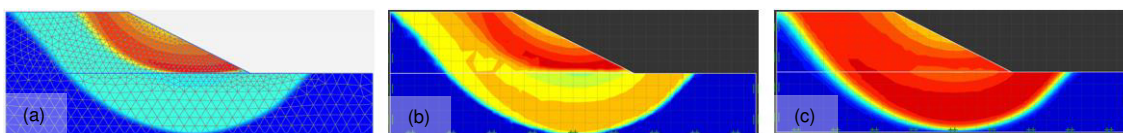


Fig. 66 Example 4 with $c_{u2} / c_{u1} = 1.5$: (a) SRFEA - Plaxis 2D; (b) SRFEA - Optum G2; (c) FELA, upper bound - Optum G2

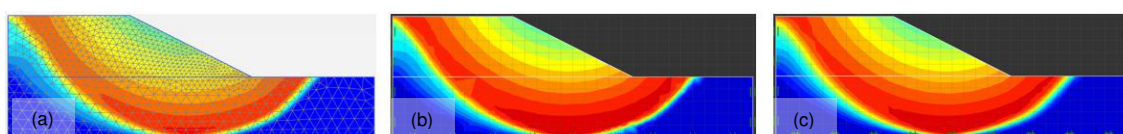


Fig. 67 Example 4 with $c_{u2} / c_{u1} = 0.75$: (a) SRFEA - Optum G2; (b) FELA, upper bound - Optum G2

In addition, limit equilibrium analyses (Morgenstern & Price) get determined for several c_{u2} / c_{u1} ratios. Fig. 68 shows that 15-noded SRFEA, FELA and LEA are in good agreement with each other.

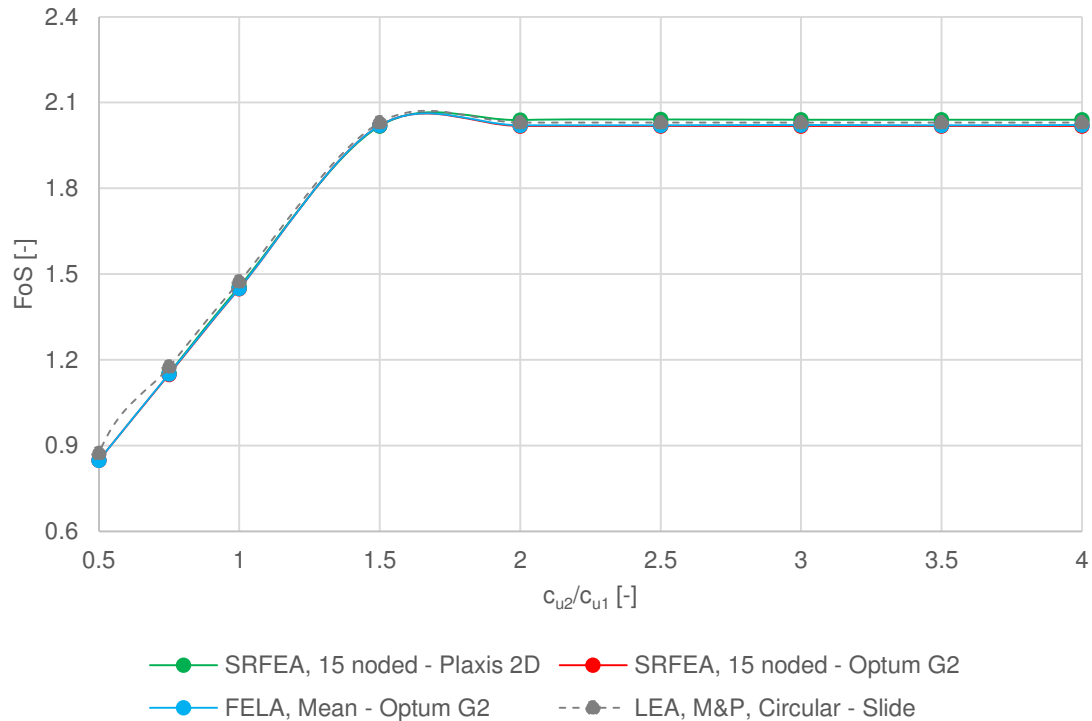


Fig. 68 Example 4: Comparison of FELA, SRFEA and LEA results

5.6 Example 5

5.6.1 General information and paper results

A homogeneous slope without foundation layer, disposed to the horizontal with 26.57° (1:2), is the object of example 5 analyses. Several horizontal water tables with a vertical distance L from the crest get analysed (Fig. 69) in order to detect which L / H ratio provides the lowest safety (Griffiths & Lane 1999).

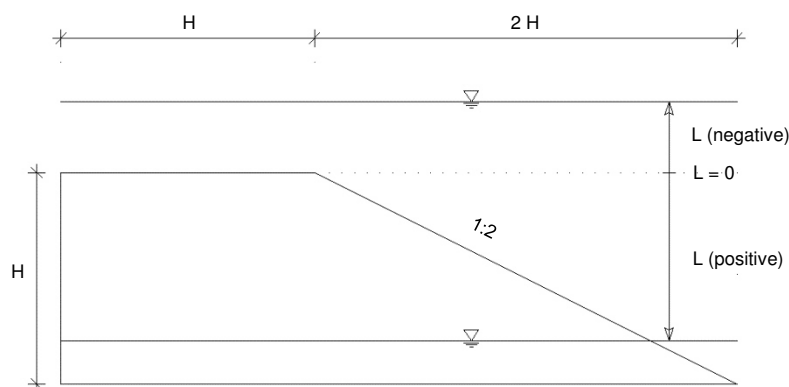


Fig. 69 Example 5: Geometry (according to Griffiths & Lane 1999)

The problem can be seen as a slow drawdown process where the water table is initially defined above the crest ($L / H = -0.2$) and gets lowered to the base ($L / H = 1$). An effective stress analysis with friction angle $\varphi' = 20^\circ$, dilatancy angle $\psi' = 0^\circ$ and $c' / \gamma H = 0.05$ provides the lowest FoS ≈ 1.3 when $L / H \approx 0.7$. The constant cohesive strength of the slope and the changing relation of soil weight and shear strength due to the drawdown process are responsible for this behaviour. As long as $L / H < 0.7$, the increased frictional strength of the soil has a proportionally smaller stabilizing effect than the increased unit weight. For larger ratios ($L / H > 0.7$), the frictional strength has a greater influence compared to the increased unit weight, therefore the safety factor rises again. A *limit equilibrium analysis* and a *finite element analysis* show that the FoS = 1.85 remains constant for $L / H < 0$. As discussed in example 1, analyses without any free surface ($L / H = 1$) lead to a FoS ≈ 1.4 (Griffiths & Lane 1999).

5.6.2 Slope stability analysis on example 5

Due to the fact that the cohesion c' , the unit-weight γ and the height H are given by the correlation $c' / \gamma H = 0.05$, the six parameter sets shown in Tab. 34 are object to SRFEA with non-associated plasticity ($\psi' = 0^\circ$) while using 6-noded elements in Plaxis 2D. The safety factors for the different L / H ratios are listed in appendix 10.4.5.

Tab. 34 Example 5: Set 1 - 6

Parameter	Unit	Set 1	Set 2	Set 3	Set 4	Set 5	Set 6
c'	(kN/m ²)	4	5	6	8	10	12
$\gamma_{unsat} = \gamma_{sat}$	(kN/m ³)	16	20	24	16	20	24
H	(m)	5	5	5	10	10	10

Fig. 70 shows that, as long as the unit-weight is kept constant and the correlation is equal to 0.05, the other two input parameters can be modified and no change in the safety factor occurs. The parameter sets 2 and 5, with minimum and maximum safety factors equal to 1.28 and 1.83, show the best accordance with the paper results. The slight differences between the results of set 2 and the ones stated in the paper can be deduced from a higher number of elements in Plaxis 2D.

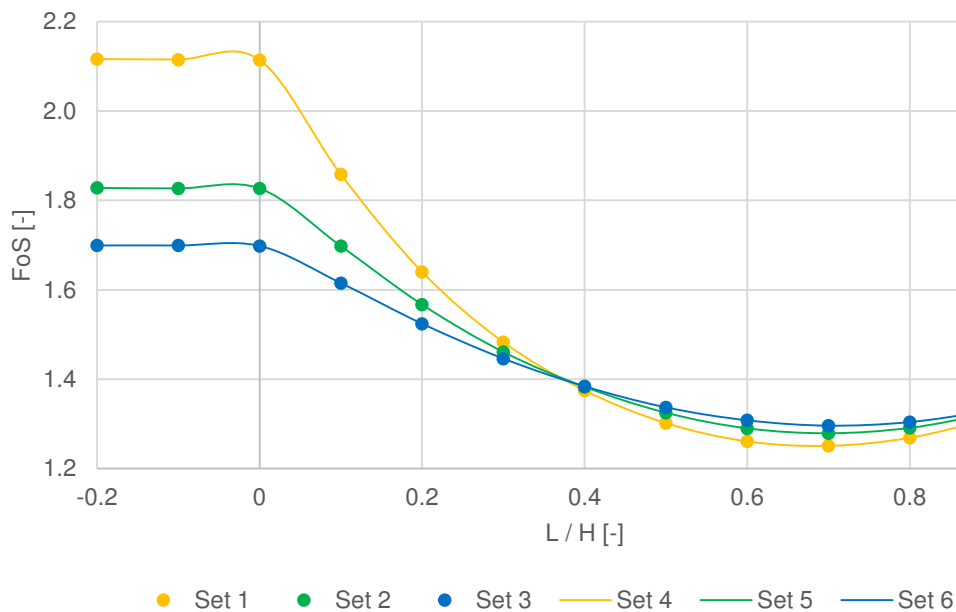


Fig. 70 Example 5: Comparison of SRFEA ($\psi' = 0^\circ$, 6-noded elements)

The following calculations are performed with parameter set 2. SRFEA with associated plasticity are in good agreement with FELA. In this connection, it is worthwhile to mention that the calculations with 6-noded elements give a slightly higher FoS. An overview of the discussed calculations can be found in appendix 10.4.5. In addition, LEA are carried out to highlight that the Morgenstern & Price method is in good agreement with *finite element analyses* ($\psi' = \varphi'$). A closer look at Fig. 71 and Fig. 72 confirm this.

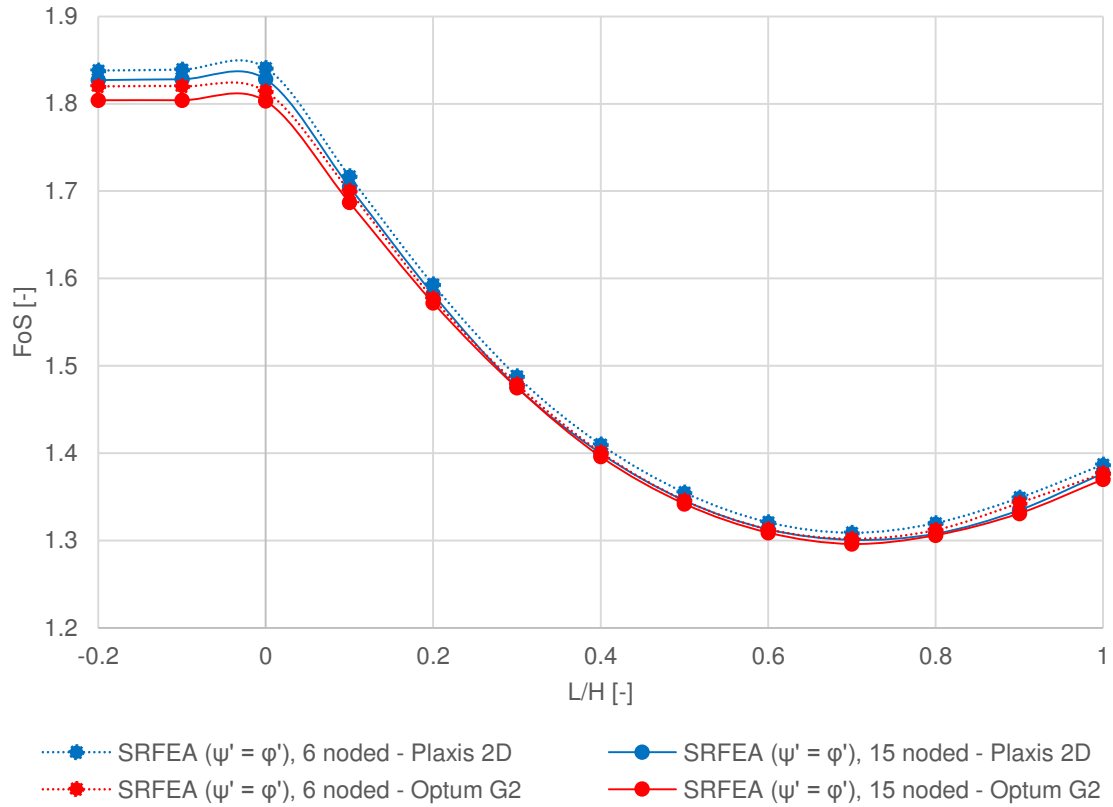


Fig. 71 Example 5: Comparison of SRFEA ($\psi' = \varphi'$) results

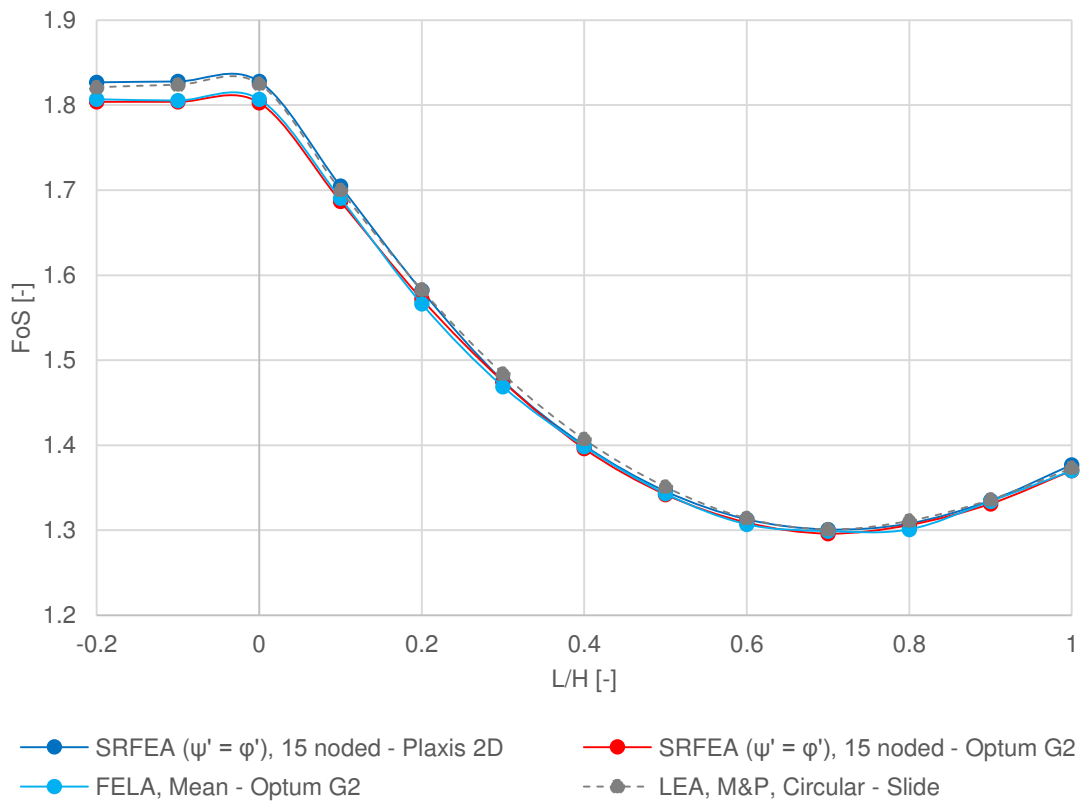


Fig. 72 Example 5: Comparison of SRFEA ($\psi' = \varphi'$), FELA and LEA results

Next, it shall be analysed how well Davis A and Davis B agree with the non-associated calculations performed in Plaxis 2D. As Tab. 35 shows, Davis A as well as Davis B (according to FELA) agree better with the 15-noded analyses. As mentioned before for associated plasticity, 6-noded analyses show a slightly higher FoS.

Tab. 35 Example 5: Comparison of Davis A and Davis B results with SRFEA ($\psi' = 0^\circ$)

Davis A ($\psi' = 0^\circ$), Davis B ($\psi' = 0^\circ$)

Parameter	$\psi' = 0^\circ$ SRFEA Plaxis 2D		Davis A SRFEA Plaxis 2D		Davis B SRFEA Optum G2		Davis A FELA Optum G2	Davis B FELA Optum G2
	15-n	6-n	15-n	6-n	15-n	6-n	Mean	Mean
- 0.2	1.81	1.83	1.72	1.73	1.79	1.80	1.70	1.77
- 0.1	1.81	1.83	1.72	1.73	1.79	1.81	1.70	1.77
0.0	1.81	1.83	1.72	1.73	1.79	1.80	1.70	1.76
0.1	1.68	1.70	1.60	1.62	1.67	1.68	1.59	1.65
0.2	1.55	1.57	1.49	1.50	1.54	1.55	1.48	1.53
0.3	1.44	1.46	1.39	1.40	1.43	1.44	1.38	1.43
0.4	1.36	1.38	1.32	1.33	1.35	1.36	1.31	1.35
0.5	1.30	1.33	1.27	1.27	1.30	1.31	1.26	1.29
0.6	1.27	1.29	1.23	1.24	1.26	1.27	1.23	1.26
0.7	1.26	1.28	1.22	1.23	1.25	1.26	1.22	1.24
0.8	1.27	1.29	1.23	1.24	1.26	1.27	1.23	1.26
0.9	1.30	1.32	1.26	1.27	1.29	1.30	1.25	1.29
1.0	1.35	1.36	1.30	1.30	1.33	1.34	1.29	1.32

Fig. 73, Fig. 74 and Fig. 75 demonstrate the conservativeness of the original and enhanced Davis approach compared to SRFEA ($\psi' = 0^\circ$). It is recognizable that Davis B clearly agrees better with non-associated analyses. When comparing both Davis approaches, according to FELA with non-associated SRFEA, it can be seen that Davis A differs at a maximum of 6.5 % while Davis B is at 2.5 %.

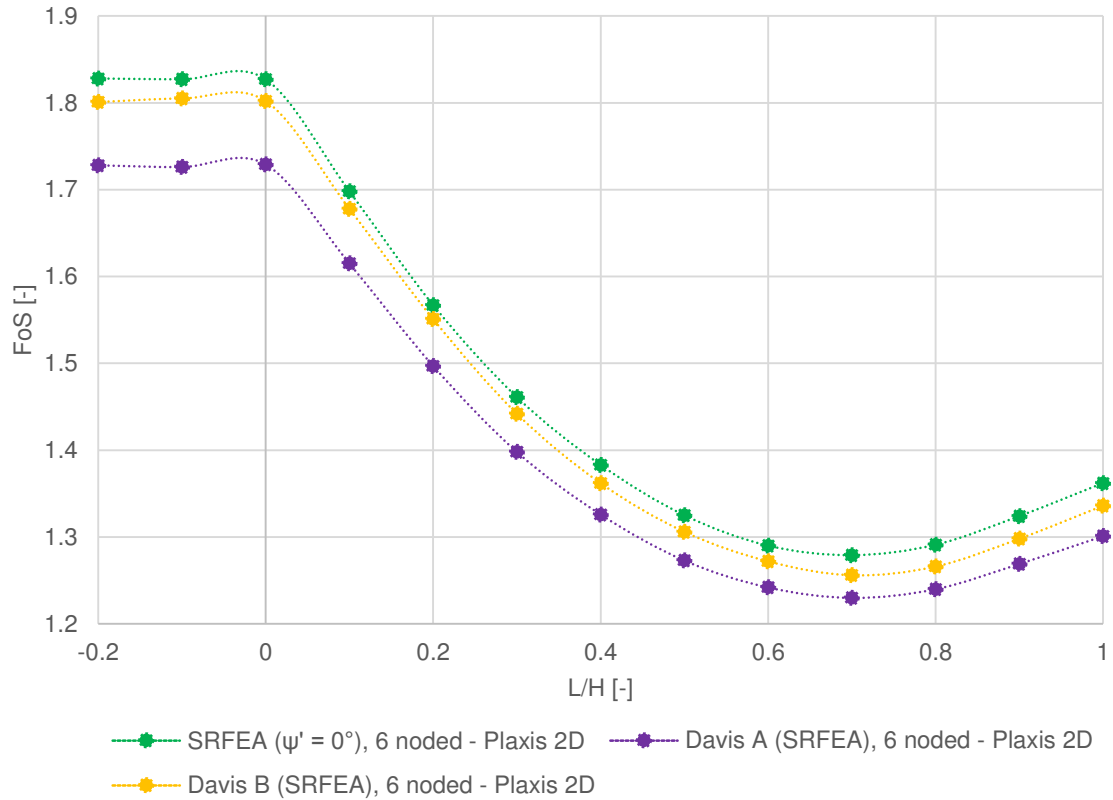


Fig. 73 Example 5 - SRFEA, 6-noded: Comparison of Davis approaches and SRFEA ($\psi' = 0^\circ$)

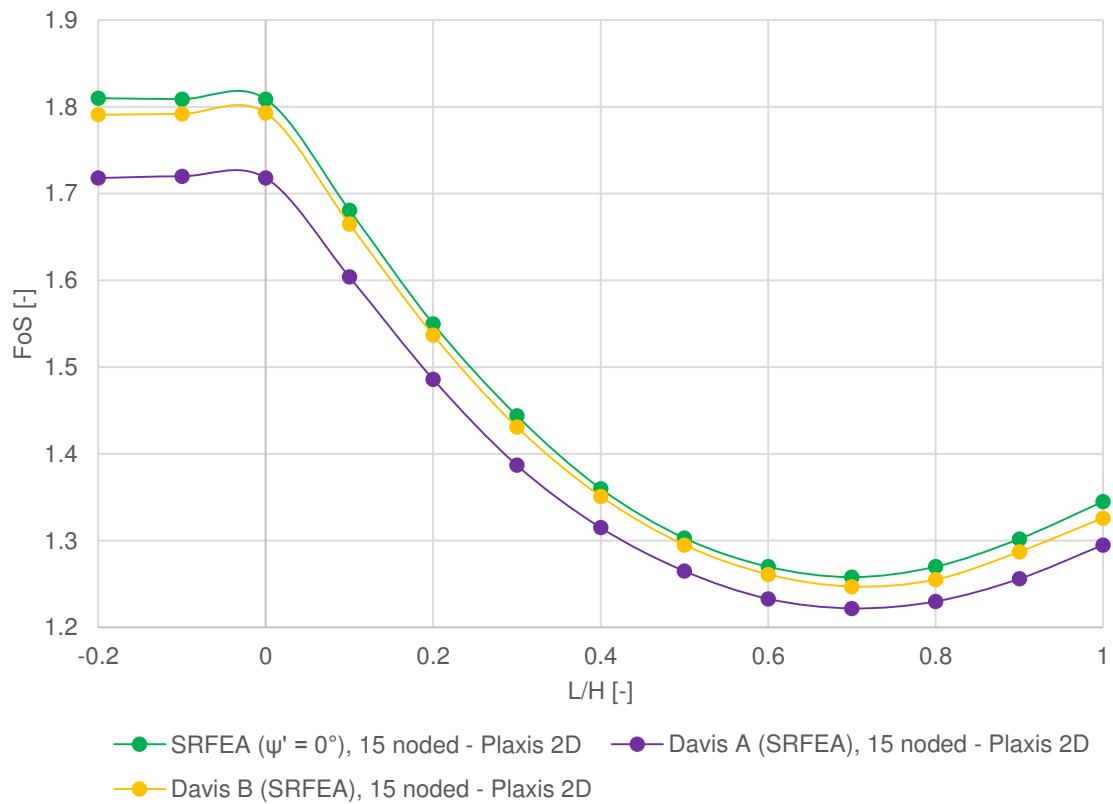


Fig. 74 Example 5 - SRFEA, 15-noded: Comparison of Davis approaches and SRFEA ($\psi' = 0^\circ$)

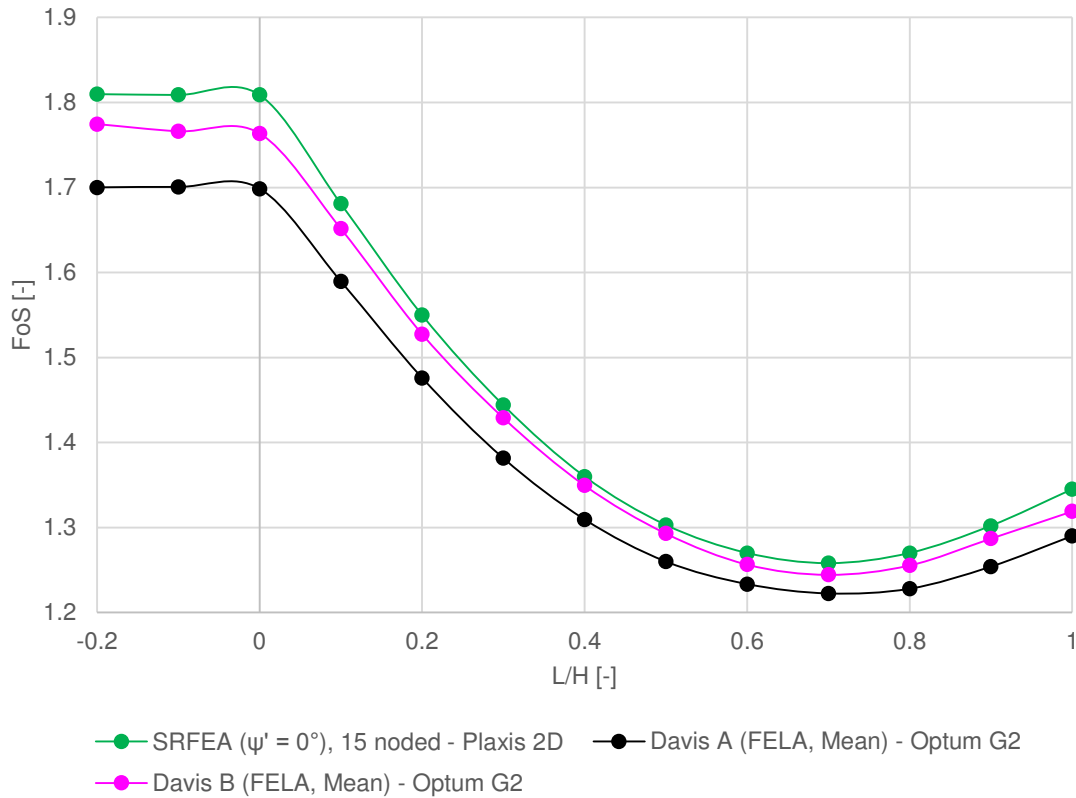


Fig. 75 Example 5 - FELA: Comparison of Davis approaches and SRFEA ($\psi' = 0^\circ$)

5.7 Example 6

5.7.1 General information and paper results

A two-side earth embankment including a free (water) surface is object of these numerical and analytical analyses. The downstream slope is disposed about 23° to the horizontal and slightly steeper than the upstream slope. The homogeneous embankment is characterized by a friction angle $\varphi' = 37^\circ$, a dilatancy angle $\psi' = 0^\circ$, a cohesion $c' = 13.8 \text{ kN/m}^2$ and an unit-weight $\gamma_{\text{unsat}} = \gamma_{\text{sat}} = 18.2 \text{ kN/m}^3$. The *limit equilibrium analysis* leads to a safety factor equal to 1.90 while considering a free (water) surface, as it is shown in Fig. 76. A second case without any free surface gives a FoS = 2.42.

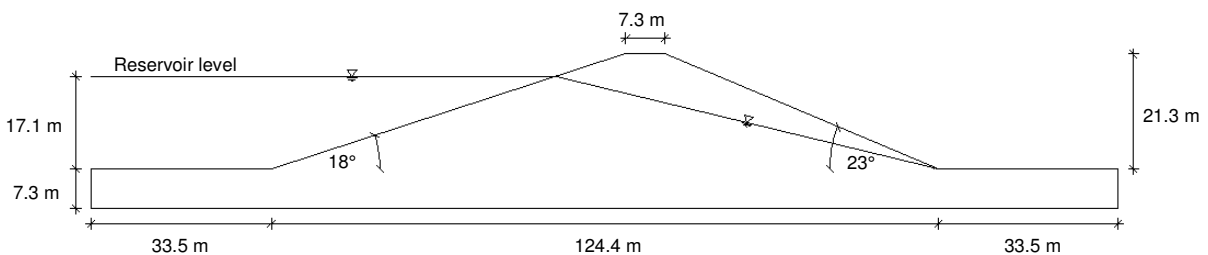


Fig. 76 Example 6: Geometry (according to Griffiths & Lane 1999)

The failure occurs for both cases on the steeper slope, whereby the corresponding failure mechanisms are slightly different. A toe failure is shown for case 2 while a deeper mechanism (cutting through the foundation layer) occurs when the free surface is considered (Griffiths & Lane 1999).

5.7.2 Slope stability analysis on example 6

The results of SRFEA, FELA and LEA will be discussed in this chapter. The two cases are considered separately. Due to the fact that both elastic parameters E' and ν are not given, the calculations are performed for Poisson's ratios $\nu_1 = 0.25$ and $\nu_2 = 0.35$. As shown in appendix 10.4.6, both sets lead to the same safety values. The Young's modulus is thereby kept constant ($E' = 10^4 \text{ kN/m}^2$), because no influence on the safety factor was determined in previous analyses. It should be noted that the results for ν_1 get discussed in this chapter.

The LEA with the Morgenstern & Price method, assuming a circular failure mechanism, leads to a FoS = 2.46, which differs approximately 1.7 % from the paper's result. Tab. 36 shows that numerical analyses, assuming associated plasticity, are in good agreement with the analytical results. The safety factors, which result from SRFEA with 6-noded elements, give higher values of 1.2 %. The failure mechanism going through the toe of the slope is shown in Fig. 77 for all SRFEA ($\psi' = \phi'$), FELA and LEA.

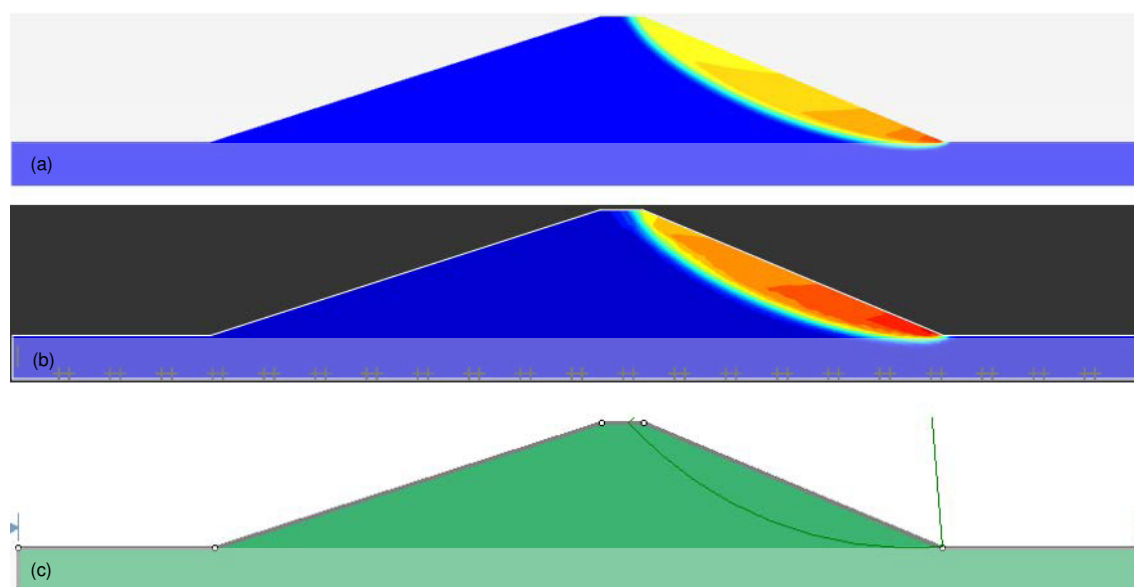


Fig. 77 Example 6 without free surface – failure mechanism: Comparison of SRFEA ($\psi' = \phi'$) with 15-noded elements (a), FELA (b) and LEA (c)

Furthermore, SRFEA in accordance with non-associated plasticity get performed with 6- as well as 15-noded elements. By comparing those safety values with Davis A and B results, it is obvious that the original Davis is way more conservative compared to the

enhanced one. Procedure A provides 20.4 % to 21.8 % lower safety factors compared to the non-associated SRFEA. On the other hand, procedure B is in very good agreement with the mentioned analyses, showing differences of 0.9 % to 2.1 % (Tab. 38).

Tab. 36 Example 6 without free surface: Comparison of SRFEA ($\psi' = \varphi'$) and FELA

Associated plasticity ($\psi' = \varphi'$)			
	SRFEA Plaxis 2D	SRFEA Optum G2	FELA Optum G2
6-noded, *Lower	2.47	2.47	*2.43
15-noded, *Upper	2.45	2.44	*2.49
*Mean	-	-	*2.46

Tab. 37 Example 6 without free surface: Comparison of Davis A and Davis B

Davis A ($\psi' = 0^\circ$), Davis B ($\psi' = 0^\circ$)					
	$\psi' = 0^\circ$ SRFEA Plaxis 2D	Davis A SRFEA Plaxis 2D	Davis B SRFEA Plaxis 2D	Davis A FELA Optum G2	Davis B FELA Optum G2
6-noded, *Lower	2.40	1.97	2.35	*1.94	*2.31
15-noded, *Upper	2.36	1.96	2.33	*1.98	*2.37
*Mean	-	-	-	*1.96	*2.34

Tab. 38 Example 6 without free surface: Comparison of Davis A and Davis B with SRFEA ($\psi' = 0^\circ$)

% Difference		
	Davis A = 100 (Davis A - SRFEA ($\psi' = 0^\circ$)) / Davis A	Davis B = 100 (Davis B - SRFEA ($\psi' = 0^\circ$)) / Davis B
SRFEA _{6-noded} Davis (SRFEA _{6-noded}) - SRFEA _{6-noded} ($\psi' = 0^\circ$)	- 21.8	- 2.1
SRFEA _{15-noded} Davis (SRFEA _{15-noded}) - SRFEA _{15-noded} ($\psi' = 0^\circ$)	- 20.4	- 1.3
FELA Davis (FELA _{Mean}) - SRFEA _{15-noded} ($\psi' = 0^\circ$)	- 20.4	- 0.9

For case 2, the same calculations are performed with an additional free surface. As mentioned in the previous chapter, the failure mechanism changes due to the defined

water table. It follows a deeper failure mechanism which cuts through the foundation layer, as shown in Fig. 78. The LEA, performed with the Morgenstern & Price method, results in a FoS = 1.92 and is in good agreement with associated *finite element analyses* shown in Tab. 39. It should be noted that SRFEA with 15-noded elements performed in Plaxis 2D result in slightly lower safety values, differing from LEA about 1.5 %.

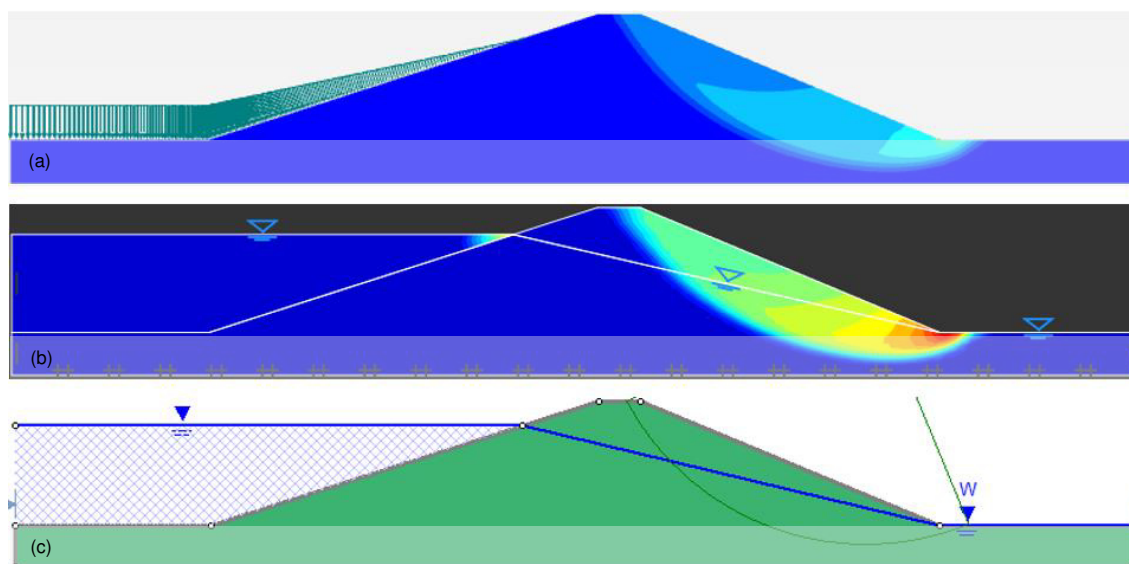


Fig. 78 Example 6 with free surface – failure mechanism: Comparison of SRFEA ($\psi' = \phi'$) with 15-noded elements (a), FELA (b) and LEA (c)

Tab. 39 Example 6 with free surface: Comparison of SRFEA ($\psi' = \phi'$) and FELA

Associated plasticity ($\psi' = \phi'$)			
	SRFEA <i>Plaxis 2D</i>	SRFEA <i>Optum G2</i>	FELA <i>Optum G2</i>
6-noded, *Lower	1.91	1.93	*1.91
15-noded, *Upper	1.90	1.92	*1.94
*Mean	-	-	*1.92

As can be seen from Tab. 40 and Tab. 41, Davis B results differ about 1.7 % to 6.9 % from non-associated analyses, whereby the calculations according to 6-noded elements deviated the most. Again, Davis A gives very conservative results.

This example is used to show one possible problem while performing the Davis approach. SRFEA may lead to different failure mechanisms, when performing associated or non-associated analyses. In such cases, Davis A and B might provide the same mechanism as SRFEA with an associated flow rule. For example 6, the failure mechanism near the top of the embankment differs from analyses with an associated

and one with a non-associated flow rule. From Fig. 79, it is apparent that the failure mechanism according to Davis B is in good agreement with SRFEA ($\psi' = \phi'$).

Tab. 40 Example 6 with free surface: Comparison of Davis A and Davis B

Davis A ($\psi' = 0^\circ$), Davis B ($\psi' = 0^\circ$)					
	$\psi' = 0^\circ$	Davis A	Davis B	Davis A	Davis B
	SRFEA	SRFEA	SRFEA	FELA	FELA
	Plaxis 2D	Plaxis 2D	Plaxis 2D	Optum G2	Optum G2
6-noded, *Lower	1.87	1.52	1.75	*1.52	*1.76
15-noded, *Upper	1.80	1.52	1.75	*1.55	*1.79
*Mean	-	-	-	*1.53	*1.77

Tab. 41 Example 6 with free surface: Comparison of Davis A and Davis B with SRFEA ($\psi' = 0^\circ$)

% Difference		
	Davis A	Davis B
	= 100 (Davis A - SRFEA ($\psi' = 0^\circ$)) / Davis A	= 100 (Davis B - SRFEA ($\psi' = 0^\circ$)) / Davis B
SRFEA _{6-noded} Davis (SRFEA _{6-noded}) - SRFEA _{6-noded} ($\psi' = 0^\circ$)	- 23.0	- 6.9
SRFEA _{15-noded} Davis (SRFEA _{15-noded}) - SRFEA _{15-noded} ($\psi' = 0^\circ$)	- 18.4	- 2.9
FELA Davis (FELA _{Mean}) - SRFEA _{15-noded} ($\psi' = 0^\circ$)	- 17.6	- 1.7

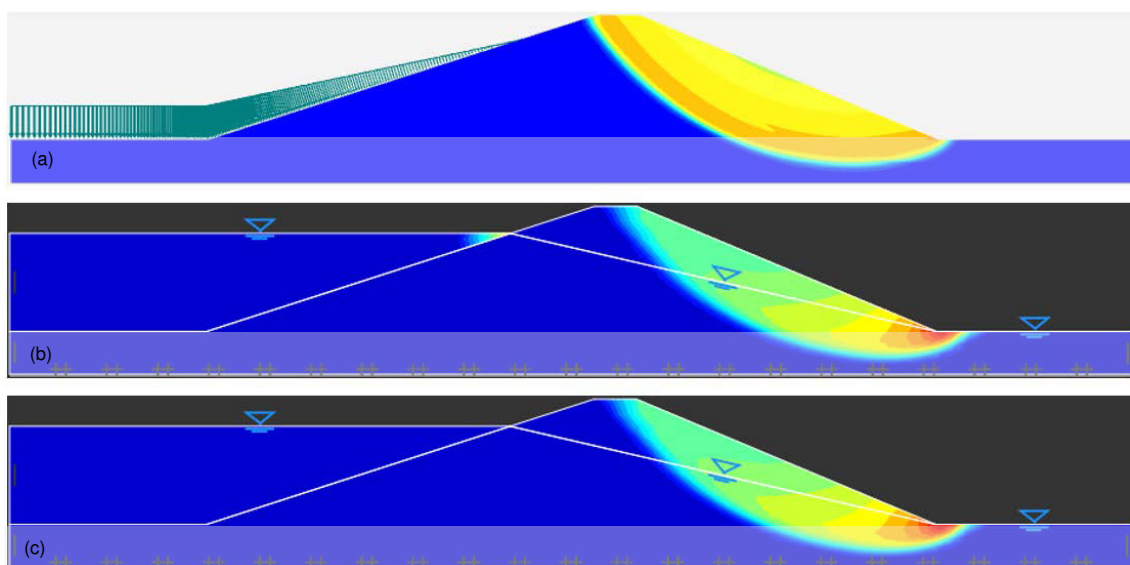


Fig. 79 Example 6 with free surface – failure mechanism: Comparison of SRFEA ($\psi' = 0^\circ$) (a), FELA (b) and FELA with Davis B ($\psi' = 0^\circ$) parameters (c)

5.8 Comparison of Davis A, Davis B and Davis C

5.8.1 General information

All slope stability analyses up to this point were performed either with associated plasticity or a dilatancy angle $\psi' = 0^\circ$. For Davis procedures B and C, the latter provide the same safety factors. For a better understanding, please refer to section 3.3.3. It has been demonstrated that procedures A and B supply conservative results.

Two geometries are used to elaborate how the effective friction angle φ' , the degree of non-associativity $\Lambda = \varphi' - \psi'$ and the cohesion c' influence the differences between Davis and non-associated SRFEA. Particular emphasis is given to the comparison of Davis B and Davis C. While procedure B is simultaneously modifying the friction angle φ' and dilatancy angle ψ' , the latter one is kept constant for procedures A and C. Therefore, Davis A and C will be compared with the standard strength reduction of Plaxis 2D, whereby the dilatancy angle ψ' is kept constant until the reduced effective friction angle φ'_{red} is the same. Thereupon, both get concurrently reduced. Since the friction angle and dilatancy angle get reduced at the same time, Davis B is compared with a user-defined strength reduction. All SRFEA are performed in Plaxis 2D with gravity loading as the initial phase.

5.8.2 Study 1: Variation of φ' and Λ

The study consists of two different geometries. *Slope 1* is disposed 26.57° (1:2) to the horizontal, while *slope 2* is inclined by 45° . The dimensions for both cases are shown in Fig. 80.

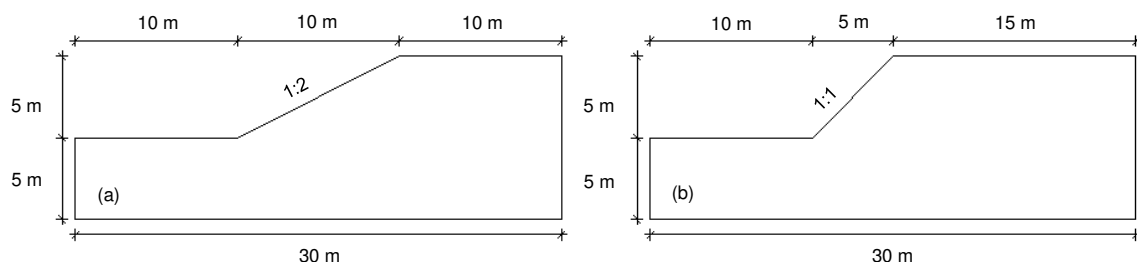


Fig. 80 Geometry of slope 1 (a) and slope 2 (b)

The homogeneous slopes are characterized by a unit-weight of $\gamma_{unsat} = 16 \text{ kN/m}^3$. However, the cohesion for both cases is different. A complete overview of the soil parameters is listed in Tab. 42. The dilatancy angle (equal to friction angle) gets reduced in intervals of five, until zero is reached. This is done for the effective friction angles φ'_1

= 25°, $\varphi'_2 = 30^\circ$, $\varphi'_3 = 35^\circ$ and $\varphi'_4 = 40^\circ$. The safety values of SRFEA are listed in appendix 10.4.7.

Tab. 42 Study 1: Soil properties

Soil parameters	Unit	Slope 1	Slope 2
Constitutive model	-	Mohr-Coulomb	Mohr-Coulomb
γ_{unsat}	(kN/m ³)	16	16
c'	(kN/m ²)	2	5
φ'	(°)	25; 30; 35; 40	25; 30; 35; 40
ψ'	(°)	φ' ; $\varphi' - n \cdot 5$; 0°	φ' ; $\varphi' - n \cdot 5$; 0°

5.8.3 Study 2: Variation of c' and λ for $\varphi' = 30^\circ$

Slope 1 is disposed 26.57° to the horizontal and will be subject to further investigations. Study 2 tries to figure out how cohesion influences the difference between Davis calculations and non-associated SRFEA. For this purpose, the effective friction angle $\varphi' = 30^\circ$ is kept constant, while the cohesion will vary between 0 and 10 kPa (Tab. 43). Again, Davis A, B and C get compared with standard as well as user-defined SRFEA. The calculations are listed in appendix 10.4.7.

Tab. 43 Study 2 - soil properties

Soil parameters	Unit	Slope 1
Constitutive model	-	Mohr-Coulomb
γ_{unsat}	(kN/m ³)	16
c'	(kN/m ²)	0; 2; 5; 10
φ'	(°)	30
ψ'	(°)	φ' ; $\varphi' - n \cdot 5$; 0°

At this point, it should be noted that Davis C might supply wrong results. It has been mentioned in Tab. 3 that in certain circumstances the reduced effective friction angle according to Davis φ^* can become smaller than ψ' . Since such a state makes no sense, $\varphi^* \geq \psi'$ has to be ensured. If one considers for example a friction angle $\varphi' = 35^\circ$, a cohesion $c' = 2$ kPa and the geometry of slope 1, Fig. 81 shows that for $\Lambda < 15^\circ$ the FoS

decreases significantly with decreasing degree of non-associativity (pink dashed line). This goes back to the fact that the reduced friction angle φ^* is smaller than the dilatancy angle ψ' for $\Lambda < 15^\circ$. The results of Davis C analyses, presented in chapter 5.8.4, are modified by a simple cut-off criterion to fulfil the condition $\varphi^* \geq \psi'$.

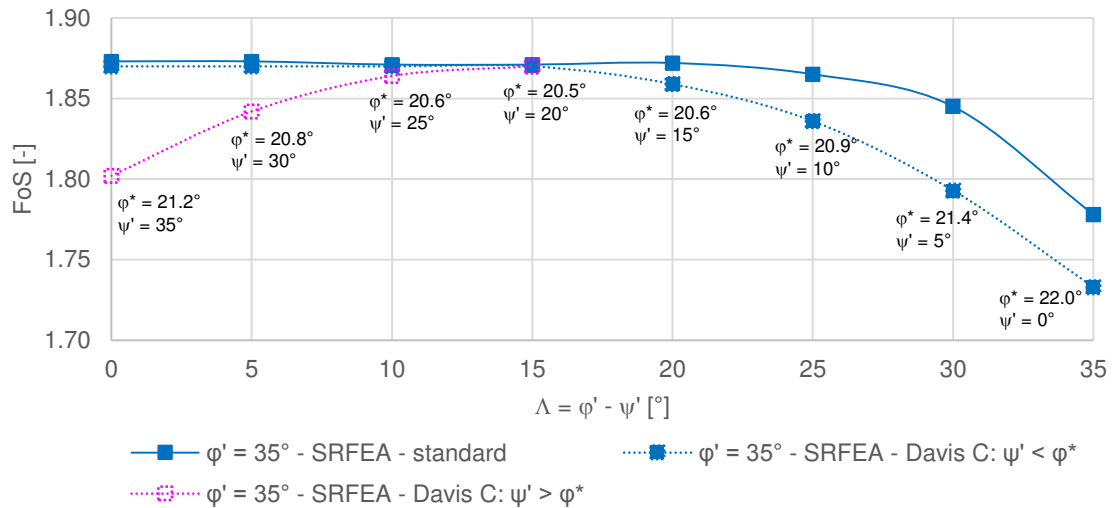


Fig. 81 Range where modification of Davis C is required to ensure $\varphi^* \geq \psi'$

5.8.4 Comparison of the results

The results are shown for *slope 1*. All statements are valid for *slope 2* as well.

At Fig. 82, it becomes clear that standard and user-defined SRFEA as well as Davis B and Davis C supply the same results for a dilatancy angle $\psi' = 0^\circ$. Section 3.3.3 explains the reasons for this. Furthermore, it becomes clear that, with an increasing degree of non-associativity ($\Lambda = \varphi' - \psi'$), the differences between all Davis approaches and standard or user-defined SRFEA become larger. Fig. 82 illustrates that with an increasing friction angle φ' those differences become significantly larger for Davis A, while differences for Davis B and C do not rise as much. As a result, the differences between the original Davis and the enhanced procedures increase. In order to gain a better understanding of this relations, Tab. 44 and Tab. 45 summarize the results for several effective friction angles, always assuming a dilatancy angle $\psi' = 0^\circ$. If one considers two extreme cases with effective friction angles φ' equal to either 25° or 40° , the differences between Davis A and standard SRFEA increase from - 5.7 % to - 24.6 %, while Davis B's rise from - 1.6 % to - 4.0 %. Hence, the differences between Davis A and Davis B rise from - 4.1 % to - 19.8 %. The results for the dilatancy angles $\psi' \geq 0^\circ$ are listed in appendix 10.4.7.

The differences between Davis B and user-defined SRFEA as well as the differences between Davis C and standard SRFEA show approximately the same values. In Fig. 83, it becomes obvious that the blue and green dashed lines have got a good correlation. The black dashed *Reference* lines represent the standard and user-defined SRFEA results. Starting from there the differences are added in the positive direction. For a better view different *Reference* values are chosen for the friction angles $\varphi' = 25^\circ - 40^\circ$.

Tab. 44 Study 1 - slope 1 ($c' = 2$ kPa): Comparison of SRFEA ($\psi' = 0^\circ$), Davis A and Davis B

SRFEA ($\psi' = 0^\circ$), Davis A, Davis B

<i>Effective friction angle φ'</i>	<i>Standard SRFEA Plaxis 2D</i>	<i>Davis A Plaxis 2D</i>	<i>Davis B Plaxis 2D</i>
$\varphi' = 25^\circ$	1.29	1.22	1.27
$\varphi' = 30^\circ$	1.55	1.39	1.49
$\varphi' = 35^\circ$	1.78	1.53	1.73
$\varphi' = 40^\circ$	2.08	1.67	2.00

Tab. 45 Study 1 - slope 1 ($c' = 2$ kPa): Comparison of Davis A and Davis B with SRFEA ($\psi' = 0^\circ$)

% Difference

<i>Effective friction angle φ'</i>	<i>Davis A vs. SRFEA = 100 (Davis A - SRFEA ($\psi' = 0^\circ$)) / Davis A</i>	<i>Davis B vs. SRFEA = 100 (Davis B - SRFEA ($\psi' = 0^\circ$)) / Davis B</i>	<i>Davis A vs. Davis B = 100 (Davis A - Davis B) / Davis A</i>
$\varphi' = 25^\circ$	- 5.7	- 1.6	- 4.1
$\varphi' = 30^\circ$	- 11.5	- 4.0	- 7.2
$\varphi' = 35^\circ$	- 16.3	- 2.9	- 13.1
$\varphi' = 40^\circ$	- 24.6	- 4.0	- 19.8

Study 2 demonstrates similar results as study 1. Keeping the friction angle constant and varying the cohesion between 0 and 10 kN/m² leads to the conclusion that with increasing cohesion Davis A becomes more conservative compared to the standard strength reduction. As it can be seen in Fig. 84 and Fig. 85, Davis B and Davis C are not strongly affected by the variation of cohesion. Again, the differences between Davis B and user-defined SRFEA as well as the differences between Davis C and standard

strength reductions are approximately the same. Despite the change of non-associativity λ , the green and blue dashed lines do match well in Fig. 85.

In conclusion, it can be said that the larger the friction angle φ' , the cohesion c' and the degree of non-associativity λ are set, the larger the differences between Davis A and standard SRFEA get. It should be noted that the differences between Davis B and user-defined SRFEA as well as Davis C and standard SRFEA are approximately the same. Both differences are not strongly affected by the cohesion c' and the friction angle φ' .

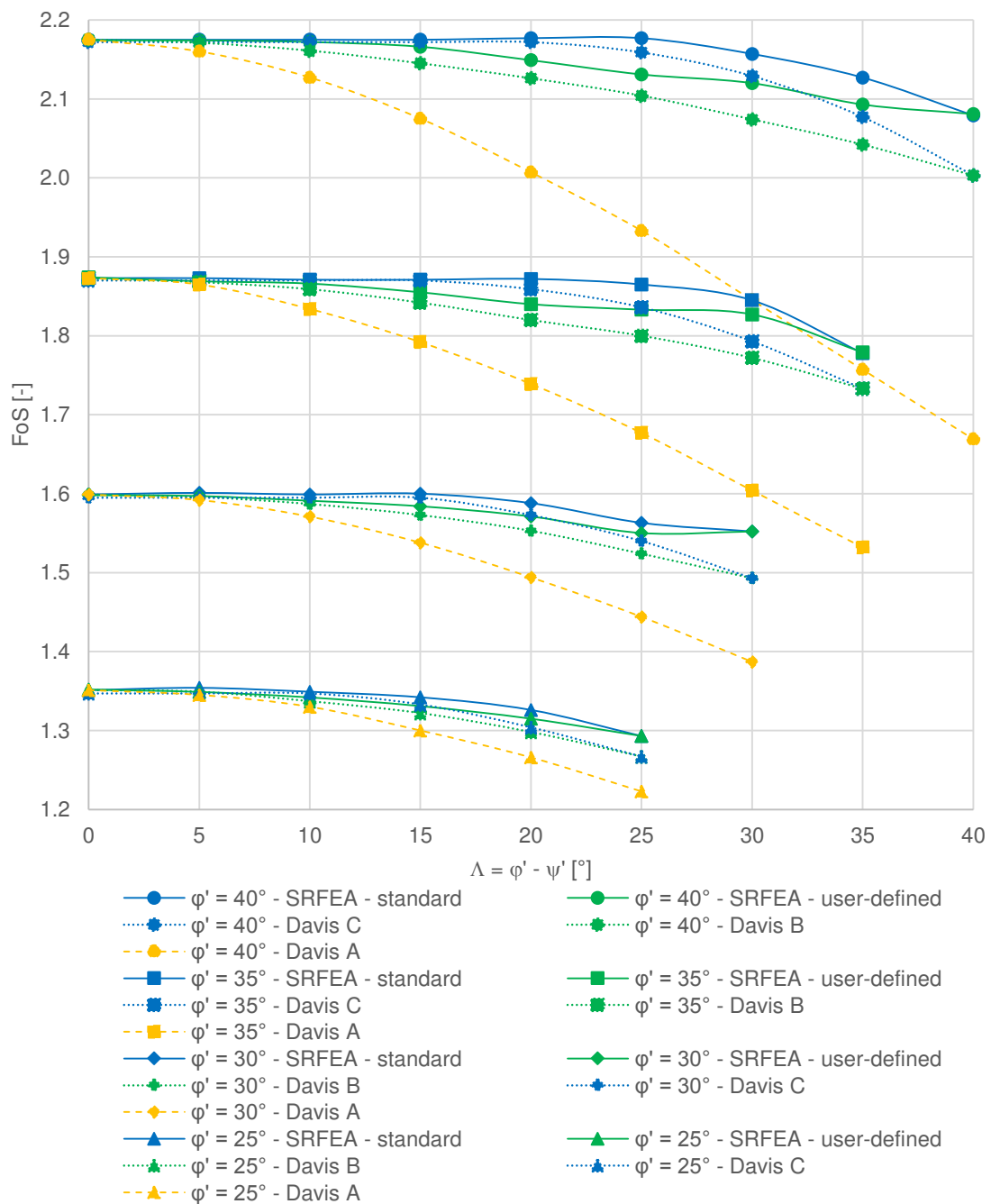


Fig. 82 Study 1 - slope 1: Standard SRFEA, user-defined SRFEA, Davis A, Davis B and Davis C results for different λ and φ'

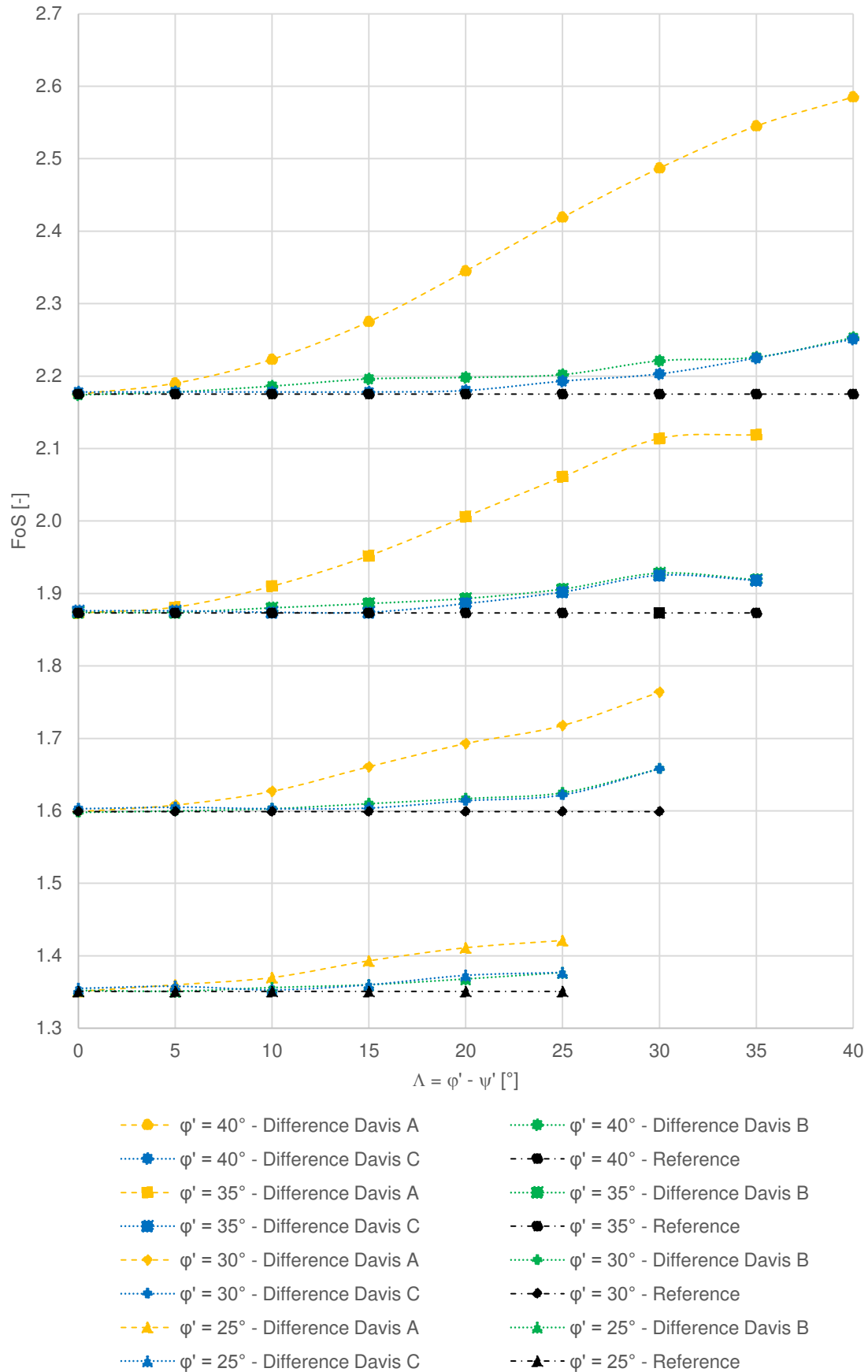


Fig. 83 Study 1 - slope 1: Differences between Davis A and standard SRFEA, Davis B and user-defined SRFEA and Davis C and standard SRFEA for different Δ and φ'

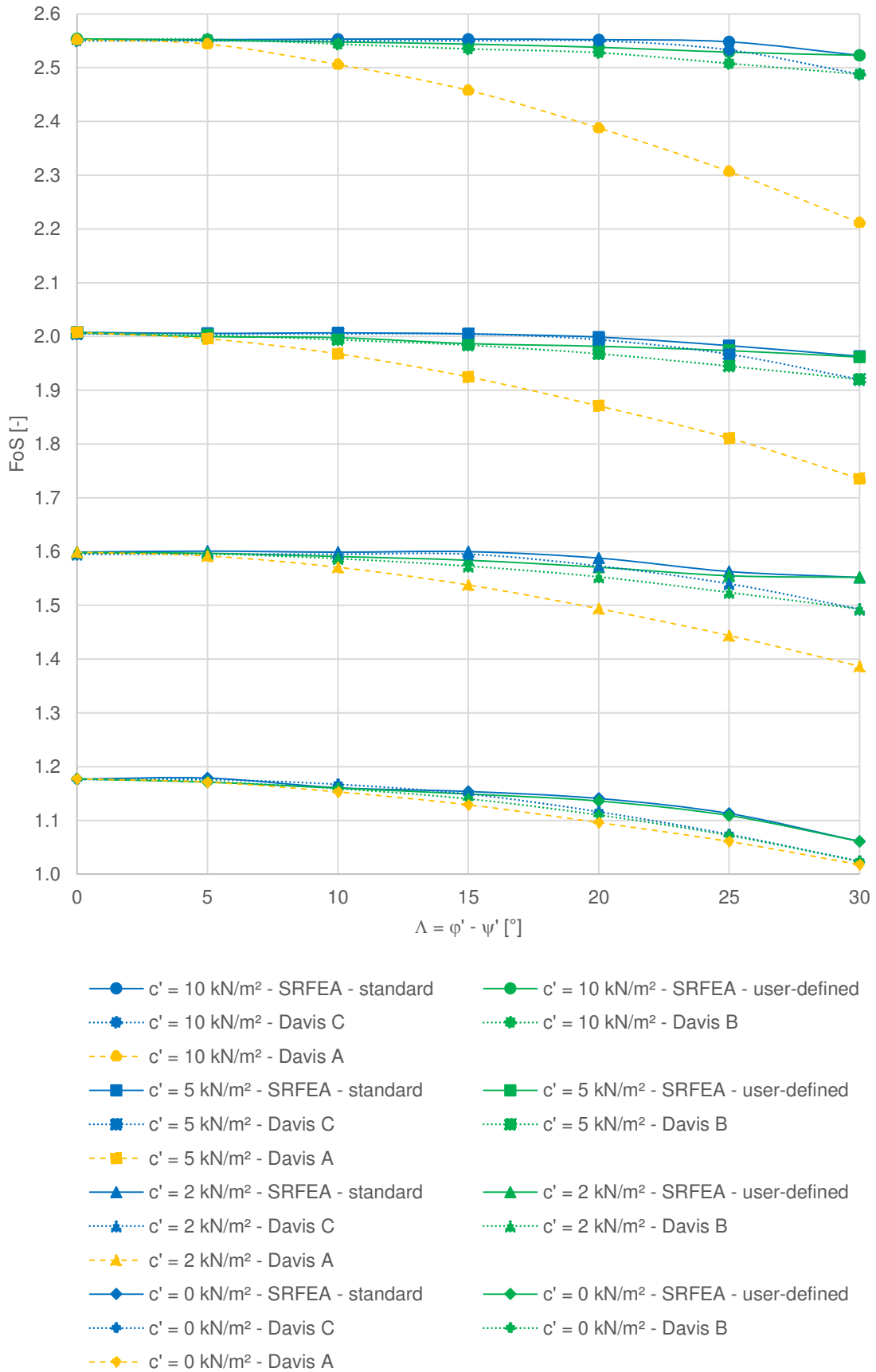


Fig. 84 Study 2 - slope 1: Standard SRFEA, user-defined SRFEA, Davis A, Davis B and Davis C results for different Δ and c'

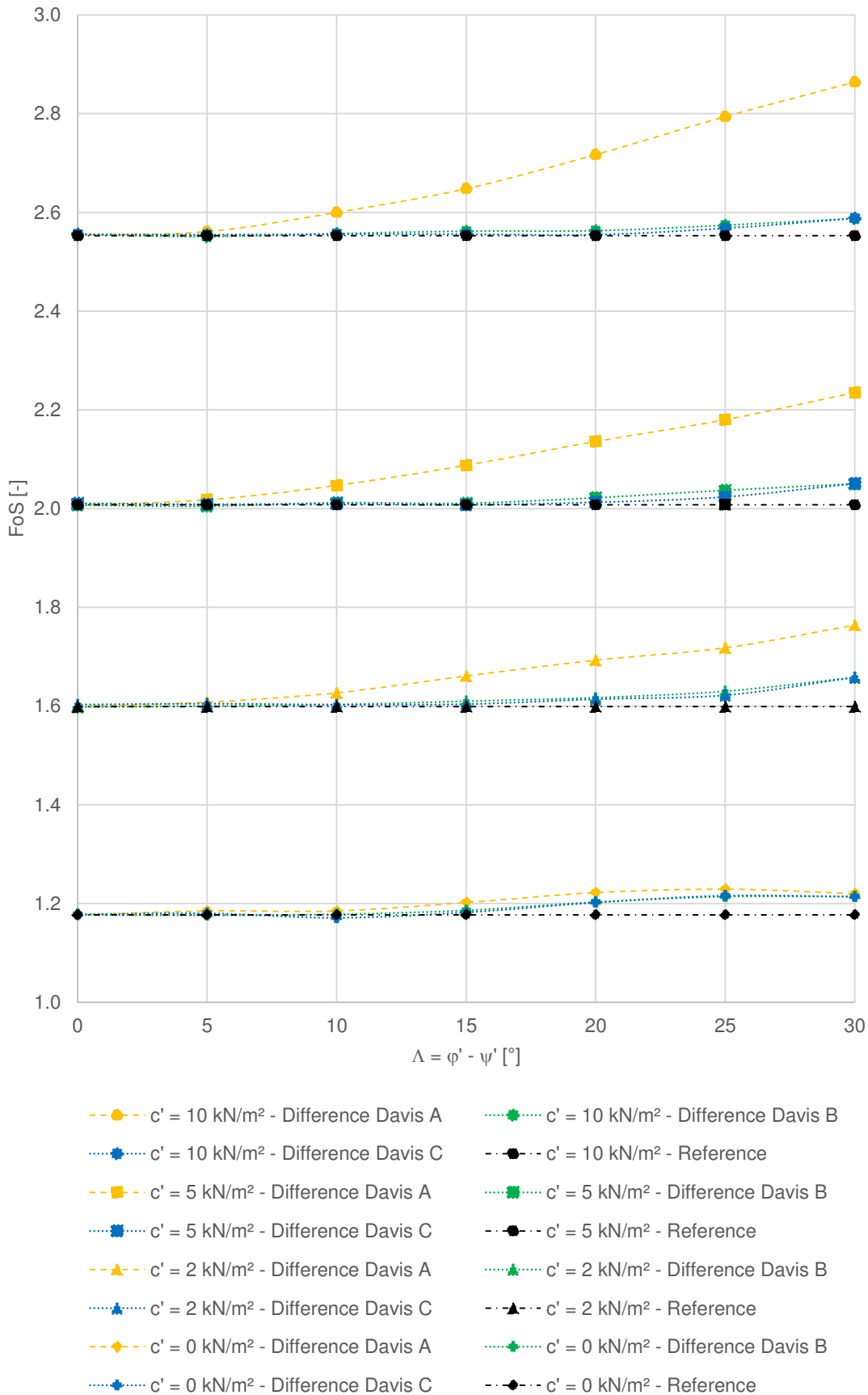


Fig. 85 Study 2 - slope 1: Differences between Davis A and standard SRFEA, Davis B and user-defined SRFEA and Davis C and standard SRFEA for different Δ and c'

6 $\varphi - \nu$ inequality

For most of Griffiths and Lane's paper examples the elastic parameters Young's modulus E' and Poisson's ratio ν were not given. The variation of these parameters show that E' has no influence on the safety factor at all, while ν can lead to small differences in some cases. The reason for this behaviour could possibly lie in the so-called $\varphi - \nu$ inequality.

6.1 Derivation of the $\varphi - \nu$ inequality

To get a better idea of the following steps, a rigid cylinder filled with homogeneous dry soil is used for the following explanations. Considered is a free top surface, between cylinder and soil no friction is acting. By assuming elastic soil properties and gravity acting on the domain, Eq. (50) and Eq. (51) define the vertical and horizontal earth pressure. The z-axis, directed positively downwards, starts on top of the free surface. The earth pressure coefficient at rest K_0 is defined according to Eq. (52).

$$\sigma_1 = -\gamma h \quad (50)$$

$$\sigma_3 = \sigma_2 = -K_0 \gamma h \quad (51)$$

$$K_0 = \frac{\nu}{1 - \nu} \quad (52)$$

It should be noted that no point in the soil can ever fail, because the system is horizontally confined. Furthermore, a Mohr-Coulomb failure criterion is used. Substituting Eq. (50) and Eq. (51) into Eq. (53) and letting the height h go towards infinity, the relation for the $\varphi - \nu$ inequality is built (Eq. (54)).

$$(1 + \sin \varphi') \sigma_3 - (1 - \sin \varphi') \sigma_1 \leq 2c \cos \varphi' \quad (53)$$

$$\sin \varphi' \geq \frac{1 - K}{1 + K} = 1 - 2\nu \quad (54)$$

Hence one can imply that the whole soil would fail if the inequality is not guaranteed ($\sin \varphi' < 1 - 2\nu$). This is particularly the case for cohesionless soils in an infinite half space or for the mentioned cylinder. Obviously, this cannot be considered to be correct (Zheng et al. 2005).

It needs to be stated that the expressions *$\varphi - \nu$ inequality satisfied* or *$\varphi - \nu$ inequality given* mean that Eq. (54) is fulfilled. If this is not the case, *$\varphi - \nu$ inequality neglected* or *$\varphi - \nu$ inequality not given* will be stated.

6.2 Scheme of analysis

In order to establish whether the $\varphi - \nu$ inequality has an influence on the computed safety factor, two scenarios get compared where the first neglects and the second satisfies the correlation. The scheme of analysis is shown in the following paragraph.

To ensure that the $\varphi - \nu$ inequality is not satisfied, the first case is assuming a limit condition for the input. The friction angle φ' and the Poisson's ratio ν have been chosen so that $\sin\varphi'$ equals $1 - 2\nu$ and thus Eq. (55) gives unity ($\theta = 1$). When considering a strength reduction with a constant ν , any further decrease of the friction angle leads to a state where the correlation is neglected.

$$\theta = \frac{\sin \varphi'}{1 - 2\nu} = 1 \quad (55)$$

Eq. (20) is used to determine friction angle $\varphi'_{mob.}$ and cohesion $c'_{mob.}$ at failure. To ensure a given inequality for scenario two, a modified Poisson's ratio $\nu_{mod.}$ is determined according to Eq. (56).

$$\nu_{mod.} = \frac{1}{2}(1 - (\sin \varphi'_{mob.}/\theta)) \quad (56)$$

The original friction angle with the modified Poisson's ratio $\nu_{mod.}$ enables a strength reduction where the inequality is always satisfied, as long as the safety factor is not increasing (Zheng et al. 2005).

To investigate if a further increase of the Poisson's ratio $\nu_{choice} > \nu_{mod.}$ shows any influence on the factor of safety, further calculations are performed for some selected examples. For the sake of completeness, it should be mentioned that any further increase of the Poisson's ratio leads to a clear fulfilment of Eq. (54).

6.3 Analysis

6.3.1 General information

All calculations are performed on a homogeneous slope, five meters high and disposed 26.57° to the horizontal (Fig. 86). The analyses consider drained conditions and a linear elastic-perfectly plastic constitutive model with a Mohr-Coulomb failure criterion. Case 1 with an effective friction angle $\varphi'_1 = 37^\circ$ and a Poisson's ratio $\nu_1 = 0.2$ as well as case 2 with an effective friction angle $\varphi'_2 = 23.6^\circ$ and a Poisson's ratio $\nu_2 = 0.3$ shall be subject to further analyses. For both parameter sets, Eq. (55) is equal to unity. The Young's

modulus E' , the unit-weight γ_{unsat} , the dilatancy angle ψ' and the cohesion c' get modified for both cases, according to Tab. 46.

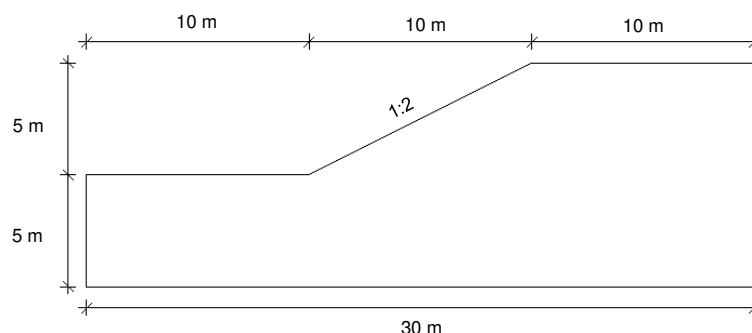


Fig. 86 $\phi - v$ inequality: Geometry of the slope

Tab. 46 $\phi - v$ inequality: Variation of the strength and stiffness parameters

Soil parameters	Unit	Case 1	Case 2
E'	(kN/m ²)	10^4 ; 10^7	10^4 ; 10^7
ν	(-)	0.2; ν_{mod} ; (ν_{choice})	0.3; ν_{mod} ; (ν_{choice})
γ_{unsat}	(kN/m ³)	16; 20	16; 20
ϕ'	(°)	37	23.6
ψ'	(°)	ϕ' ; $\phi' / 3$; $\phi' / 4$; 0	ϕ' ; $\phi' / 3$; $\phi' / 4$; 0
c'	(kN/m ²)	0; 2; 4	2; 4

In the first phase, gravity loading is applied in Plaxis 2D, followed by a SRFEA. To monitor the change in failure points, a nil-step gets additionally inserted after the initial phase. Plaxis 2D uses a tolerated error of 1 % and these tolerances might cause an additional load redistribution in the nil-step, as shown in Fig. 87 (Brinkgreve et al. 2016). It should be stressed at this point that the amount of failure points is smaller compared to the initial phase.

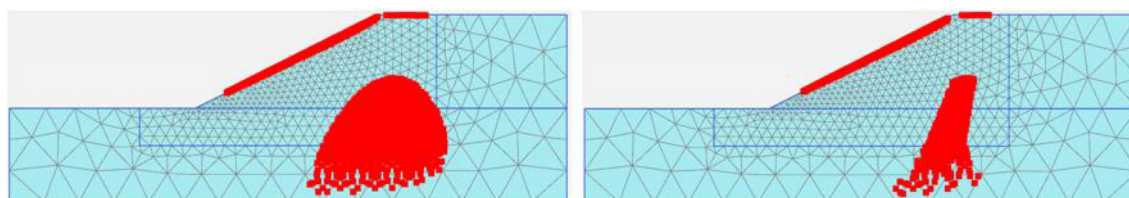


Fig. 87 $\phi - v$ inequality - failure points: Comparison of gravity loading and the following nil-step ($\phi'_1 = 37^\circ$, $\nu_1 = 0.2$, $c' = 2$ kN/m², $E' = 10^4$ kN/m², $\gamma_{unsat} = 16$ kN/m³)

Besides any standard and user-defined SRFEA, Davis procedures A, B and C are carried out in Plaxis 2D. For all calculations, the domain is discretised by 1035 15-noded elements. In addition, SRFEA, FELA, Davis A, Davis B and Davis C are performed in Optum G2 with an adaptive mesh refinement. An overview of the calculations for both cases is shown in appendix 10.5.

6.3.2 Comparison of the results

Analyses with the soil properties according to Tab. 47 are the subject of the following discussion. It should be noted that all statements hold true for the other calculations as well.

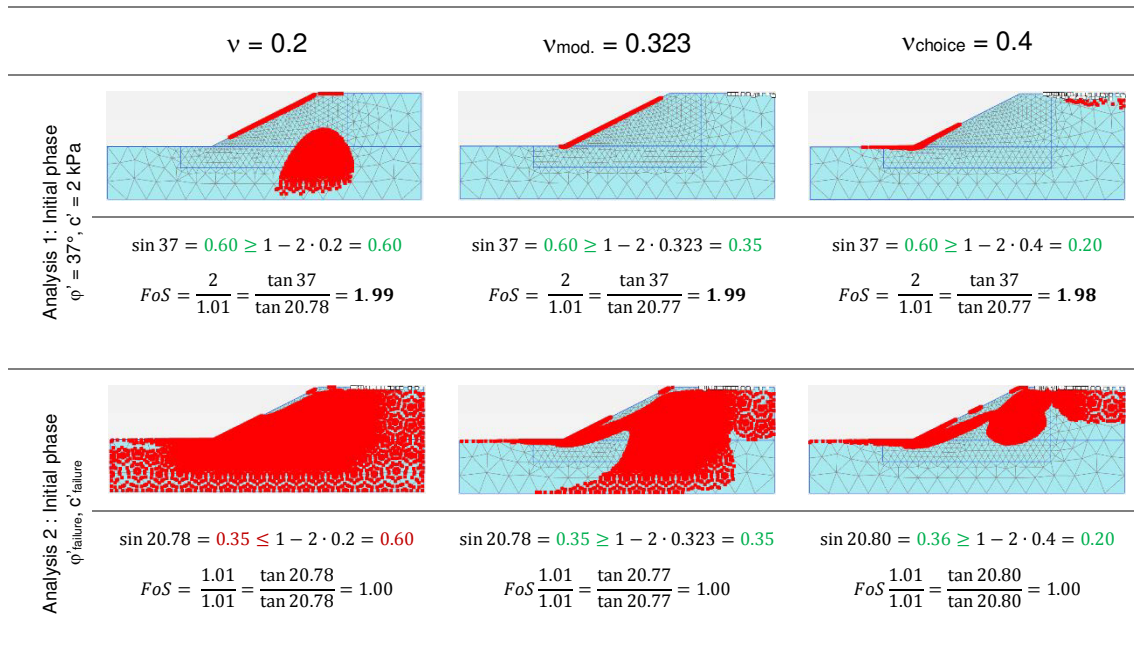
Tab. 47 φ - ν inequality: Soil parameters used for the evaluation

Soil parameters	Unit	Case 1
E'	(kN/m ²)	10 ⁴
ν	(-)	0.2; ν_{mod} ; ν_{choice}
γ_{unsat}	(kN/m ³)	16
φ'	(°)	37
ψ'	(°)	φ' ; $\varphi' / 3$; $\varphi' / 4$; 0
c'	(kN/m ²)	2

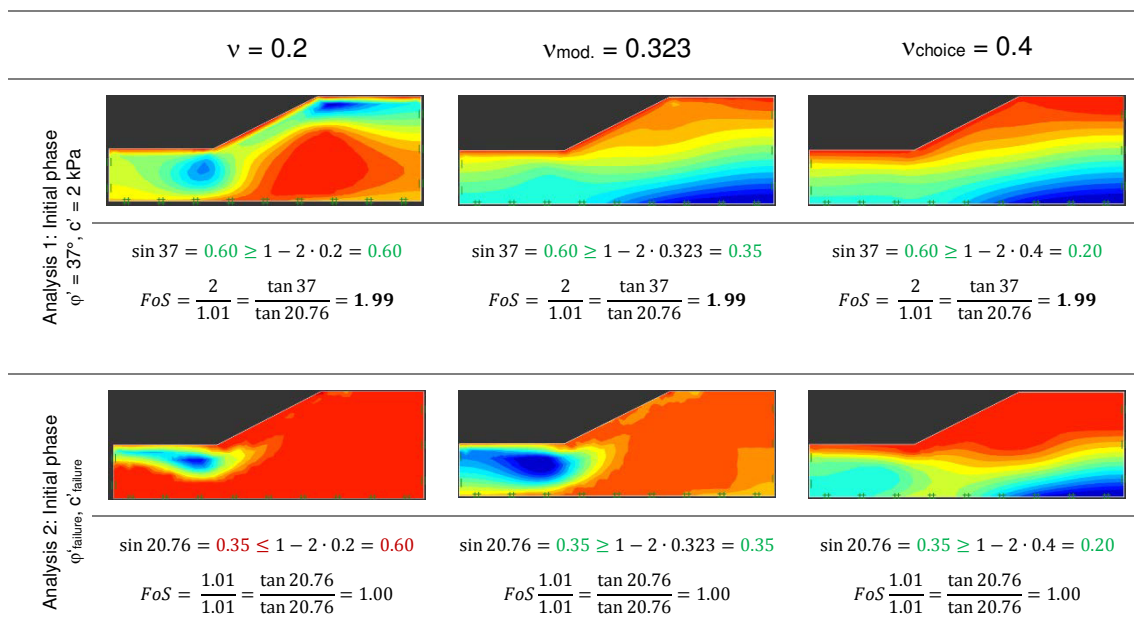
In the first part, SRFEA with associated plasticity and FELA are going to be compared for different Poisson's ratios ν . Special emphases is put on the development of failure points. Alongside the development of those failure points, it is of main interest to clarify if the φ - ν inequality affects the factor of safety. For this particular case, additional safety analyses are made with a Poisson's ratio of $\nu_{choice} = 0.4$. In order to gain a better understanding of the following tables, it should be said that for each Poisson's ratio (ν , ν_{mod} , ν_{choice}) two safety analyses (analysis 1, analysis 2) are performed. The effective friction angle and cohesion listed in Tab. 47 are used as input parameters for analysis 1, while the resulting friction angle and cohesion at failure ($\varphi'_{mob.}$, $c'_{mob.}$) are the input parameters for analysis 2. Logically, this also means that the safety factor of the latter analysis has to be equal to unity (FoS = 1). The amount and the distribution of failure points (or yield function for Optum G2) shown in the initial phase of analysis 2 are important, because they represent the failure condition of analysis 1. Summarized in one sentence, the upper figures show the plastic points at the initial state, while the figures

at the bottom represent the state of failure (this statement refers to Tab. 48, Tab. 49, Tab. 50). Tab. 48, Tab. 49 and Tab. 50 clearly indicate the significant influence the Poisson's ratio ν has on the amount of plastic points. The amount of plastic points is further decreasing for the chosen Poisson's ratio $\nu_{\text{choice}} = 0.4$. Furthermore it could be seen that the $\phi - \nu$ inequality does not influence the safety factors. By varying ν between 0.2 and 0.4, the FoS does not change remarkably for SRFEA and FELA. The safety values differ between 1.98 and 2.00.

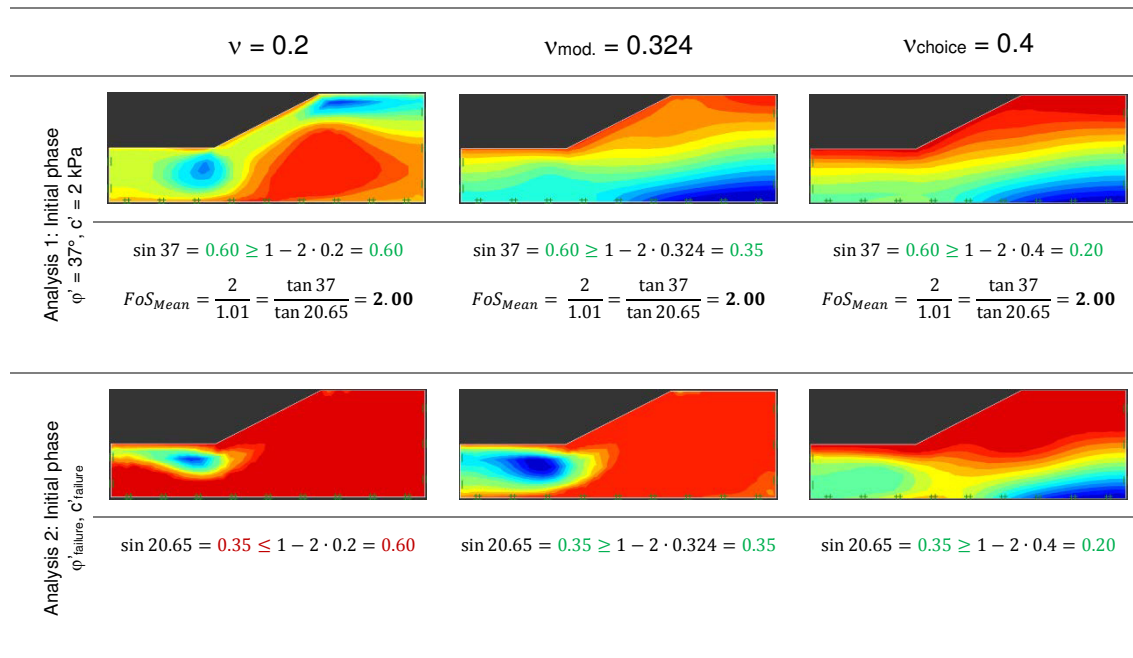
Tab. 48 Failure points: SRFEA ($\psi' = \phi'$), Plaxis 2D



Tab. 49 Yield function: SRFEA ($\psi' = \phi'$), Optum G2



Tab. 50 Yield function: FELA, upper-bound ($\psi' = \phi'$), Optum G2



Finally, it is important to emphasize that changes in Poisson's ratio do not affect the safety factor for any associated SRFEA, FELA and Davis approaches at all. The variation of strength and stiffness parameters, according to Tab. 46, have also no impact on this finding, as it can be seen in appendix 10.5.

The statements herein hold true for SRFEA with non-associated plasticity as well. As shown in Tab. 51, the safety values are approximately constant for all the Poisson's ratios.

Tab. 51 ϕ - ν inequality: SRFEA results according to non-associated plasticity (Plaxis 2D)

Dilatancy angle	$\nu = 0.2$	$\nu_{mod.} = \text{variable}$	$\nu_{choice} = 0.4$
$\psi' = 0^\circ$	1.88	1.87	1.87
$\psi' = \phi' / 4$	1.98	1.97	1.96
$\psi' = \phi' / 3$	1.99	1.98	1.98
$\psi' = \phi'$	1.99	1.99	1.98

In rare cases, the study identifies larger differences in FoS for several Poisson's ratios. By assuming a unit-weight $\gamma_{unsat} = 20 \text{ kN/m}^3$, a Young's modulus $E' = 10^4 \text{ kN/m}^2$, an effective friction angle $\phi' = 37^\circ$, a dilatancy angle $\psi' = 0^\circ$ and varying the cohesions c' between 0 and 4 kPa, the computed safety factors for $\nu = 0.2$ and $\nu_{mod.}$ differ slightly. On

the other hand, Davis A and Davis B do not show these differences. The observed behaviour can be explained through the bifurcation of the failure mechanism. As mentioned in section 3.1.4, large differences between the effective friction angle and the dilatancy angle may lead to changes in the failure mechanism. Consequently, no precise definition of the safety factor is possible.

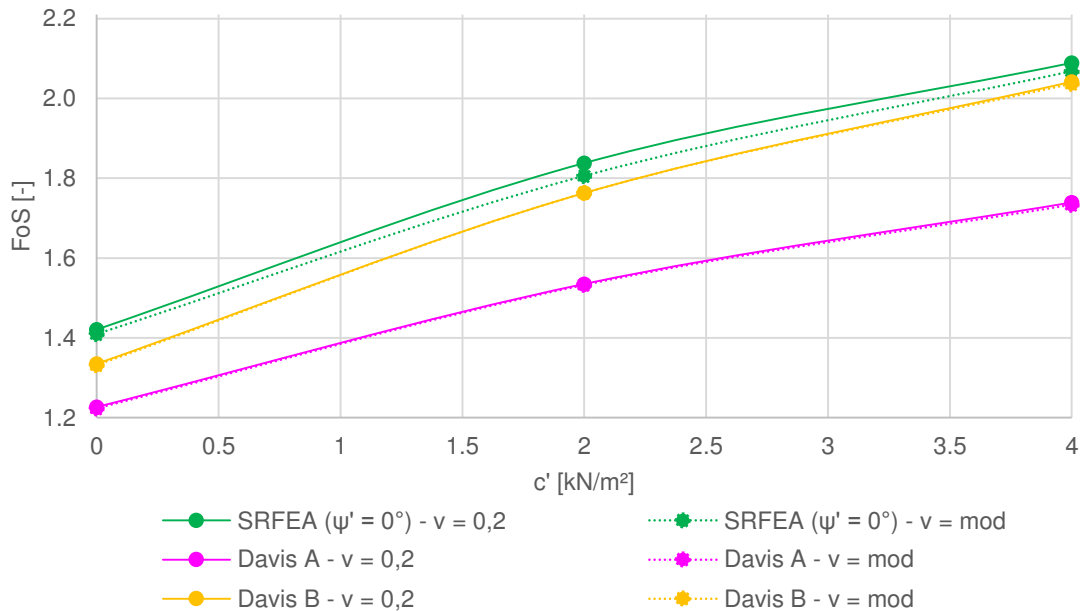


Fig. 88 $\phi - \nu$ inequality: Comparison of SRFEA, Davis A and Davis B for different ν ($\gamma_{\text{unsat}} = 16$ kN/m³, $E' = 10^4$ kN/m², $\varphi'_1 = 37^\circ$, $\psi' = 0^\circ$)

Subsequently, the example was taken to demonstrate the bifurcation of a failure mechanism. This behaviour has already been introduced in section 3.1.4. As Fig. 89 shows, the choice of safety value is decisive for the resulting modified Poisson's ratio ν_{mod} . Those Poisson's ratios differ up to 5 %, depending on the chosen FoS. Running a SRFEA with modified Poisson's ratios ν_{mod} can show that the erratic distributions are not weakened and still deviate of 2.5 % from the previous calculations, according to $\nu = 0.146$ (Fig. 90).

In conclusion, it can be said that the Poisson's ratio is not affecting the safety factor for any analyses but is particularly responsible for the amount of plastic points in a domain. Differences in the FoS arising from the variation of ν are related to the bifurcation of the failure mechanism. Furthermore, it has been shown that the $\phi - \nu$ inequality does not influence the erratic behaviour of the $\phi - c$ reduction in combination with non-associated plasticity.

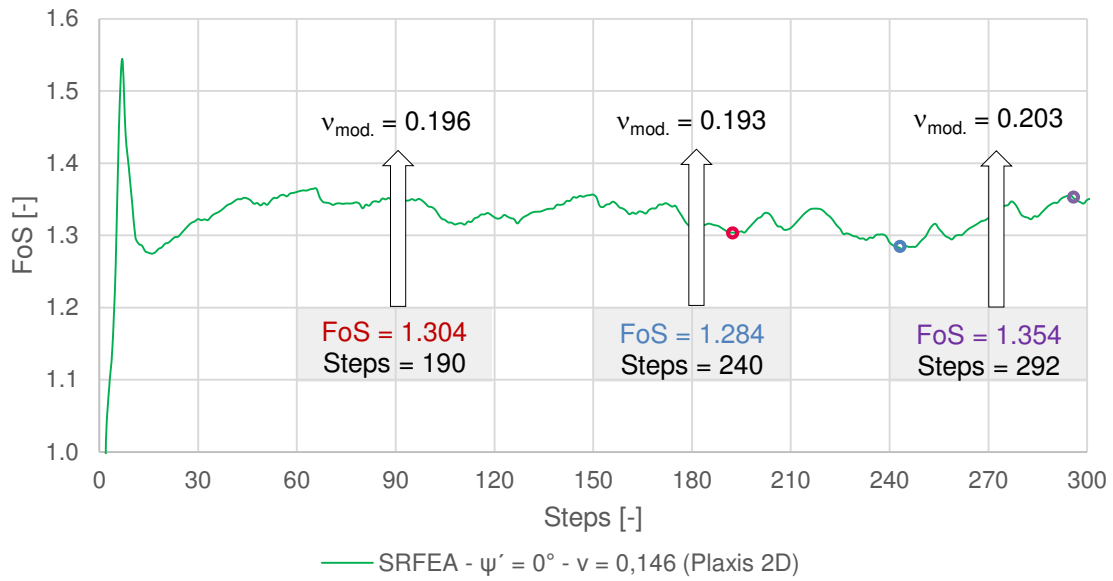


Fig. 89 ϕ - ν inequality: SRFEA ($\psi' = 0^\circ$) according to $\nu = 0.146$

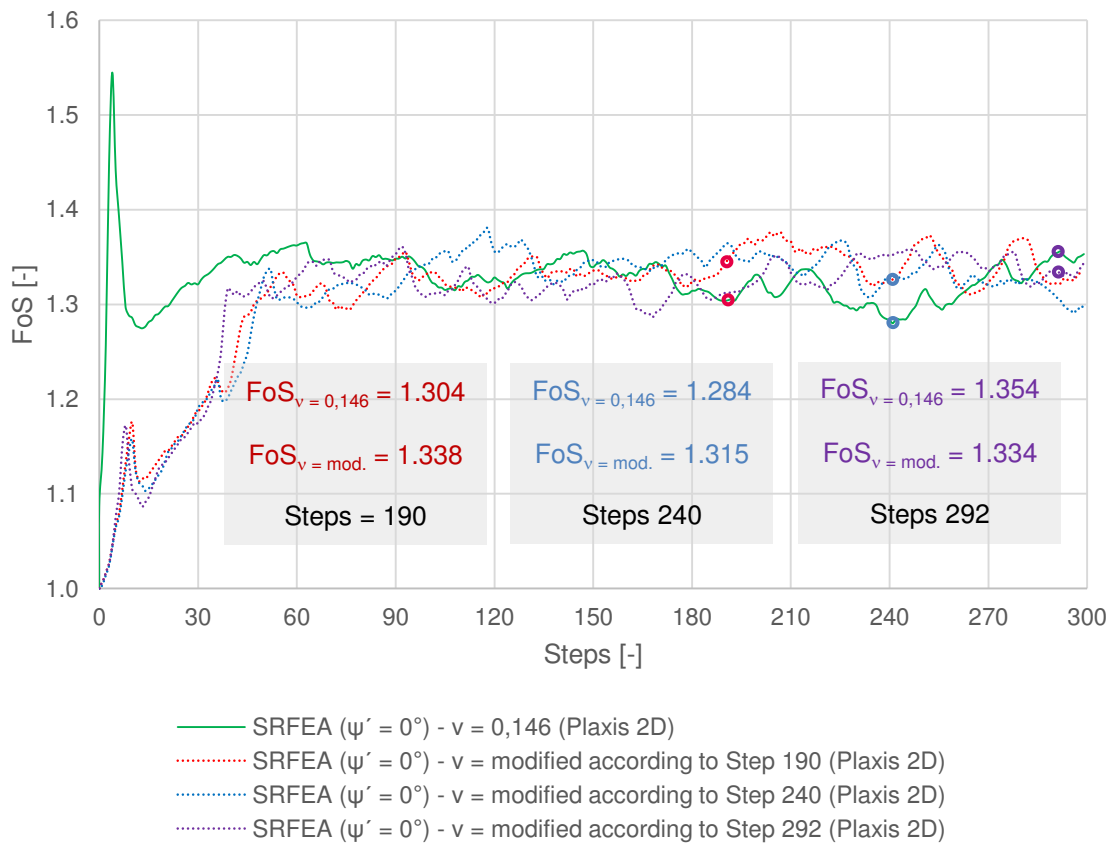


Fig. 90 ϕ - ν inequality : SRFEA ($\psi' = 0^\circ$) according to ν_{mod}

7 Influence of the initial stress condition on the FoS

As several studies that have been investigated in this thesis have shown, Poisson's ratio does not affect the FoS. The initial phase was determined by gravity loading. Chapter 7.1 and 7.2 are going to make an attempt to answer the following two questions: Do the statements on the $\varphi - v$ inequality hold true if the initial stresses are calculated by a K_0 procedure? Has the K_0 value any influence on the factor of safety?

In Plaxis 2D, the initial stress distribution by using gravity loading gets determined by considering the self-weight, according to Eq. (52). By using an elastic-perfectly plastic constitutive model, the ratio of the horizontal to the vertical effective stresses is strongly affected by the Poisson's ratio. The procedure satisfies the equilibrium for all geometries. In contrast, a K_0 procedure calculates the stresses according to Eq. (57) whereby the mayor and minor principal stresses remain vertical and horizontal. It follows that K_0 becomes an input parameter (default: $K_0 = 1 - \sin\varphi'$). The vertical stresses are in equilibrium with the self-weight of the soil, but the K_0 procedure does not ensure any failure criterion in the complete stress field. Only in the case of a horizontal soil surface, soil layers and phreatic levels, a complete equilibrium is guaranteed (Brinkgreve et al. 2016).

$$K_0 = \frac{\sigma'_{xx}}{\sigma'_{yy}} \quad (57)$$

7.1 $\varphi - v$ inequality with K_0 procedure

To answer the first of the above mentioned questions, SRFEA are performed on two slopes in Plaxis 2D. Looking at the figure below, one can see that slope 1 is disposed 26.57° ($1:2$) to the horizontal, while slope 2 is 45° ($1:1$) steep.

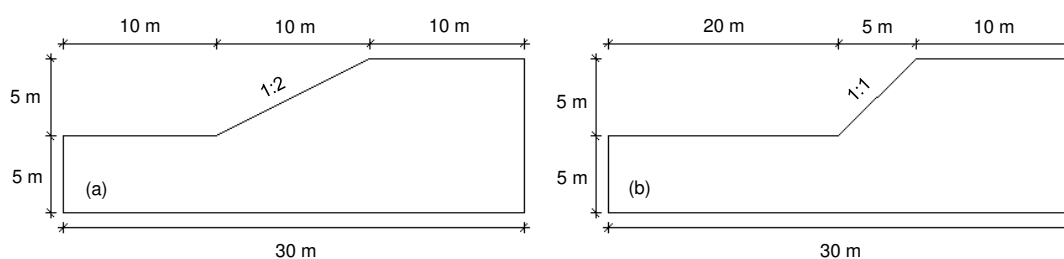


Fig. 91 Geometry of slope 1 (a) and slope 2 (b)

The homogeneous slopes are characterized by a unit-weight $\gamma_{\text{unsat}} = 16 \text{ kN/m}^3$. However, the cohesion for both cases is different. Note that for both slopes, SRFEA according to associated and non-associated plasticity are performed. A complete overview of the soil

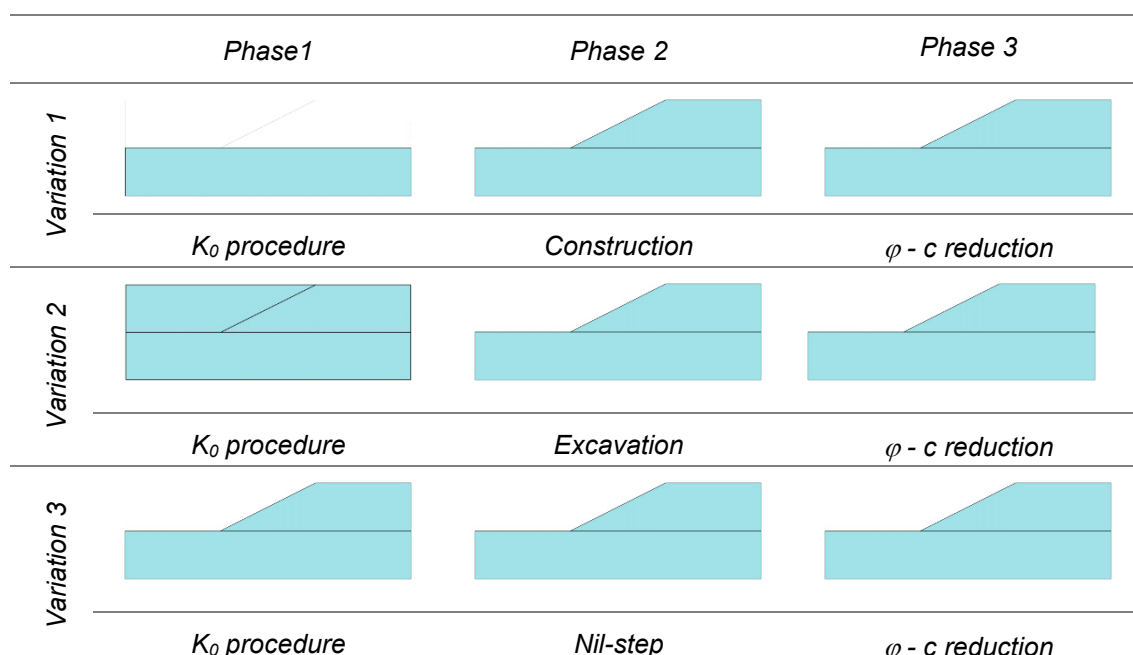
parameters is listed in Tab. 52. The discussion of results will be made for slope 1 with associated plasticity. The statements apply for all calculations performed in this study. The results are attached in appendix 10.6. For slope 1, about 1509 15-noded triangular elements are used to discretize the domain.

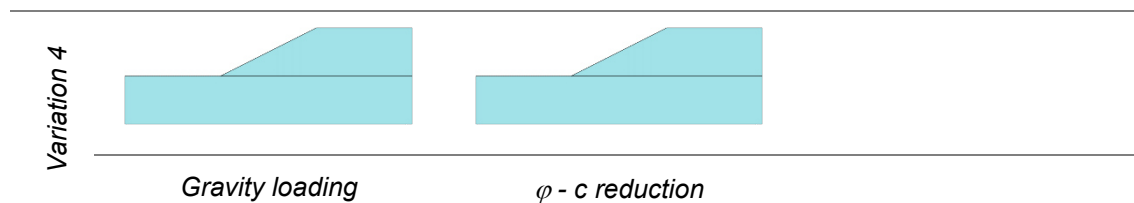
Tab. 52 Soil parameters used for analyses

Soil parameters	Unit	Slope 1	Slope 2
E'	(kN/m ²)	10 ⁴	10 ⁴
ν	(-)	0.2; ν_{mod} ; ν_{choice}	0.2; ν_{mod} ; ν_{choice}
γ_{unsat}	(kN/m ³)	16	16
φ'	(°)	37	37
ψ'	(°)	φ' ; 0	φ' ; 10
c'	(kN/m ²)	1	4

Three variations of slope stability analyses with K_0 procedure as the initial phase are the subject for further studies. The initial phase is followed by either a construction phase, an excavation phase or a nil-step. A standard $\varphi - c$ reduction is used to determine the factor of safety in phase 3. Furthermore, SRFEA with initial phase gravity loading are calculated as well (variation 4). In order to gain a better understanding, Tab. 53 highlights the phases of each variation.

Tab. 53 Variation 1 - 4: Calculation phases (Plaxis 2D)





In the same way as described in 6.2, SRFEA are performed with Poisson's ratios ν , ν_{mod} and ν_{choice} . For variations 1 - 3 the K_0 value is determined according to Eq. (52) to ensure a comparable initial stress distribution in all initial phases. It is important to note that the direction and magnitude of major (σ'_1) and minor (σ'_3) principle stresses are different for variations 1 - 4 in the initial phase, depending on the geometry and the chosen method (K_0 procedure, gravity loading). However, a basis for comparison can be achieved. The K_0 value gets modified depending on the Poisson's ratio (Tab. 54).

Tab. 54 K_0 values for the several Poisson's ratios

$\nu = 0.2$	$\nu_{mod} = 0.308$	$\nu_{choice} = 0.4$
$K_0 = \frac{0.2}{1 - 0.2} = 0.25$	$K_0 = \frac{0.308}{1 - 0.308} = 0.45$	$K_0 = \frac{0.4}{1 - 0.4} = 0.67$


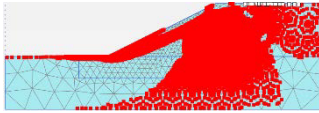
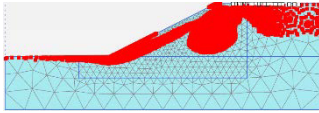
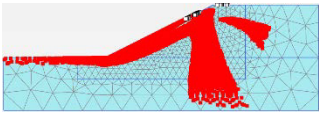
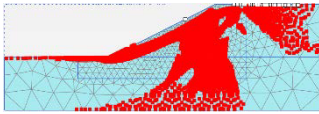
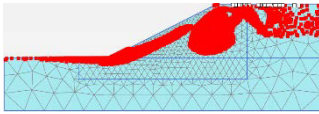

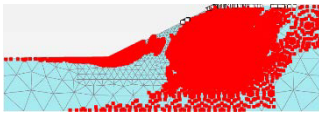
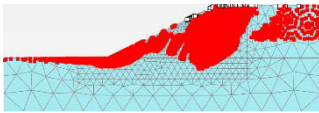


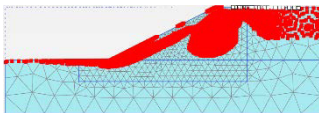
For each variation and Poisson's ratio, SRFEA are performed according to the original strength parameters and strength parameters at failure (FoS = 1). The failure points of the latter ones are shown in Tab. 55. The underlined phase is subject of discussion (left column in Tab. 55).

The calculations show that the FoS is not affected by the variation of Poisson's ratio and K_0 value respectively. As can be seen in Tab. 55, the factors of safety for variations 1 - 4 vary between 1.80 and 1.81. On the other hand, the amount of failure points strongly decreases again with an increasing Poisson's ratio (see also chapter 6.3.2).

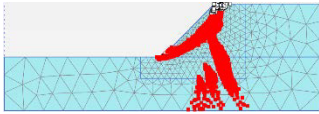
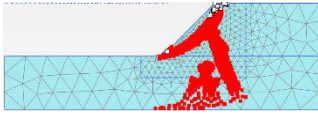
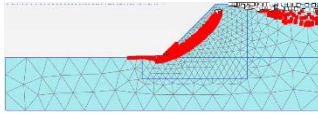
The amount and distribution of failure points is similar for variations 1, 3 and 4. Variations 2, however, shows less failure points. The reason for this is that the excavation phase is an unloading process. Therefore, failure points can become elastic again. Contrary to the expectations, the amount of failure points is increasing for a Poisson's ratio $\nu_{mod} = 0.308$. This increase of failure points remains unclarified. The increase of failure points is not present on slope 2 (Tab. 56). The amount of tension points at the crown of the embankment is increasing with an increasing Poisson's ratio. This becomes particularly obvious in Tab. 56. In order to be able to draw more conclusions, further analyses are needed. To conclude this chapter, it should be underlined that SRFEA with a K_0

procedure as the initial phase do confirm all statements made on the $\varphi - \nu$ inequality. The factor of safety is not affected by the Poisson's ratio, but the amount of failure points diminishes with an increasing ν .

Tab. 55 Slope 1 - SRFEA ($\psi' = \varphi'$): Failure points and safety factors for several ν

	$\nu = 0.2$	$\nu_{mod} = 0.308$	$\nu_{choice} = 0.4$
Variation 1: K_0 procedure + construction + safety phase	 <p> $\sin 22.69 = 0.38 \leq 1 - 2 \cdot 0.2 = 0.60$ $FoS = \frac{1}{0.56} = \frac{\tan 37}{\tan 22.69} = 1.80$ </p>	 <p> $\sin 22.68 = 0.39 \geq 1 - 2 \cdot 0.308 = 0.39$ $FoS = \frac{1}{0.56} = \frac{\tan 37}{\tan 22.68} = 1.80$ </p>	 <p> $\sin 22.69 = 0.39 \geq 1 - 2 \cdot 0.4 = 0.20$ $FoS = \frac{1}{0.56} = \frac{\tan 37}{\tan 22.69} = 1.80$ </p>
Variation 2: K_0 procedure + excavation + safety phase	 <p> $\sin 22.66 = 0.38 \leq 1 - 2 \cdot 0.2 = 0.60$ $FoS = \frac{1}{0.55} = \frac{\tan 37}{\tan 22.66} = 1.81$ </p>	 <p> $\sin 22.69 = 0.39 \geq 1 - 2 \cdot 0.308 = 0.39$ $FoS = \frac{1}{0.56} = \frac{\tan 37}{\tan 22.69} = 1.80$ </p>	 <p> $\sin 22.70 = 0.39 \geq 1 - 2 \cdot 0.4 = 0.20$ $FoS = \frac{1}{0.56} = \frac{\tan 37}{\tan 22.70} = 1.80$ </p>
Variation 3: K_0 procedure + NI-step + safety phase	 <p> $\sin 22.63 = 0.38 \leq 1 - 2 \cdot 0.2 = 0.60$ $FoS = \frac{1}{0.55} = \frac{\tan 37}{\tan 22.63} = 1.81$ </p>	 <p> $\sin 22.67 = 0.39 \geq 1 - 2 \cdot 0.308 = 0.39$ $FoS = \frac{1}{0.55} = \frac{\tan 37}{\tan 22.67} = 1.80$ </p>	 <p> $\sin 22.67 = 0.39 \geq 1 - 2 \cdot 0.4 = 0.20$ $FoS = \frac{1}{0.55} = \frac{\tan 37}{\tan 22.67} = 1.80$ </p>
Variation 4: Gravity loading + safety phase	 <p> $\sin 22.64 = 0.38 \leq 1 - 2 \cdot 0.2 = 0.60$ $FoS = \frac{1}{0.55} = \frac{\tan 37}{\tan 22.64} = 1.81$ </p>	 <p> $\sin 22.65 = 0.39 \geq 1 - 2 \cdot 0.308 = 0.39$ $FoS = \frac{1}{0.55} = \frac{\tan 37}{\tan 22.65} = 1.81$ </p>	 <p> $\sin 22.70 = 0.39 \geq 1 - 2 \cdot 0.4 = 0.20$ $FoS = \frac{1}{0.56} = \frac{\tan 37}{\tan 22.70} = 1.80$ </p>

Tab. 56 Slope 2 - SRFEA ($\psi' = \varphi'$): Failure points and safety factors for the several ν

	$\nu = 0.2$	$\nu_{mod} = 0.267$	$\nu_{choice} = 0.4$
Variation 2: K_0 procedure + excavation + safety phase			
	$\sin 27.84 = 0.47 \leq 1 - 2 \cdot 0.2 = 0.60$ $FoS = \frac{4}{2.80} = \frac{\tan 37}{\tan 27.84} = 1.43$	$\sin 27.87 = 0.47 \geq 1 - 2 \cdot 0.267 = 0.47$ $FoS = \frac{1}{2.81} = \frac{\tan 37}{\tan 27.87} = 1.43$	$\sin 28.02 = 0.47 \geq 1 - 2 \cdot 0.4 = 0.20$ $FoS = \frac{4}{2.82} = \frac{\tan 37}{\tan 28.02} = 1.42$

7.2 Influence of K_0 on the FoS

In 7.1 the K_0 value and the Poisson's ratio got modified in a simultaneous manner, according to Eq. 52. The following study can be considered isolated from the $\varphi - \nu$ inequality and should clarify the effect from the K_0 value on the FoS. The two slopes of the previous chapter are object to further SRFEA with associated and non-associated plasticity. To prove if the K_0 value influences the FoS, the variations 1 to 3 are considered for both slopes again. By keeping the Poisson's ratio ($\nu = 0.2$) constant, the initial stress distribution is established for a K_0 value equal to 0.25 and 0.40. The first value results from Eq. 52 while the latter one corresponds to the default value $K_0 = 1 - \sin\varphi'$. An overview of all the calculations is found in appendix 10.6. As Tab. 57 shows, the initial stress state does not affect the obtained safety value. For an explanation of this behaviour, slope 1 with associated plasticity will be utilized.

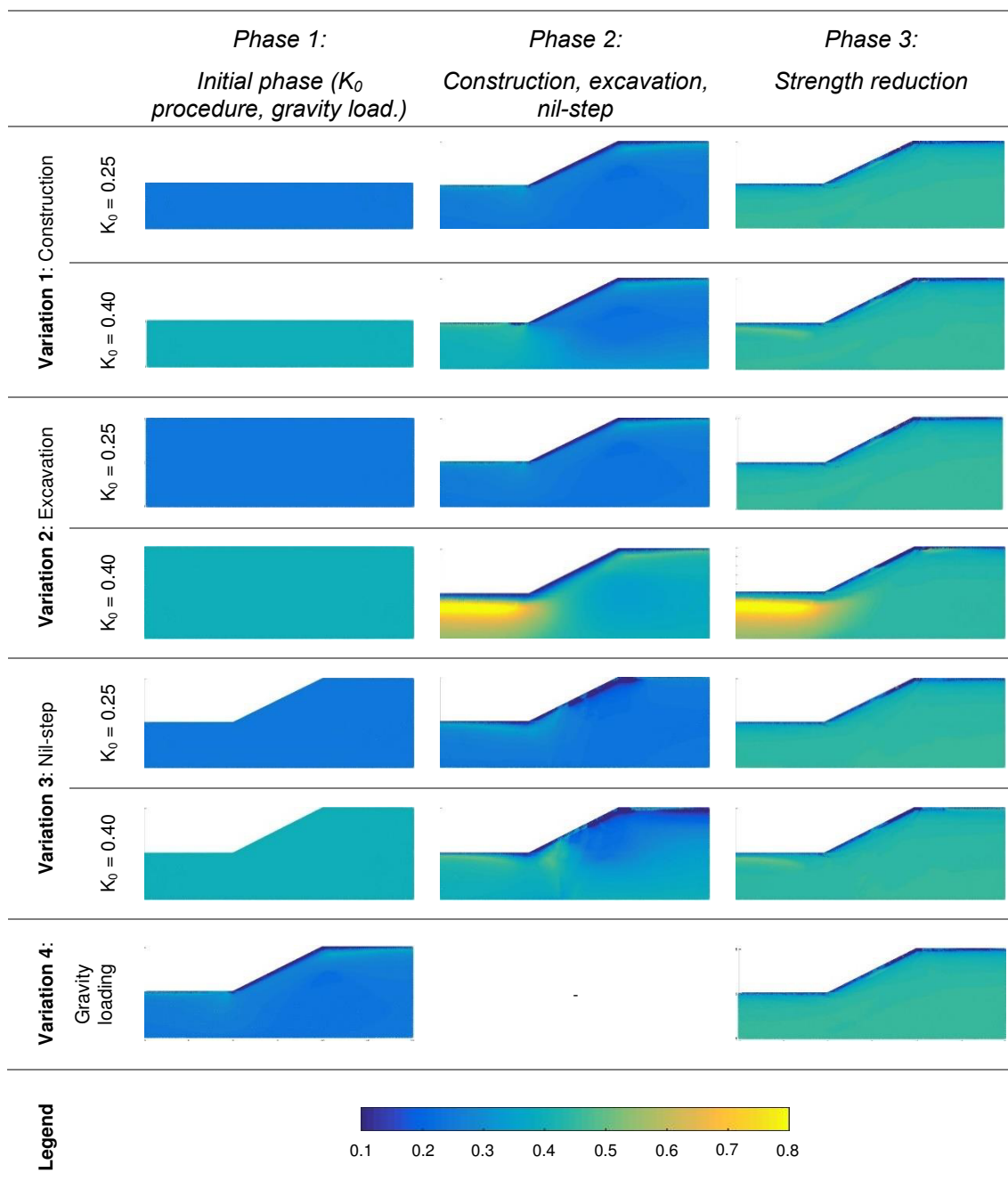
Tab. 57 SRFEA results (FoS) according to associated and non-associated plasticity

	<i>Slope 1</i>				<i>Slope 2</i>			
	$\psi' = 0^\circ$		$\psi' = \varphi'$		$\psi' = 0^\circ$		$\psi' = \varphi'$	
K_0	0.25	0.40	0.25	0.40	0.25	0.40	0.25	0.40
<i>Variation 1: Construction</i>	1.72	1.72	1.80	1.80	1.37	1.37	1.43	1.43
<i>Variation 2: Excavation</i>	1.72	1.71	1.81	1.81	1.37	1.37	1.43	1.43
<i>Variation 3: Nil-step</i>	1.70	1.71	1.81	1.81	1.36	1.36	1.43	1.43
<i>Variation 4: Gravity load.</i>	1.72		1.81		1.37		1.43	

In order to gain a better understanding of the stress distribution, the ratio of minor principle stress σ'_3 over major principle stress σ'_1 for the several variations and phases is plotted in Tab. 58. Due to the fact that no rotation of the principle stresses occurs in a K_0 procedure, the illustrated ratio is equal to K_0 . As it can be clearly seen, the ratio is constant for the whole domain (as it is an input to the analysis). In phase 2, the different initial stress conditions cause divergent σ'_3 / σ'_1 ratios. It is notable that all three variations with an initial K_0 value equal to 0.25 are in exceptional agreement with the initial phase of variation 4 (gravity loading). The second phases based on $K_0 = 0.4$ are in good agreement as well. Variation 2 leads to higher ratios below the toe of the embankment.

Due to the excavation, the minor principle stresses rotate and become relatively large compared to the diminishing major principle stresses. The followed strength reduction analyses show that the ratios of principle stresses are almost the same for all the variations. The exception here is again variation 2 with an initial $K_0 = 0.4$. The reason for this is the same as discussed above.

Tab. 58 Slope 1 - SRFEA ($\psi' = \varphi'$): σ'_3 / σ'_1



To demonstrate that the initial stress distribution does not affect the factor of safety, the stress paths of point A and B are considered in more detail. Both points are located within

the failure mechanism, as it is shown in Fig. 92. The corresponding stress paths for variations 1 to 4 are shown in Fig. 93 and Fig. 94. However, it must be said that the starting points of each stress path are marked by an orange node. Equal factors of safety must result in stress paths reaching the same Mohr-Coulomb failure criterion. By looking at Fig. 93 and Fig. 94, it becomes clear that the stress paths always end at the same Mohr-Coulomb failure criterion, unaffected by their starting point.

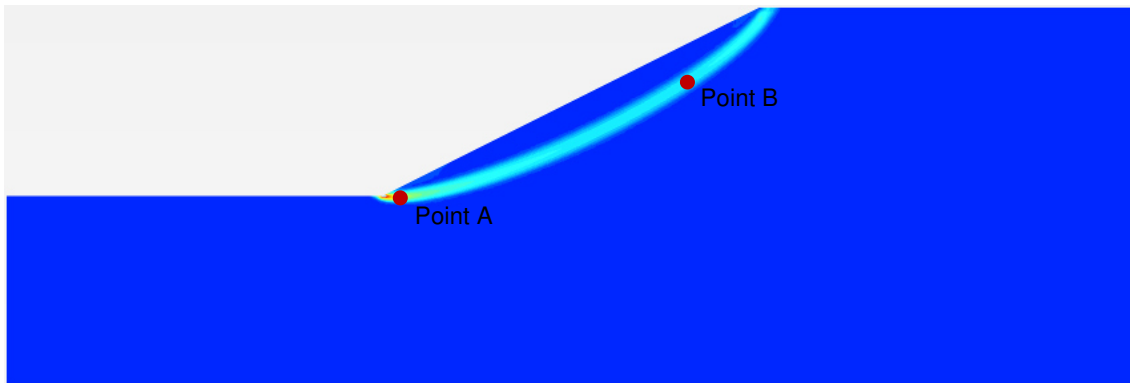


Fig. 92 Location of point A and point B

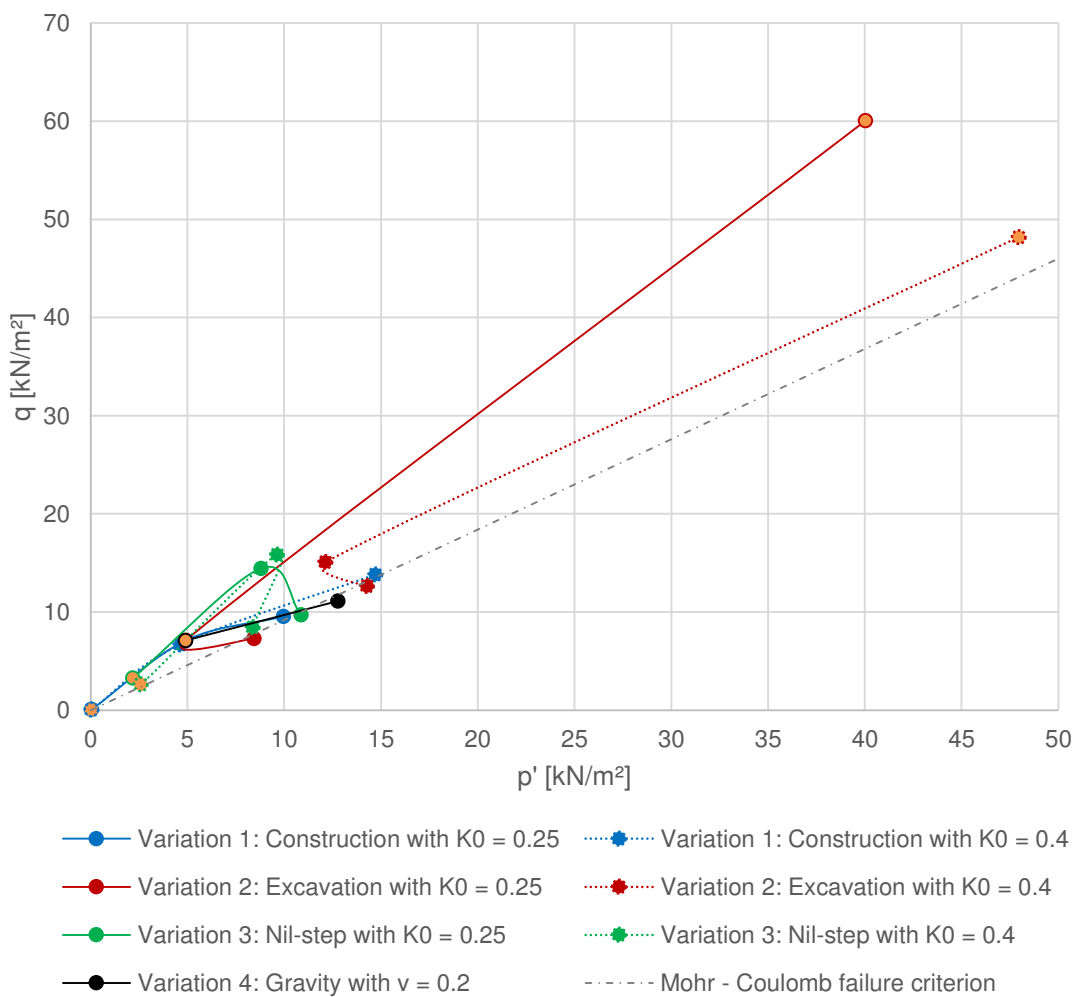


Fig. 93 Stress paths of point A

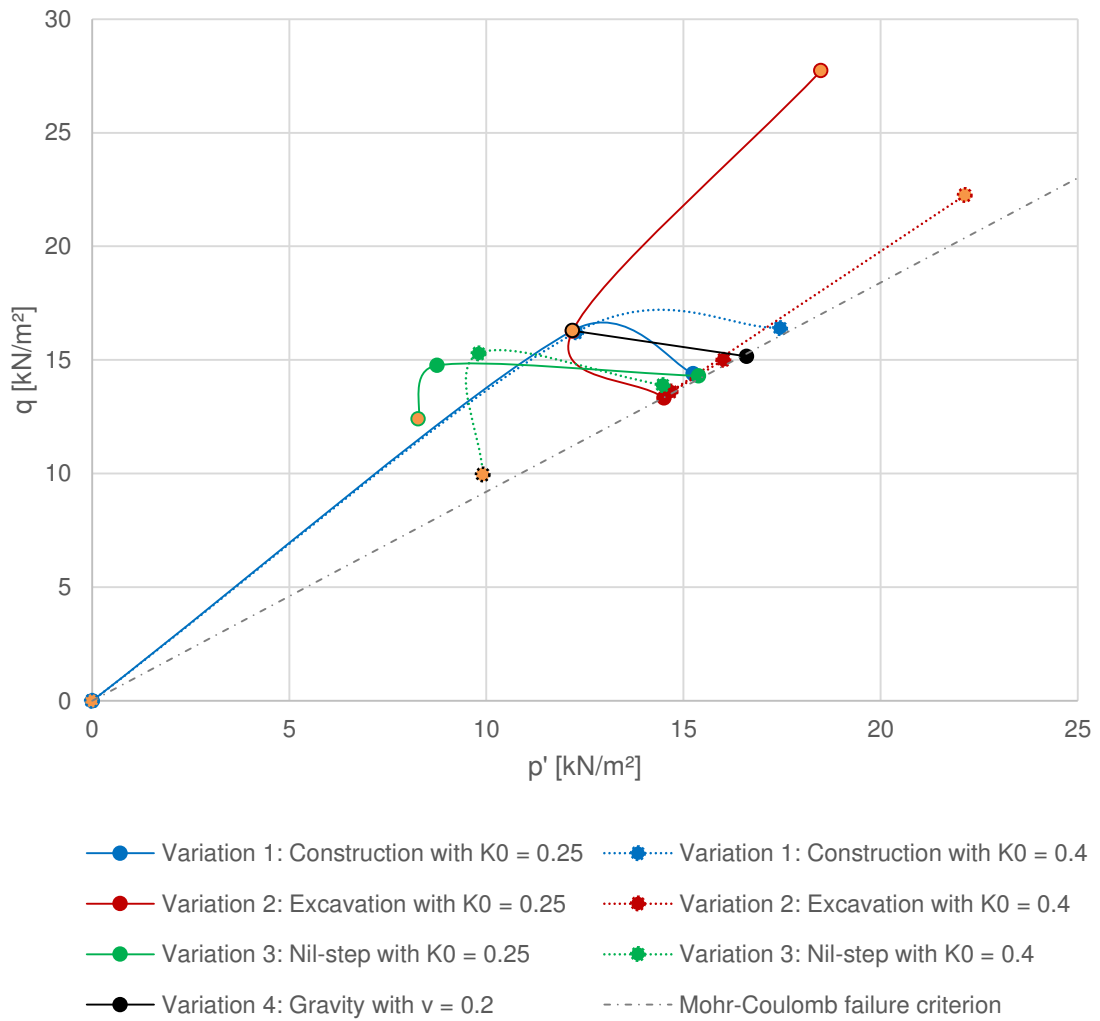


Fig. 94 Stress paths of point B

8 Conclusion

The results presented in this thesis confirm that the *limit equilibrium analysis* (LEA), the *finite element limit analysis* (FELA) and the *strength reduction finite element analysis* (SRFEA) assuming associated plasticity are in good agreement with each other. At the same time it is shown, that by using an adaptive mesh refinement, it is possible to remarkably reduce the number of elements. It has been determined in Griffiths & Lane (1999) that *a priori* knowledge of the failure mechanism is required in order to avoid an overestimation of the factor of safety. Cases with $\varphi' \neq \psi'$ demonstrated a lower FoS provided by the SRFEA compared to a LEA. It should be noted that for steep slopes with a high degree of non-associativity ($\Lambda = \varphi' - \psi'$), the failure mechanism changes during a $\varphi - c$ reduction. As a consequence, no clear definition of the FoS is possible.

The numerical instabilities of non-associated *displacement based finite element analyses* can be avoided by using the Davis approach with reduced strength parameters in combination with an associated flow rule. The original concept (Davis A) leads to very conservative results when the factor of safety is expressed by strength parameters. For the enhanced procedures Davis B and Davis C, the reduction factor β is not constant anymore. It was established that three iterative determinations of β are in general sufficient that the safety factor remains the same. These stability analyses on two reinforced slopes as well as on six examples (Griffiths & Lane 1999) showed that the modified procedures lead to slightly conservative results too but are in better agreement with the non-associated SRFEA.

Further parameter studies have proven that an increasing friction angle φ' , cohesion c' and degree of non-associativity Λ lead to larger differences between Davis A and the standard SRFEA. The dilatancy angle is kept constant in a standard strength reduction until the reduced friction angle amounts to the same value. Once $\varphi'_{red.}$ equals ψ' , both strength parameters are simultaneously reduced. Therefore a user-defined SRFEA has been used, on the other hand, where the friction and dilatancy angle are reduced concurrently from the beginning. Since the difference of the friction angle φ' to the dilatancy angle ψ' characterizes the amount of non-associativity, the latter method is considered to be more appropriate. It should be noted that the differences between Davis B and the user-defined SRFEA as well as between Davis C and the standard SRFEA are approximately the same. While the degree of non-associativity Λ has a noticeable influence on those differences, a change in the cohesion c' shows no effect.

It should be mentioned that Davis B and Davis C do not always have to be conservative compared to non-associated SRFEA. E.g. in the case of a vertical pile where the confined situation of the boundary value problem leads to the mobilisation of normal forces along the skin. Such a scenario where the FoS obtained with non-associated plasticity is smaller than the FoS obtained with the modified Davis approach was never achieved in this study.

In a further section, it was proved that the $\varphi - \nu$ inequality does not influence the factor of safety. Small differences in the FoS arising from the variation of ν are related to varying failure mechanism. The Poisson's ratio ν , however, plays an important role for the amount of failure points. It appears that the amount of failure points diminishes with an increasing ν .

Final analyses proved that the initial stress state has no impact on the FoS. If a point which is situated along the failure mechanism is considered, it is of no importance where the stress path starts (in the initial phase), failure will always occur at the same reduced strength parameters ($\varphi'_{mob.}$, $c'_{mob.}$), thus Mohr-Coulomb criterion.

9 Literatur

- Abramson, L.W.; Lee, T.S.; Sharma, S.; Boyce, G.M. (2002)
Slope Stabilisation and Stabilisation Methods. Second edition, 329-461, New York: John Wiley & Sons, Inc.
- Aryal, K.P. (2006)
Slope Stability Evaluations by Limit Equilibrium and Finite Element Methods. Ph.D. Thesis, Norwegian University of Science and Technology.
- Bishop, A. W. (1955)
The use of slip circles in the stability analysis of earth slopes. *Géotechnique* 5, No. 1, 7-17, <http://dx.doi.org/10.1680/geot.1955.5.1.7>.
- Brinkgreve, R.B.J.; Kumarswamy, S.; Swolfs, W.M. (2016)
PLAXIS 2D 2016 - User Manual. Delft, The Netherlands: Plaxis bv.
- Chen, W.F. (2007)
Limit Analysis and Soil Plasticity. pp. 1-122, J.Ross publishing
- Davis, E. H. (1968)
Theories of plasticity and failure of soil masses. In *Soil mechanics: selected topics.* (ed. I. K. Lee), pp.341–354. New York, NY, USA: Elsevier.
- Doherty, J. P.; Muir Wood, D. (2013)
An extended Mohr-Coulomb (EMC) model for predicting the settlement of shallow foundations on sand. *Géotechnique* 63, 661-673.
- Egger, D. (2012)
Untersuchung zur Böschungsstabilität mittels FE-Methode. Master's thesis, Institute of Soil Mechanics and Foundation Engineering, Graz University of Technology.
- Fellenius, W. (1936)
Calculations of the Stability of Earth Dams. *Proceedings of the Second Congress of Large Dams.* Vol. 4, pp. 445-63, Washington D. C.
- Griffiths, D.V.; Lane, P.A. (1999)
Slope stability analysis by finite elements. *Géotechnique* 49, No. 3, 387-403, <http://dx.doi.org/10.1680/geot.1999.49.3.387>.
- Janbu, N. (1954)
Proceedings of the European conference on stability of earth slopes, Stockholm, Sweden, Vol. 3, pp. 43-49. Stockholm, Sweden: International Society of Soil Mechanics and Foundation Engineering.
- Krabbenhøft, K., Lyamin, A. V., Hjjaj, M. & Sloan, S. W. (2005)
A new discontinuous upper bound limit analysis formulation. *Int. J. Numer. Methods Engng* 63, No. 7, 1069–1088.
- Krabbenhøft, K.; Lyamin, A.V.; Krabbenhøft, J. (2016)
Optum G2 2016 - User Manual. Newcastle, Australia: Optum Computational Engineering.

- Lyamin, A.V.; Sloan, S.W. (2002a).
Lower bound limit analysis using nonlinear programming. *Int. J. Numer. Methods Engng* 55, No. 5, 573–611.
- Lyamin, A.V.; Sloan, S.W. (2002b).
Upper bound limit analysis using linear finite elements and nonlinear programming. *Int. J. Numer. Analyt. Methods Geomech.* 26, No. 2, 181-216.
- Morgenstern, N. R.; Price, V. E. (1965)
The analysis of the stability of general slip surfaces. *Géotechnique* 15, No. 1, 79-93, <http://dx.doi.org/10.1680/geot.1965.15.1.79>.
- Nash, D. (1987)
Comprehensive Review of Limit Equilibrium Methods of Stability Analysis. Chapter 2, pp. 11-75, New York: John Wiley & Sons, Inc.
- Nordal, S. (2014)
Advanced Course Geotechnical Engineering: Lecture notes and background material. Institutt for bygg, anlegg og transport, Norwegian University of Science and Technology.
- Schanz, T. (1998)
Zur Modellierung des mechanischen Verhaltens von Reibungsmaterialien. Habilitation, Stuttgart Universität.
- Schweiger, H.F. (2016)
Computational Geotechnics: Lecture notes. Institute of Soil Mechanics and Foundation Engineering, Graz University of Technology.
- Sloan, S. W. (2013)
51st Rankine lecture: geotechnical stability analysis. *Géotechnique* 63, No. 7, 531-572, <http://dx.doi.org/10.1680/geot.12.RL.001>.
- Smith, I.M.; Griffiths, D.V. (1998)
Programming the finite element method, 3rd edn. Chichester: Wiley.
- Spencer, E. (1967).
A method of analysis of the stability of embankments assuming parallel inter-slice forces. *Géotechnique* 17, No. 1, 11-26, <http://dx.doi.org/10.1680/geot.1967.17.1.11>.
- Tschuchnigg, F.; Schweiger, H.F.; Sloan, S.W. (2015a)
Slope stability analysis by means of finite element limit analysis and finite element strength reduction techniques. Part I: Numerical studies considering non-associated plasticity. *Computers and Geotechnics* 70, 169-177, <http://dx.doi.org/10.1016/j.compgeo.2015.06.018>.
- Tschuchnigg, F.; Schweiger, H.F.; Sloan, S.W. (2015b)
Slope stability analysis by means of finite element limit analysis and finite element strength reduction techniques. Part II: Back analyses of a case history. *Computers and Geotechnics* 70, 178-189, <http://dx.doi.org/10.1016/j.compgeo.2015.07.019>.
- Tschuchnigg, F.; Schweiger, H.F.; Sloan, S.W.; Lyamin, A.V.; Raissakis, I. (2015)
Comparison of finite-element limit analysis and strength reduction techniques. *Géotechnique* 65, No. 4, 249-257, <http://dx.doi.org/10.1680/geot.14.P.022>.

Zheng, H.; Liu, D.F.; Li, C.G. (2005)

Slope stability analysis based on elasto-plastic finite element method. International Journal for Numerical Methods in Engineering 64, 1871-1888, <http://dx.doi.org/10.1002/nme.1406>.

10 Appendix

10.1 Safety analysis of Optum G2

10.1.1 FELA (Optum G2)

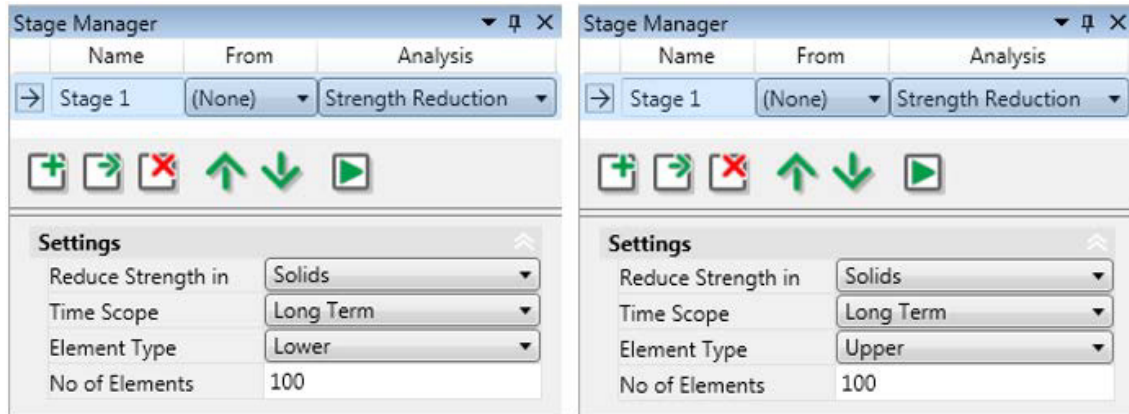


Fig. 95 FELA - Optum G2: *Strength Reduction* (in *Solids*) with (a) *Lower* and (b) *Upper* element type

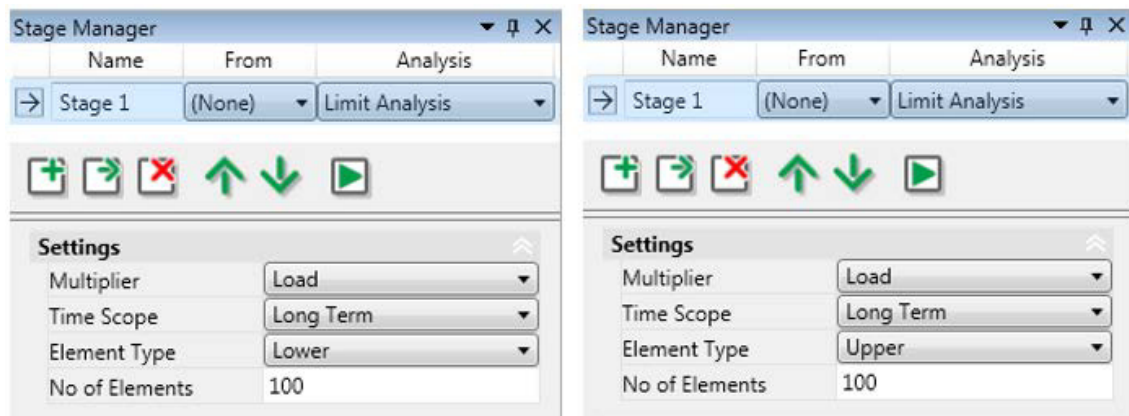


Fig. 96 FELA - Optum G2: *Limit Analysis* (Multiplier: *Load*) with (a) *Lower* and (b) *Upper* element type

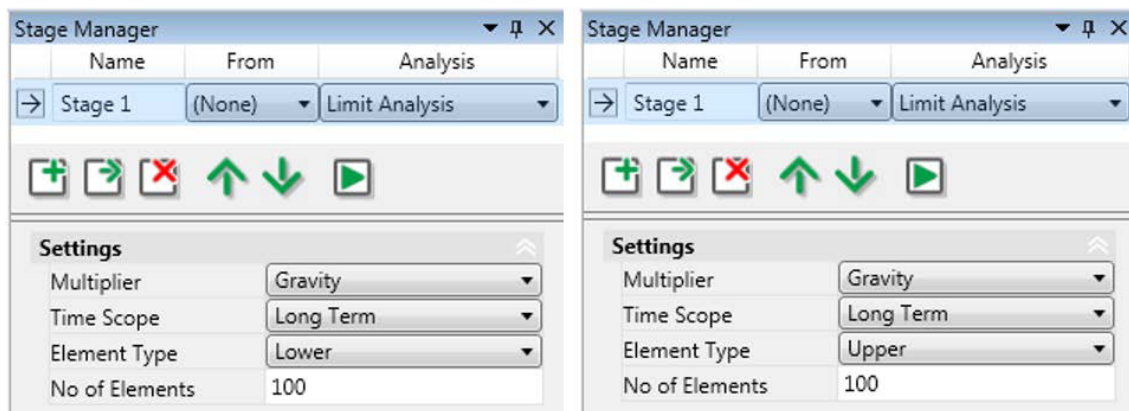


Fig. 97 FELA - Optum G2: *Limit Analysis* (Multiplier: *Gravity*) with (a) *Lower* and (b) *Upper* element type

10.1.2 SRFEA (Optum G2)

Tab. 59 Strength reduction in the soil (according to Krabbenhøft et al. 2016)

Parameters reduced	
Mohr-Coulomb	$c', \tan\phi'$
Drucker-Prager	K, M
Tesca	c_u
Hoek-Brown	σ_{ci}, m_i
GSK	$c', \tan\phi'_1, \tan\phi'_2$
Modified Cam Clay	$\tan\phi'$
Hardening Mohr-Coulomb (HMC)	$c', \tan\phi'$

Tab. 60 Strength reduction in structural elements (according to Krabbenhøft et al. 2016)

Parameters reduced	
Beams	N_P, M_P (Set A) or σ_0 (Set B)
Geogrids	N_P (Set A) or σ_0 (Set B)
Fixed-End Anchors	N_P (Set A) or σ_0 (Set B)
Connectors	N_P (Set A) or σ_0 (Set B)

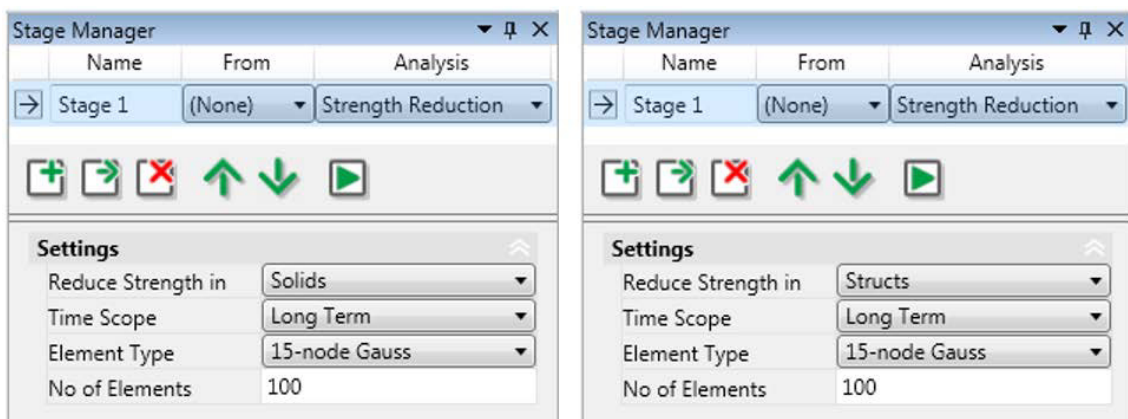


Fig. 98 SRFEA - Optum G2: (a): Strength reduction in the soil (*Solids*), (b) strength reduction in the structural elements (*Struts*)

10.2 Reinforced embankment

10.2.1 Influence of construction steps on the FoS

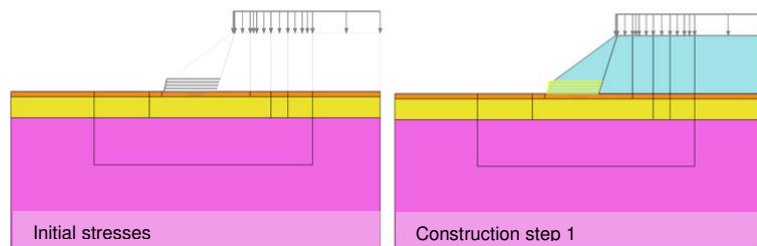


Fig. 99 Construction in one step

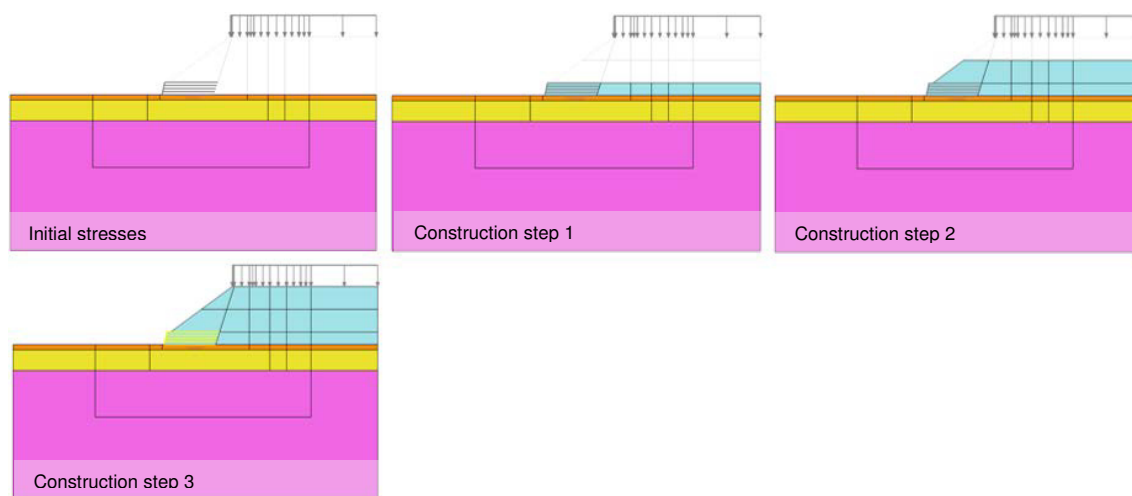


Fig. 100 Construction in three steps

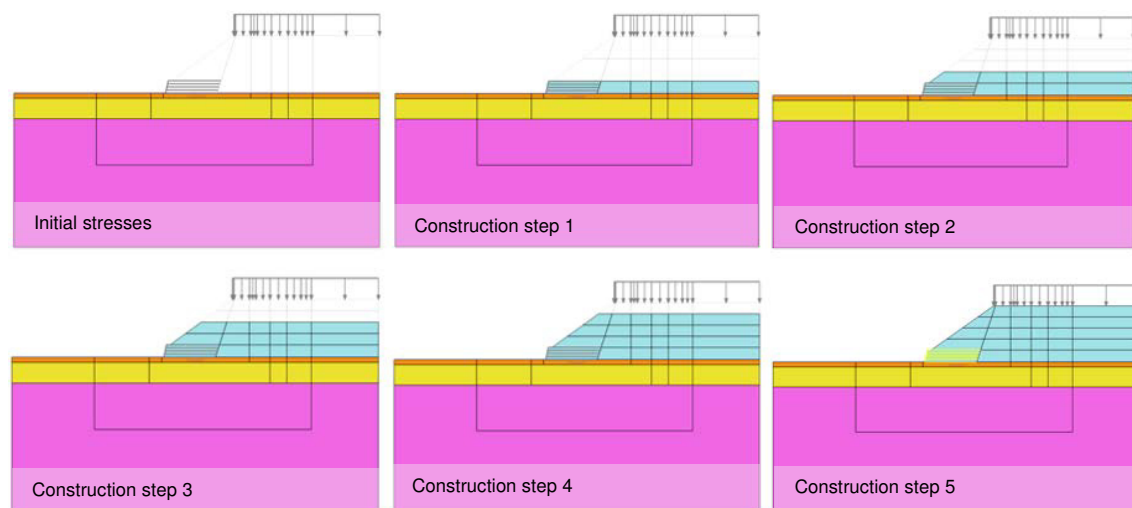


Fig. 101 Construction in five steps

Tab. 61 Influence of construction steps on the factor of safety: Overview of the safety factors

SRFEA ($\psi' = 0^\circ$)			
	<i>Construction in 1 step</i>	<i>Construction in 3 steps</i>	<i>Construction in 5 steps</i>
LC1	1.52	1.52	1.53
LC2	1.42	1.41	1.42
LC3	1.28	1.27	1.27

10.2.2 Safety analyses on modified cross section 1 and cross section 2

Tab. 62 Modified cross section 1: Comparison of SRFEA and LEA

LEA, SRFEA			
	<i>Loading condition 1</i>	<i>Loading condition 2</i>	<i>Loading condition 3</i>
LEA (M-P)	1.59	1.49	1.37
SRFEA ($\psi' = \varphi'$)	1.54	1.45	1.33
SRFEA ($\psi' = 0^\circ$)	1.40	1.31	1.17

Tab. 63 Modified cross section 1: Differences between SRFEA and LEA

% Differences			
	<i>Loading condition 1</i>	<i>Loading condition 2</i>	<i>Loading condition 3</i>
$\frac{LEA (M-P) - SRFEA (\psi' = \varphi')}{LEA (M-P)} = 100 (LEA (M-P) - SRFEA (\psi' = \varphi')) / LEA (M-P)$	3.1	2.7	2.9
$\frac{LEA (M-P) - SRFEA (\psi' = 0^\circ)}{LEA (M-P)} = 100 (LEA (M-P) - SRFEA (\psi' = 0^\circ)) / LEA (M-P)$	11.9	12.1	14.6

Tab. 64 Modified cross section 2: Comparison of SRFEA and LEA

LEA, SRFEA			
	<i>Loading condition 1</i>	<i>Loading condition 2</i>	<i>Loading condition 3</i>
LEA (M-P)	1.62	1.51	1.33
SRFEA ($\psi' = \varphi'$)	1.56	1.46	1.28
SRFEA ($\psi' = 0^\circ$)	1.42	1.33	1.14

Tab. 65 Modified cross section 1: Differences between SRFEA and LEA

% Differences			
	<i>Loading condition 1</i>	<i>Loading condition 2</i>	<i>Loading condition 3</i>
<i>LEA (M-P) - SRFEA ($\psi' = \varphi'$)</i> = 100 (LEA (M-P) - SRFEA ($\psi' = \varphi'$)) / LEA (M-P)	3.7	3.3	3.8
<i>LEA (M-P) - SRFEA ($\psi' = 0^\circ$)</i> = 100 (LEA (M-P) - SRFEA ($\psi' = 0^\circ$)) / LEA (M-P)	12.3	11.9	14.3

10.2.3 Cross section 2: Influence of strength parameters φ' and c' on FoS

A non-associated flow rule ($\psi' = 0^\circ$) is used for the calculations. In addition, it should be noted that 400 steps are used to perform the $\varphi - c$ reduction.

Tab. 66 Cross section 1: Influence of strength parameters φ' and c' on FoS

SRFEA ($\psi' = 0^\circ$)			
	<i>Loading condition 1</i>	<i>Loading condition 2</i>	<i>Loading condition 3</i>
$\varphi' = 35^\circ; c' = 2 \text{ kPa}$	1.16	1.04	1.04
$\varphi' = 35^\circ; c' = 5 \text{ kPa}$	1.48	1.36	1.23
$\varphi' = 37^\circ; c' = 2 \text{ kPa}$	1.22	1.16	1.13
$\varphi' = 37^\circ; c' = 5 \text{ kPa}$	1.52	1.42	1.28

10.2.4 Influence of extensional stiffness and tensile strength N_p on FoS

Tab. 67 EA = 750 kN/m²: Variation of tensile strength

SRFEA ($\psi' = 0^\circ$)					
	<i>Linear elastic</i>	$N_p = 50 \text{ kN/m}$	$N_p = 15 \text{ kN/m}^2$	$N_p = 10 \text{ kN/m}$	$N_p = 5 \text{ kN/m}$
<i>Loading condition 1</i>	1.53	1.53	1.53	1.53	1.50
<i>Loading condition 2</i>	1.42	1.43	1.43	1.43	1.40
<i>Loading condition 3</i>	1.24	1.23	1.23	1.23	1.24

Tab. 68 EA = 500 kN/m²: Variation of tensile strength

SRFEA ($\psi' = 0^\circ$)					
	Linear elastic	$N_p = 50 \text{ kN/m}$	$N_p = 10 \text{ kN/m}^2$	$N_p = 5 \text{ kN/m}$	$N_p = 2.5 \text{ kN/m}$
Loading condition 1	1.57	1.57	1.54	1.49	1.33
Loading condition 2	1.43	1.44	1.44	1.40	1.26
Loading condition 3	1.25	1.24	1.23	1.21	1.18

10.2.5 Mesh study: Safety values for SRFEA and FELA

Tab. 69 SRFEA ($\psi' = \varphi'$): Plaxis 2D - no adaptive mesh refinement

15-noded		6-noded	
No of elements	FoS _{15-noded}	No of elements	FoS _{6-noded}
62	1.92	62	2.23
75	1.89	75	2.18
103	1.81	103	1.99
213	1.74	213	1.91
406	1.70	406	1.83
637	1.70	637	1.82
821	1.70	821	1.81
1060	1.69	1060	1.78
1537	1.69	1696	1.76
3056	1.68	3056	1.73
4992	1.67	4992	1.71
10913	1.66	10913	1.69

Tab. 70 SRFEA ($\psi' = \varphi'$): Optum G2 - no adaptive mesh refinement

<i>15-noded</i>		<i>6-noded</i>	
No of elements	FoS _{15-noded}	No of elements	FoS _{6-noded}
495	1.72	483	1.94
588	1.72	580	1.88
687	1.72	673	1.85
757	1.69	759	1.81
883	1.69	880	1.79
971	1.69	969	1.78
1065	1.69	1057	1.78
1142	1.69	1132	1.78
1269	1.69	1279	1.78
1327	1.69	1324	1.78

Tab. 71 SRFEA ($\psi' = \varphi'$): Optum G2 - adaptive mesh refinement

<i>15-noded</i>		<i>6-noded</i>	
No of elements	FoS _{15-noded}	No of elements	FoS _{6-noded}
359	1.71	371	1.85
591	1.69	583	1.77
637	1.68	635	1.74
772	1.67	780	1.71
916	1.66	964	1.70
1071	1.66	1127	1.69
1273	1.66	1333	1.68

Tab. 72 FELA: Optum G2 - no adaptive mesh refinement

<i>Lower-bound</i>		<i>Upper-bound</i>	
No of elements	FoS _{LB}	No of elements	FoS _{UB}
495	0.68	483	2.06
588	1.16	580	2.00
683	1.29	673	1.97
757	1.34	759	1.89
955	1.46	969	1.88
1065	1.52	1057	1.84
1142	1.48	1132	1.84
1269	1.50	1279	1.84
1327	1.48	1324	1.84
5120	1.60	5120	1.75

Tab. 73 FELA: Optum G2 - adaptive mesh refinement

<i>Lower-bound</i>		<i>Upper-bound</i>	
No of elements	FoS _{LB}	No of elements	FoS _{UB}
359	0.83	371	1.96
583	1.41	573	1.85
626	1.54	649	1.79
784	1.59	748	1.75
916	1.60	956	1.72
1105	1.91	1149	1.72
1246	1.62	1302	1.71
4453	1.63	5201	1.68

10.3 Upstream slope

10.3.1 Input parameters for modelling soil nails and Maccaferri grid

Tab. 74 Input parameters for the Maccaferri grid

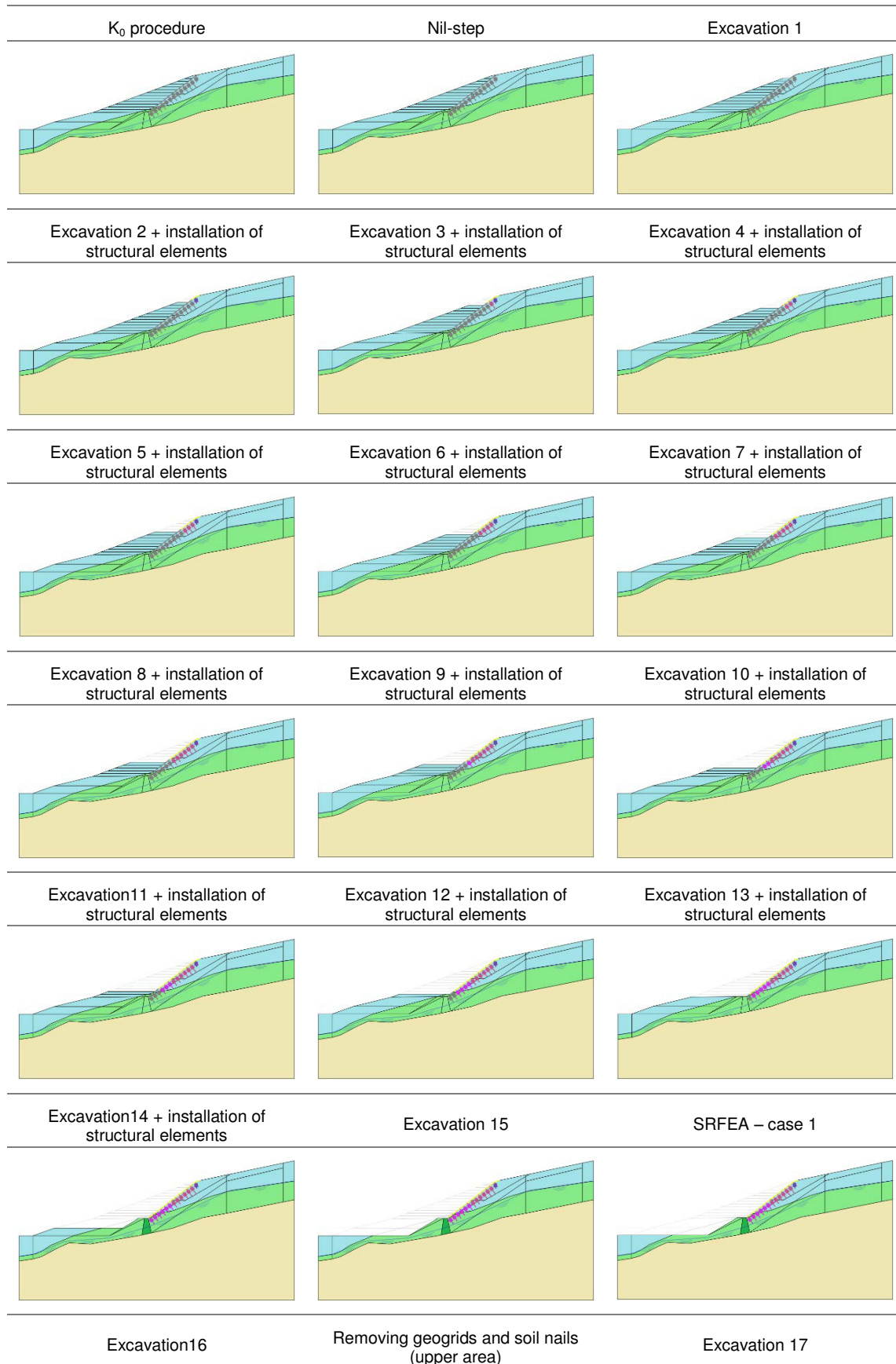
	<i>Plaxis 2D</i>	<i>Optum G2</i>
<i>Set type</i>	Geogrids	Geogrids
<i>Material type</i>	Elastoplastic	Elastoplastic
<i>EA (kN/m)</i>	2000	2000
<i>N_p (kN/m)</i>	40	40

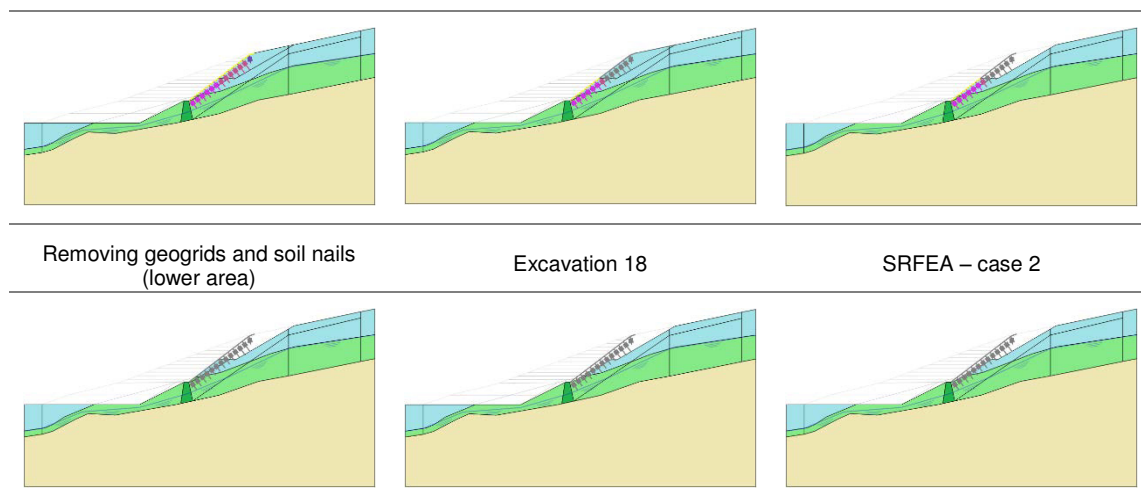
Tab. 75 Input parameters for the soil nails

	<i>Plaxis 2D</i>	<i>Optum G2 2</i>
<i>Set type</i>	Embedded beam row	Nail Rows
<i>Material type</i>	Elastoplastic	Elastic
<i>E' (MPa)</i>	200000	200000
<i>γ (kN/m³)</i>	7850	-
<i>D (cm)</i>	2.7	2.7
<i>L_{Spacing} (m)</i>	2; 2.5; 3	2; 2.5; 3
<i>N_p (kN)</i>	104	-
<i>T_{skin,axial} (kN/m)</i>	34 (start, max = end, max)	34
<i>T_{skin,lateral} (kN/m)</i>	5 (start = end)	5

10.3.2 Excavation steps for SRFEA

Tab. 76 Single phases for SRFEA performed in Plaxis 2D

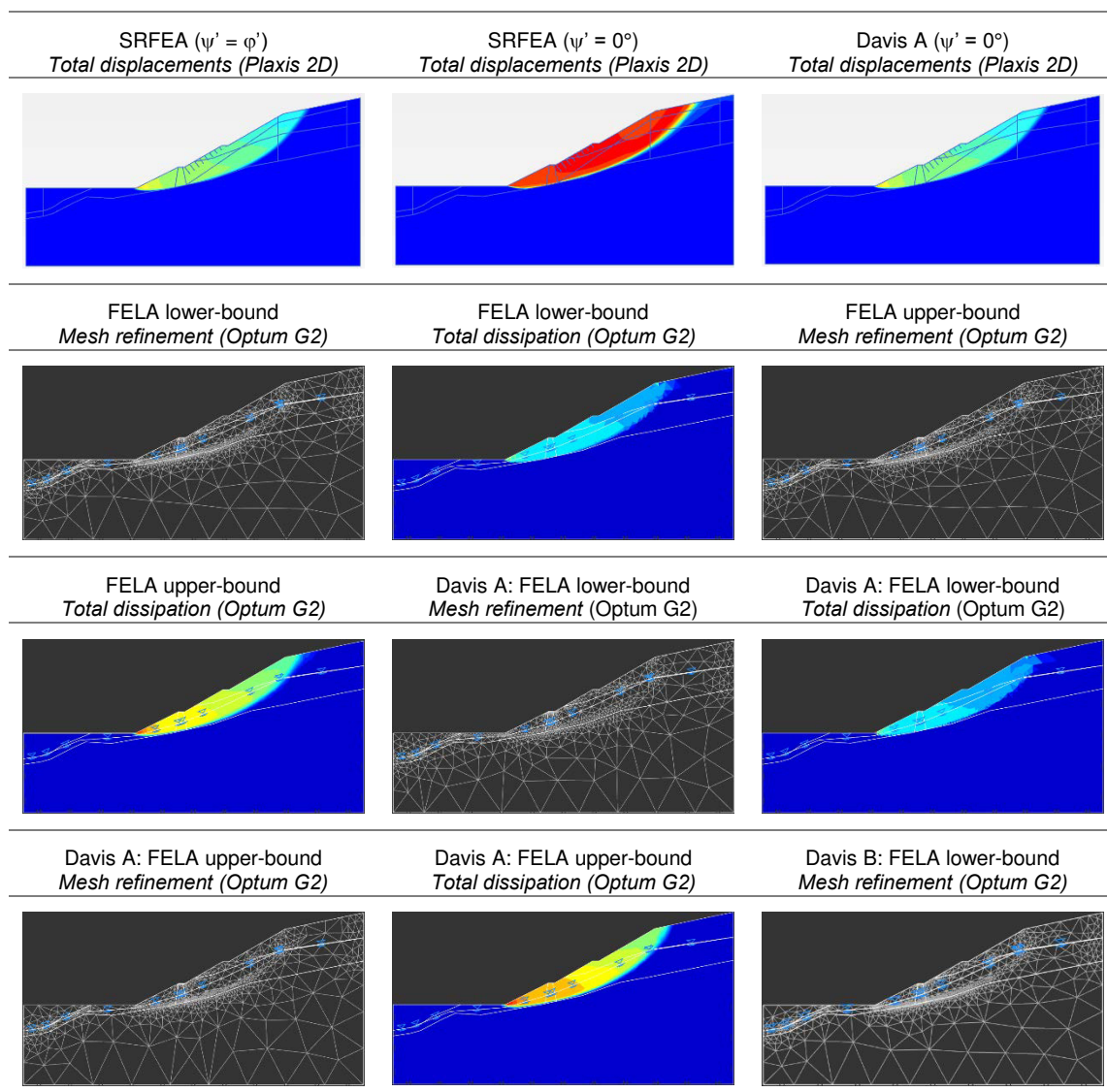


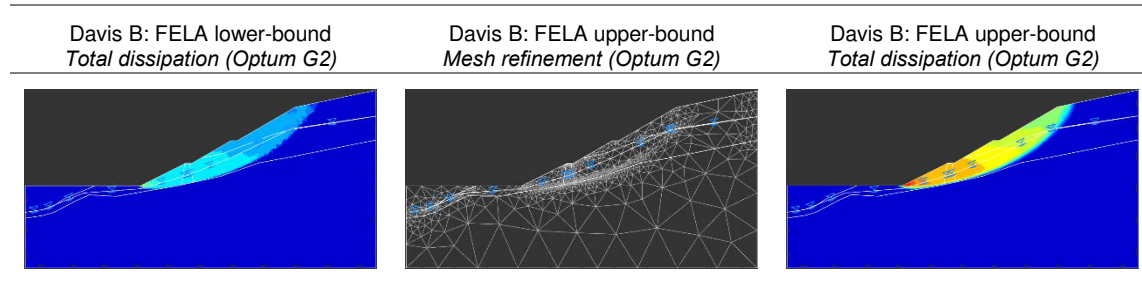


10.3.3 Additional studies on the upstream slope

- Original water table, without modifying the water pressure in Optum G2

Tab. 77 Original water table (no modifications in Optum G2): Comparison of total displacements and mesh refinements





Tab. 78 Original water table (no modifications in Optum G2): Comparison of SRFEA results

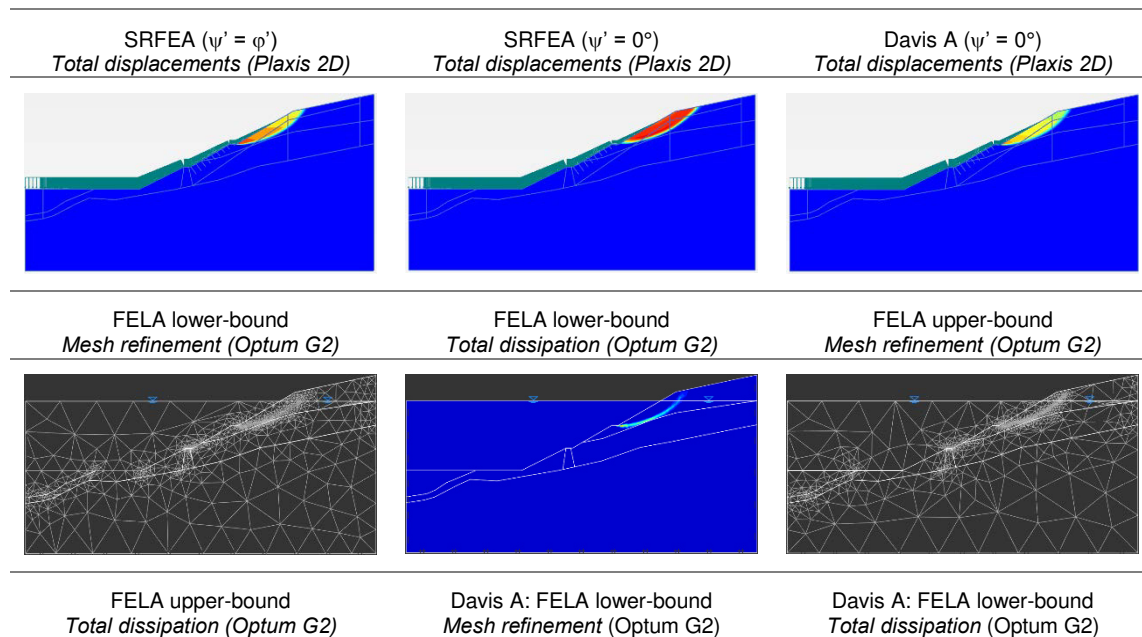
SRFEA			
	$\varphi' = \psi'$ <i>Plaxis 2D</i>	$\psi' = 0^\circ$ <i>Plaxis 2D</i>	<i>Davis A</i> ($\psi' = 0^\circ$) <i>Plaxis 2D</i>
<i>FoS</i>	1.29	1.19	1.10

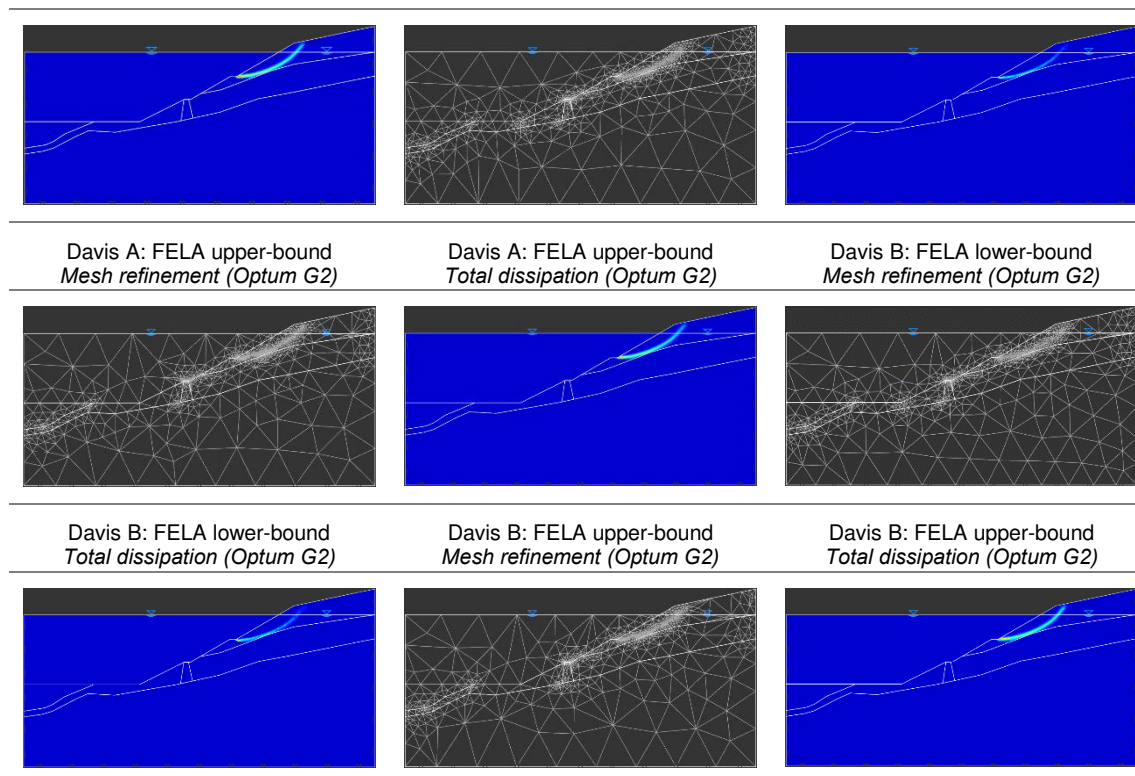
Tab. 79 Original water table (no modifications in Optum G2): Comparison of FELA results

FELA			
	$\varphi' = \psi'$ <i>Optum G2</i>	<i>Davis A</i> ($\psi' = 0^\circ$) <i>Optum G2</i>	<i>Davis B</i> ($\psi' = 0^\circ$) <i>Optum G2</i>
<i>FoS_{Mean}</i>	1.35	1.15	1.21

- Horizontal water table

Tab. 80 Horizontal water table (no modifications in Optum G2): Comparison of total displacements and mesh refinements





Tab. 81 Horizontal water table (no modifications in Optum G2): Comparison of SRFEA results

SRFEA			
	$\varphi' = \psi'$ Plaxis 2D	$\psi' = 0^\circ$ Plaxis 2D	Davis A ($\psi' = 0^\circ$) Plaxis 2D
FoS	1.55	1.49	1.33

Tab. 82 Horizontal water table: Safety factors according to FELA

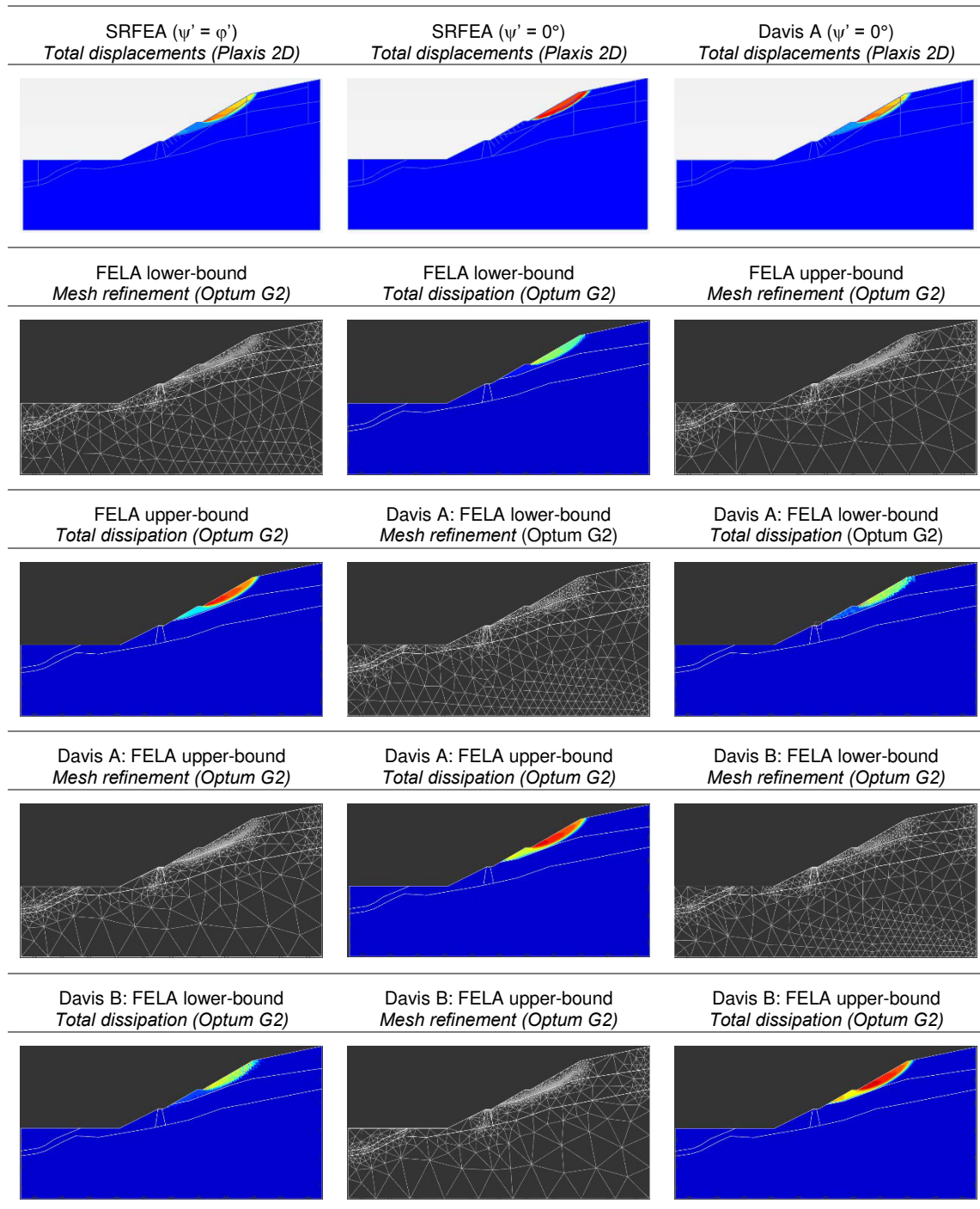
FELA			
	$\varphi' = \psi'$ Optum G2	Davis A ($\psi' = 0^\circ$) Optum G2	Davis B ($\psi' = 0^\circ$) Optum G2
FoS_{Mean}	1.55	1.33	1.43

Tab. 83 Horizontal water table (no modifications in Optum G2): Comparison of Davis A and Davis B with SRFEA ($\psi' = 0^\circ$)

% Difference	
Davis A	Davis B
$= 100 \text{ (FELA (Davis A) - SRFEA } (\psi' = 0^\circ)) / \text{FELA (Davis A)}$	$= 100 \text{ (FELA (Davis B) - SRFEA } (\psi' = 0^\circ)) / \text{FELA (Davis B)}$
- 12.0	- 4.2

- No water table

Tab. 84 No water table: Comparison of total displacements and mesh refinements



Tab. 85 No water table: Comparison of SRFEA results

SRFEA			
	$\varphi' = \psi'$ <i>Plaxis 2D</i>	$\psi' = 0^\circ$ <i>Plaxis 2D</i>	Davis A ($\psi' = 0^\circ$) <i>Plaxis 2D</i>
<i>FoS</i>	1.52	1.44	1.30

Tab. 86 No water table: Comparison of FELA results

FELA			
	$\varphi' = \psi'$ Optum G2	Davis A ($\psi' = 0^\circ$) Optum G2	Davis B ($\psi' = 0^\circ$) Optum G2
FoS _{Mean}	1.52	1.30	1.39

Tab. 87 No water table: Comparison of Davis A and Davis B with SRFEA ($\psi' = 0^\circ$)

% Difference	
Davis A	Davis B
$= 100 (\text{FELA (Davis A)} - \text{SRFEA } (\psi' = 0^\circ)) / \text{FELA (Davis A)}$	$= 100 (\text{FELA (Davis B)} - \text{SRFEA } (\psi' = 0^\circ)) / \text{FELA (Davis B)}$
- 10.8	- 3.6

10.4 Slope stability analyses based on six paper examples

10.4.1 Example 1

Tab. 88 Example 1: Check calculations

Parameters		SRFEA ($\psi' = 0^\circ$) (Plaxis 2D)				LEA (Slide) M-P Circular
		~200 elements		~1000 elements		
		15-n	6-n	15-n	6-n	
Set 1: H = 5 m $\gamma = 16 \text{ kN/m}^3$ $c' = 4 \text{ kN/m}^2$	$E' = 10^4 \text{ kN/m}^2 - \nu = 0.25$	1.35	1.39	1.35	1.36	1.37
	$E' = 10^4 \text{ kN/m}^2 - \nu = 0.35$	1.35	1.39	1.34	1.36	
	$E' = 10^6 \text{ kN/m}^2 - \nu = 0.25$	1.35	1.39	1.35	1.36	
	$E' = 10^6 \text{ kN/m}^2 - \nu = 0.35$	1.35	1.39	1.34	1.36	
Set 2: H = 5 m $\gamma = 20 \text{ kN/m}^3$ $c' = 5 \text{ kN/m}^2$	$E' = 10^4 \text{ kN/m}^2 - \nu = 0.25$	1.35	1.39	1.35	1.36	1.37
	$E' = 10^4 \text{ kN/m}^2 - \nu = 0.35$	1.35	1.39	1.34	1.36	
	$E' = 10^6 \text{ kN/m}^2 - \nu = 0.25$	1.35	1.39	1.35	1.36	
	$E' = 10^6 \text{ kN/m}^2 - \nu = 0.35$	1.35	1.39	1.34	1.36	
Set 3: H = 10 m $\gamma = 16 \text{ kN/m}^3$ $c' = 8 \text{ kN/m}^2$	$E' = 10^4 \text{ kN/m}^2 - \nu = 0.25$	1.35	1.39	1.35	1.36	1.37
	$E' = 10^4 \text{ kN/m}^2 - \nu = 0.35$	1.35	1.39	1.34	1.36	
	$E' = 10^6 \text{ kN/m}^2 - \nu = 0.25$	1.35	1.39	1.35	1.36	
	$E' = 10^6 \text{ kN/m}^2 - \nu = 0.35$	1.35	1.39	1.34	1.36	
Set 4: H = 10 m $\gamma = 20 \text{ kN/m}^3$ $c' = 10 \text{ kN/m}^2$	$E' = 10^4 \text{ kN/m}^2 - \nu = 0.25$	1.35	1.39	1.35	1.36	1.37
	$E' = 10^4 \text{ kN/m}^2 - \nu = 0.35$	1.35	1.39	1.34	1.36	
	$E' = 10^6 \text{ kN/m}^2 - \nu = 0.25$	1.35	1.39	1.35	1.36	
	$E' = 10^6 \text{ kN/m}^2 - \nu = 0.35$	1.35	1.39	1.34	1.36	

Tab. 89 Example 1: Further calculations for set 1 - part 1

Parameters	SRFEA ($\psi' = 0^\circ$) (Plaxis 2D)		SRFEA ($\psi' = \varphi'$) (Plaxis 2D)		Davis A SRFEA (Plaxis 2D)		Davis B SRFEA (Plaxis 2D)		SRFEA ($\psi' = \varphi'$) (Optum G2)				
	~200 elements		~1000 elements		~1000 elements		~1000 elements		~900 elements				
	15-n	6-n	15-n	6-n	15-n	6-n	15-n	6-n	15-n	6-n			
Set 1	$E' = 10^4 \text{ kN/m}^2$ $-\nu = 0.25$	1.35	1.39	1.35	1.36	1.38	1.39	1.30	1.30	1.33	1.34	1.37	1.38
	$E' = 10^4 \text{ kN/m}^2$ $-\nu = 0.35$	1.35	1.39	1.34	1.36	1.38	1.39	1.29	1.30	1.33	1.34	1.37	1.38
	$E' = 10^6 \text{ kN/m}^2$ $-\nu = 0.25$	1.35	1.39	1.35	1.36	1.38	1.39	1.30	1.30	1.33	1.34	1.37	1.38
	$E' = 10^6 \text{ kN/m}^2$ $-\nu = 0.35$	1.35	1.39	1.34	1.36	1.38	1.39	1.29	1.30	1.33	1.34	1.37	1.38

Tab. 90 Example 1: Further calculations for set 1 - part 2

Parameters	FELA (Optum G2)			Davis A - FELA (Optum G2)			Davis B - FELA (Optum G2)			LEA (Slide)	
	Lower	Upper	Mean	Lower	Upper	Mean	Lower	Upper	Mean	M-P Circ.	
Set 1	~900 elements			~900 elements			~900 elements			1.37	
	$E' = 104 \text{ kN/m}^2$ $- \nu = 0.25$	1.36	1.38	1.37	1.28	1.30	1.29	1.31	1.33		1.32
	$E' = 104 \text{ kN/m}^2$ $- \nu = 0.35$	1.36	1.38	1.37	1.28	1.30	1.29	1.31	1.33		1.32
	$E' = 106 \text{ kN/m}^2$ $- \nu = 0.25$	1.36	1.38	1.37	1.28	1.30	1.29	1.31	1.33		1.32
	$E' = 106 \text{ kN/m}^2$ $- \nu = 0.35$	1.36	1.38	1.37	1.28	1.30	1.29	1.31	1.33	1.32	

10.4.2 Example 2

Tab. 91 Example 2: Check calculations

Parameters	SRFEA ($\psi' = 0^\circ$) (Plaxis 2D)				LEA (Slide)	
	~250 elements		~1000 elements		M-P Circular	
	15-n	6-n	15-n	6-n		
Set 1: H = 5 m $\gamma = 16 \text{ kN/m}^3$ $c' = 4 \text{ kN/m}^2$	$E' = 10^4 \text{ kN/m}^2 - \nu = 0.25$	1.33	1.39	1.32	1.35	1.37
	$E' = 10^4 \text{ kN/m}^2 - \nu = 0.35$	1.33	1.39	1.33	1.35	
	$E' = 10^6 \text{ kN/m}^2 - \nu = 0.25$	1.33	1.39	1.32	1.35	
	$E' = 10^6 \text{ kN/m}^2 - \nu = 0.35$	1.33	1.39	1.33	1.35	
Set 2: H = 5 m $\gamma = 20 \text{ kN/m}^3$ $c' = 5 \text{ kN/m}^2$	$E' = 10^4 \text{ kN/m}^2 - \nu = 0.25$	1.33	1.39	1.32	1.35	1.37
	$E' = 10^4 \text{ kN/m}^2 - \nu = 0.35$	1.33	1.39	1.33	1.35	
	$E' = 10^6 \text{ kN/m}^2 - \nu = 0.25$	1.33	1.39	1.32	1.35	
	$E' = 10^6 \text{ kN/m}^2 - \nu = 0.35$	1.33	1.39	1.33	1.35	
Set 3: H = 10 m $\gamma = 16 \text{ kN/m}^3$ $c' = 8 \text{ kN/m}^2$	$E' = 10^4 \text{ kN/m}^2 - \nu = 0.25$	1.32	1.39	1.32	1.35	1.37
	$E' = 10^4 \text{ kN/m}^2 - \nu = 0.35$	1.32	1.39	1.33	1.35	
	$E' = 10^6 \text{ kN/m}^2 - \nu = 0.25$	1.33	1.39	1.32	1.35	
	$E' = 10^6 \text{ kN/m}^2 - \nu = 0.35$	1.33	1.39	1.33	1.35	
Set 4: H = 10 m $\gamma = 20 \text{ kN/m}^3$ $c' = 10 \text{ kN/m}^2$	$E' = 10^4 \text{ kN/m}^2 - \nu = 0.25$	1.33	1.39	1.32	1.35	1.37
	$E' = 10^4 \text{ kN/m}^2 - \nu = 0.35$	1.33	1.39	1.33	1.35	
	$E' = 10^6 \text{ kN/m}^2 - \nu = 0.25$	1.33	1.39	1.32	1.35	
	$E' = 10^6 \text{ kN/m}^2 - \nu = 0.35$	1.33	1.39	1.33	1.35	

Tab. 92 Example 2: Further calculations for set 1 - part 1

Parameters	SRFEA ($\psi' = 0^\circ$) (Plaxis 2D)		SRFEA ($\psi' = \varphi'$) (Plaxis 2D)		Davis A SRFEA (Plaxis 2D)		Davis B SRFEA (Plaxis 2D)		SRFEA ($\psi' = \varphi'$) (Optum G2)				
	~250 elements		~1000 elements		~1000 elements		~1000 elements		~1000 elements		~900 elements		
	15-n	6-n	15-n	6-n	15-n	6-n	15-n	6-n	15-n	6-n	15-n	6-n	
Set 1	$E' = 10^4$ kN/m ² $\nu = 0.25$	1.33	1.39	1.32	1.35	1.36	1.37	1.28	1.29	1.31	1.32	1.36	1.37
	$E' = 10^4$ kN/m ² $\nu = 0.35$	1.33	1.39	1.33	1.35	1.36	1.37	1.28	1.29	1.31	1.32	1.36	1.37
	$E' = 10^6$ kN/m ² $\nu = 0.25$	1.33	1.39	1.32	1.35	1.36	1.37	1.28	1.29	1.31	1.32	1.36	1.37
	$E' = 10^6$ kN/m ² $\nu = 0.35$	1.33	1.39	1.33	1.35	1.36	1.37	1.28	1.29	1.31	1.32	1.36	1.37

Tab. 93 Example 2: Further calculations for set 1 - part 2

Parameters	FELA (Optum G2)			Davis A FELA (Optum G2)			Davis B FELA (Optum G2)			LEA (Slide)	
	~900 elements			~900 elements			~900 elements			M-P	
	Lower	Upper	Mean	Lower	Upper	Mean	Lower	Upper	Mean	Circ.	
Set 1	$E' = 10^4$ kN/m ² $\nu = 0.25$	1.35	1.38	1.36	1.27	1.29	1.28	1.30	1.33	1.31	1.37
	$E' = 10^4$ kN/m ² $\nu = 0.35$	1.35	1.38	1.36	1.27	1.29	1.28	1.30	1.33	1.31	
	$E' = 10^6$ kN/m ² $\nu = 0.25$	1.35	1.38	1.36	1.27	1.29	1.28	1.30	1.33	1.31	
	$E' = 10^6$ kN/m ² $\nu = 0.35$	1.35	1.38	1.36	1.27	1.29	1.28	1.30	1.33	1.31	

10.4.3 Example 3

Tab. 94 Example 3: Overview of the calculations

Parameters		SRFEA (Plaxis 2D)		SRFEA (Optum G2)		FELA (Optum G2)			LEA (Slide)					
		~1750 elements		~1000 elements		~1250 elements			Jambu simpl.	M-P Circ.	Janbu simpl. 3 l. w.	M-P 3 l. w.		
		6-n	15-n	6-n	15-n	Lower	Upper	Mean	Circ.	Circ.	3 l. w.	3 l. w.		
H = 5 m γ = 16 kN/m³ c _{u1} = 20 kN/m²	E _u = 5000 kN/m²	c _{u2} /c _{u1} = 1	1.47	1.46	1.46	1.45	1.44	1.46	1.45	1.41	1.47	2.28	2.44	
		c _{u2} /c _{u1} = 0.9	1.45	1.44	1.44	1.43	1.42	1.45	1.44	1.39	1.45	2.06	2.21	
	v _u = 0.495 (0.5)	c _{u2} /c _{u1} = 0.8	1.44	1.42	1.42	1.41	1.40	1.43	1.42	1.37	1.43	1.83	1.96	
		c _{u2} /c _{u1} = 0.7	1.41	1.39	1.40	1.39	1.37	1.41	1.39	1.35	1.41	1.60	1.72	
	c _{u2} /c _{u1} = 0.6	1.38	1.36	1.37	1.36	1.34	1.38	1.36	1.33	1.38	1.37	1.47		
		c _{u2} /c _{u1} = 0.5	1.24	1.17	1.20	1.17	1.15	1.20	1.17	1.31	1.36	1.14	1.22	
	c _{u2} /c _{u1} = 0.4	1.01	-	0.97	0.95	0.93	0.98	0.95	1.28	1.33	0.92	0.98		
		c _{u2} /c _{u1} = 0.3	-	-	0.75	0.72	0.71	0.75	0.73	1.26	1.31	0.69	0.73	
	c _{u2} /c _{u1} = 0.2	-	-	0.51	0.50	0.49	0.52	0.50	1.21	1.24	0.46	0.48		
		c _{u2} /c _{u1} = 0.1	-	-	0.28	0.27	0.26	0.28	0.27	1.12	1.11	0.23	0.24	
	H = 5 m γ = 20 kN/m³ c _{u1} = 25 kN/m²	E _u = 5000 kN/m²	c _{u2} /c _{u1} = 1	1.47	1.46	1.46	1.45	1.44	1.46	1.45	1.41	1.47	2.28	2.44
			c _{u2} /c _{u1} = 0.9	1.45	1.44	1.44	1.43	1.42	1.45	1.44	1.39	1.45	2.06	2.21
v _u = 0.495 (0.5)		c _{u2} /c _{u1} = 0.8	1.44	1.42	1.42	1.41	1.40	1.43	1.42	1.37	1.43	1.83	1.96	
		c _{u2} /c _{u1} = 0.7	1.41	1.39	1.40	1.39	1.37	1.41	1.39	1.35	1.41	1.60	1.72	
c _{u2} /c _{u1} = 0.6		1.38	1.36	1.37	1.36	1.34	1.38	1.36	1.33	1.38	1.37	1.47		
		c _{u2} /c _{u1} = 0.5	1.24	1.17	1.20	1.17	1.15	1.20	1.17	1.31	1.36	1.14	1.22	
c _{u2} /c _{u1} = 0.4		1.01	-	0.97	0.95	0.93	0.98	0.95	1.28	1.33	0.92	0.98		
		c _{u2} /c _{u1} = 0.3	-	-	0.75	0.72	0.71	0.75	0.73	1.26	1.31	0.69	0.73	
c _{u2} /c _{u1} = 0.2		-	-	0.51	0.50	0.49	0.52	0.50	1.21	1.24	0.46	0.48		
		c _{u2} /c _{u1} = 0.1	-	-	0.28	0.27	0.26	0.28	0.27	1.12	1.11	0.23	0.24	
H = 10 m γ = 16 kN/m³ c _{u1} = 40 kN/m²		E _u = 5000 kN/m²	c _{u2} /c _{u1} = 1	1.47	1.46	1.46	1.45	1.44	1.46	1.45	1.41	1.47	2.28	2.44
			c _{u2} /c _{u1} = 0.9	1.45	1.44	1.44	1.43	1.42	1.45	1.44	1.39	1.45	2.06	2.21
	v _u = 0.495 (0.5)	c _{u2} /c _{u1} = 0.8	1.44	1.42	1.42	1.41	1.40	1.43	1.42	1.37	1.43	1.83	1.96	
		c _{u2} /c _{u1} = 0.7	1.41	1.39	1.40	1.39	1.37	1.41	1.39	1.35	1.41	1.60	1.72	
	c _{u2} /c _{u1} = 0.6	1.38	1.36	1.37	1.36	1.34	1.38	1.36	1.33	1.38	1.37	1.47		
		c _{u2} /c _{u1} = 0.5	1.24	1.17	1.20	1.17	1.15	1.20	1.17	1.31	1.36	1.14	1.22	
	c _{u2} /c _{u1} = 0.4	1.01	-	0.97	0.95	0.93	0.98	0.95	1.28	1.33	0.92	0.98		
		c _{u2} /c _{u1} = 0.3	-	-	0.75	0.72	0.71	0.75	0.73	1.26	1.31	0.69	0.73	
	c _{u2} /c _{u1} = 0.2	-	-	0.51	0.50	0.49	0.52	0.50	1.21	1.24	0.46	0.48		
		c _{u2} /c _{u1} = 0.1	-	-	0.28	0.27	0.26	0.28	0.27	1.12	1.11	0.23	0.24	
	H = 10 m γ = 20 kN/m³ c _{u1} = 50 kN/m²	E _u = 5000 kN/m²	c _{u2} /c _{u1} = 1	1.47	1.46	1.46	1.45	1.44	1.46	1.45	1.41	1.47	2.28	2.44
			c _{u2} /c _{u1} = 0.9	1.45	1.44	1.44	1.43	1.42	1.45	1.44	1.39	1.45	2.06	2.21
v _u = 0.495 (0.5)		c _{u2} /c _{u1} = 0.8	1.44	1.42	1.42	1.41	1.40	1.43	1.42	1.37	1.43	1.83	1.96	
		c _{u2} /c _{u1} = 0.7	1.41	1.39	1.40	1.39	1.37	1.41	1.39	1.35	1.41	1.60	1.72	
c _{u2} /c _{u1} = 0.6		1.38	1.36	1.37	1.36	1.34	1.38	1.36	1.33	1.38	1.37	1.47		
		c _{u2} /c _{u1} = 0.5	1.24	1.17	1.20	1.17	1.15	1.20	1.17	1.31	1.36	1.14	1.22	
c _{u2} /c _{u1} = 0.4		1.01	-	0.97	0.95	0.93	0.98	0.95	1.28	1.33	0.92	0.98		
		c _{u2} /c _{u1} = 0.3	-	-	0.75	0.72	0.71	0.75	0.73	1.26	1.31	0.69	0.73	
c _{u2} /c _{u1} = 0.2		-	-	0.51	0.50	0.49	0.52	0.50	1.21	1.24	0.46	0.48		
		c _{u2} /c _{u1} = 0.1	-	-	0.28	0.27	0.26	0.28	0.27	1.12	1.11	0.23	0.24	

10.4.4 Example 4

Tab. 95 Example 4: Overview of the calculations

Parameters		SRFEA (Plaxis 2D)		SRFEA (Optum G2)		FELA (Optum G2)			LEA (Slide)	
		~1450 elements		~1000 elements		~1050 elements			M-P	
		6-n	15-n	6-n	15-n	Lower	Upper	Mean	Circular	
H = 5 m $\gamma = 16 \text{ kN/m}^3$ $c_{u1} = 20 \text{ kN/m}^2$	$E_{s1} = 5000 \text{ kN/m}^2$ $\nu_{s1} = 0.495 (0.5)$	$c_{u2}/c_{u1} = 4$	2.07	2.04	2.05	2.02	1.99	2.05	2.02	2.03
		$c_{u2}/c_{u1} = 3.5$	2.07	2.04	2.04	2.02	1.99	2.05	2.02	2.03
		$c_{u2}/c_{u1} = 3$	2.07	2.04	2.04	2.02	1.99	2.05	2.02	2.03
		$c_{u2}/c_{u1} = 2.5$	2.07	2.04	2.04	2.02	1.99	2.05	2.02	2.03
		$c_{u2}/c_{u1} = 2$	2.07	2.04	2.04	2.02	1.99	2.05	2.02	2.03
		$c_{u2}/c_{u1} = 1.5$	2.04	2.02	2.04	2.02	1.99	2.05	2.02	2.03
		$c_{u2}/c_{u1} = 1$	1.47	1.46	1.46	1.45	1.44	1.46	1.45	1.47
		$c_{u2}/c_{u1} = 0.75$	1.17	1.15	1.16	1.15	1.14	1.16	1.15	1.18
		$c_{u2}/c_{u1} = 0.5$	-	-	0.86	0.85	0.84	0.86	0.85	0.87
		$c_{u2}/c_{u1} = 0.25$	-	-	0.55	0.54	0.53	0.55	0.54	-
		$c_{u2}/c_{u1} = 4$	2.07	2.04	2.05	2.02	1.99	2.05	2.02	-
		$c_{u2}/c_{u1} = 3.5$	2.07	2.04	2.04	2.02	1.99	2.05	2.02	-
		$c_{u2}/c_{u1} = 3$	2.07	2.04	2.04	2.02	1.99	2.05	2.02	-
		$c_{u2}/c_{u1} = 2.5$	2.07	2.04	2.04	2.02	1.99	2.05	2.02	-
H = 5 m $\gamma = 20 \text{ kN/m}^3$ $c_{u1} = 25 \text{ kN/m}^2$	$E_{s1} = 7000 \text{ kN/m}^2$ $\nu_{s1} = 0.495 (0.5)$	$c_{u2}/c_{u1} = 4$	2.07	2.04	2.04	2.02	1.99	2.05	2.02	-
		$c_{u2}/c_{u1} = 3.5$	2.07	2.04	2.04	2.02	1.99	2.05	2.02	-
		$c_{u2}/c_{u1} = 3$	2.07	2.04	2.04	2.02	1.99	2.05	2.02	-
		$c_{u2}/c_{u1} = 2.5$	2.07	2.04	2.04	2.02	1.99	2.05	2.02	-
		$c_{u2}/c_{u1} = 2$	2.07	2.04	2.04	2.02	1.99	2.05	2.02	-
		$c_{u2}/c_{u1} = 1.5$	2.04	2.02	2.04	2.02	1.99	2.05	2.02	-
		$c_{u2}/c_{u1} = 1$	1.47	1.46	1.46	1.45	1.44	1.46	1.45	-
		$c_{u2}/c_{u1} = 0.75$	1.17	1.15	1.16	1.15	1.14	1.16	1.15	-
		$c_{u2}/c_{u1} = 0.5$	-	-	0.86	0.85	0.84	0.86	0.85	-
		$c_{u2}/c_{u1} = 0.25$	-	-	0.55	0.54	0.53	0.55	0.54	-
		$c_{u2}/c_{u1} = 4$	2.07	2.04	2.05	2.02	1.99	2.05	2.02	2.03
		$c_{u2}/c_{u1} = 3.5$	2.07	2.04	2.04	2.02	1.99	2.05	2.02	2.03
		$c_{u2}/c_{u1} = 3$	2.07	2.04	2.04	2.02	1.99	2.05	2.02	2.03
		$c_{u2}/c_{u1} = 2.5$	2.07	2.04	2.04	2.02	1.99	2.05	2.02	2.03
$c_{u2}/c_{u1} = 2$	2.07	2.04	2.04	2.02	1.99	2.05	2.02	2.03		
H = 10 m $\gamma = 16 \text{ kN/m}^3$ $c_{u1} = 40 \text{ kN/m}^2$	$E_{s1} = 5000 \text{ kN/m}^2$ $\nu_{s1} = 0.495 (0.5)$	$c_{u2}/c_{u1} = 4$	2.07	2.04	2.04	2.02	1.98	2.05	2.01	2.03
		$c_{u2}/c_{u1} = 3.5$	2.07	2.04	2.04	2.02	1.98	2.05	2.01	2.03
		$c_{u2}/c_{u1} = 3$	2.07	2.04	2.04	2.02	1.98	2.05	2.01	2.03
		$c_{u2}/c_{u1} = 2.5$	2.07	2.04	2.04	2.02	1.98	2.05	2.01	2.03
		$c_{u2}/c_{u1} = 2$	2.07	2.04	2.04	2.02	1.98	2.05	2.01	2.03
		$c_{u2}/c_{u1} = 1.5$	2.04	2.02	2.04	2.02	1.98	2.05	2.01	2.03
		$c_{u2}/c_{u1} = 1$	1.47	1.46	1.46	1.45	1.43	1.46	1.44	1.47
		$c_{u2}/c_{u1} = 0.75$	1.17	1.15	1.16	1.15	1.14	1.16	1.15	1.18
		$c_{u2}/c_{u1} = 0.5$	-	-	0.86	0.85	0.84	0.86	0.85	0.87
		$c_{u2}/c_{u1} = 0.25$	-	-	0.55	0.54	0.53	0.55	0.54	-
		$c_{u2}/c_{u1} = 4$	2.07	2.04	2.04	2.02	1.98	2.05	2.01	-
		$c_{u2}/c_{u1} = 3.5$	2.07	2.04	2.04	2.02	1.98	2.05	2.01	-
		$c_{u2}/c_{u1} = 3$	2.07	2.04	2.04	2.02	1.98	2.05	2.01	-
		$c_{u2}/c_{u1} = 2.5$	2.07	2.04	2.04	2.02	1.98	2.05	2.01	-
$c_{u2}/c_{u1} = 2$	2.07	2.04	2.04	2.02	1.98	2.05	2.01	-		
H = 10 m $\gamma = 20 \text{ kN/m}^3$ $c_{u1} = 50 \text{ kN/m}^2$	$E_{s1} = 7000 \text{ kN/m}^2$ $\nu_{s1} = 0.495 (0.5)$	$c_{u2}/c_{u1} = 4$	2.07	2.04	2.04	2.02	1.98	2.05	2.01	2.03
		$c_{u2}/c_{u1} = 3.5$	2.07	2.04	2.04	2.02	1.98	2.05	2.01	2.03
		$c_{u2}/c_{u1} = 3$	2.07	2.04	2.04	2.02	1.98	2.05	2.01	2.03
		$c_{u2}/c_{u1} = 2.5$	2.07	2.04	2.04	2.02	1.98	2.05	2.01	2.03
		$c_{u2}/c_{u1} = 2$	2.07	2.04	2.04	2.02	1.98	2.05	2.01	2.03
		$c_{u2}/c_{u1} = 1.5$	2.04	2.02	2.04	2.02	1.98	2.05	2.01	2.03
		$c_{u2}/c_{u1} = 1$	1.47	1.46	1.46	1.45	1.43	1.46	1.44	1.47
		$c_{u2}/c_{u1} = 0.75$	1.17	1.15	1.16	1.15	1.14	1.16	1.15	1.18
		$c_{u2}/c_{u1} = 0.5$	-	-	0.86	0.85	0.84	0.86	0.85	0.87
		$c_{u2}/c_{u1} = 0.25$	-	-	0.55	0.54	0.53	0.55	0.54	-
		$c_{u2}/c_{u1} = 4$	2.07	2.04	2.04	2.02	1.98	2.05	2.01	-
		$c_{u2}/c_{u1} = 3.5$	2.07	2.04	2.04	2.02	1.98	2.05	2.01	-
		$c_{u2}/c_{u1} = 3$	2.07	2.04	2.04	2.02	1.98	2.05	2.01	-
		$c_{u2}/c_{u1} = 2.5$	2.07	2.04	2.04	2.02	1.98	2.05	2.01	-
$c_{u2}/c_{u1} = 2$	2.07	2.04	2.04	2.02	1.98	2.05	2.01	-		

10.4.5 Example 5

Tab. 96 Example 5: Check calculations

Parameters		SRFEA ($\psi' = 0^\circ$) (Plaxis 2D)					
		H = 5 m			H = 10 m		
		Set 1 $\gamma_{\text{unsat}} = 16 \text{ kN/m}^3$ $\gamma_{\text{sat}} = 16 \text{ kN/m}^3$ $c' = 4 \text{ kN/m}^2$ H = 5 m	Set 2 $\gamma_{\text{unsat}} = 20 \text{ kN/m}^3$ $\gamma_{\text{sat}} = 20 \text{ kN/m}^3$ $c' = 5 \text{ kN/m}^2$ H = 5 m	Set 3 $\gamma_{\text{unsat}} = 24 \text{ kN/m}^3$ $\gamma_{\text{sat}} = 24 \text{ kN/m}^3$ $c' = 6 \text{ kN/m}^2$ H = 5 m	Set 4 $\gamma_{\text{unsat}} = 16 \text{ kN/m}^3$ $\gamma_{\text{sat}} = 16 \text{ kN/m}^3$ $c' = 8 \text{ kN/m}^2$ H = 10 m	Set 5 $\gamma_{\text{unsat}} = 20 \text{ kN/m}^3$ $\gamma_{\text{sat}} = 20 \text{ kN/m}^3$ $c' = 10 \text{ kN/m}^2$ H = 10 m	Set 6 $\gamma_{\text{unsat}} = 24 \text{ kN/m}^3$ $\gamma_{\text{sat}} = 24 \text{ kN/m}^3$ $c' = 12 \text{ kN/m}^2$ H = 10 m
		δ -n	δ -n	δ -n	δ -n	δ -n	δ -n
$E' = 10^4 \text{ kN/m}^2$ $\nu = 0.25$	L/H = -0.2	2.12	1.83	1.70	2.12	1.83	1.70
	L/H = -0.1	2.12	1.83	1.70	2.12	1.83	1.70
	L/H = 0	2.11	1.83	1.70	2.11	1.83	1.70
	L/H = 0.1	1.86	1.70	1.62	1.86	1.70	1.62
	L/H = 0.2	1.64	1.57	1.52	1.64	1.57	1.52
	L/H = 0.3	1.48	1.46	1.45	1.48	1.46	1.45
	L/H = 0.4	1.38	1.38	1.38	1.38	1.38	1.38
	L/H = 0.5	1.30	1.33	1.34	1.30	1.33	1.34
	L/H = 0.6	1.26	1.29	1.31	1.26	1.29	1.31
	L/H = 0.7	1.25	1.28	1.30	1.25	1.28	1.30
	L/H = 0.8	1.27	1.29	1.30	1.27	1.29	1.30
	L/H = 0.9	1.31	1.32	1.33	1.31	1.32	1.33
	L/H = 1	1.36	1.36	1.36	1.36	1.36	1.36

Tab. 97 Example 5: Further calculations for set 2

Parameters	SRFEA ($\psi = 0^\circ$) (Piaxis 2D)		SRFEA ($\psi = \varphi$) (Piaxis 2D)		Davis A - SRFEA (Piaxis 2D)		Davis B - SRFEA (Piaxis 2D)		SRFEA ($\psi = \varphi$) (Optum G2)		FELA (Optum G2)		Davis A - FELA (Optum G2)		Davis B - FELA (Optum G2)		LEA (Slide)				
	6-n	15-n	6-n	15-n	6-n	15-n	6-n	15-n	6-n	15-n	Lower	Upper	Mean	Lower	Upper	Mean		M-P			
Set 2 H = 5 m $\gamma_{unsat} = 20 \text{ kN/m}^3$ $\gamma_{sat} = 20 \text{ kN/m}^3$ $c' = 5 \text{ kN/m}^2$	L/H = -0.2	1.81	1.84	1.83	1.72	1.80	1.79	1.82	1.80	1.82	1.79	1.82	1.81	1.68	1.72	1.70	1.76	1.79	1.77	1.82	
	L/H = -0.1	1.83	1.81	1.84	1.83	1.72	1.81	1.79	1.82	1.80	1.79	1.82	1.81	1.68	1.72	1.70	1.75	1.79	1.77	1.82	
	L/H = 0	1.83	1.81	1.84	1.83	1.72	1.81	1.79	1.82	1.80	1.79	1.82	1.81	1.68	1.72	1.70	1.75	1.79	1.77	1.82	
	L/H = 0.1	1.70	1.68	1.72	1.71	1.62	1.60	1.68	1.67	1.70	1.69	1.68	1.70	1.69	1.58	1.60	1.59	1.64	1.66	1.65	1.70
	L/H = 0.2	1.57	1.55	1.59	1.58	1.50	1.49	1.55	1.54	1.58	1.57	1.55	1.58	1.57	1.47	1.49	1.48	1.52	1.54	1.53	1.58
	L/H = 0.3	1.46	1.44	1.49	1.48	1.40	1.39	1.44	1.43	1.48	1.48	1.45	1.48	1.47	1.37	1.39	1.38	1.42	1.44	1.43	1.48
	L/H = 0.4	1.38	1.36	1.41	1.40	1.33	1.32	1.36	1.35	1.40	1.40	1.39	1.41	1.40	1.30	1.32	1.31	1.34	1.36	1.35	1.41
	L/H = 0.5	1.33	1.30	1.36	1.35	1.27	1.27	1.31	1.30	1.35	1.34	1.33	1.35	1.34	1.25	1.27	1.26	1.28	1.31	1.29	1.35
	L/H = 0.6	1.29	1.27	1.32	1.31	1.24	1.23	1.27	1.26	1.31	1.31	1.29	1.32	1.31	1.21	1.24	1.23	1.24	1.27	1.26	1.31
	L/H = 0.7	1.28	1.26	1.31	1.30	1.23	1.22	1.26	1.25	1.30	1.30	1.29	1.31	1.30	1.21	1.23	1.22	1.23	1.26	1.24	1.30
	L/H = 0.8	1.29	1.27	1.32	1.31	1.24	1.23	1.27	1.26	1.31	1.31	1.29	1.32	1.30	1.22	1.24	1.23	1.25	1.27	1.26	1.31
	L/H = 0.9	1.32	1.30	1.35	1.34	1.27	1.26	1.30	1.29	1.34	1.33	1.32	1.35	1.33	1.24	1.27	1.25	1.27	1.30	1.29	1.34
L/H = 1	1.36	1.35	1.39	1.38	1.30	1.30	1.34	1.33	1.38	1.37	1.35	1.39	1.37	1.28	1.30	1.29	1.31	1.33	1.32	1.37	
Set 5 H = 10 m $\gamma_{unsat} = 20 \text{ kN/m}^3$ $\gamma_{sat} = 20 \text{ kN/m}^3$ $c' = 10 \text{ kN/m}^2$	L/H = -0.2	1.82	1.81	1.82	1.81	1.82	1.81	1.82	1.80	1.82	1.80	1.82	1.81	1.82	1.80	1.82	1.80	1.82	1.80	1.82	
	L/H = -0.1	1.82	1.81	1.82	1.81	1.82	1.81	1.82	1.80	1.82	1.80	1.82	1.81	1.82	1.80	1.82	1.80	1.82	1.80	1.82	1.82
	L/H = 0	1.82	1.81	1.82	1.81	1.82	1.81	1.82	1.80	1.82	1.80	1.82	1.81	1.82	1.80	1.82	1.80	1.82	1.80	1.82	1.82
	L/H = 0.1	1.70	1.68	1.72	1.71	1.62	1.60	1.68	1.67	1.70	1.69	1.68	1.70	1.69	1.58	1.60	1.59	1.64	1.66	1.65	1.70
	L/H = 0.2	1.57	1.55	1.59	1.58	1.50	1.49	1.55	1.54	1.58	1.57	1.55	1.58	1.57	1.47	1.49	1.48	1.52	1.54	1.53	1.58
	L/H = 0.3	1.46	1.44	1.49	1.48	1.40	1.39	1.44	1.43	1.48	1.48	1.45	1.48	1.47	1.37	1.39	1.38	1.42	1.44	1.43	1.48
	L/H = 0.4	1.38	1.36	1.41	1.40	1.33	1.32	1.36	1.35	1.40	1.40	1.39	1.41	1.40	1.30	1.32	1.31	1.34	1.36	1.35	1.41
	L/H = 0.5	1.33	1.30	1.36	1.35	1.27	1.27	1.31	1.30	1.35	1.34	1.33	1.35	1.34	1.25	1.27	1.26	1.28	1.31	1.29	1.35
	L/H = 0.6	1.29	1.27	1.32	1.31	1.24	1.23	1.27	1.26	1.31	1.31	1.29	1.32	1.31	1.21	1.24	1.23	1.24	1.27	1.26	1.31
	L/H = 0.7	1.28	1.26	1.31	1.30	1.23	1.22	1.26	1.25	1.30	1.30	1.29	1.31	1.30	1.21	1.23	1.22	1.23	1.26	1.24	1.30
	L/H = 0.8	1.29	1.27	1.32	1.31	1.24	1.23	1.27	1.26	1.31	1.31	1.29	1.32	1.30	1.22	1.24	1.23	1.25	1.27	1.26	1.31
	L/H = 0.9	1.32	1.30	1.35	1.34	1.27	1.26	1.30	1.29	1.34	1.33	1.32	1.35	1.33	1.24	1.27	1.25	1.27	1.30	1.29	1.34
L/H = 1	1.36	1.35	1.39	1.38	1.30	1.30	1.34	1.33	1.38	1.37	1.35	1.39	1.37	1.28	1.30	1.29	1.31	1.33	1.32	1.37	

10.4.6 Example 6

Tab. 98 Example 6: Overview of the calculations - part 1

Parameters		SRFEA ($\psi' = 0^\circ$) (Plaxis 2D)		SRFEA ($\psi' = \varphi'$) (Plaxis 2D)		Davis A - SRFEA (Plaxis 2D)		Davis B - SRFEA (Plaxis 2D)		SRFEA ($\psi' = \varphi'$) (Optum G2)	
		~1250 elements		~1250 elements		~1250 elements		~1250 elements		~850 elements	
		6-n	15-n	6-n	15-n	6-n	15-n	6-n	15-n	6-n	15-n
No free surface	$E' = 10^4 \text{ kN/m}^2$ $\nu = 0.25$	2.40	2.36	2.47	2.45	1.97	1.96	2.35	2.33	2.47	2.44
	$E' = 10^4 \text{ kN/m}^2$ $\nu = 0.35$	2.40	2.36	2.47	2.45	1.97	1.95	2.34	2.34	2.47	2.44
With a free surface	$E' = 10^4 \text{ kN/m}^2$ $\nu = 0.25$	1.87	1.80	1.91	1.90	1.52	1.52	1.75	1.75	1.93	1.92
	$E' = 10^4 \text{ kN/m}^2$ $\nu = 0.35$	1.87	1.80	1.91	1.90	1.52	1.51	1.75	1.74	1.93	1.92

Tab. 99 Example 6: Overview of the calculations - part 2

Parameters		FELA (Optum G2)			Davis A - FELA (Optum G2)			Davis B - FELA (Optum G2)			LEA (Slide)
		~850 elements			~850 elements			~850 elements			M-P Circular
		Lower	Upper	Mean	Lower	Upper	Mean	Lower	Upper	Mean	
No free surface	$E' = 10^4 \text{ kN/m}^2$ $\nu = 0.25$	2.43	2.49	2.46	1.94	1.98	1.96	2.31	2.37	2.34	2.46
	$E' = 10^4 \text{ kN/m}^2$ $\nu = 0.35$	2.43	2.49	2.46	1.94	1.98	1.96	2.31	2.37	2.34	
With a free surface	$E' = 10^4 \text{ kN/m}^2$ $\nu = 0.25$	1.91	1.94	1.92	1.52	1.55	1.53	1.76	1.79	1.77	1.92
	$E' = 10^4 \text{ kN/m}^2$ $\nu = 0.35$	1.91	1.94	1.92	1.52	1.55	1.53	1.76	1.79	1.77	

10.4.7 Comparison of Davis A, Davis B and Davis C

Tab. 100 Study 1 - slope 1: Overview of the calculations

Parameters		SRFEA (Plaxis 2D)						Davis A (Plaxis 2D)			Davis B (Plaxis 2D)			Davis C (Plaxis 2D)			
		15 noded $\nu = 0.2$			15 noded: user-defined MC $\nu = 0.2$			15 noded $\nu = 0.2$			15 noded $\nu = 0.2$			15 noded $\nu = 0.2$			
		ϕ' failure	c' failure	FoS	ϕ' failure	c' failure	G	FoS	ϕ' failure	c' failure	FoS	ϕ' failure	c' failure	FoS	ϕ' failure	c' failure	FoS
$\phi' = 40^\circ$	$\psi = 40^\circ$	21.10	0.92	2.18	21.11	0.92	4166.67	2.17	21.10	0.92	2.18	21.10	0.92	2.18	19.91	0.86	2.17
	$\psi = 35^\circ$	21.10	0.92	2.18	21.11	0.92	4166.67	2.17	21.11	0.92	2.16	21.10	0.92	2.17	20.47	0.89	2.17
	$\psi = 30^\circ$	21.10	0.92	2.18	21.12	0.92	4166.67	2.17	21.09	0.92	2.13	21.09	0.92	2.16	20.86	0.91	2.17
	$\psi = 25^\circ$	21.10	0.92	2.18	21.18	0.92	4166.67	2.17	21.08	0.92	2.08	21.10	0.92	2.15	21.07	0.92	2.17
	$\psi = 20^\circ$	21.08	0.92	2.18	21.33	0.93	4166.67	2.15	21.09	0.92	2.01	21.10	0.92	2.13	21.12	0.92	2.17
	$\psi = 15^\circ$	21.08	0.92	2.18	21.49	0.94	4166.67	2.13	21.07	0.92	1.93	21.08	0.92	2.10	21.11	0.92	2.16
	$\psi = 10^\circ$	21.26	0.93	2.16	21.59	0.94	4166.67	2.12	21.12	0.92	1.85	21.10	0.92	2.07	21.09	0.92	2.13
	$\psi = 5^\circ$	21.53	0.94	2.13	21.85	0.96	4166.67	2.09	21.11	0.92	1.76	21.11	0.92	2.04	21.09	0.92	2.08
$\psi = 0^\circ$	21.98	0.96	2.08	21.96	0.96	4166.67	2.08	21.06	0.92	1.67	21.12	0.92	2.00	21.12	0.92	2.00	
$\phi' = 35^\circ$	$\psi = 35^\circ$	20.50	1.07	1.87	20.49	1.07	4166.67	1.87	20.50	1.07	1.87	20.50	1.07	1.87	19.84	1.03	1.87
	$\psi = 30^\circ$	20.50	1.07	1.87	20.54	1.07	4166.67	1.87	20.48	1.07	1.87	20.51	1.07	1.87	20.23	1.05	1.87
	$\psi = 25^\circ$	20.52	1.07	1.87	20.57	1.07	4166.67	1.87	20.51	1.07	1.83	20.50	1.07	1.86	20.46	1.07	1.87
	$\psi = 20^\circ$	20.52	1.07	1.87	20.68	1.08	4166.67	1.86	20.51	1.07	1.79	20.52	1.07	1.84	20.53	1.07	1.87
	$\psi = 15^\circ$	20.51	1.07	1.87	20.83	1.09	4166.67	1.84	20.51	1.07	1.74	20.55	1.07	1.82	20.54	1.07	1.86
	$\psi = 10^\circ$	20.58	1.07	1.87	20.91	1.09	4166.67	1.83	20.51	1.07	1.68	20.51	1.07	1.80	20.51	1.07	1.84
	$\psi = 5^\circ$	20.78	1.08	1.85	20.97	1.09	4166.67	1.83	20.55	1.07	1.60	20.49	1.07	1.77	20.52	1.07	1.79
	$\psi = 0^\circ$	21.50	1.12	1.78	21.48	1.12	4166.67	1.78	20.53	1.07	1.53	20.53	1.07	1.73	20.53	1.07	1.73
$\phi' = 30^\circ$	$\psi = 30^\circ$	19.85	1.25	1.60	19.86	1.25	4166.67	1.60	19.85	1.25	1.60	19.85	1.25	1.60	19.57	1.23	1.60
	$\psi = 25^\circ$	19.83	1.25	1.60	19.88	1.25	4166.67	1.60	19.84	1.25	1.59	19.85	1.25	1.60	19.81	1.25	1.60
	$\psi = 20^\circ$	19.85	1.25	1.60	19.95	1.26	4166.67	1.59	19.84	1.25	1.57	19.84	1.25	1.59	19.90	1.25	1.60
	$\psi = 15^\circ$	19.84	1.25	1.60	20.03	1.26	4166.67	1.58	19.83	1.25	1.54	19.83	1.25	1.57	19.83	1.25	1.60
	$\psi = 10^\circ$	19.98	1.26	1.59	20.18	1.27	4166.67	1.57	19.85	1.25	1.49	19.82	1.25	1.55	19.85	1.25	1.57
	$\psi = 5^\circ$	20.27	1.28	1.56	20.43	1.29	4166.67	1.55	19.83	1.25	1.44	19.85	1.25	1.52	19.84	1.25	1.54
	$\psi = 0^\circ$	20.41	1.29	1.55	20.41	1.29	4166.67	1.55	19.82	1.25	1.39	19.83	1.25	1.49	19.83	1.25	1.49
	$\phi' = 25^\circ$	$\psi = 25^\circ$	19.04	1.48	1.35	19.03	1.48	4166.67	1.35	19.04	1.48	1.35	19.04	1.48	1.35	18.99	1.48
$\psi = 20^\circ$		19.00	1.48	1.35	19.07	1.48	4166.67	1.35	19.04	1.48	1.35	19.02	1.48	1.35	19.09	1.48	1.35
$\psi = 15^\circ$		19.07	1.48	1.35	19.16	1.49	4166.67	1.34	19.02	1.48	1.33	19.05	1.48	1.34	19.05	1.48	1.35
$\psi = 10^\circ$		19.16	1.49	1.34	19.31	1.50	4166.67	1.33	19.06	1.48	1.30	19.03	1.48	1.32	19.03	1.48	1.33
$\psi = 5^\circ$		19.37	1.51	1.33	19.52	1.52	4166.67	1.32	19.05	1.48	1.27	19.04	1.48	1.30	19.07	1.48	1.30
$\psi = 0^\circ$		19.83	1.55	1.29	19.83	1.55	4166.67	1.29	19.06	1.48	1.22	19.05	1.48	1.27	19.05	1.48	1.27

Tab. 101 Study 1 - slope 2: Overview of the calculations

Parameters		SRFEA (Plaxis 2D)						Davis A (Plaxis 2D)		Davis B (Plaxis 2D)			Davis C (Plaxis 2D)				
		15 noded $\nu = 0.2$			15 noded: user-defined MC $\nu = 0.2$			15 noded $\nu = 0.2$		15 noded $\nu = 0.2$			15 noded $\nu = 0.2$				
		ϕ' failure	c' failure	FoS	ϕ' failure	c' failure	G	FoS	ϕ' failure	c' failure	FoS	ϕ' failure	c' failure	FoS	ϕ' failure	c' failure	FoS
$\phi' = 40^\circ$	$\psi = 40^\circ$	27.01	3.04	1.65	27.00	3.04	4166.67	1.65	27.01	3.04	1.65	27.01	3.04	1.65	26.33	2.95	1.64
	$\psi = 35^\circ$	27.00	3.04	1.65	27.00	3.04	4166.67	1.65	27.03	3.04	1.64	27.01	3.04	1.64	26.80	3.01	1.64
	$\psi = 30^\circ$	27.05	3.04	1.64	27.04	3.04	4166.67	1.64	27.10	3.05	1.60	27.01	3.04	1.63	27.04	3.04	1.64
	$\psi = 25^\circ$	27.05	3.04	1.64	27.35	3.08	4166.67	1.62	27.12	3.05	1.56	27.08	3.05	1.60	27.06	3.04	1.64
	$\psi = 20^\circ$	27.12	3.05	1.64	27.63	3.12	4166.67	1.60	27.05	3.04	1.52	27.12	3.05	1.58	27.07	3.05	1.63
	$\psi = 15^\circ$	27.37	3.08	1.62	27.96	3.16	4166.67	1.58	27.09	3.05	1.46	26.99	3.04	1.55	27.00	3.04	1.60
	$\psi = 10^\circ$	27.84	3.15	1.59	28.31	3.21	4166.67	1.56	27.09	3.05	1.39	27.07	3.05	1.51	27.09	3.05	1.55
	$\psi = 5^\circ$	28.40	3.22	1.55	28.76	3.27	4166.67	1.53	27.01	3.04	1.33	27.11	3.05	1.46	27.01	3.04	1.49
$\psi = 0^\circ$	29.30	3.34	1.50	29.34	3.35	4166.67	1.49	26.99	3.04	1.26	27.05	3.04	1.41	27.05	3.04	1.41	
$\phi' = 35^\circ$	$\psi = 35^\circ$	25.61	3.42	1.46	25.58	3.42	4166.67	1.46	25.61	3.42	1.46	25.61	3.42	1.46	25.24	3.37	1.46
	$\psi = 30^\circ$	25.59	3.42	1.46	25.62	3.42	4166.67	1.46	25.59	3.42	1.45	25.60	3.42	1.46	25.53	3.41	1.46
	$\psi = 25^\circ$	25.56	3.42	1.46	25.71	3.44	4166.67	1.45	25.57	3.42	1.43	25.60	3.42	1.45	25.61	3.42	1.46
	$\psi = 20^\circ$	25.58	3.42	1.46	25.98	3.48	4166.67	1.44	25.62	3.42	1.40	25.59	3.42	1.43	25.59	3.42	1.45
	$\psi = 15^\circ$	25.81	3.45	1.45	26.30	3.53	4166.67	1.42	25.60	3.42	1.36	25.57	3.42	1.40	25.59	3.42	1.43
	$\psi = 10^\circ$	26.23	3.52	1.42	26.60	3.58	4166.67	1.40	25.62	3.42	1.31	25.61	3.42	1.37	25.63	3.43	1.39
	$\psi = 5^\circ$	26.80	3.61	1.39	27.02	3.64	4166.67	1.37	25.57	3.42	1.26	25.67	3.43	1.33	25.58	3.42	1.34
	$\psi = 0^\circ$	27.52	3.72	1.34	27.45	3.71	4166.67	1.35	25.58	3.42	1.20	25.54	3.41	1.29	25.54	3.41	1.29
$\phi' = 30^\circ$	$\psi = 30^\circ$	24.01	3.86	1.30	24.01	3.86	4166.67	1.30	24.01	3.86	1.30	24.01	3.86	1.30	23.97	3.85	1.29
	$\psi = 25^\circ$	24.01	3.86	1.30	24.05	3.86	4166.67	1.29	24.04	3.86	1.29	24.04	3.86	1.29	24.11	3.88	1.29
	$\psi = 20^\circ$	23.98	3.85	1.30	24.19	3.89	4166.67	1.29	24.05	3.86	1.27	24.05	3.86	1.28	24.05	3.86	1.29
	$\psi = 15^\circ$	24.14	3.88	1.29	24.38	3.92	4166.67	1.27	24.03	3.86	1.24	24.06	3.87	1.26	24.10	3.87	1.27
	$\psi = 10^\circ$	24.48	3.94	1.27	24.76	3.99	4166.67	1.25	24.09	3.87	1.21	24.03	3.86	1.24	24.07	3.87	1.25
	$\psi = 5^\circ$	24.98	4.04	1.24	25.22	4.08	4166.67	1.23	23.99	3.85	1.17	24.01	3.86	1.20	24.03	3.86	1.21
	$\psi = 0^\circ$	25.49	4.13	1.21	25.49	4.13	4166.67	1.21	24.02	3.86	1.12	24.01	3.86	1.16	24.01	3.86	1.16
	$\phi' = 25^\circ$	$\psi = 25^\circ$	22.30	4.40	1.14	22.30	4.40	4166.67	1.14	22.30	4.40	1.14	22.30	4.40	1.14	22.31	4.40
$\psi = 20^\circ$		22.19	4.37	1.14	22.37	4.41	4166.67	1.13	22.25	4.39	1.14	22.26	4.39	1.14	22.32	4.40	1.14
$\psi = 15^\circ$		22.28	4.39	1.14	22.50	4.44	4166.67	1.13	22.26	4.39	1.12	22.30	4.40	1.12	22.25	4.39	1.13
$\psi = 10^\circ$		22.55	4.45	1.12	22.68	4.48	4166.67	1.									

Tab. 102 Study 2 - slope 1: Overview of the calculations

Parameters		SRFEA (Plaxis 2D)						Davis A (Plaxis 2D)			Davis B (Plaxis 2D)			Davis C (Plaxis 2D)				
		15 noded $\nu = 0.2$			15 noded: user-defined MC $\nu = 0.2$			15 noded $\nu = 0.2$			15 noded $\nu = 0.2$			15 noded $\nu = 0.2$				
		$\phi'_{failure}$	$c'_{failure}$	FoS	$\phi'_{failure}$	$c'_{failure}$	G	FoS	$\phi'_{failure}$	$c'_{failure}$	FoS	$\phi'_{failure}$	$c'_{failure}$	FoS	$\phi'_{failure}$	$c'_{failure}$	FoS	
$c' = 10 \text{ kN/m}^2$	$\phi' = 30^\circ$	$\psi = 30^\circ$	12.74	3.92	2.55	12.74	3.92	4166.67	2.55	12.75	3.92	2.55	12.75	3.92	2.55	12.17	3.74	2.55
		$\psi = 25^\circ$	12.75	3.92	2.55	12.75	3.92	4166.67	2.55	12.73	3.91	2.54	12.73	3.91	2.55	12.46	3.83	2.55
		$\psi = 20^\circ$	12.74	3.92	2.55	12.77	3.92	4166.67	2.55	12.74	3.92	2.51	12.74	3.92	2.54	12.65	3.89	2.55
		$\psi = 15^\circ$	12.74	3.92	2.55	12.79	3.93	4166.67	2.54	12.72	3.91	2.46	12.74	3.92	2.54	12.75	3.92	2.55
		$\psi = 10^\circ$	12.75	3.92	2.55	12.82	3.94	4166.67	2.54	12.72	3.91	2.39	12.71	3.91	2.53	12.74	3.92	2.55
		$\psi = 5^\circ$	12.77	3.92	2.55	12.86	3.95	4166.67	2.53	12.72	3.91	2.31	12.73	3.91	2.51	12.72	3.91	2.53
	$\psi = 0^\circ$	12.89	3.96	2.52	12.89	3.96	4166.67	2.52	12.74	3.92	2.21	12.74	3.92	2.49	12.74	3.92	2.49	
$c' = 5 \text{ kN/m}^2$	$\phi' = 30^\circ$	$\psi = 30^\circ$	16.04	2.49	2.01	16.05	2.49	4166.67	2.01	16.04	2.49	2.01	16.04	2.49	2.01	15.57	2.41	2.01
		$\psi = 25^\circ$	16.06	2.49	2.01	16.10	2.50	4166.67	2.00	16.06	2.49	2.00	16.06	2.49	2.00	15.86	2.46	2.01
		$\psi = 20^\circ$	16.05	2.49	2.01	16.12	2.50	4166.67	2.00	16.07	2.49	1.97	16.07	2.49	1.99	16.03	2.49	2.01
		$\psi = 15^\circ$	16.06	2.49	2.01	16.20	2.52	4166.67	1.99	16.08	2.50	1.93	16.05	2.49	1.98	16.06	2.49	2.01
		$\psi = 10^\circ$	16.11	2.50	2.00	16.24	2.52	4166.67	1.98	16.08	2.50	1.87	16.05	2.49	1.97	16.05	2.49	1.99
		$\psi = 5^\circ$	16.23	2.52	1.98	16.30	2.53	4166.67	1.97	16.04	2.49	1.81	16.06	2.49	1.95	16.05	2.49	1.97
	$\psi = 0^\circ$	16.39	2.55	1.96	16.40	2.55	4166.67	1.96	16.07	2.49	1.74	16.06	2.49	1.92	16.06	2.49	1.92	
$c' = 0 \text{ kN/m}^2$	$\phi' = 30^\circ$	$\psi = 30^\circ$	26.13	0.00	1.18	26.13	0.00	4166.67	1.18	26.13	0.00	1.18	26.13	0.00	1.18	26.08	0.00	1.18
		$\psi = 25^\circ$	26.09	0.00	1.18	26.25	0.00	4166.67	1.17	26.14	0.00	1.17	26.14	0.00	1.17	26.14	0.00	1.18
		$\psi = 20^\circ$	26.44	0.00	1.16	26.46	0.00	4166.67	1.16	26.18	0.00	1.15	26.15	0.00	1.16	26.16	0.00	1.17
		$\psi = 15^\circ$	26.58	0.00	1.15	26.68	0.00	4166.67	1.15	26.17	0.00	1.13	26.13	0.00	1.14	26.14	0.00	1.15
		$\psi = 10^\circ$	26.84	0.00	1.14	26.94	0.00	4166.67	1.14	26.20	0.00	1.10	26.16	0.00	1.11	26.19	0.00	1.12
		$\psi = 5^\circ$	27.42	0.00	1.11	27.50	0.00	4166.67	1.11	26.14	0.00	1.06	26.17	0.00	1.07	26.19	0.00	1.07
	$\psi = 0^\circ$	28.55	0.00	1.06	28.55	0.00	4166.67	1.06	26.16	0.00	1.02	26.16	0.00	1.02	26.16	0.00	1.02	
$c' = 2 \text{ kN/m}^2$	$\phi' = 30^\circ$	$\psi = 30^\circ$	19.85	1.25	1.60	19.86	1.25	4166.67	1.60	19.85	1.25	1.60	19.85	1.25	1.60	19.84	1.25	1.60
		$\psi = 25^\circ$	19.83	1.25	1.60	19.88	1.25	4166.67	1.60	19.84	1.25	1.59	19.85	1.25	1.60	19.84	1.25	1.60
		$\psi = 20^\circ$	19.85	1.25	1.60	19.95	1.26	4166.67	1.59	19.84	1.25	1.57	19.84	1.25	1.59	19.83	1.25	1.60
		$\psi = 15^\circ$	19.84	1.25	1.60	20.03	1.26	4166.67	1.58	19.83	1.25	1.54	19.83	1.25	1.57	19.83	1.25	1.60
		$\psi = 10^\circ$	19.98	1.26	1.59	20.18	1.27	4166.67	1.57	19.85	1.25	1.49	19.82	1.25	1.55	19.85	1.25	1.57
		$\psi = 5^\circ$	20.27	1.28	1.56	20.43	1.29	4166.67	1.56	19.83	1.25	1.44	19.85	1.25	1.52	19.84	1.25	1.54
	$\psi = 0^\circ$	20.41	1.29	1.55	20.41	1.29	4166.67	1.55	19.82	1.25	1.39	19.83	1.25	1.49	19.83	1.25	1.49	

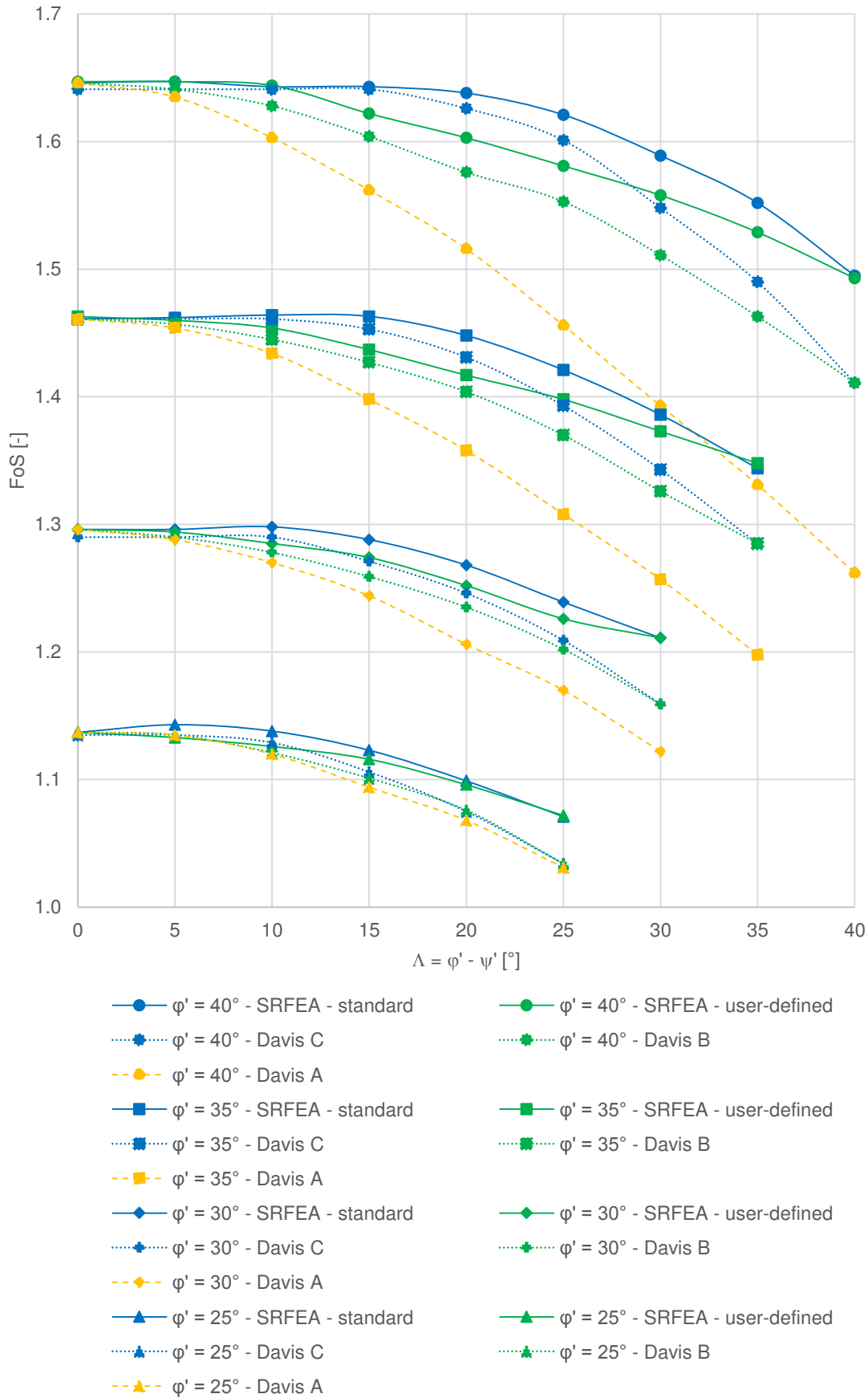


Fig. 102 Study 1 - slope 2: Standard SRFEA, user-defined SRFEA, Davis A, Davis B as well as Davis C results for different Δ and φ'

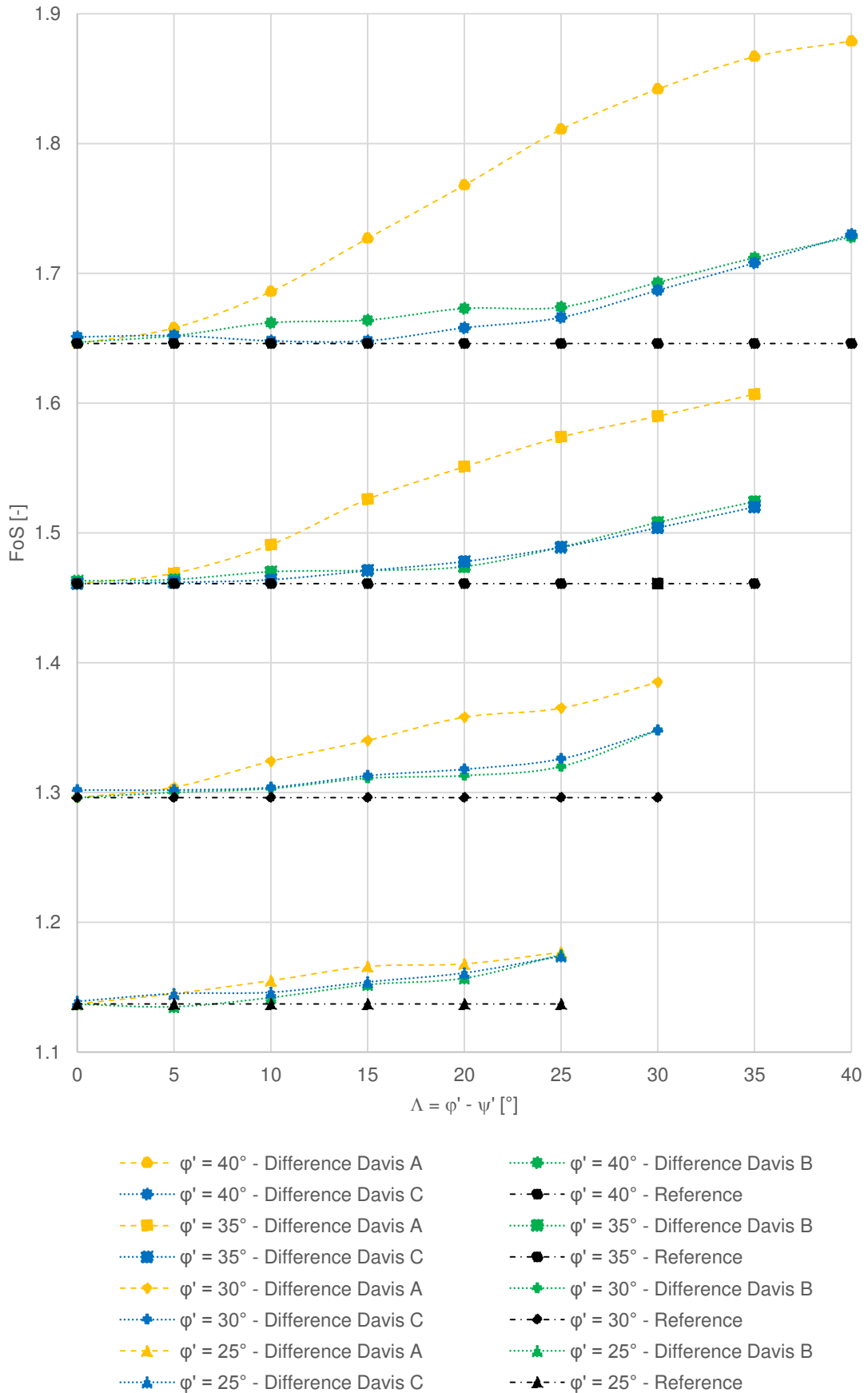


Fig. 103 Study 1 - slope 2: Differences between Davis A and standard SRFEA, Davis B and user-defined SRFEA as well as Davis C and standard SRFEA for different Δ and ϕ'

Tab. 104 Case 2: Overview of the calculations

Parameters	SRFEA ($\psi' \neq \phi'$) (Plaxis 2D)	SRFEA ($\psi' = \phi'$) (Plaxis 2D)	Davis A SRFEA (Plaxis 2D)	Davis B SRFEA (Plaxis 2D)	Davis C SRFEA (Plaxis 2D)	SRFEA ($\psi' = \phi'$) (Optum G2)	Davis A FELA (Optum G2)	Davis B FELA (Optum G2)	Davis C FELA (Optum G2)
	15 noded $\nu = 0.3$ modified FoS	15 noded $\nu = 0.3$ modified FoS	15 noded $\nu = 0.3$ modified FoS	15 noded $\nu = 0.3$ modified FoS	15 noded $\nu = 0.3$ modified FoS	Lower, Upper $\nu = 0.3$ modified FoS _{Mea}	Lower, Upper $\nu = 0.3$ modified FoS _{Mea}	Lower, Upper $\nu = 0.3$ modified FoS _{Mea}	Lower, Upper $\nu = 0.3$ modified FoS _{Mea}
$E' = 10^4 \text{ kN/m}^2$ $\gamma_{\text{unsat}} = 16 \text{ kN/m}^3$ $\psi = \phi/4$ $\psi = \phi/3$	$\psi = 0$ 1.23	1.18	1.17	1.21	1.20	1.28	1.18	1.21	1.21
	$\psi = \phi/4$ 1.26	1.22	1.22	1.24	1.25	1.28	1.22	1.24	1.24
	$\psi = \phi/3$ 1.27	1.23	1.23	1.25	1.26	1.28	1.24	1.25	1.25
	$\psi = 0$ 1.17	1.12	1.12	1.14	1.14	1.22	1.13	1.15	1.15
	$\psi = \phi/4$ 1.20	1.16	1.16	1.18	1.18	1.22	1.17	1.19	1.19
	$\psi = \phi/3$ 1.21	1.17	1.18	1.19	1.19	1.19	1.18	1.19	1.20
$c' = 2 \text{ kN/m}^2$ $E' = 10^7 \text{ kN/m}^2$ $\gamma_{\text{unsat}} = 16 \text{ kN/m}^3$ $\psi = \phi/4$ $\psi = \phi/3$	$\psi = 0$ 1.22	1.18	1.17	1.21	1.20	1.28	1.18	1.21	1.21
	$\psi = \phi/4$ 1.26	1.22	1.22	1.24	1.25	1.28	1.22	1.24	1.25
	$\psi = \phi/3$ 1.27	1.23	1.23	1.25	1.26	1.28	1.24	1.25	1.26
	$\psi = 0$ 1.17	1.12	1.12	1.14	1.14	1.22	1.13	1.15	1.15
	$\psi = \phi/4$ 1.20	1.16	1.16	1.18	1.18	1.22	1.17	1.19	1.19
	$\psi = \phi/3$ 1.21	1.17	1.18	1.19	1.19	1.19	1.18	1.19	1.20
$E' = 10^7 \text{ kN/m}^2$ $\gamma_{\text{unsat}} = 16 \text{ kN/m}^3$ $\psi = \phi/4$ $\psi = \phi/3$	$\psi = 0$ 1.20	1.16	1.16	1.18	1.18	1.22	1.17	1.19	1.19
	$\psi = \phi/4$ 1.21	1.17	1.18	1.19	1.19	1.22	1.18	1.19	1.20
	$\psi = \phi/3$ 1.21	1.17	1.18	1.19	1.19	1.22	1.18	1.19	1.20
	$\psi = 0$ 1.51	1.41	1.41	1.48	1.48	1.54	1.41	1.48	1.48
	$\psi = \phi/4$ 1.53	1.46	1.46	1.51	1.51	1.54	1.47	1.51	1.52
	$\psi = \phi/3$ 1.53	1.48	1.48	1.51	1.51	1.52	1.48	1.51	1.53
$c' = 4 \text{ kN/m}^2$ $E' = 10^4 \text{ kN/m}^2$ $\gamma_{\text{unsat}} = 20 \text{ kN/m}^3$ $\psi = \phi/4$ $\psi = \phi/3$	$\psi = 0$ 1.40	1.32	1.32	1.38	1.37	1.44	1.33	1.38	1.38
	$\psi = \phi/4$ 1.43	1.37	1.37	1.40	1.41	1.44	1.37	1.41	1.42
	$\psi = \phi/3$ 1.43	1.39	1.38	1.41	1.41	1.44	1.39	1.42	1.43
	$\psi = 0$ 1.51	1.41	1.41	1.48	1.48	1.54	1.41	1.48	1.48
	$\psi = \phi/4$ 1.53	1.46	1.46	1.51	1.50	1.54	1.47	1.51	1.52
	$\psi = \phi/3$ 1.53	1.48	1.48	1.51	1.51	1.52	1.48	1.51	1.53
$E' = 10^7 \text{ kN/m}^2$ $\gamma_{\text{unsat}} = 20 \text{ kN/m}^3$ $\psi = \phi/4$ $\psi = \phi/3$	$\psi = 0$ 1.40	1.32	1.32	1.38	1.37	1.44	1.33	1.38	1.38
	$\psi = \phi/4$ 1.43	1.37	1.37	1.40	1.41	1.44	1.37	1.41	1.42
	$\psi = \phi/3$ 1.43	1.39	1.38	1.41	1.41	1.44	1.39	1.42	1.43
	$\psi = 0$ 1.51	1.41	1.41	1.48	1.48	1.54	1.41	1.48	1.48
	$\psi = \phi/4$ 1.53	1.46	1.46	1.51	1.50	1.54	1.47	1.51	1.52
	$\psi = \phi/3$ 1.53	1.48	1.48	1.51	1.51	1.52	1.48	1.51	1.53
$E' = 10^7 \text{ kN/m}^2$ $\gamma_{\text{unsat}} = 20 \text{ kN/m}^3$ $\psi = \phi/4$ $\psi = \phi/3$	$\psi = 0$ 1.40	1.32	1.32	1.38	1.37	1.44	1.33	1.38	1.38
	$\psi = \phi/4$ 1.43	1.37	1.37	1.40	1.41	1.44	1.37	1.41	1.42
	$\psi = \phi/3$ 1.43	1.39	1.38	1.41	1.41	1.44	1.39	1.42	1.43
	$\psi = 0$ 1.51	1.41	1.41	1.48	1.48	1.54	1.41	1.48	1.48
	$\psi = \phi/4$ 1.53	1.46	1.46	1.51	1.50	1.54	1.47	1.51	1.52
	$\psi = \phi/3$ 1.53	1.48	1.48	1.51	1.51	1.52	1.48	1.51	1.53

10.6 Influence of the initial stress condition on the FoS

Tab. 105 φ - ν inequality with K_0 procedure: Overview of the calculations

Parameters			SRFEA ($\psi' = 0^\circ$) (Plaxis 2D)			SRFEA ($\psi' = \varphi'$) (Plaxis 2D)		
			15 noded			15 noded		
			$\nu = 0.2$ FoS	$\nu = \text{modified}$ FoS	$\nu = \text{choice}$ FoS	$\nu = 0.2$ FoS	$\nu = \text{modified}$ FoS	$\nu = \text{choice}$ FoS
$c' = 1 \text{ kN/m}^2$	$E' = 10^4 \text{ kN/m}^2$ $\gamma_{\text{unsat}} = 16 \text{ kN/m}^3$	Construction	1.72	1.71	1.71	1.80	1.80	1.80
		Excavation	1.72	1.68	1.71	1.81	1.80	1.80
		Nil step	1.70	1.71	1.71	1.81	1.80	1.80
		Gravity	1.72	1.71	1.72	1.81	1.81	1.80
$c' = 4 \text{ kN/m}^2$	$E' = 10^4 \text{ kN/m}^2$ $\gamma_{\text{unsat}} = 16 \text{ kN/m}^3$	Construction	1.37	1.37	1.37	1.43	1.42	1.41
		Excavation	1.37	1.37	1.37	1.43	1.43	1.42
		Nil step	1.36	1.36	1.36	1.43	1.42	1.41
		Gravity	1.37	1.37	1.37	1.43	1.42	1.42

Tab. 106 Influence of K_0 on FoS: Overview of the calculations with $K_0 = 0.25$

Parameters			SRFEA ($\psi' = 0^\circ$) (Plaxis 2D)	SRFEA ($\psi' = \varphi'$) (Plaxis 2D)
			15 noded	15 noded
			$K_0 = 0.25$ FoS	$K_0 = 0.25$ FoS
$c' = 1 \text{ kN/m}^2$	$E' = 10^4 \text{ kN/m}^2$ $\gamma_{\text{unsat}} = 16 \text{ kN/m}^3$	Construction	1.72	1.80
		Excavation	1.72	1.81
		Nil step	1.70	1.81
		Gravity	1.72	1.81
$c' = 4 \text{ kN/m}^2$	$E' = 10^4 \text{ kN/m}^2$ $\gamma_{\text{unsat}} = 16 \text{ kN/m}^3$	Construction	1.37	1.43
		Excavation	1.37	1.43
		Nil step	1.36	1.43
		Gravity	1.37	1.43

Tab. 107 Influence of K_0 on FoS: Overview of the calculations with $K_0 = 0.4$

Parameters			SRFEA ($\psi' = 0^\circ$) (Plaxis 2D)	SRFEA ($\psi' = \varphi'$) (Plaxis 2D)
			15 noded	15 noded
			$K_0 = 0.4$ FoS	$K_0 = 0.4$ FoS
$c' = 1 \text{ kN/m}^2$	$E' = 10^4 \text{ kN/m}^2$ $\gamma_{\text{unsat}} = 16 \text{ kN/m}^3$	Construction	1.72	1.80
		Excavation	1.71	1.81
		Nil step	1.71	1.81
		Gravity	1.72	1.81
$c' = 4 \text{ kN/m}^2$	$E' = 10^4 \text{ kN/m}^2$ $\gamma_{\text{unsat}} = 16 \text{ kN/m}^3$	Construction	1.37	1.43
		Excavation	1.37	1.43
		Nil step	1.36	1.43
		Gravity	1.37	1.43